NUREG/CR-6300
BMI-2184

Refinement and Evaluation of Crack-Opening-Area Analyses for Circumferential Through-Wall Cracks in Pipes

Manuscript Completed: March 1995
Date Published: April 1995

Prepared by
S. Rahman, F. Brust, N. Ghadiali, Y. H. Choi[1],
P. Krishnaswamy, F. Moberg[2], B. Brickstad[2],
G. Wilkowski

Battelle
505 King Avenue
Columbus, OH 43201

Prepared for
Division of Engineering Technology
Office of Nuclear Regulatory Research
U.S. Nuclear Regulatory Commission
Washington, DC 20555-0001
NRC Job Code B5702

[1]Korea Institute of Nuclear Safety
P.O. Box 16, Daeduk-danji, Taejeon Republic of Korea

[2]Swedish Plant Inspection Ltd. Alstromergatan 12
S-100 29 Stockholm, P.O. Box 49306 Sweden

DISCLAIMER

ABSTRACT

Leak-before-break (LBB) analyses for circumferentially cracked pipes are currently being conducted in the nuclear industry to justify elimination of pipe whip restraints and jet impingement shields which are present because of the expected dynamic effects from pipe rupture. The application of the LBB methodology frequently requires calculation of leak rates. The leak rates depend on the crack-opening area of the through-wall crack in the pipe. In addition to LBB analyses which assume a hypothetical flaw size, there is also interest in the integrity of actual leaking cracks corresponding to current leakage detection requirements in NRC Regulatory Guide 1.45, or for assessing temporary repair of Class 2 and 3 pipes that have leaks as are being evaluated in ASME Section XI.

This study was requested by the NRC to review, evaluate, and refine current analytical models for crack-opening-area analyses of pipes with circumferential through-wall cracks. Twenty-five pipe experiments were analyzed to determine the accuracy of the predictive models. Several practical aspects of crack-opening such as; crack-face pressure, off-center cracks, restraint of pressure-induced bending, cracks in thickness transition regions, weld residual stresses, crack-morphology models, and thermal-hydraulic analysis, were also investigated.

CONTENTS

CONTENTS

CONTENTS

CONTENTS

LIST OF FIGURES

LIST OF FIGURES

LIST OF FIGURES

LIST OF FIGURES

LIST OF FIGURES

LIST OF FIGURES

LIST OF TABLES

LIST OF TABLES

LIST OF TABLES

EXECUTIVE SUMMARY

Leak-before-break (LBB) analyses for circumferentially cracked pipes are currently being conducted in the nuclear industry to justify elimination of pipe whip restraints and jet impingement shields which are present because of the expected dynamic effects from pipe rupture. The application of the LBB methodology frequently requires calculation of leak rates. These leak rates depend on the crack-opening area of a through-wall crack in the pipe. In addition to LBB analyses, which assume a hypothetical flaw size, there is also interest in the integrity of actual leaking cracks corresponding to current leakage detection requirements in NRC Regulatory Guide 1.45, or for assessing temporary repair of Class 2 and 3 pipes that have leaks as are being evaluated in ASME Section XI. The results in this report are applicable to various aspects of these practical concerns.

Traditionally, the developments of crack-opening models have been focussed on idealized conditions for analyzing cracked pipes. For example, it is generally assumed that a simple circumferential through-wall crack exists in the pipe with the crack located in the center of the bending plane. The crack-opening area is calculated when this pipe is subjected to remote loads that may include pure bending, pure tension, or combined bending and tension. However, in reality, the loading conditions, the pipe and crack geometries, and the boundary conditions can be more complicated. For example, a crack in a pipe may become off-centered due to random imperfections around the pipe circumference, or the pipe may be restrained from pressure-induced bending if the crack is close to a nozzle. Additionally, the crack may be located at a thickness transition (e.g., a girth-weld crack in a nozzle), or the pipe may have significant weld residual stresses in addition to remote bending loads. Other scenarios can also be envisioned. Currently, there are no engineering methods or guidelines available to analyze pipes for these practical conditions. While some of these aspects are applicable to LBB analyses, other aspects are more applicable to evaluating flaw stability for a real rather than a hypothetical flaw.

The objectives of this study were to review, evaluate, and refine current analytical models for conducting crack-opening-area analyses of pipes with circumferential through-wall cracks. A separate report on the accuracy of load predictions by various analyses for circumferential cracks is published as NUREG/CR-6235 "Assessment of Short Through-Wall Cracks in Pipes - Experiments and Analyses." Also, the effects of combined loading with torsional stresses are being addressed in a separate report NUREG/CR-6299 "Effect of Toughness Anisotropy and Combined Tension, Torsion and Bending Loads on Fracture Behavior of Ferritic Nuclear Pipe."

The objectives of this study were accomplished in the following eight stages.

1. Review and Comparison of Predictive Models with Experimental Data

An in-depth review was conducted to evaluate current models for predicting crack-opening in circumferentially cracked pipes. The results from twenty-five full-scale pipe fracture experiments, conducted in the Degraded Piping Program, the International Piping Integrity Research Group (IPIRG) Program, and the Short Cracks in Piping and Piping Welds Program, were used to verify five different estimation methods as well as finite element analysis predictions. The results showed the following.

From Finite Element Analyses

- The results from several finite element analyses showed that the crack-opening shape for a pipe would approximately follow an elliptical profile. Both large-diameter pipes with short cracks and small-diameter pipes with long cracks were analyzed under pure bending and combined bending plus tension to reach this conclusion.

- The finite element predictions of the center-crack-opening displacement for Experiment 1.1.1.21 containing a short through-wall crack (θ/π = 6.25 percent) were in very good agreement with the experimental data from the pipe test.

- The differences in the GE/EPRI functions from the previously developed solutions (EPRI NP-3607) and the present study appear to be most important for small crack sizes (e.g., when θ/π = 1/16 and 1/8). The present solutions were developed using the 20-noded three-dimensional solid elements and the deformation theory algorithm of the ABAQUS code. The solutions presented here are believed to be the more accurate of the two solutions, because full three-dimensional elements were used instead of shell elements. The functions in the EPRI NP-3607 report appear to produce results that are too stiff, and, indeed, solutions for large n were not possible due to convergence problems. No convergence problems were experienced in the present work.

- For pipes under combined bending and pressure, the influence functions for a specific pipe (R_m/t = 10, θ/π = 1/16, and n = 5) were compared to determine the effects of hoop stress on a pipe. The results suggest that the hoop stress due to pressure will increase h_1, and hence, the J-integral. The mid-thickness crack-opening displacement (h_2) will also increase slightly due to local crack bulging. The load-point displacement (h_3) and the pipe rotation (h_4) will be significantly reduced due to stiffening of the pipe under additional hoop stresses.

From Estimation Analyses for Cracks in Base Metals

- Among the five estimation methods considered in this study, the LBB.ENG2 and GE/EPRI methods provided the most accurate predictions of crack-opening displacements up to crack-initiation load for the pipe experiments with cracks in the base metal that involved either pure bending or tension loads. For pipes under combined bending and tension, there were mixed trends in the crack-opening predictions by all estimation methods, except the Paris/Tada method which underpredicted crack-opening by the largest margin.

- The results for ten complex-cracked[(a)] pipes subjected to pure bending showed that in most cases, the LBB.ENG2 estimation method overestimated crack-opening displacements in experiments at all load levels regardless of the J-R curves. One primary reason for this is the use of an adjusted pipe radius and pipe thickness of an equivalent through-wall-cracked pipe and a simple through-wall-cracked pipe formula for analyzing a complex-cracked pipe.

(a) A complex crack is defined as a finite length circumferential through-wall crack with a surface crack in the remaining ligament of the circumferential plane. Sometimes referred to as a compound crack.

From Estimation Analyses for Cracks in Girth Welds

- There were underpredictions and overpredictions of crack-opening by the LBB.ENG2, LBB.ENG3, GE/EPRI, and LBB.NRC methods for welded pipe experiments that were subjected to pure bending. The Paris/Tada method significantly underpredicted crack-opening displacement in all five experiments.

- The comparisons of the J-R curves obtained from compact tension specimens and η-factor analyses of J-R curves from stainless SAW pipe Experiments 4141-1 and 4141-5 revealed that differences in the weld thickness and procedure between the pipe and the C(T) specimens could provide widely different fracture toughness properties. (The pipe was about half the thickness of the C(T) specimens made from welded plates in this case.) Using the pipe J-R curves for these two experiments, the predicted crack-opening results by most estimation methods were in better agreement with the pipe fracture data. Among the five estimation methods, the LBB.ENG3 and LBB.NRC methods provided the best results for crack-opening and load predictions in the stainless steel cracked SAW pipe experiments.

- The analysis of a bimetallic pipe experiment showed that reasonably good predictions of crack-opening could be obtained by using the tensile properties of the A516 Grade 70 carbon steel pipe and the J-R curve of A516 Grade 70/Inconel 182 weld fusion-line. The results from the GE/EPRI and LBB.ENG2 methods were in good agreement with the test data. (Additional results on this bimetallic weld pipe test are given in NUREG/CR-6297 "Fracture Evaluations of Fusion Line Cracks in Nuclear Pipe Bimetallic Welds."

2. Statistical Evaluation of Current Predictive Models

Standard statistical analyses were performed to assess the accuracy of the predictive models in estimating the center-crack-opening displacement for pipes analyzed in this study. The statistics involved calculation of the mean and coefficient of variation (COV) of the predictive crack-opening ratio defined as the ratio between the experimental and predicted values of the center-crack-opening displacement when the applied load is 40 percent of the experimental maximum load. (Note, the fracture behavior at this load is essentially elastic.) The results showed the following:

From Analyses of Simple Through-Wall-Cracked Pipes

- When all TWC pipe experiments were considered, all of the predictive models underpredicted the mean value of the COD (i.e., mean ratio greater than 1). The GE/EPRI methods (with the original and newly developed influence functions from this work) predicted experimental COD with very good accuracy in terms of the mean value of the crack-opening ratio, but their predicted COVs were much higher. The differences between the statistics for the GE/EPRI method based on the original influence functions and those from the present study were not significant. The LBB.ENG2 and LBB.ENG3 methods slightly underpredicted the mean experimental COD with much lower COVs. The LBB.NRC method underpredicted the COD more than the LBB.ENG2 or LBB.ENG3 methods with higher values of COV. Among all methods, the Paris/Tada method underpredicted COD by the largest margin in terms of both mean and COV of the predicted crack-opening ratio.

- For pipes under pure bending loads, the LBB.ENG2 (mean ratio = 1.07) and LBB.ENG3 (mean ratio = 1.10) methods slightly underpredicted the experimental COD when the mean values were compared. The LBB.NRC (mean ratio = 1.16) and Paris/Tada method (mean ratio = 1.60) also underpredicted the COD with the Paris/Tada method underpredicting the most. It is interesting to note that the GE/EPRI methods (mean ratio = 0.84 and 0.74 for original and newly developed influence functions, respectively) overpredicted the mean COD for this loading condition.

- For a pipe under pure tension from pressure loading, similar trends were exhibited by the GE/EPRI, LBB.ENG2, and LBB.ENG3 methods. The comparisons of the COD predictions by the LBB.ENG2 and LBB.ENG3 methods with the experimental data were excellent.

- For pipes under combined bending and tension, all methods considered in this study underpredicted the experimental COD. The qualitative behavior is similar to that exhibited for the results of all pipe experiments discussed earlier. On a quantitative scale, however, the magnitudes of underprediction were much higher regardless of the methods used. Once again, the Paris/Tada method significantly underpredicted the COD.

- The mean results for pipes with short cracks indicate that the crack-opening would be underpredicted by the Paris/Tada, LBB.NRC, LBB.ENG2, and LBB.ENG3 methods and overpredicted by the GE/EPRI method. A similar trend was found for pipes under pure bending. The results for pipes with cracks in girth welds also reveal a similar qualitative behavior. For the girth weld cracks, the LBB.ENG2 and LBB.ENG3 methods predicted crack-opening displacement with reasonable accuracy with mean ratios close to one.

From Analyses of Complex-Cracked Pipes

- Complex-cracked pipe experiments, i.e., a pipe with a 360-degree circumferential surface crack and a finite length through-wall crack, were also analyzed using only the LBB.ENG2 method. Regardless of whether a constraint factor was applied to the J-R curves, the LBB.ENG2 method overpredicted (in terms of the mean value) crack-opening displacement for pipes with complex cracks. This is clearly opposite to the behavior exhibited by this method in analyzing simple through-wall-cracked pipes. Further breakdown of the statistics for shallow cracks ($d/t \leq 0.5$) and deep cracks ($d/t \geq 0.5$) reveals that this estimation method provides better predictions of the experimental COD if the depth of the 360-degree surface crack is smaller. For example, the mean values of the crack-opening ratio were 0.77 for shallow cracks and 0.33 for deep cracks. Nevertheless, the LBB.ENG2 predictions for complex-cracked pipes were much larger than the experimental COD values. This overprediction of the LBB.ENG2 method is due to the over-simplification in the estimation formulas for TWC pipes used for predicting the COD of complex-cracked pipes. Hence, further developments are necessary to improve crack-opening models for complex-cracked pipes.

- In analyzing pipes with a leaking crack that may potentially be a complex crack, it may not be always possible to estimate accurately the depth of the internal surface crack

unless detailed nondestructive examination is performed. For such a crack, if the depth of the surface crack is overestimated, the current analysis methods would overpredict crack-opening. Hence, for a given leak rate, this will cause the crack length to be underestimated resulting overprediction of the pipe's maximum load-carrying capacity. On the other hand, if the depth of the surface crack is underestimated or ignored, the predictive methods would underestimate crack-opening, and hence, also underestimate the load-carrying capacity of the pipe.

3. Sensitivity Analysis

A sensitivity study was performed to evaluate the effects of crack-face pressure, Ramberg-Osgood fit parameters, and errors in the elastic modulus on the crack-opening predictions. The results showed that:

- In general, the crack-face pressure would increase the crack-opening displacement. The magnitude of this increase depends on the crack size, pressure on the crack face, and the applied remote moment. For a linear-elastic analysis, when the crack size is small ($\theta/\pi \leq 1/16$), the crack-face pressure can be neglected. For a large crack size ($\theta/\pi \geq 1/4$), if the crack-face pressure is close to the pipe pressure and the applied remote moment is comparable to the moment due to the crack-face pressure, its effects can become important. However, since the ratio of the crack-face pressure to the pipe pressure increases with the crack-opening, the possibility of having a large crack-face pressure and small applied moment is very unlikely. Hence, the effects of crack-face pressure for large cracks would also be negligible.

- The Ramberg-Osgood fit in various strain regions of actual tensile data showed distinct variations in the parameters, α and n, particularly when the low-strain and high-strain regions were considered. The effects of these variations on the crack-opening predictions were more significant for stainless steel pipe than for carbon steel pipe. In particular, when α and n were based on fitting the stress-strain curve in the low-strain region, the predicted crack-opening displacements in the stainless steel pipe were much lower than the experimental data.

- If the crack-opening analysis is linear-elastic, an accurate estimate of the elastic modulus can become important. In one stainless pipe test (Experiment 1.1.1.26), the elastic modulus was measured to be 157.5 GPa (22.84×10^6 psi), considerably lower than handbook values which typically vary from 179.27 GPa (26×10^6 psi) to 182.7 GPa (26.5×10^6 psi) for austenitic materials. Hence, the crack-opening displacement could be underpredicted by 13.8 percent to 16.0 percent by using these two handbook values for the elastic modulus instead of the measured value, .

4. Analysis of Off-Centered Cracks

An analytical effort was undertaken to investigate the crack-opening characteristics of a pipe with an off-centered crack. Methods were developed by both finite element and estimation analyses to predict the crack-opening area for an off-centered crack. The results showed that:

- The crack-opening area for a pipe with an off-centered crack can be determined by normal analysis procedures for a centered crack by resolving the applied moment to the

effective moment at the center of the off-centered crack and assuming an elliptical profile for the crack-opening shape. This was an important finding since for leak-rate calculations, accuracy in the prediction of crack-opening area is more significant than that of the entire crack-opening shape.

- From the numerical analyses, the effects of off-centered cracks were determined considering only the crack-opening area for pipe fracture evaluations. Their effects on the load-carrying capacity and the fracture stability of a leaking crack had not been assessed. From a qualitative viewpoint, one can, however, argue that when a crack is off-centered, the crack-driving force, be it stress-intensity factor in linear-elastic fracture or J-integral in elastic-plastic fracture, will be lower than that for a centered crack. This assumes that the bending plane is the same for normal moments and seismic moments. However, it is possible that the bending planes will differ between normal operating stresses and under seismic loading. Hence, an off-centered crack, which may increase the length of the leakage flaw due to reduced crack-opening, can have positive effects on the load-carrying capacity of pipes. It would be interesting to see how they would be countered by the positive effects related to the structural integrity of the pipes.

5. Evaluation of Restraint of Pressure-Induced Bending

A numerical study was conducted to evaluate the effects of restraint of induced bending due to pressure on the crack-opening of a simple through-wall-cracked pipe on a pipe system. The results suggest that:

- The restraint of the induced bending due to an axial (pressure) tension increases the failure stresses, but can decrease the crack-opening at a given load. If the pipe system restrains the bending (i.e., from cracks being close to a nozzle or restraint from the rest of the piping system), then the actual leak rate would be less than the leak rate calculated by using analyses that assume that the pipe is free to rotate. This will cause the actual leakage crack size to be larger than calculated by the current analysis methods for the same leak rate.

- When the crack angle was small ($\theta/\pi \leq 1/8$), the restraint effects were also small and may be neglected. However, for larger crack angles ($\theta/\pi \geq 1/4$), the crack-opening displacement for the case where the induced bending is restrained could be significantly smaller than the crack-opening displacement for the unrestrained condition. Hence, the restraint effects should not be ignored in the crack-opening and leak-rate analyses, particularly for small-diameter pipes where the leaking crack size could be large for typical plant stresses and leakage detection requirements.

- From the numerical results presented in this report, the potential reduction of crack-opening area due to restraint of pressure-induced bending have been evaluated for some specific cases. On the other hand, it is also recognized that for a pipe which restrains bending from pressure loads, the load-carrying capacity of the pipe will also tend to increase. However, since the normal operating plus seismic loads have a higher percentage of bending than axial membrane loads, the beneficial effects on the fracture loads may not be as great. Nevertheless, the restraint of pressure-induced bending, which may increase the length of the leakage flaw, can have positive effects on the

maximum load-carrying capacity of pipes. It would be useful to also quantify a possible increase in the failure loads and then evaluate how it would counter the effects of crack-opening-area reduction.

From one pipe system experiment in the IPIRG-1 program, it was experimentally determined that a guillotine break did not occur until the growing through-wall crack was 95 percent around the circumference. From pressure loads alone, it was expected that a break would occur once the crack reached 65 percent of the circumference. The 95-percent crack length corresponded to the pressure-induced failure if the induced bending was restrained. (This crack was located 3.4 pipe diameters from an elbow.) This is strong evidence of the effect of pressure-induced bending restraint on increasing the load-carrying capacity in a pipe system.

6. Analysis of a Girth Weld Nozzle Crack at a Thickness Transition

A pipe containing a crack in a girth weld at a nozzle with a thickness taper on both sides was analyzed to evaluate its crack-opening characteristics. Elastic-plastic finite element analyses were performed to assess the effects of a typical thickness transition and geometric constraint associated with heavy integrally reinforced nozzles on the crack-opening displacement of a carbon steel nozzle containing a circumferential through-wall crack. In this analysis an angled safety injection nozzle on a cold-leg pipe was analyzed. The main result from this study is summarized below.

- Due to thickness gradients on both sides of the crack, the component of crack-opening displacement in the thinner side of the crack was much larger than that in the thicker side, thereby breaking the symmetry of the crack-opening shape with respect to the crack length. The differences in these components can be significant when the applied moment is large to induce plasticity.

7. Evaluation of Weld Residual Stresses

An analytical study was conducted to assess the magnitude of weld residual stresses in pipe and their effects on the crack-opening-area analysis. Standard finite element analyses were performed to determine the effects of the residual stresses. The key findings are summarized below.

- The prescribed residual stress field from ASME Section XI technical basis document IWB-3640 affected the crack-opening for the thicker-wall large-diameter pipe much less than that for the thinner-wall small-diameter pipe. For the large-diameter pipe with residual stresses and an applied moment yielding a bending stress of 0.5 times the ASME Service Level A stress limit, the center-crack-opening displacement:

  - increased by 9.46 percent at the inside surface,
  - decreased by 5.17 percent at the middle surface, and
  - increased by 7.11 percent at the outer surface of the pipe.

  For the small-diameter pipe when the residual stresses were included with an applied moment giving a bending stress of 0.5 times the ASME Service Level A limit, the center-crack-opening displacement:

- increased by 30.9 percent at the inside surface,
- decreased by 57.2 percent at the mid-thickness, and
- decreased by 21.1 percent at the outside surface.

Relative comparisons of the crack-opening results for these two pipes indicate that at any given applied bending stress, the residual stress effects are more severe for the thin-walled small-diameter pipe than for the thick-walled large-diameter pipe.

- For both thicker-wall large-diameter pipe and thinner-wall small-diameter pipe, plots of crack-opening displacement versus applied moment showed that at some value of this applied moment, the crack-opening could be zero when residual stresses were included. For the thinner-wall small-diameter pipe, the analysis predicted that due to the residual stress, the outer surface of the pipe would close (thus prevent any leakage) when the applied load was equal to 28.6 percent of the ASME Service Level A stress limit. Similar calculations could also be made for the middle surface of both pipes, but the trends in the results suggest that for closure to occur, the applied stresses would have to be very small, i.e., 2.60 and 10.5 percent of the ASME Service Level A stress limit for the thicker-wall large-diameter and thinner-wall small-diameter pipes, respectively.

- The finite element modeling in the residual stress analyses conducted in this work probably overpredicts their significance on the crack-opening because of the modelling technique used. This analysis applied the residual stress field as a load-controlled crack face pressure, whereas the residual stresses are strain induced over the weld region. A more sophisticated finite element analysis (e.g., a thermo-plastic analysis) is needed to account for these effects.

8. Improved Model of Crack Morphology

An improved crack-morphology model was developed to conduct thermal-hydraulic analysis for leak-rate predictions. The model involved improved definitions of surface roughness, number of turns, and path deviation factors as a function of center-crack-opening displacement which are key input parameters for calculating the leak rate in a cracked pipe. Simple linear interpolator models were developed based on local and global definitions of crack-morphology variables such as roughness, number of turns, and the deviation of straightness. These crack morphology variables were measured from current service data. Standard statistical analyses of these data were conducted to determine the mean and standard deviation of the crack-morphology parameters for several types of cracking mechanisms and pipe materials. Using these statistics, one can evaluate the effects of crack-morphology variability on the leak rate or leakage size flaw.

9. Modifications of the SQUIRT Code

Two modified versions of the SQUIRT code, which was originally developed in the International Piping Integrity Research Group Program, were created to conduct improved leak-rate and crack-opening-area analyses. These modifications reflect recent changes in the fracture-mechanics modules including adding new GE/EPRI influence functions developed at Battelle. A separate estimation scheme, known as the LBB.ENG2 method, was also added to the already existing GE/EPRI method for elastic-plastic fracture-mechanics analyses. In addition, the modified versions of SQUIRT include corrections of minor bugs and errors that were identified during the course of the Short Cracks in Piping and Piping Welds Program.

ACKNOWLEDGMENTS

This work is supported by the U.S. Nuclear Regulatory Commission (NRC) through the Electrical, Materials and Mechanical Engineering Branch of the Office of Nuclear Regulatory Research under Contract No. NRC-04-90-069. Mr. A. Hiser was the NRC program manager during most of this work and Mr. M. Mayfield was the program manager at the end of the program.

Dr. Young Hwan Choi of Korea Institute of Nuclear Safety (KINS) performed sensitivity calculations for Ramberg-Osgood parameters, obtained measurements of nozzle geometry, and conducted a few analyses while he was a visiting scientist at Battelle during this program. We thank him for his diligent efforts.

We would like to thank the following persons who provided technical information of value: Dr. N. Miura of Central Research Institute of Electric Power Industry, who analyzed some of the pipe fracture experiments; Dr. R. Mohan of Battelle, who conducted some of the finite element analyses for crack-opening profile; Dr. N. Bonora of University of Rome, who helped in the calculations for analysis of off-center cracks; Dr. S. Doctor of Battelle Pacific Northwest Laboratory, who provided information to assess crack morphology parameters for thermal fatigue cracks in cast stainless steel; and Dr. D. Paul, who provided general comments on thermal-hydraulic analysis and the SQUIRT code.

We would also like to thank others at Battelle who have helped in these efforts. Mr. T. Kilinski and Mr. D. Rudland developed several plots for this report. We thank Mrs. B. Blanton, Mrs. Verna Kreachbaum, and Ms. Adele Armitage for typing this report; Dr. A. Hopper, Dr. D. Snediker, and Mr. P. Scott for editorial comments; and Mr. D. Hayes and Ms. J. Ward for drafting assistance.

NOMENCLATURE

1. Symbols

A_c	Area of crack-opening
A_{ce}	Elastic area of crack-opening
a	Half of crack length at mean pipe diameter
a_e	Half of effective crack length at mean pipe diameter
â	Length of pipe with reduced thickness in the LBB.ENG2 and LBB.ENG3 methods
b	Half of pipe circumference at mean pipe diameter
C	Power-law coefficient for modeling J-resistance curve
C_D	Coefficient of discharge
C_F	Constraint factor for a complex-cracked pipe
c	Half of uncracked ligament of the pipe at mean pipe diameter
D_i	Inside diameter of pipe
D_m	Mean diameter of pipe
D_o	Outside diameter of pipe
d	Depth of surface crack in complex-cracked pipe
E	Modulus of elasticity
E_i	Modulus of elasticity for material i (i = 1 or 2)
$F(a/b,R_m/t)$	Elastic function related to stress intensity factor
$F_B(\theta)$	Elastic geometry function for bending
F_{CP}	Resultant force due to crack-face pressure
F_V	Total concentrated load in four-point bending
$H_B(n,\theta)$	Function defined by the LBB.ENG2 method for bending
$H_B(n_1,n_2,\theta)$	Function defined by the LBB.ENG3 method for bending
h_1,h_2,h_3,h_4	Fully plastic influence functions for the GE/EPRI method
h_1^B	Fully plastic influence function for J-integral under pure bending
h_2^B	Fully plastic influence function for COD under pure bending
h_2^{B+T}	Fully plastic influence function for COD under combined bending and tension
h_2^T	Fully plastic influence function for COD under pure tension
I	Moment of inertia of uncracked pipe cross-section
$I_B(\theta)$	Nondimensional LEFM function for a pipe in bending

$I_T(\theta)$	Nondimensional LEFM function for a pipe in tension
J	J-integral (energy release rate)
J_e	Elastic component of J
J_D	Deformation J
J_D-R	Deformation J-R curve
J_{Ic}	Plane strain Mode-I J at crack initiation by ASTM E813
J_M	Modified J
J_M-R	Modified J-R curve
J_M^{CC}	Modified J-resistance of complex-cracked pipe
J_M^{TWC}	Modified J-resistance of through-wall-cracked pipe
J_p	Plastic component of J
J_R, J-R	J-integral resistance (curve)
K_G	Correction factor for global path deviation
K_{G+L}	Correction factor for global plus local path deviation
K_I	Stress intensity factor
K_i	Function defined by the LBB.ENG3 method for material i (i = 1 or 2)
$\hat{K}$	Function defined by the LBB.ENG2 method
$\hat{K}_i$	Function defined by the LBB.ENG3 method for material i (i = 1 or 2)
L	Half of total pipe length
L_a	Flow-path length
$L_B(n,\theta)$	Function defined by the LBB.ENG2 method for bending
$L_B(n_1,n_2,\theta)$	Function defined by the LBB.ENG3 method for bending
L_F	Distance between the fixed plane and the nozzle section with largest wall thickness
L_R	Restraint length
L_w	Width of weld in a pipe
M	Bending moment
M_{CP}	Additional bending moment due to crack-face pressure
M_i^*	Elastic bending moment corresponding to reference stress, σ_{0i}, for material i (i = 1 or 2)
M_{nsc}	Net-section-collapse moment
M_{RP}	Rigid-plastic moment for a pipe
M_0	Limit moment of a pipe at reference stress, σ_0

M_{0i}	Moment defined by the LBB.ENG3 method for material i (i = 1 or 2)
m	Power-law exponent for modeling J-resistance curve
n	Strain-hardening exponent in Ramberg-Osgood model
n_i	Strain-hardening exponent in Ramberg-Osgood model for material i (i = 1 or 2)
n_t	Total number of turns in the flow path
n_{tL}	Total local number of turns in the flow path
P	Axial Load on a pipe
P_0	Axial limit load at reference stress under pure tension
P_0'	Axial limit load at reference stress under combined bending and tension
p	Internal pressure in the pipe
p_c	Crack-face pressure
R_i	Inside radius of the pipe
R_m	Mean radius of the pipe
R_m^*	Adjusted mean radius of the complex-cracked pipe
r	A dummy parameter with a value of unity
r_t	Distance between centroid of the cracked area and centroidal axis of the uncracked pipe
r_b	Distance between centroidal axis of uncracked pipe and neutral axis of the cracked pipe
r_y	Plastic-zone radius
S	Residual stress
S_m	Code-specified nominal design stress
t	Pipe wall thickness
t_e	Equivalent thickness of uncracked pipe in the LBB.ENG2 and LBB.ENG3 methods
t^*	Adjusted wall thickness of the complex-cracked pipe
u	Co-ordinate distance (radial) from the inner surface of the pipe
V_1, V_2, V_3	Elastic influence functions for the GE/EPRI method
V_1^B	Elastic influence function for crack-opening displacement under pure bending
V_1^T	Elastic influence function for crack-opening displacement under pure tension
v_p^c	Plastic component of load-point displacement due to presence of a crack
α	Coefficient of Ramberg-Osgood model
α_i	Coefficient of Ramberg-Osgood model for material i (i = 1 or 2)
β_1	2 for plane stress; 6 for plane strain

$\Gamma(u)$	Gamma function
γ	Plasticity correction factor
Δ	Total axial stretch in a pipe under tension
Δa	Crack length extension at a crack tip
Δ^c	Axial stretch under tension due to presence of a crack
Δ_e^c	Elastic component of Δ^c
Δ_p^c	Plastic component of Δ^c
δ	Center-crack-opening displacement
$\delta(\psi)$	Center-crack-opening displacement for a crack off-centered by an angle, ψ
δ_e	Elastic component of δ
δ_M	Center-crack-opening displacement under remote moment without residual stress
δ_{M+RS}	Center-crack-opening displacement under remote moment with residual stress
δ_{NOR}	Normalized center-crack-opening displacement
δ_p	Plastic component of δ
δ_s	Scaled center-crack-opening displacement
δ_{uns}	Unscaled center-crack-opening displacement
δ_1	Center-crack-opening displacement without crack-face pressure
δ_2	Center-crack-opening displacement with crack-face pressure
δ_∞	Center-crack-opening displacement when restraint length is infinity
ϵ	Total Strain
ϵ_0	Reference strain in Ramberg-Osgood model
ϵ_{0i}	Reference strain in Ramberg-Osgood model for material i (i = 1 or 2)
ζ	A dummy variable
η	Geometric factor used in J-integral analysis
θ	Half of total crack angle
θ_e	Half of total effective crack angle
κ	Load function for plastic-zone size correction in the GE/EPRI method
λ	Load factor for pipes under combined bending and tension
μ	Surface roughness
μ_G	Global surface roughness
μ_L	Local surface roughness
ν	Poisson's ratio
ξ	An angle from the crack tip

σ	Stress
σ_B	Nominal bending stress
σ_T	Nominal tensile stress
σ_f	Flow stress
σ_{ref}	Axial reference stress
σ_{ten}	Axial tension stress
σ_y	Yield strength
σ_u	Ultimate strength
σ_0	Reference stress in Ramberg-Osgood model
σ_{0i}	Reference stress in Ramberg-Osgood model for material i (i = 1 or 2)
ϕ^c	Load-point rotation due to presence of a crack
ϕ_e^c	Elastic component of ϕ^c
ϕ_p^c	Plastic component of ϕ^c
ψ	Off-center angle from pipe bending plane for a through-wall-cracked pipe

2. Acronyms and Initialisms

ASME	American Society of Mechanical Engineers
ASTM	American Society for Testing Materials
BWR	Boiling water reactor
CC	Complex crack
COA	Crack-opening area
COD	Crack-opening displacement
C(T)	Compact (tension) specimen
DTNSRDC	David Taylor Naval Ship R&D Center (currently called Naval Surface Warfare Center)
EDF	Electricité de France
EPFM	Elastic-plastic fracture mechanics
EPRI	Electric Power Research Institute
FEA	Finite element analysis
FEM	Finite element method
GE	General Electric
HRR	Hutchinson-Rice-Rosengren

ID	Inside diameter
IGSCC	Intergranular stress corrosion cracking
IPIRG	International Piping Integrity Research Group
J-R	J-resistance
LBB	Leak-before-break
LEFM	Linear-elastic fracture mechanics
NED	Nuclear Engineering and Design
NRC	Nuclear Regulatory Commission
NUREG/CR	Nuclear Regulatory Commission contractor report
OD	Outside diameter
PICEP	Pipe Crack Evaluation Program
PNL	Battelle Pacific Northwest Laboratory
PWR	Pressurized water reactor
SAW	Submerged-arc weld
SA-SAW	Solution-annealed submerged-arc weld
SIF	Stress-intensity factor
SMAW	Shielded-metal arc weld
SQUIRT	Seepage Quantification of Upsets in Reactor Tubes
TWC	Through-wall-cracked
TIG	Tungsten inert-gas (weld)
3D	Three-dimensional

PREVIOUS REPORTS IN SERIES

Previous Reports from this Program

"Short Cracks in Piping and Piping Welds," First Semiannual Report, NUREG/CR-4599, Vol. 1, No. 1, March 1991.

"Short Cracks in Piping and Piping Welds," Second Semiannual Report, NUREG/CR-4599, Vol. 1, No. 2, April 1992.

"Short Cracks in Piping and Piping Welds," Third Semiannual Report, NUREG/CR-4599, Vol. 2, No. 1, September 1992.

"Short Cracks in Piping and Piping Welds," Fourth Semiannual Report, NUREG/CR-4599, Vol. 2, No. 2, May 1993.

"Short Cracks in Piping and Piping Welds," Fifth Semiannual Report, NUREG/CR-4599, Vol. 3, No. 1, October 1993.

"Short Cracks in Piping and Piping Welds," Sixth Semiannual Report, NUREG/CR-4599, Vol. 3, No. 2, March 1994.

"Short Cracks in Piping and Piping Welds," Final Program Report, NUREG/CR-4599, BMI-2173, Vol. 4, No. 1, April 1995.

"Assessment of Short Through-Wall Circumferential Cracks in Pipes - Experiments and Analyses," NUREG/CR-6235, April 1995.

"Fracture Evaluations of Fusion-Line Cracks in Nuclear Pipe Bimetallic Welds," NUREG/CR-6297, April 1995.

"Effects of Toughness Anisotropy and Combined Loading on Fracture Behavior of Ferritic Nuclear Pipe," NUREG/CR-6299, April 1995.

"Effect of Dynamic Strain Aging on the Strength and Toughness of Nuclear Ferritic Piping at LWR Temperatures," NUREG/CR-6226, October 1994.

"Probabilistic Pipe Fracture Evaluations for Leak-Rate-Detection Applications," NUREG/CR-6004, April 1995.

"Validity Limits in J-Resistance Curve Determination -- Volume 1: An Assessment of the J_M Parameter," NUREG/CR-6264 Volume 1, February 1995.

"Validity Limits in J-Resistance Curve Determination -- Volume 2: A Computational Approach to Ductile Crack Growth Under Large-Scale Yielding Conditions," NUREG/CR-6264 Volume 2, February 1995.

"Stainless Steel Submerged Arc Weld Fusion Line Toughness," NUREG/CR-6251, April 1995.

Previous Related Documents from NRC's Degraded Piping Program

"Degraded Piping Program - Phase II," Semiannual Report, NUREG/CR-4082, Vol. 1, Oct. 1984.

"Degraded Piping Program - Phase II," Semiannual Report, NUREG/CR-4082, Vol. 2, June 1985.

"Degraded Piping Program - Phase II," Semiannual Report, NUREG/CR-4082, Vol. 3, March 1986.

"Degraded Piping Program - Phase II," Semiannual Report, NUREG/CR-4082, Vol. 4, July 1986.

"Degraded Piping Program - Phase II," Semiannual Report, NUREG/CR-4082, Vol. 5, Dec. 1986.

"Degraded Piping Program - Phase II," Semiannual Report, NUREG/CR-4082, Vol. 6, April 1988.

"Degraded Piping Program - Phase II," Semiannual Report, NUREG/CR-4082, Vol. 7, March 1989.

"Degraded Piping Program - Phase II," Semiannual Report, NUREG/CR-4082, Vol. 8, March 1989.

"NRC Leak-Before-Break (LBB.NRC) Analysis Method for Circumferentially Through-Wall Cracked Pipes Under Axial Plus Bending Loads," Topical Report, NUREG/CR-4572, March 1986.

"Elastic-Plastic Finite Element Analysis of Crack Growth in Large Compact Tension and Circumferentially Through-Wall-Cracked Pipe Specimen--Results of the First Battelle/NRC Analysis Round Robin," Topical Report, NUREG/CR-4573 September 1986.

"An Experimental and Analytical Assessment of Circumferential Through-Wall Cracked Pipes Under Pure Bending," Topical Report, NUREG/CR-4574, June 1986.

"Predictions of J-R Curves With Large Crack Growth From Small Specimen Data," Topical Report, NUREG/CR-4575, August 1986.

"An Assessment of Circumferentially Complex-Cracked Pipe Subjected to Bending," Topical Report, NUREG/CR-4687, September 1986.

"Analysis of Cracks in Stainless Steel TIG Welds," Topical Report, NUREG/CR4806, November 1986.

"Approximate Methods for Fracture Analyses of Through-Wall Cracked Pipes," Topical Report, NUREG/CR-4853, January 1987.

"Assessment of Design Basis for Load-Carrying Capacity of Weld-Overlay Repair," Topical Report," NUREG/CR-4877, February 1987.

"Analysis of Experiments on Stainless Steel Flux Welds," Topical Report, NUREG/CR-4878, February 1987.

"Experimental and Analytical Assessment of Circumferentially Surface-Cracked Pipes Under Bending," Topical Report, NUREG/CR-4872, April 1987.

Previous Related Documents from NRC's International Piping Integrity Research Group (IPIRG) Program

"Evaluation and Refinement of Leak-Rate Estimation Models," Topical Report, NUREG/CR-5128, Revision 1, June 1994.

"Loading Rate Effects on Strength and Fracture Toughness of Pipe Steels Used in Task 1 of the IPIRG Program," Topical Report, NUREG/CR-6098, October 1993.

"Stability of Cracked Pipe Under Inertial Stresses--Subtask 1.1 Final Report," NUREG/CR-6233, Vol. 1, August 1994.

1.0 INTRODUCTION

1.1 Overview

Leak-before-break (LBB) analyses for circumferentially cracked pipes are currently being conducted in the nuclear industry to justify elimination of design requirements to account for dynamic effects during pipe rupture. This allows elimination of hardware, such as pipe whip restraints and jet impingement shields, which can impede accessibility to pipes and increase radiation exposure during maintenance operation and in-service inspection. In an LBB analysis for nuclear piping systems, the following approach is employed. First, it is necessary to show that the pipe system is not susceptible to fatigue, stress-corrosion cracking, creep, or waterhammer. Second, as a worst-case assumption, it is assumed that a through-wall crack exists with a maximum credible flaw size, which can be detected under normal operating loads. It is then desired that this through-wall crack will remain stable at normal operating plus safe shutdown earthquake loads. Further details of LBB methods are described in NUREG/CR-1061 Volume 3 (Ref. 1.1), and the Draft Standard Review Plan, Section 3.6.3 (Ref. 1.2) of the U.S. Nuclear Regulatory Commission (NRC).

The application of the LBB methodology frequently requires determination of leak rates. In addition to LBB analyses which assume a hypothetical flaw size, there is also interest in the integrity of actual leaking cracks corresponding to current leakage detection requirements in NRC Regulatory Guide 1.45, or for assessing temporary repair of Class 2 and 3 pipes that have leaks as are being evaluated in ASME Section XI. Generally, the leak-rate calculations are performed for one of the following two purposes:

(1) Given a flaw size, pipe dimensions, material stress-strain properties, and loading, the fluid leak rate through the crack needs to be determined. The aim is to estimate whether the given flaw size would result in a reliably detectable leak rate. Therefore, the aim is to underestimate rather than overestimate the crack-opening area (COA).

(2) Given a leak rate, the COA needs to be determined. Then, knowing the COA, pipe dimensions, material properties, and loading, the aim is to estimate the flaw size, which could subsequently be used to determine the pipe's load-carrying capacity. For this purpose, it is more desirable to overestimate than underestimate the COA.

For either of the two purposes, accurate models are needed to predict COA for subsequent leak-rate evaluations. Besides the finite element method, there are a number of engineering (or estimation) methods which are available in the current literature to determine the crack-opening characteristics of a pipe with a circumferential crack. However, due to the lack of systematic studies involving combined experimental and analytical efforts, the accuracy of these methods for different pipe materials, crack geometries, and loading conditions have yet to be evaluated.

Traditionally, the developments of the COA models have been focussed on idealized conditions for analyzing cracked pipes. For example, it is generally assumed that a simple circumferential through-wall crack exists in the base metal or the weld metal of the pipe with the crack located in the center of the bending plane. The crack-opening area is calculated when this pipe is subjected to remote loads that may include pure bending or pure tension (generally pressure induced) or combined

bending and tension. In reality, the loading conditions, the pipe and crack geometries, and the boundary conditions can be more complicated. For example, the crack in a pipe may become off-centered due to random imperfections around the pipe circumference, or pressure-induced bending may be restrained if the crack is close to a nozzle, or the crack may be located at the thickness transition (e.g., girth-weld crack in a nozzle), or the pipe may have significant weld residual stresses in addition to remote bending loads, etc. Currently, there are no engineering methods or guidelines available to analyze pipes under these conditions. While some of these aspects are applicable to LBB analyses, other aspects are more applicable to evaluating flaw stability for a real rather than a hypothetical flaw.

1.2 Objectives of the Study

The objectives of this study are to review, evaluate, and refine current analytical models for conducting crack-opening-area analyses of pipes with circumferential cracks. These were accomplished here in the following eight distinct stages:

(1) Review and Evaluation of Current Predictive Models. An in-depth review was conducted to evaluate the adequacy of current predictive models for performing crack-opening-area analyses of circumferentially cracked pipes. The results from twenty-five full-scale pipe fracture experiments, conducted in the past Degraded Piping Program (Ref. 1.3), the International Piping Integrity Research Group Program [IPIRG] (Ref. 1.4), and the Short Cracks in Piping and Piping Welds Program (Ref. 1.5), were used to verify the analytical models.

(2) Sensitivity Analysis. A sensitivity study was performed to evaluate the effects of crack-face pressure, Ramberg-Osgood fit parameters, and errors in elastic modulus on crack-opening-area analysis.

(3) Analysis of Off-Centered Cracks. An analytical effort was undertaken to investigate the crack-opening characteristics of a pipe with an off-centered crack. From the results of these analyses, recommendations were made on how an off-centered crack under elastic loads could be analyzed based on the fracture-mechanics equations for a centered crack.

(4) Evaluation of Restraint of Pressure-Induced Bending. A numerical study was conducted to evaluate the effects of restraint of induced bending due to pressure on the crack-opening of a pipe with simple through-wall cracks. From the results of analyses, it was found when the restraint of bending effects become important and how they should be taken into account.

(5) Analysis of a Girth Weld Nozzle Crack at a Thickness Transition. A pipe containing a crack in a girth weld at a nozzle with a thickness taper on both sides was analyzed to evaluate its crack-opening characteristics. Elastic-plastic finite element analyses were performed to assess the effects of a typical thickness transition and geometric constraint associated with heavy, integrally reinforced nozzles on the crack-opening displacement of a carbon steel nozzle containing a circumferential through-wall crack.

(6) Evaluation of Weld Residual Stresses. A simplified numerical study was conducted to assess the magnitude of weld residual stresses in a pipe and their effects on the crack-opening-area analysis. Standard finite element analyses were performed to determine if the residual stresses should be considered and when they could become important for crack-opening evaluations.

(7) Improved Model of Crack Morphology. An improved crack morphology model was developed for performing thermal-hydraulic analysis in LBB applications. The model involved local and global definitions of surface roughness, number of turns, and path deviation factors which are key input parameters for determining the leak rate in a cracked pipe. Following review of service cracks in actual plant piping, the statistical properties of these crack-morphology parameters were estimated for several types of cracking mechanism and pipe materials.

(8) Modifications of the SQUIRT Code. Two modified versions of the SQUIRT code, originally developed in the past IPIRG Program (Ref. 1.4), were created to conduct improved leak-rate and crack-opening-area analyses. These modifications reflect recent changes in the fracture-mechanics modules including new GE/EPRI influence functions developed at Battelle (Ref. 1.6). A separate estimation scheme, known as the LBB.ENG2 method, was also added to the already existing GE/EPRI method for elastic-plastic fracture-mechanics analyses. In addition, the modified versions of SQUIRT include corrections of minor bugs and errors that were identified during the course of the Short Cracks in Piping and Piping Welds Program (Ref. 1.5).

1.3 Outline of the Report

Section 2 provides a state-of-the-art review of the current deterministic models for crack-opening-area analysis of circumferentially cracked pipes.

Section 3 discusses the results for evaluating the analytical models by comparing crack-opening predictions with the corresponding pipe fracture data.

Section 4 presents the results of sensitivity studies involving crack-face pressure, Ramberg-Osgood material constants, and errors in elastic modulus values.

Section 5 discusses the analytical efforts to predict the crack-opening characteristics of a pipe with an off-centered crack.

Section 6 describes the numerical analyses to evaluate the effects of restraint of induced bending due to pipe pressure on the crack-opening.

Section 7 contains the results of a computational study to assess the crack-opening characteristics of a pipe with a crack in a thickness taper that can occur when a crack develops in a girth weld of a nozzle.

Section 8 discusses typical residual stresses in a pipe weld and presents analytical results related to the effects of residual stresses on the crack-opening displacements of thick-walled large-diameter and thin-walled small-diameter pipes.

Section 9 describes the improved models of crack-morphology parameters and their statistical characterization for conducting leak-rate computations in a pipe for LBB applications.

Section 10 reports the developments of two modified versions of the SQUIRT code for leak-rate calculations.

Finally, Section 11 summarizes the principal contributions made from this study and draws conclusions regarding crack-opening-area analyses in pipes with circumferential cracks.

1.4 References

1.1 "Report to the U.S. Nuclear Regulatory Commission Piping Review Committee," Prepared by the Pipe Break Task Group, NUREG/CR-1061, Vol. 3, U.S. Nuclear Regulatory Commission, Washington, D.C., November 1984.

1.2 Published for public comment on "Standard Review Plan, Section 3.6.3 Leak-Before-Break Evaluation Procedures," *Federal Register*, Vol. 52, No. 167, Notices, pp. 32626 to 32633, Friday, August 28, 1987.

1.3 Wilkowski, G. M., Ahmad, J., Barnes, C. R., Brust, F., Ghadiali, N., Guerrieri, D., Jones, D., Kramer, G., Landow, M., Marschall, C. W., Olson, R., Papaspyropoulos, V., Pasupathi, V., Rosenfeld, M., Scott. P., and Vieth, P., "Degraded Piping Program - Phase II: Summary of Technical Results and Their Significance to Leak-Before-Break and In-Service Flaw Acceptance Criteria, March 1984 - January 1989," NUREG/CR-4082, Vol. 8, U.S. Nuclear Regulatory Commission, Washington, D.C., March 1989.

1.4 Schmidt, R. A., Wilkowski, G. M., and Mayfield, M. E., "The International Piping Integrity Research Group (IPIRG) Program: An Overview," *Transactions of the 11th International Conference on Structural Mechanics in Reactor Technology, Vol. G2: Fracture Mechanics and Non-Destructive Evaluation - 2*, Edited by H. Shibata, Tokyo, Japan, Paper No. G23/1, pp. 177-188, August 1991.

1.5 Wilkowski, G. M., and others, "Short Cracks in Piping and Piping Program," Semiannual reports by Battelle, NUREG/CR-4599, Vols. 1 to 3, Nos. 1 and 2, U.S. Nuclear Regulatory Commission, Washington, D.C., 1991-1994.

1.6 Brust, F., Rahman, S., and Ghadiali, N, "Elastic-Plastic Analysis of Small Cracks in Tubes," *Proceedings of the 11th Conference on Offshore Mechanics and Arctic Engineering*, Calgary, Canada, June 1992.

2.0 ANALYTICAL MODELS

2.1 Introduction

For the prediction of crack-opening in a through-wall-cracked (TWC) pipe, it is desirable to have a mathematical model which is sufficiently accurate, relatively simple, and inexpensive to use. For example, a detailed finite element analysis, while generally accurate, would have very limited use because it would be expensive and time-consuming to be used routinely. What is needed is a relatively simple equation, or a set of equations, to estimate the crack-opening area (COA).

Simple mathematical models, often referred to as estimation models, are almost invariably based on assumptions necessary to minimize the need for elaborate numerical analyses. Typically, such assumptions lead to simpler representations of the material's stress-strain behavior, flaw shape and orientation, loading, and the boundary conditions (Ref. 2.1). Nevertheless, fracture mechanics models are required to evaluate the fracture response and crack-opening of a through-wall-cracked pipe. The available models can be broadly classified as:

(1) the linear-elastic fracture mechanics (LEFM) models, and

(2) the elastic-plastic fracture mechanics (EPFM) models.

This section provides a short summary of these models to predict the crack-opening displacement (COD) in a through-wall-cracked pipe with particular emphasis on the EPFM models. Improvements and refinement of some of the models made in this study are also discussed. Section 3 will show how well these models perform by making direct comparisons with the experimental pipe fracture data.

2.2 Linear-Elastic Fracture Mechanics Models

The linear-elastic fracture mechanics models are based on the assumption that even at the maximum applied loads of interest, the material behavior everywhere in a pipe containing a through-wall crack remains linear-elastic. A number of linear-elastic solutions for through-wall cracks in pipes are available in the current literature. For examples, see the work done by Erdogan (Ref. 2.2), Erdogan and Delale (Ref. 2.3), Sanders (Refs. 2.4 and 2.5), and Yoo and Pan (Ref. 2.6). Many of these elastic solutions in the literature appear in terms of the stress intensity factor (SIF) rather than the COD or COA. However, the available SIF solutions can be utilized to determine COD and COA using Castigliano's theorem, as described in Reference 2.7 or, alternatively, in the work of Wuthrich (Ref. 2.8).

The well-known GE/EPRI method (Refs. 2.9 to 2.11) also permits the elastic calculation of COD for a through-wall-cracked pipe under various loading conditions. However, the main purpose of this method is for use as an elastic-plastic fracture-mechanics method. Further details of this method in the complete range between elastic and elastic-plastic conditions are described in Section 2.4.1.

Neglecting the crack-tip plasticity in LEFM models leads to underestimates of COA for a given load acting on the pipe. Alternatively, for a prescribed remote displacement or rotation, an LEFM model will tend to overestimate the COA. In many practical situations, where the flaw size is small compared with the pipe circumference and where the loads are low, the error (positive or negative) caused by neglecting crack-tip plasticity should be insignificantly small.

2.3 Elastic-Plastic Fracture Mechanics Models

There are two basic types of elastic-plastic fracture mechanics methods used for predicting COD in a circumferential TWC pipe. They are:

(1) Finite element or numerical methods, and

(2) Engineering approximation (estimation) methods

A finite element analysis can always be performed to determine the crack-opening displacements and precise crack-opening area for a given pipe geometry and material. However, for most practical applications of leak-before-break (LBB), a full finite element computation is not always needed. Also, such computations are too time-consuming and expensive to be used for routine LBB evaluations. Rather, compilations of finite element solutions for specific pipe and crack geometries and material constants, for instance from the GE/EPRI handbook, are typically used for crack-opening and fracture assessments (Refs. 2.9 to 2.11). The solutions available in the GE/EPRI handbook method (Ref. 2.9) were improved in the Short Cracks in Piping and Piping Welds Program at Battelle (Ref. 2.12).

The estimation methods for predicting the fracture response and corresponding COD for TWC pipe involve either incorporating a plastic-zone correction into an elastic solution or approximating the crack compliance reduction via a reduced section analogy. The plastic-zone correction methods are the Paris/Tada method (Ref. 2.13) and the LBB.NRC method (Ref. 2.14), which will be discussed in Sections 2.4.2 and 2.4.3, respectively. A method based on the reduced thickness analogy is called the LBB.ENG2 method (Refs. 2.15 to 2.17), and is discussed in Section 2.4.4. Finally, a modification to the LBB.ENG2 method for predicting the J-integral and COD in a welded pipe, known as the LBB.ENG3 method (Refs. 2.18 to 2.20) is discussed in Section 2.4.5.

2.3.1 Idealization of Material Properties

In general, the fracture response and COA predictions by the estimation models require an analytic description of the material properties. For example, it is generally assumed that the constitutive law characterizing the material's stress-strain response can be represented by the well-known Ramberg-Osgood model

$$\frac{\epsilon}{\epsilon_0} = \frac{\sigma}{\sigma_0} + \alpha \left[\frac{\sigma}{\sigma_0}\right]^n \quad (2\text{-}1)$$

in which σ_0 is a reference stress usually assumed to be the yield stress, $\epsilon_0 = \sigma_0/E$ is the associated reference strain, E is the modulus of elasticity, and α and n are strain-hardening parameters usually chosen from a best fit of laboratory data. This representation of the stress-strain curve is necessary, since the J-integral and COD in most estimation schemes are formulated based on a power-law idealization.

In characterizing the fracture toughness of the materials, the ASTM J-resistance curve (J-R curve) is typically used. The J-R curve, which is usually generated from small specimens cut from the pipe (e.g., the compact tension [C(T)] specimen), can be conveniently modeled by a power-law equation of the form

$$J_R(\Delta a) = J_{Ic} + C\left[\frac{\Delta a}{r}\right]^m \quad (2\text{-}2)$$

in which Δa is the crack length extension during crack growth, J_{Ic} is the fracture toughness at crack initiation, and C and m are the power-law parameters from a best fit of the experimental data. In Equation 2-2, r is a convenient normalizing parameter with a value of unity and the same units as Δa. For example, if J and Δa are expressed in kJ/m^2 and mm, the dimension of C also becomes kJ/m^2 if r = 1 mm. Because the C(T) specimens are small, large extrapolation of the data is often required in order to predict crack growth in a pipe, particularly for the large diameter pipes. Note that "Δa" here is the physical crack extension, i.e., without blunting. This is because blunting is automatically accounted for in the finite element method as well as in the pipe estimation schemes.

2.3.2 Crack-Opening-Area Analysis for J-controlled Crack Growth

In order to evaluate crack-opening displacements for a growing crack, the criteria for crack growth must be specified. Recent analytical, experimental, and computational studies on this subject indicate that the energy release rate, also known as the J-integral (Refs. 2.21 and 2.22), is the most viable fracture parameter for characterizing crack initiation, stable crack growth, and subsequent instability in ductile materials. This suggests that J can be conveniently used to assess structural integrity for both leak-before-break and in-service flaw acceptance criteria in the degraded piping systems. It is, however, noted that the parameter J still possesses some theoretical limitations. For example, the Hutchinson-Rice-Rosengren (HRR) singular field (Refs. 2.21 to 2.23) may not be valid in the case of certain amounts of crack extension where J ceases to act as an amplifier for this singular field. Nevertheless, the possible error is considered tolerable if the relative amount of crack extension stays within a certain limit, and if elastic unloading and nonproportional plastic loading zones around a crack tip are surrounded by a much larger zone of nearly proportional loading controlled by the HRR field (Ref. 2.24). Under this condition of J-dominance, both the onset and limited amount of crack growth can be correlated to the critical values of J and J-resistance curve, respectively (Ref. 2.25).

The applications of the J-integral in describing crack driving force, crack growth, and subsequent crack-opening in a pipe are well-established for pure bending or pure tension loads (Refs. 2.9 to 2.20). Discussions of the conditions for achieving J-dominance and the suitability of J as a fracture parameter for combined bending and tensile loadings have been presented by Shih (Ref. 2.26) and Shih and Hutchinson (Ref. 2.27) by studying the single-edge notch specimen. Additional studies based on finite element analysis of the single-edge notch specimen subjected to combined tension and bending have recently appeared (Refs. 2.28 and 2.29). An important result obtained by Sonnerlind and Kaiser (Ref. 2.29) indicates that the value of J is essentially independent of whether tension is applied followed by bending; bending then tension; or both tension and bending are applied proportionally. This is not intuitively obvious since such loading clearly violates the hypothesis (necessary for the valid J-tearing theory) of proportional loading. Further discussions on the validity of J for combined bending and tension are available in Reference 2.30. Details of finite element analyses for combined loads and the results produced by the incremental and deformation plasticity theories are given in a separate topical report (NUREG/CR-6235).

2.4 Review of Estimation Models for EPFM Analysis

Consider a simple through-wall-cracked pipe with mean radius, R_m, wall thickness, t, and a crack angle, 2θ, located in the center of the bending plane. Several loading conditions can be considered. For example, the pipe may be under a pure bending moment, M; or pure tension (axial), P, due to internal pipe pressure, p; or combined bending (M) and tension (P). Figure 2.1 shows a schematic representation of a through-wall-cracked pipe subjected to combined bending and tension. In a typical estimation scheme, it is generally assumed that the load-point rotation and axial displacement (or stretch) due to the presence of a crack, ϕ^c and Δ^c, the relevant crack-driving force, J, and center-crack-opening displacement, δ, allow additive decomposition into elastic and plastic components given by

$$\phi^c = \phi_e^c + \phi_p^c \tag{2-3}$$

$$\Delta^c = \Delta_e^c + \Delta_p^c \tag{2-4}$$

$$J = J_e + J_p \tag{2-5}$$

$$\delta = \delta_e + \delta_p \tag{2-6}$$

where the subscripts "e" and "p" refer to the elastic and plastic contributions, respectively. In the elastic range, ϕ_e^c and M, and Δ_e^c and P are uniquely related. In addition, if the deformation theory of

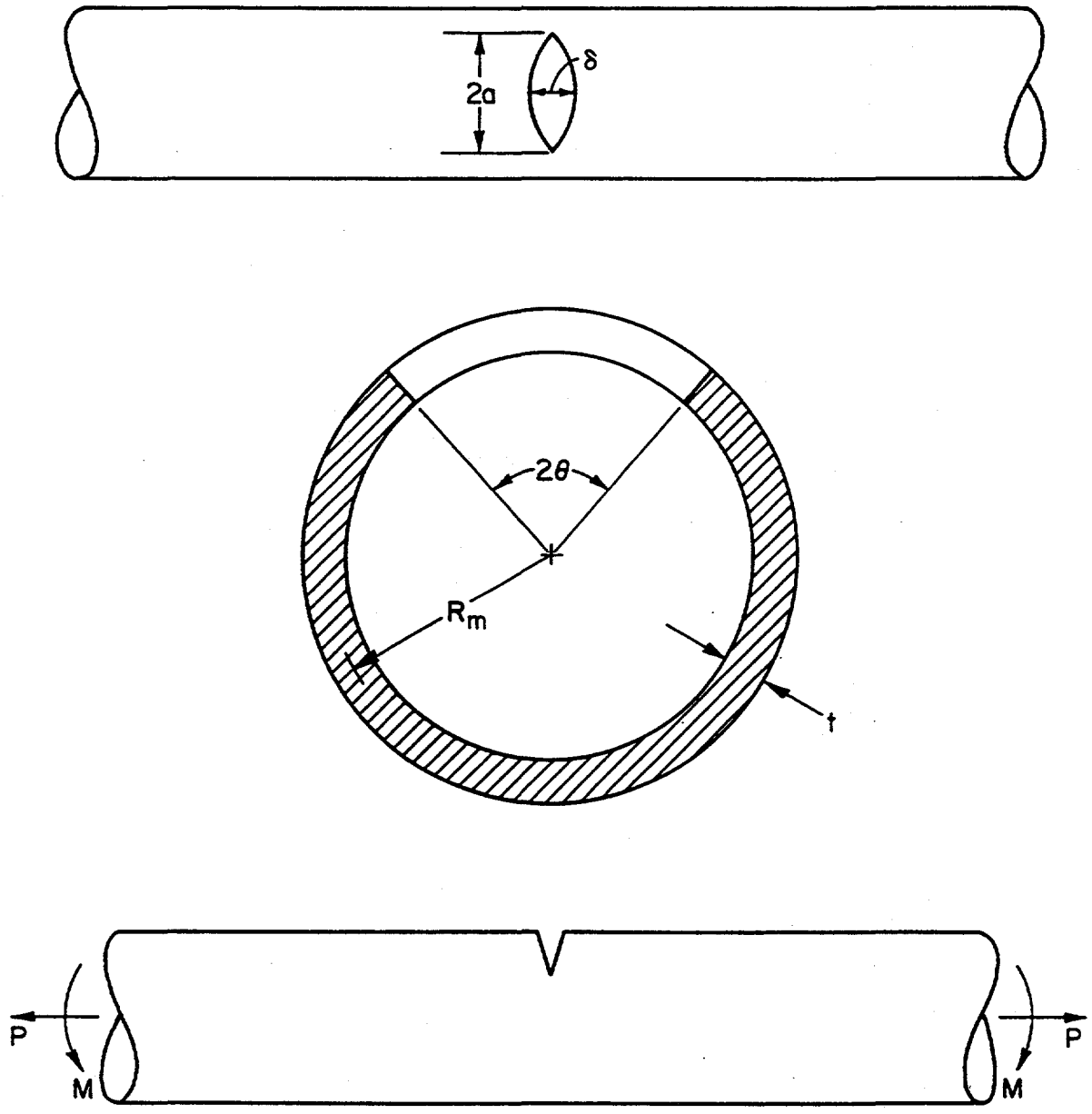

Figure 2.1 Schematic representation of pipe with a circumferential through-wall crack subjected to bending and tension

T-6300-F3.1

plasticity holds, a unique relationship also exists between ϕ_p^c and M and Δ_p^c and P. These relationships provide important information in determining J or COD in a pipe (Refs. 2.9 to 2.20).

In the rest of this section, several estimation methods currently available in the literature are reviewed for predicting fracture response and crack-opening displacements of a circumferential TWC pipe under various loads. Five different estimation methods are considered:

(1) The GE/EPRI method (Refs. 2.9 to 2.11),

(2) the Paris/Tada method (Ref. 2.13),

(3) the LBB.NRC method (Ref. 2.14),

(4) the LBB.ENG2 method (Refs. 2.15 to 2.17), and

(5) the LBB.ENG3 method (Refs. 2.18 to 2.20).

In the following paragraphs, a short summary for each of these estimation schemes is provided with the estimation formulas for both J-integral and COD. The evaluations of COD are discussed for various loading conditions, e.g., pure bending, pure tension, and combined bending and tension. For brevity, the J-integral evaluations are discussed only for pure bending.

2.4.1 The GE/EPRI Method

2.4.1.1 J-integral

The GE/EPRI method is based on a compilation of finite element solutions for TWC pipes using the deformation theory of plasticity. These solutions are catalogued in References 2.9 to 2.11 for various geometric and material parameters. For pure bending in pipes containing a through-wall crack, the J-integral is calculated by Equation 2-5 in which the elastic component J_e, and the plastic component J_p, are given by (Refs. 2.9 and 2.10)

$$J_e = \pi a \left[\frac{R_m}{I}\right]^2 F^2(a/b, R_m/t)\frac{M^2}{E} \tag{2-7}$$

$$J_p = \alpha \sigma_0 \epsilon_0 c \frac{a}{b} h_1^B(a/b, n, R_m/t) \left[\frac{M}{M_0}\right]^{n+1} \tag{2-8}$$

where $a = R_m\theta$ is half of the crack length at the mean diameter, $b = \pi R_m$ is half of the mean pipe circumference, $c = R_m(\pi-\theta)$ is half of the uncracked ligament of the pipe, $I \simeq \pi R_m^3 t$ is the moment of inertia of an uncracked pipe cross-section about its centroidal axis, $F(\theta/\pi, R_m/t)$ and

h_1^B (a/b,n,R_m/t) are the elastic and plastic influence functions, respectively, for the J-integral under pure bending that are tabulated in Reference 2.10, and

$$M_0 = 4\sigma_0 R_m^2 t \left[\cos\frac{\theta}{2} - \frac{1}{2}\sin\theta\right] \tag{2-9}$$

is a reference moment representing the limit moment for a TWC pipe also under pure bending if σ_0 is the collapse stress. Similar functional forms can be written for the tension case and the combined bending and tension case with the corresponding influence functions compiled in the pertinent references.

2.4.1.2 Center-Crack-Opening Displacement

The following are the elastic and plastic solutions for the center-crack-opening displacement of a pipe under various loading conditions:

Bending. The elastic and plastic parts of the center-crack-opening displacement for the case of pure bending, as defined by the GE/EPRI method, are (Refs. 2.9 to 2.11)

$$\delta_e = 4a\frac{R_m}{I}V_1^B(a/b, R_m/t)\frac{M}{E} \tag{2-10}$$

$$\delta_p = \alpha\epsilon_0 a h_2^B(a/b, n, R_m/t)\left[\frac{M}{M_0}\right]^n \tag{2-11}$$

where V_1^B(a/b,R_m/t) and h_2^B(a/b,n,R_m/t) are the elastic and plastic influence functions, respectively, for COD under pure bending.

Tension. The GE/EPRI influence functions for the case of a pure tension load, P, were compiled using a tensile load caused by the end-capped pipe with internal pressure, p, applied at the ends of the pipe. The corresponding equations for the elastic and plastic CODs are (Refs. 2.9 to 2.11)

$$\delta_e = \frac{2a}{\pi R_m t}V_1^T(a/b, R_m/t)\frac{P}{E} \tag{2-12}$$

$$\delta_p = \alpha \epsilon_0 a h_2^T (a/b, n, R_m/t) \left[\frac{P}{P_0} \right]^n \tag{2-13}$$

where $V_1^T(a/b,R_m/t)$ and $h_2^T(a/b,n,R_m/t)$ are the elastic and plastic influence functions, respectively, for crack-opening displacement under pure tension, P is the axial tensile force due to an internal pipe pressure, and

$$P_0 = 2\sigma_0 R_m t \left[\pi - \theta - 2\sin^{-1} \left(\frac{1}{2} \sin\theta \right) \right] \tag{2-14}$$

is a reference load representing the limit load of a TWC pipe under pure tension if σ_0 is the collapse stress.

Combined Bending and Tension. For a pipe subjected to a combined bending and tension loading, the elastic and plastic CODs are (Refs. 2.9 to 2.11)

$$\delta_e = 4a \frac{R_m}{I} V_1^B (a/b, R_m/t) \frac{M}{E} + \frac{2a}{\pi R_m t} V_1^T (a/b, R_m/t) \frac{P}{E} \tag{2-15}$$

$$\delta_p = \alpha \epsilon_0 a h_2^{B+T} (a/b, n, R_m/t, \lambda) \left[\frac{P}{P_0'} \right]^n \tag{2-16}$$

where $h_2^{B+T}(a/b,n,R_m/t,\lambda)$ is the plastic influence function for crack-opening displacement under combined bending and tension,

$$P_0' = \frac{1}{2} \left[-\frac{\lambda P_0^2 R_m}{M_0} + \sqrt{\left[\frac{\lambda P_0^2 R_m}{M_0} \right]^2 + 4P_0^2} \right] \tag{2-17}$$

is another reference load representing the limit load of a TWC pipe under combined bending and tension if σ_0 is the collapse stress, and $\lambda = M/PR_m$ is the load factor.

The values of the above influence functions for TWC pipes under pure bending, pure tension, and combined bending and tension were compiled by Kumar et al. (Refs. 2.9 and 2.10) and Kishida and Zahoor (Ref. 2.11) for specific pipe geometries (e.g., R_m/t = 5, 10, and 20), crack sizes (a/b = 1/16, 1/8, 1/4, and 1/2), and material constants (n = 1, 2, 3, 5, 7). For a pipe with an arbitrary geometry and material properties, the corresponding influence functions can be evaluated from multiple interpolation of these functions at the pre-determined values of R_m/t, a/b (i.e., θ/π), n, and λ. See References 2.9 to 2.11 for further details on these functions.

2.4.1.3 Plastic-Zone Size Correction in the GE/EPRI Method

In Reference 2.31, it has been claimed that the linear-elastic solutions of J, COD, and other fracture parameters of interest underestimate the actual values when M/M_0 exceeds 0.5 and the plastic components of the above parameters are too small, e.g., for large n values. This is the apparent reason why Kumar et al. (Ref. 2.10) extended the plastic-zone size formula established by Rice (Ref. 2.21) for the antiplane shear problem. According to Reference 2.10, the effective crack length (half), a_e, is given by

$$a_e = a + \kappa r_y \tag{2-18}$$

where

$$r_y = \frac{1}{\beta_1 \pi} \frac{n-1}{n+1} \left[\frac{K_I}{\sigma_0} \right]^2 \tag{2-19}$$

K_I is the mode-I stress intensity factor, and

$$\kappa = \begin{cases} \dfrac{1}{1 + (M/M_0)^2} & \text{(pure bending)} \\ \dfrac{1}{1 + (P/P_0)^2} & \text{(pure tension)} \end{cases} \tag{2-20}$$

The value of β_1 in Equation 2-19 depends on the state of stress, e.g., $\beta_1 = 2$ for plane stress and $\beta_1 = 6$ for plane strain. For a through-wall-cracked pipe under pure bending or tension, the stress state is dominated by the plane stress condition (i.e., $\beta_1 = 2$).

Equation 2-18 was developed in order to increase the value of elastic J or COD when the applied load becomes closer to the reference load, e.g., when M becomes closer to M_0. There is no sound technical justification for the choice of the $1/[1 + (M/M_0)^2]$ or $1/[1 + (P/P_0)^2]$ function in Equation 2-20 except ensuring the continuity of the partial derivatives of J with respect to applied load at $M = M_0$ or $P = P_0$. Past experience at Battelle suggests that when using the GE/EPRI method for TWC pipes, the plastic-zone correction in the elastic solution may be a contributor to the overprediction of applied crack-driving force. Nevertheless, it has been suggested in References 2.9 to 2.11 to use the plastic-zone correction in the elastic solution, i.e.,

$$J_e(a,M) = J_e(a_e,M) \tag{2-21}$$

$$\delta_e(a,M) = \delta_e(a_e,M) \tag{2-22}$$

for a pipe under pure bending. Similar plastic-zone corrections can also be used for a pipe subjected to pure tension or combined bending and tension.

2.4.2 The Paris/Tada Method

2.4.2.1 J-integral

In the Paris/Tada method (Ref. 2.13), J is obtained using an interpolation between the linear-elastic and fully-plastic limit-load solutions. In effect, the procedure uses the techniques developed in References 2.32 and 2.33 for a planar fracture specimen appropriately adapted for a through-wall-cracked pipe. Thus, J calculated by this method depends only on the cracked-pipe geometry and flow stress, and does not explicitly account for hardening behavior of the material.

For linear-elastic and rigid-plastic conditions in through-wall-cracked pipes, the moment-rotation and J-rotation relations are well-established (Ref. 2.13). The Paris/Tada method interpolates between these two solutions by artificially increasing the crack size using a plastic-zone size correction and substituting this artificially increased crack size into the elastic solution to obtain the moment-rotation relation in the elastic-plastic regime. This procedure is based on the Irwin estimate (Ref. 2.34) of the size of the plastic zone that is given by

$$\theta_e = \theta + \frac{1}{\beta_1 \pi R_m}\left(\frac{K_I}{\sigma_y}\right)^2 \tag{2-23}$$

where θ_e is the effective crack angle (half), σ_y is the yield strength of the material, and $\beta_1 = 2$ or 6 depending on whether plane stress or plane strain conditions apply, respectively. The estimate of the plastic-zone size in Equation 2-23 is only accurate for small plastic zones. Because Paris/Tada attempts to estimate J throughout the entire range between elastic and rigid plastic response, a method was developed to interpolate between elastic and fully plastic conditions. This interpolation method amounts to modifying β_1 in Equation 2-23. Then, β_1 is not 2 or 6, but rather is determined in a somewhat complicated fashion which depends on the current load, as detailed in Reference 2.13.

From linear-elastic fracture mechanics, it can be shown that the moment and the elastic rotation are related via (Refs. 2.13 to 2.15 and 2.18 to 2.20)

$$M = \frac{E\pi R_m^2 t}{I_B(\theta)}\phi_e^c \tag{2-24}$$

where $I_B(\theta)$ is a bending compliance function defined in Reference 2.13. Using the effective crack size, θ_e (i.e., applying a plastic-zone correction) and total rotation, ϕ^c in place of θ and ϕ_e^c in Equation 2-24 and the expression for a rigid-plastic moment, the final equations for J_e and J_p by the Paris/Tada method for the case of pure bending are (Ref. 2.13)

$$J_e = \frac{K_I^2}{E} \tag{2-25}$$

$$J_p = \frac{\sigma_y R_m [\sin(\theta/2) + \cos\theta]}{M_{RP}(\theta)} \int_0^{\phi_p^c} M(\theta)\, d\phi_p^c \tag{2-26}$$

where

$$K_I = \frac{M}{\pi R_m^2 t} F_B(\theta) \sqrt{\pi R_m \theta} \tag{2-27}$$

is the stress intensity factor for a TWC pipe under pure bending with $F_B(\theta)$ representing the appropriate geometry function and M_{RP} is the rigid-plastic moment from limit-load analysis given by

$$M_{RP} = 4\sigma_f R_m^2 t \left[\cos\frac{\theta}{2} - \frac{1}{2}\sin\theta\right] \tag{2-28}$$

where σ_f is the flow stress of the material. Explicit functional forms of $F_B(\theta)$ and $I_B(\theta)$ are given in References 2.13.

2.4.2.2 Center-Crack-Opening Displacement

According to Reference 2.13, the elastic crack-opening area, A_{ce}, for a TWC pipe under combined bending and tension can be derived from the energy method (Castigliano's theorem) which gives

$$A_{ce} = \frac{\pi R_m^2}{E} [\sigma_B I_B(\theta) + \sigma_T I_T(\theta)] \tag{2-29}$$

where $I_T(\theta)$ is the tensile compliance function defined in Reference 2.13, $\sigma_B = M/(\pi R_m^2 t)$ is the nominal bending stress at the mean pipe diameter, and $\sigma_T = P/2\pi R_m t$ is the nominal tensile (axial) stress for an uncracked pipe section. Further simplification of Equation 2-29, details of which are given in Reference 2.13, yields

$$A_{ce} \simeq \frac{\pi R_m^2}{E} I_T(\theta) \left[\sigma_B \frac{3+\cos\theta}{4} + \sigma_T \right] \tag{2-30}$$

Equations 2-29 and 2-30 are valid only for the linear-elastic condition. However, for the elastic-plastic condition, Paris and Tada extended these equations by incorporating plastic-zone corrections discussed previously. Accordingly, for an EPFM analysis, the crack-opening area is given by

$$A_c \simeq \frac{\pi R_m^2}{E} I_T(\theta_e) \left[\sigma_B \frac{3+\cos\theta_e}{4} + \sigma_T \right] \tag{2-31}$$

where θ_e is half of the effective crack angle already defined in Equation 2-23. Assuming an elliptical crack-opening shape, the total center-crack-opening displacement is

$$\delta \simeq \frac{2R_m^2}{aE} I_T(\theta_e) \left[\sigma_B \frac{3+\cos\theta_e}{4} + \sigma_T \right] \tag{2-32}$$

Setting $\sigma_T = 0$ or $\sigma_B = 0$ in Equation 2-32, one can compute the COD under pure bending or pure tension, respectively.

2.4.3 The LBB.NRC Method

2.4.3.1 J-integral

The LBB.NRC method (Ref. 2.14) for TWC pipes subjected to bending is similar to the Paris/Tada method described earlier. However, the elastic geometry function, $F_B(\theta)$, was derived independently based on Sanders' elastic solutions (Refs. 2.4 and 2.5). The plastic component of rotation due to a crack is written as

$$\phi_p^c = \alpha \left[\frac{\sigma}{\sigma_f} \right]^{n-1} \phi_e^c \tag{2-33}$$

with $\phi_e^c = \phi_e^c(\theta_e)$ from the Paris/Tada solution. Hence, the elastic component of rotation is increased by an interpolation type of Irwin plastic-zone correction and the plastic component of rotation is increased or decreased depending on the current applied stress level. In the LBB.NRC method, the effects of strain-hardening are incorporated in the evaluation of the J-integral.

2.4.3.2 Center-Crack-Opening Displacement

The crack-opening area calculations by the LBB.NRC method are almost identical to those by the Paris/Tada method discussed earlier. According to Reference 2.14, Equations 2-31 and 2-32 are also used to compute COA and COD, respectively. However, in these equations, the effective crack angle, θ_e is not the same as in the Paris/Tada method. The β_1 term in the equation for plastic-zone correction (see Equation 2-23) in the Paris/Tada and the LBB.NRC method is calculated by forcing the solution to reach the limit load of a cracked pipe for large values of the stress intensity factor. Further details on the derivation of β_1 are available in References 2.13 and 2.14.

2.4.4 The LBB.ENG2 Method

2.4.4.1 J-integral

The LBB.ENG2 method was originally developed by Brust (Ref. 2.15) to compute the energy release rate and crack-opening for through-wall-cracked pipes. It involves an equivalence criterion incorporating a reduced thickness analogy for simulating system compliance due to the presence of a crack in a pipe. Detailed derivations of both elastic and plastic components of the J-integral in this method are available in References 2.15 to 2.17. Only the final expressions are presented here.

For a pipe under pure bending, the elastic component of J, J_e, by the LBB.ENG2 method is identical to that by the Paris/Tada method and hence, is given by Equation 2-25. However, the equation for the geometry function, $F_B(\theta)$, was obtained from the LBB.NRC method. The plastic component of J, J_p, was calculated by invoking the energy interpretation of J and hence, by integrating the moment-rotation ($M\text{-}\phi_p^c$) curve. The $M\text{-}\phi_p^c$ relation was derived from the solution of the ordinary differential equations for a beam representing an uncracked pipe with a reduced thickness (stiffness) and power-law constitutive properties. The reduced (equivalent) thickness was approximated by forcing the limit moment of this uncracked pipe to be equal to that of the actual cracked pipe. Finally, the plastic component of J, J_p, is given by (Refs. 2.15 to 2.17)

$$J_p = \frac{\alpha}{E\sigma_0^{n-1}} \frac{\pi R_m}{2(n+1)} H_B(n,\theta) L_B(n,\theta) I_B(\theta) \left[\frac{M}{\pi R_m^2 t}\right]^{n+1} \qquad (2\text{-}34)$$

where

$$H_B(n,\theta) = \frac{4\theta F_B(\theta)^2}{I_B(\theta)} + \frac{1}{L_B(n,\theta)} \frac{\partial L_B(n,\theta)}{\partial \theta} \tag{2-35}$$

$$L_B(n,\theta) = \left[\frac{\pi}{4\left\{ \cos\left[\frac{\theta}{2}\right] - \frac{1}{2}\sin\theta \right\}} \right]^{n-1} \left[\frac{\pi}{4\hat{K}} \right]^n \tag{2-36}$$

$$I_B(\theta) = 4\int_0^\theta \theta F_B(\theta)^2 \, d\theta \tag{2-37}$$

$$\hat{K} = \frac{\sqrt{\pi}}{2} \frac{\Gamma\left[1+\frac{1}{2}n\right]}{\Gamma\left[\frac{3}{2}+\frac{1}{2}n\right]} \tag{2-38}$$

with

$$\Gamma(u) = \int_0^\infty \zeta^{u-1} \exp(-\zeta) \, d\zeta \tag{2-39}$$

representing the gamma function. Further details on the simplified forms of these functions are available in References 2.15 to 2.17.

2.4.4.2 Center-Crack-Opening Displacement

Bending. For the case of a pure bending load, the elastic COD solution is the same as in the GE/EPRI method (i.e., Equation 2-10). Initially, there were attempts to use some of the closed-form solutions, for instance, as developed in References 2.6; however, these analytical solutions were smaller by a factor of three compared with the numerical solutions as well as with the experimental data. Therefore, the numerical solutions of the GE/EPRI method were selected for the elastic component of COD in this method. The plastic component of COD is obtained from

$$\delta_p = R_m \left[1 + \sin\frac{\theta}{2}\right] \phi_p^c \tag{2-40}$$

where the plastic rotation in the presence of a crack, ϕ_p^c, is given by (Refs. 2.15 to 2.17)

$$\phi_p^c = L_B(n,\theta)\frac{\alpha}{E\sigma_0^{n-1}}\frac{I_B(\theta)}{\left(\pi R_m^2 t\right)^n}M^n \qquad (2\text{-}41)$$

The term $R_m[1+\sin(\theta/2)]$ in Equation 2-40 is the distance from the rigid-plastic neutral axis to the center of the crack.

Tension. For the pure tension load case, the estimate of δ has a functional form similar to that for the bending case. The crack-opening displacement is again separated into elastic and plastic components. The elastic COD is given by the same equation of the GE/EPRI method (i.e., Equation 2-12). The plastic COD is given by

$$\delta_p = \frac{\alpha\epsilon_0\left[\frac{\sigma_T}{\sigma_0}\right]^{n-1}}{1-\frac{\theta}{\pi}-\frac{2}{\pi}\sin^{-1}\left[\frac{1}{2}\sin\theta\right]} + R_m\left[1+\sin\frac{\theta}{2}\right]\phi_p^c \qquad (2\text{-}42)$$

In Equation 2-42, the first term is due to the tension load and the second term is due to the induced bending caused by the tension load on the cracked pipe. Note that ϕ_p^c in this equation is the plastic rotation in the presence of the crack that is caused only by the pressure- or tension-induced bending. This bending moment can be inserted in Equation 2-41 to obtain ϕ_p^c.

Combined Bending and Tension. For combined bending and tension, the elastic COD is obtained by superposing the solutions for pure bending and pure tension, which are given by Equations 2-10 and 2-12, respectively. The plastic COD is given by the same form as shown by Equation 2-42, but the ϕ_p^c in that equation now includes both the applied moment and the induced bending due to tension.

2.4.5 The LBB.ENG3 Method

2.4.5.1 J-integral

The LBB.ENG3 method, developed by Rahman and Brust (Refs. 2.18 to 2.20), improves the computation of the J-integral and COD for TWCs in pipe welds by incorporating weld-metal strength properties. The method is similar to the LBB.ENG2 method and is also based on an equivalence criterion incorporating reduced thickness analogy for simulating system compliance due to the presence of a crack in the pipe. Figure 2.2 shows a schematic for the reduced section analogy by the LBB.ENG3 method for analyzing welded pipes with a through-wall crack in the center of the weld.

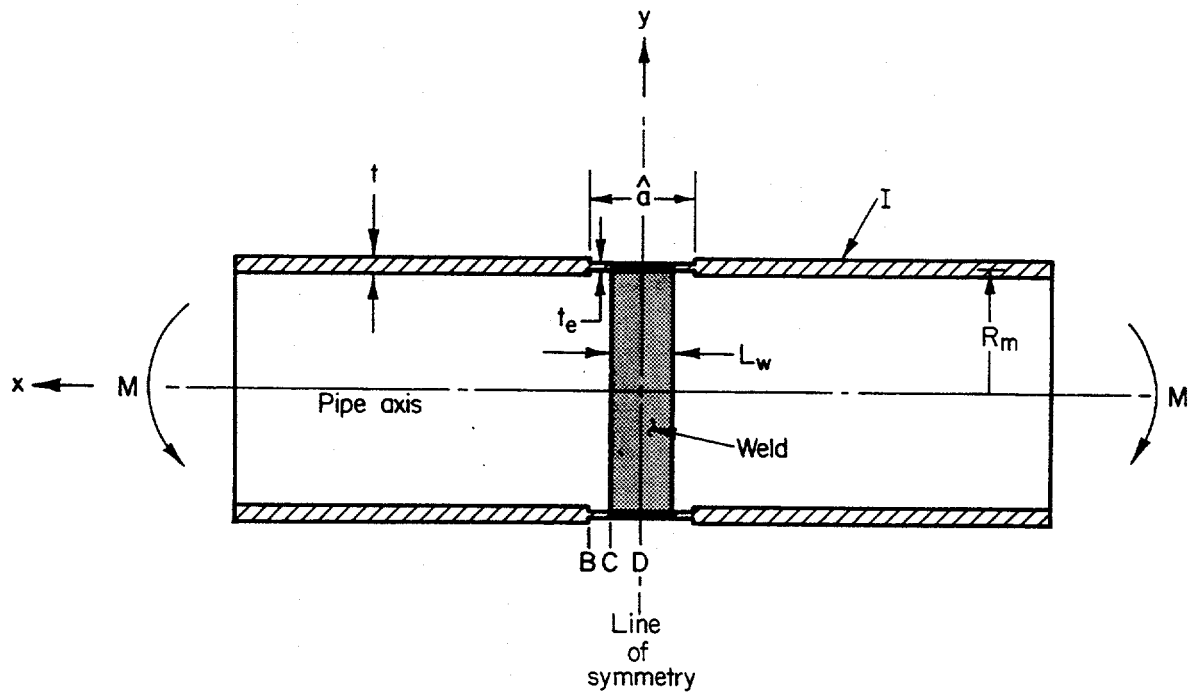

Figure 2.2 Reduced section analogy in the LBB.ENG3 method

T-6300-F2.2

The elastic solution obtained by this method is identical to that obtained by the LBB.ENG2 or the LBB.NRC method and is given by Equation 2-25 (for pure bending) presented earlier. The plastic solution for the J-integral, also under pure bending, is

$$J_p = \frac{\alpha_1}{E_1 \sigma_{01}^{\,n_1-1}} \frac{\pi R_m}{2(n_1+1)} H_B(n_1,n_2,\theta)\, L_B(n_1,n_2,\theta)\, I_B(\theta) \left[\frac{M}{\pi R_m^2 t}\right]^{n_1+1} \qquad (2\text{-}43)$$

in which the additional subscripts "1" and "2" on the variables E, σ_0, α, and n are needed to represent base and weld metal properties, respectively. In Equation 2-43, $H_B(n_1,n_2,\theta)$ and $L_B(n_1,n_2,\theta)$ are the algebraic functions defined by

$$H_B(n_1,n_2,\theta) = \frac{1}{I_B(\theta)} \frac{\partial I_B(\theta)}{\partial \theta} + \frac{1}{L_B(n_1,n_2,\theta)} \frac{\partial L_B(n_1,n_2,\theta)}{\partial \theta} \qquad (2\text{-}44)$$

and

$$L_B(n_1,n_2,\theta) = \frac{\left[\frac{M}{M_{01}}\right]^{n_1}\left[\frac{\hat{a}}{2}-\frac{L_w}{2}\right]\left[\frac{t}{t_e}\right]^{n_1}+\left[\frac{M}{M_{02}}\right]^{n_2}\frac{L_w}{2}\left[\frac{t}{t_e}\right]^{n_2}}{\left[\frac{M}{M_1^*}\right]\epsilon_{01}\left[\frac{\hat{a}}{2}-\frac{L_w}{2}\right]\frac{t}{t_e}+\left[\frac{M}{M_2^*}\right]\epsilon_{02}\frac{L_w}{2}\frac{t}{t_e}} \times \frac{1}{\alpha_1\left[\frac{M}{M_1^*}\right]^{n_1-1}} \quad (2\text{-}45)$$

respectively, where for material i (i = 1 for base metal, i = 2 for weld metal), σ_{0i} is the reference stress, α_i and n_i are the Ramberg-Osgood parameters, $\epsilon_{0i} = \sigma_{0i}/E_i$ is the associated reference strain, L_w is the width of the weld in the pipe, â is the length of reduced thickness, t_e is the equivalent thickness of the pipe, $M_i^* = \sigma_{0i}I/R_m$ is the elastic bending moment corresponding to reference stress, σ_{0i}, and

$$M_{0i} = \frac{4K_iI\hat{K}_i}{\pi R_m} \quad (2\text{-}46)$$

with $K_i = \sigma_{0i}/(\alpha_i\epsilon_{0i})^{1/n_i}$ and

$$\hat{K}_i = \frac{\sqrt{\pi}}{2}\frac{\Gamma\left[1+\frac{1}{2}n_i\right]}{\Gamma\left[\frac{3}{2}+\frac{1}{2}n_i\right]} \quad (2\text{-}47)$$

Clearly, the $H_B(n_1,n_2,\theta)$ and $L_B(n_1,n_2,\theta)$ functions in Equation 2-43 are more complex than their counterparts are in Equation 2-34 due to the inclusion of both base and weld metal properties. See References 2.18 to 2.20 for fundamental details on the development of the LBB.ENG3 method.

2.4.5.2 Center-Crack-Opening Displacement

The equations for the estimates of COD by the LBB.ENG3 method are identical to those of the LBB.ENG2 method, except the plastic rotation due to the presence of a crack is evaluated considering the tensile properties of both the base and weld metals. According to this method, ϕ_p^c can be obtained from

$$\phi_p^c = L_B(n_1,n_2,\theta)\frac{\alpha_1}{E_2\sigma_{01}^{n_1-1}}\frac{I_B(\theta)}{\left(\pi R_m^2 t\right)^{n_1}}M^{n_1} \quad (2\text{-}48)$$

Once again, further details can be found in References 2.18 to 2.20.

Note that Equations 2-43 and 2-48 have characteristics similar to those of Equations 2-34 and 2-41 required to calculate J_p and ϕ_p^c, respectively, for a base-metal crack (the LBB.ENG2 method). However, from Equations 2-43 and 2-48, it can be seen that the tensile strength properties of both base and weld metals are accounted for in calculating the J-integral and plastic rotation. Equations 2-43 and 2-48 are strongly dependent on the base metal properties, but the weld metal properties are also considered via L_B- and H_B-functions. When differences in the base metal and weld metal properties vanish, it can be shown that Equations 2-43 and 2-48 degenerate to Equations 2-34 and 2-31, respectively, as one would expect. Hence, the LBB.ENG2 method can be treated as a special case of the more general LBB.ENG3 method.

2.4.6 Other Methods

In addition to the estimation methods discussed above, there are a few other methods to estimate COA for TWC pipes. For example, Wuthrich (Ref. 2.8) has given an expression for COA for through-wall axial and circumferential cracks in pipes subjected to membrane forces. The results are presented as the product of a plasticity correction factor, γ, and the area of crack opening, A_{ce}, calculated by linear-elastic analysis, that is,

$$A_c = \gamma A_{ce} \quad (2\text{-}49)$$

Wuthrich gives γ based on both Irwin (Ref. 2.34) and Dugdale (Ref. 2.35) plastic-zone corrections for small-scale yielding. A comparison of the two approaches, made in Reference 2.1, suggests that for small values of σ/σ_y (σ is the nominal applied stress) the two approaches give approximately the same result. For larger values of σ/σ_y, the plasticity correction factors associated with the two approaches deviate from each other. But for larger σ/σ_y values the small-scale yielding condition is violated and neither approach should be expected to be accurate. Instead, it may be more appropriate to use another model based on the assumption that the uncracked ligament is fully yielded. One such model, proposed by Smith (Ref. 2.36), gives the following expression for COA for a circumferential through-wall crack in a pipe under pure bending:

$$A_c = 4R_m^2\phi_p^c\left[1-\cos\frac{\theta}{2}+\frac{1}{2}\sin\theta\right] \quad (2\text{-}50)$$

While both the linear-elastic and the small-scale yielding models are useful in specific situations, they cannot be expected to provide accurate COA estimates over the entire range of load magnitudes, flaw sizes, and material types of interest in nuclear piping systems. The main reason is that a large

number of situations are such that the crack-tip plastic deformation can be characterized by neither linear elasticity nor small-scale yielding. Rather, the analysis problem is elastic-plastic, requiring nonlinear analysis methods. Specific examples showing comparisons with pipe test data are given in Section 3 of this report.

2.5 The New NRC/Battelle Influence Functions

Earlier studies on fracture response and crack-opening in pipes were concerned for the most part with larger cracks (i.e., $\theta/\pi \geq 30$ percent) where the nominal failure stresses were below yield. The estimation methods developed to date, some of which are described here, are well-suited for analyzing pipes with large cracks. The ability of these methods to predict crack-opening for small cracks ($\theta/\pi \leq 12$ percent) has not been established even though such small cracks are often the concern in practical LBB analyses. A short crack is typical of one for LBB analyses in large diameter pipes. Indeed, the finite element solutions compiled in the GE/EPRI handbook (Ref. 2.10) appear quite inadequate for small-size cracks. This section of the report presents new results from a series of finite element analyses conducted at Battelle that are tabulated in the spirit of the GE/EPRI handbook (Ref. 2.10). The explicit details of the finite element calculations and modeling procedures are discussed in a separate topical report (NUREG/CR-6235) from the Short Cracks in Piping and Piping Welds Program (Ref. 2.12). Some of these new results have also been published in a recent technical paper by Brust, Rahman, and Ghadiali (Ref. 2.37).

Specifically, the solutions to improve the F-, V-, and h-functions were generated for Ramberg-Osgood coefficients n = 1, 2, 3, 5, 7, 10 and for several crack angles (2θ) for the following three cases:

1. Short through-wall cracks under bending (θ/π = 1/16, 1/8),
2. Long through-wall cracks under bending (θ/π = 1/4, 1/2), and
3. Short through-wall cracks under combined bending and tension (θ/π = 1/16, 1/8).

2.5.1 Short Through-Wall Cracks Under Pure Bending

2.5.1.1 Finite Element Model and Analysis Matrix

Six finite element meshes were developed, one for each case listed in Table 2.1. A typical finite element mesh and geometric definitions are illustrated in Figure 2.3. A quarter model was used by taking advantage of symmetry. Twenty-noded, isoparametric, brick elements were used with focused elements at the crack tip. Only one element through the pipe wall was used, and, as such, the tabulated results should be considered as average values through the pipe wall.

The elastic solutions were developed using the elastic properties of the pipe. A deformation theory plasticity algorithm in the ABAQUS (Ref. 2.38) finite element code was used to generate the plastic solution. Because a through-wall-cracked pipe subjected to bending is a plane stress problem, the special (hybrid) elements in the ABAQUS library which adequately handle plastic incompressibility are not necessary. A reduced (2 x 2) Gaussian quadrature integration rule was utilized.

Table 2.1 Matrix of finite element calculations for short through-wall-cracked pipes under pure bending (total of 30 analyses)

Model No.	Model Name	R_m/t	n[(a)]	θ/π	Remarks	Loading
1	CASE1A3DM	5	1,2,3,5,7,10	0.0625	5 Runs	Bending
2	CASE2A3DM	10	1,2,3,5,7,10	0.0625	5 Runs	Bending
3	CASE3A3DM	20	1,2,3,5,7,10	0.0625	5 Runs	Bending
4	CASE1B3DM	5	1,2,3,5,7,10	0.1250	5 Runs	Bending
5	CASE2B3DM	10	1,2,3,5,7,10	0.1250	5 Runs	Bending
6	CASE3B3DM	20	1,2,3,5,7,10	0.1250	5 Runs	Bending

(a) n = 1 is elastic

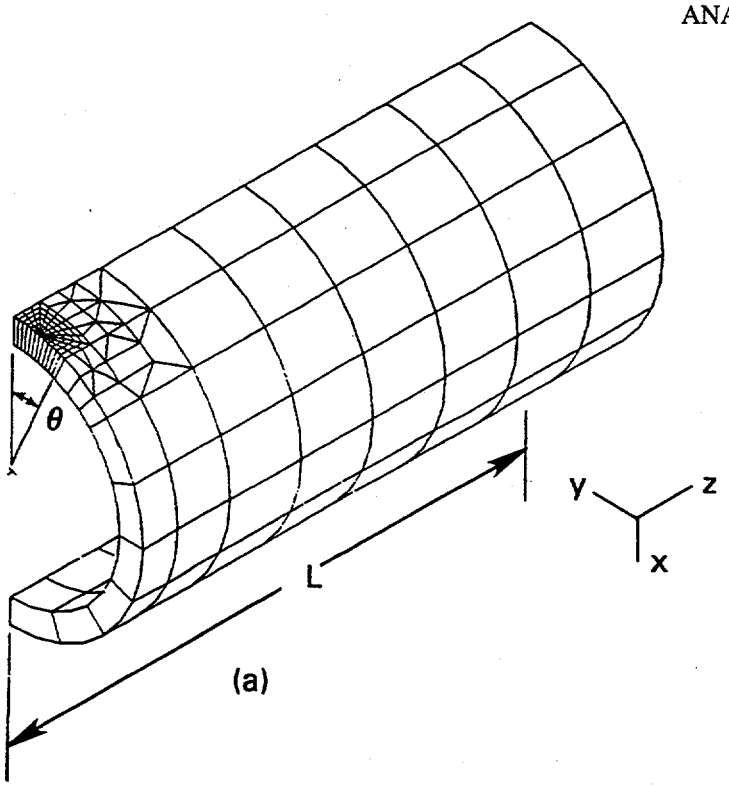

(a) Mesh for finite element analysis (1/4 model)

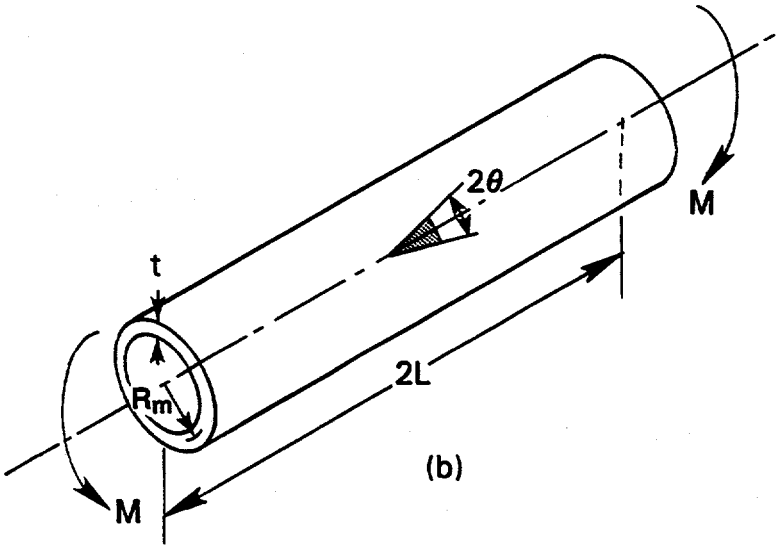

(b) Circumferentially cracked-pipe geometry

Figure 2.3 Typical finite element mesh and geometric definitions

T-6300-F2.3

2.5.1.2 Results of Analysis

Both elastic and fully plastic (deformation theory) computations were made for bending loads for each of the six cases defined in Table 2.1.

Past studies at Battelle suggest that the original GE/EPRI compilations are accurate in predicting J for large crack sizes. Hence, a comparison was made for a specific pipe case with $R_m/t=10$, $\theta/\pi = 1/2$, and $n = 3$ to verify the accuracy of the results from these new analyses. Table 2.2 lists the plastic h-functions for a pipe under pure bending obtained from Reference 2.10 and the present study. The comparisons for h_1 (J-integral) indicate little difference between the results of these two finite element solutions. However, the values of the h_2- (COD) and h_4-functions (load-point rotation) from Reference 2.10 are 10.5 and 17.3 percent higher, respectively, than those predicted by the present study.

Tables 2.3 through 2.6 provide the solutions compiled for all of the cases listed in Table 2.1. Table 2.3 provides the elastic solution, while Tables 2.4 to 2.6 provide the plastic solutions for $R_m/t = 5$, 10, and 20, respectively. Note that the GE/EPRI handbook method did not provide solutions for $n = 10$ and some of the $n = 7$ cases due to numerical difficulties.

Table 2.2 Check case $R_m/t = 10$, $\theta/\pi = 1/2$, and $n = 3$ (pure bending)

Influence Functions	GE/EPRI (Ref. 2.10)	3D-Solid ABAQUS (this report)
h_1 (J-integral)	2.105	2.008
h_2 (Crack-opening displacement)	3.331	3.015
h_4 (Load-point rotation)	3.232	2.756

2.5.2 Long Through-Wall Cracks Under Pure Bending

In order to be consistent with the functions developed for short through-wall cracks using ABAQUS 3D-solid elements, additional calculations were also performed for longer cracks. The methodology used to compute these functions is identical to that for short cracks.

2.5.2.1 Finite Element Model and Analysis Matrix

Six finite element meshes were developed, one for each case listed in Table 2.7. The details of the mesh, solution techniques, etc., were similar to those for short cracks.

Table 2.3 F-, V_1-, V_3-functions for short through-wall-cracked pipes under pure bending (ABAQUS - 3D solid element solution)[a]

Crack Size	Function	$R_m/t = 5$	$R_m/t = 10$	$R_m/t = 20$
$\theta/\pi = 1/16$	F	1.022	1.049	1.097
	V_1	1.234	1.206	1.111
	V_3	0.028	0.035	0.098
$\theta/\pi = 1/8$	F	1.103	1.208	1.418
	V_1	1.388	1.480	1.482
	V_3	0.126	0.160	0.231

(a) This represents the n = 1 case of Table 2.1

Table 2.4 Tabulation of h-functions for short through-wall-cracked pipes under pure bending for $R_m/t = 5$ (ABAQUS - 3D solid element solution)

Crack Size	Function	n = 2	n = 3	n = 5	n = 7	n = 10
$\theta/\pi = 1/16$	h_1	5.202	5.451	5.766	5.681	5.263
	h_2	6.686	6.896	7.003	6.715	6.087
	h_4	0.553	0.826	1.452	1.879	2.371
$\theta/\pi = 1/8$	h_1	4.575	4.484	3.976	3.372	2.464
	h_2	5.972	5.820	4.999	4.164	2.959
	h_4	0.958	1.194	1.454	1.461	1.291

Table 2.5 Tabulation of h-functions for short through-wall-cracked pipes under pure bending for $R_m/t = 10$ (ABAQUS - 3D solid element solution)

Crack Size	Function	n = 2	n = 3	n = 5	n = 7	n = 10
$\theta/\pi = 1/16$	h_1	5.588	6.225	6.761	6.784	6.749
	h_2	6.701	7.422	7.739	7.632	7.527
	h_4	0.745	1.156	1.802	2.220	2.826
$\theta/\pi = 1/8$	h_1	5.694	5.791	5.512	4.790	3.823
	h_2	6.619	6.654	6.319	5.329	4.221
	h_4	1.234	1.550	1.886	1.864	1.713

Table 2.6 Tabulation of h-functions for short through-wall-cracked pipes under pure bending for $R_m/t = 20$ (ABAQUS - 3D solid element solution)

Crack Size	Function	n = 2	n = 3	n = 5	n = 7	n = 10
$\theta/\pi = 1/16$	h_1	6.272	7.044	8.022	8.756	8.815
	h_2	7.155	7.073	8.050	8.787	8.812
	h_4	0.979	1.505	2.348	3.087	3.770
$\theta/\pi = 1/8$	h_1	8.019	8.448	8.281	7.748	6.524
	h_2	7.934	7.498	7.491	7.160	5.890
	h_4	1.730	2.216	2.738	2.963	2.728

Table 2.7 Matrix of finite element calculations for long through-wall-cracked pipes under pure bending (total of 30 analyses)[a]

Model No.	Model Name	R_m/t	n[a]	θ/π	Remarks	Loading
1	CASE4A3DM	5	1,2,3,5,7,10	0.5000	5 runs	Bending
2	CASE4B3DM	10	1,2,3,5,7,10	0.5000	5 runs	Bending
3	CASE4C3DM	20	1,2,3,5,7,10	0.5000	5 runs	Bending
4	CASE5A3DM	5	1,2,3,5,7,10	0.2500	5 runs	Bending
5	CASE5B3DM	10	1,2,3,5,7,10	0.2500	5 runs	Bending
6	CASE5C3DM	20	1,2,3,5,7,10	0.2500	5 runs	Bending

(a) n = 1 is the elastic case.

2.5.2.2 Results of Analyses

Tables 2.8 through 2.11 provide the solutions compiled for all the cases listed in Table 2.7. Table 2.8 provides the elastic solution, while Tables 2.9 to 2.11 provide the plastic solutions for R_m/t = 5, 10 and 20, respectively.

2.5.3 Short Through-Wall-Cracked Pipe Under Combined Bending and Tension

The GE/EPRI estimation scheme can be used to calculate fracture parameters such as J, COD, displacements, and rotations, for through-wall-cracked pipes under combined bending and tension using the following two approaches:

(1) In the first approach, a nondimensional parameter λ is used to define a proportionality relationship between pressure (or tension) and moment, M. The GE/EPRI plastic functions h_1, h_2, h_3, and h_4 are now also a function of λ. This approach, although theoretically rigorous, is not very convenient for pipes subjected to a fixed internal pressure and varying bending moment, which is the case in nuclear piping for Boiling Water Reactor (BWR) and Pressurized Water Reactor (PWR) systems. Due to the addition of one more variable (λ), the number of variables h is a function of increases from three to four. Consequently, the matrix of finite element calculations for determining these h-functions can become enormously large. Nevertheless, some limited solutions of h-functions using λ were compiled in Reference 2.11.

(2) In the second approach, it is proposed that the plastic h-functions be evaluated for a fixed internal pressure and increasing bending moment using procedures similar to those used for tension and bending alone. For example, the calculated h values can be

Table 2.8 F-, V_1-, V_3-functions for long through-wall-cracked pipes under pure bending (ABAQUS - 3D solid element solution)[a]

Crack Size	Function	$R_m/t = 5$	$R_m/t = 10$	$R_m/t = 20$
$\theta/\pi = 1/4$	F	1.434	1.697	2.120
	V_1	2.008	2.379	3.079
	V_3	0.327	0.439	0.637
$\theta/\pi = 1/2$	F	2.552	3.031	3.902
	V_1	5.331	7.165	11.585
	V_3	3.792	5.228	8.567

(a) This represents the n = 1 case of Table 2.7

Table 2.9 Tabulation of h-functions for long through-wall-cracked pipes under pure bending for $R_m/t = 5$ (ABAQUS - 3D solid element solution)

Crack Size	Function	n = 2	n = 3	n = 5	n = 7	n = 10
$\theta/\pi = 1/4$	h_1	4.109	3.720	2.671	1.821	1.019
	h_2	5.319	4.706	3.283	2.189	1.194
	h_4	1.298	1.543	1.426	1.082	0.641
$\theta/\pi = 1/2$	h_1	1.981	1.408	0.684	0.418	0.154
	h_2	3.478	2.271	1.019	0.598	0.215
	h_4	2.927	2.034	0.936	0.543	0.196

Table 2.10 Tabulation of h-functions for long through-wall-cracked pipes under pure bending for $R_m/t = 10$ (ABAQUS - 3D solid element solution)

Crack Size	Function	n = 2	n = 3	n = 5	n = 7	n = 10
$\theta/\pi = 1/4$	h_1	5.952	5.169	3.475	2.895	1.689
	h_2	6.629	5.757	3.853	3.209	1.844
	h_4	1.676	1.896	1.712	1.593	1.006
$\theta/\pi = 1/2$	h_1	2.887	2.008	1.060	0.579	0.267
	h_2	4.693	3.015	1.452	0.777	0.349
	h_4	4.038	2.756	1.364	0.592	0.116

Table 2.11 Tabulation of h-functions for long through-wall-cracked pipes under pure bending for $R_m/t = 20$ (ABAQUS - 3D solid element solution)

	Function	n = 2	n = 3	n = 5	n = 7	n = 10
$\theta/\pi = 1/4$	h_1	9.469	8.147	7.474	7.983	3.165
	h_2	8.916	7.704	5.173	2.970	1.055
	h_4	2.375	2.555	2.044	1.361	0.548
$\theta/\pi = 1/2$	h_1	5.009	3.893	2.300	2.096	1.051
	h_2	7.913	5.773	3.052	1.517	0.623
	h_4	6.611	5.023	2.727	1.379	0.572

determined for an internal pressure of 15.51 MPa (2,250 psi) and 7.24 MPa (1,050 psi) for operating conditions at PWR and BWR plants, respectively. This is the approach undertaken at Battelle to conduct new finite element calculations of the h-functions. The calculations were performed only for the PWR pressure condition i.e., for p = 15.51 MPa (2,250 psi). No similar calculations were done for the BWR pressure condition (7.24 MPa [1,050 psi]) or any other pressure. However, using the h-functions for PWR pressure should provide overpredictions of J and COD for cracked pipes at BWR pressures.

2.5.3.1 Finite Element Model and Analysis Matrix

Six finite element meshes were developed, one for each case listed in Table 2.12. A typical finite element mesh and geometric definition are illustrated in Figure 2.3. A quarter model was used to take advantage of symmetry. Twenty-noded isoparametric brick elements were used with focused elements at the crack tip. Only one element through the pipe wall was used, and, as such, the tabulated results should be considered as average values through the pipe wall.

2.5.3.2 Results of Analysis

The plastic h-functions for pipes in Table 2.12 that are subjected to combined bending and tension due to an internal pressure of 15.51 MPa (2,250 psi) are given in Tables 2.13 through 2.15 for R_m/t = 5, 10, and 20, respectively.

2.5.4 Discussions of the Results

The differences between the solutions developed previously (Refs. 2.9 to 2.11) and the present results appear to be most important for small crack sizes (e.g., when θ/π = 1/16 and 1/8). The present solutions were developed using the three-dimensional solid elements (20-noded brick elements) and the deformation theory algorithm of ABAQUS. The solutions presented here are believed to be the more accurate of the two solutions because full three-dimensional elements were used instead of relying on shell elements. The analyses presented in Reference 2.10 appeared to produce results that are too stiff, and, indeed, solutions for large n were not possible as convergence problems occurred. Using the NRC/Battelle influence function analysis, no convergence problems were experienced. The problems with the short-crack solutions of Reference 2.10 are discussed in much more detail in References 2.15 and 2.16.

The plots of the new F-function results and the corresponding GE/EPRI solutions are seen in Figure 2.4(a) as a function of R_m/t for θ/π = a/b = 1/16. The differences are about three percent. Figure 2.4(b) shows two plots of V_1 that are related to the elastic crack-opening displacement. The values of V_1 obtained from the present work and the GE/EPRI solution show different trends as a function of R_m/t. From Figure 2.4(b), the largest difference is about 20 percent for R_m/t = 5. Comparisons of h_1 (J-integral) and h_2 (crack-opening displacement) values are presented in Figures 2.5 and 2.6, respectively. The h_1 and h_2 values differ less than 25 percent between the two solutions.

No comparisons were made for the h_4 functions. The original GE/EPRI h_4 functions are negative for most small-crack cases that were developed in Reference 2.10 and were obviously in error.

Table 2.12 Matrix of finite element calculations for short through-wall-cracked pipes under combined bending and tension (total of 30 analyses)

Model No.	Model Name	R_m/t	n	θ/π	Remarks	Loading
1	CASE1A3DTM	5	2,3,5,7,10	0.0625	5 Runs	Tension & bending
2	CASE2A3DTM	10	2,3,5,7,10	0.0625	5 Runs	Tension & bending
3	CASE3ADTM	20	2,3,5,7,10	0.0625	5 Runs	Tension & bending
4	CASE1B3DTM	5	2,3,5,7,10	0.1250	5 Runs	Tension & bending
5	CASE2B3DTM	10	2,3,5,7,10	0.1250	5 Runs	Tension & bending
6	CASE3B3DTM	20	2,3,5,7,10	0.1250	5 Runs	Tension & bending

Table 2.13 Tabulation of h-functions for short through-wall-cracked pipes under combined bending and tension for $R_m/t = 5$ (p = 15.51 MPa [2,250 psi])

Crack Size	Function	n = 2	n = 3	n = 5	n = 7	n = 10
$\theta/\pi = 1/16$	h_1	5.408	5.725	6.060	5.967	5.341
	h_2	6.851	7.115	7.232	6.979	6.153
	h_3	1.245	1.299	1.772	1.868	1.446
	h_4	2.746	1.591	2.045	2.917	3.472
$\theta/\pi = 1/8$	h_1	4.837	4.682	4.338	3.996	3.064
	h_2	6.182	5.918	5.312	4.766	3.580
	h_3	2.013	1.662	1.423	1.232	0.813
	h_4	3.279	2.020	2.285	2.608	2.133

Table 2.14 Tabulation of h-functions for short through-wall-cracked pipes under combined bending and tension for $R_m/t = 10$ (p = 15.51 MPa [2,250 psi])

Crack Size	Function	n = 2	n = 3	n = 5	n = 7	n = 10
$\theta/\pi = 1/16$	h_1	5.929	6.409	7.157	8.052	8.312
	h_2	6.973	7.460	8.108	8.923	9.009
	h_3	1.524	1.643	2.264	2.647	2.702
	h_4	2.507	1.893	3.199	6.191	9.048
$\theta/\pi = 1/8$	h_1	6.051	6.066	6.206	5.618	6.294
	h_2	6.888	6.868	6.844	6.181	6.578
	h_3	1.652	1.533	1.459	1.187	1.585
	h_4	2.624	2.089	3.055	3.036	4.495

Table 2.15 Tabulation of h-functions for short through-wall-cracked pipes under combined bending and tension for $R_m/t = 20$ (p = 15.51 MPa [2,250 psi])

Crack Size	Function	n = 2	n = 3	n = 5	n = 7	n = 10
$\theta/\pi = 1/16$	h_1	6.734	7.484	10.251	13.544	15.243
	h_2	7.561	8.292	10.924	14.078	15.813
	h_3	1.210	1.369	2.479	3.696	3.870
	h_4	2.144	2.264	6.069	11.739	17.100
$\theta/\pi = 1/8$	h_1	8.621	8.917	10.846	13.282	13.836
	h_2	8.375	8.705	10.383	12.479	13.051
	h_3	1.289	1.367	1.577	2.223	2.317
	h_4	2.689	2.778	5.160	7.720	9.046

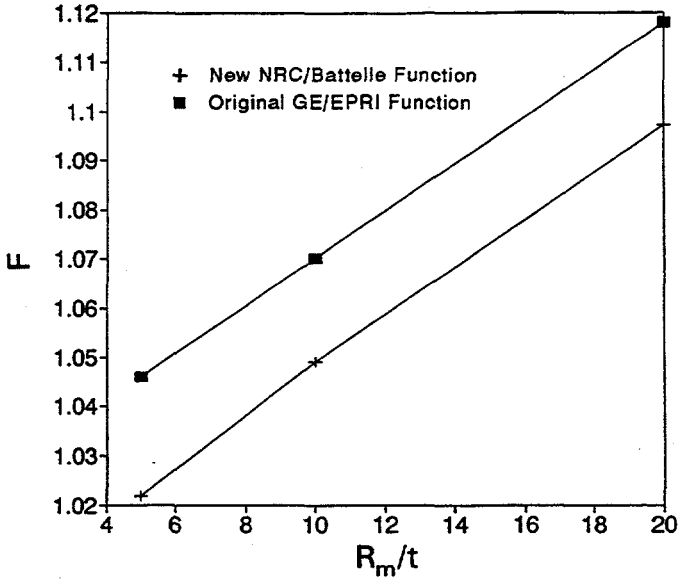

(a) F-function for θ/π = 1/16 (F relates elastic stress intensity factor to stress)

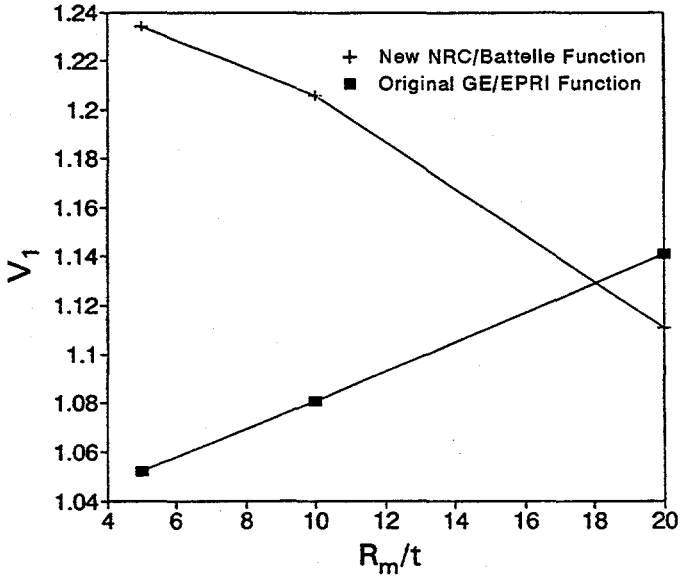

(b) V_1-function for θ/π = 1/16 (V_1 relates elastic center-crack-opening displacement to moment)

Figure 2.4 Comparison of ABAQUS FEM results to past GE/EPRI solutions for elastic functions

T-6300-F2.4

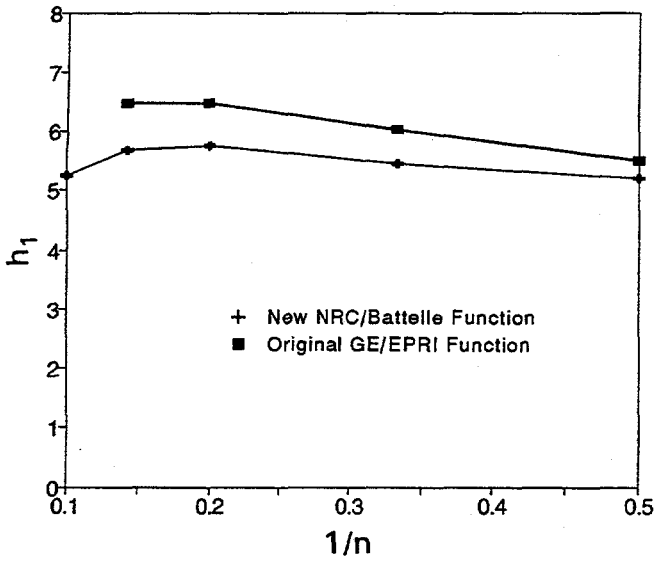

(a) $R_m/t = 5$, $\theta/\pi = 1/16$

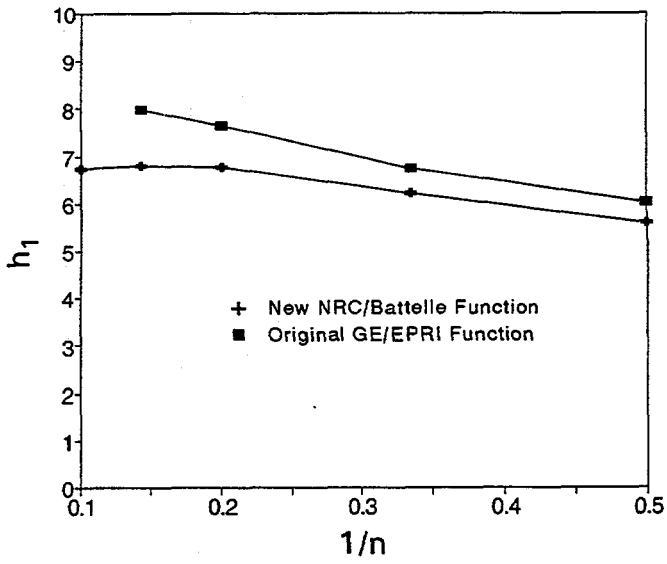

(b) $R_m/t = 10$, $\theta/\pi = 1/16$

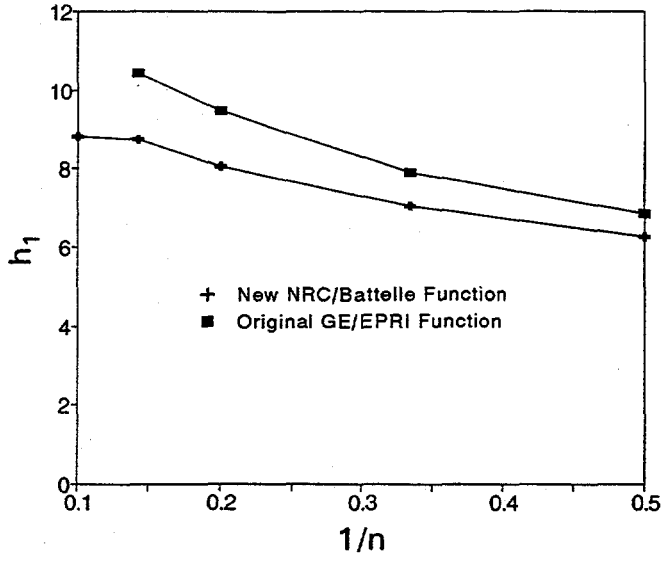

(c) $R_m/t = 20$, $\theta/\pi = 1/16$

Figure 2.5 Comparison of ABAQUS FEM results to past GE/EPRI solutions for h_1 fully plastic functions (h_1 relates fully plastic J to moment)

T-6300-F2.5

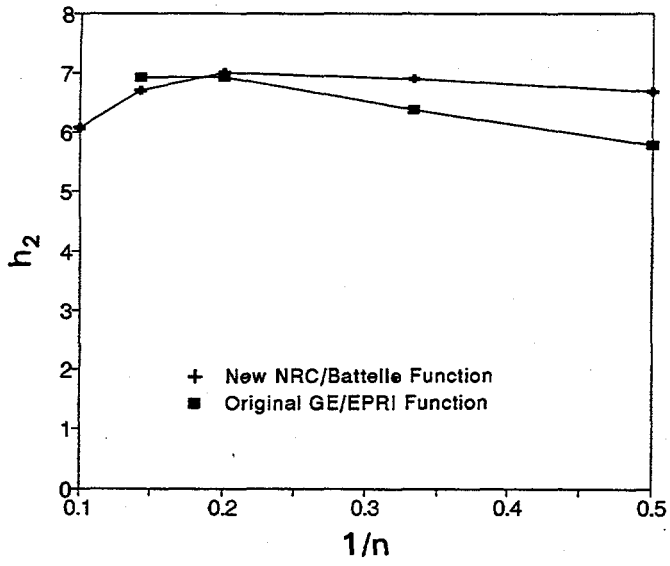

(a) $R_m/t = 5$, $\theta/\pi = 1/16$

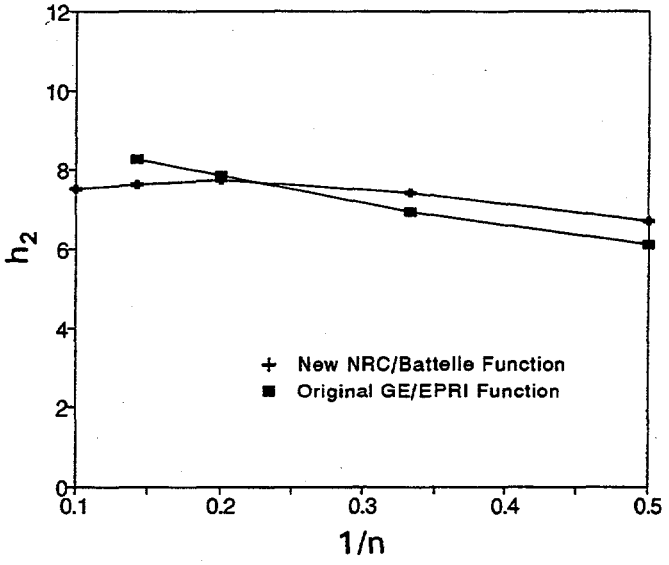

(b) $R_m/t = 10$, $\theta/\pi = 1/16$

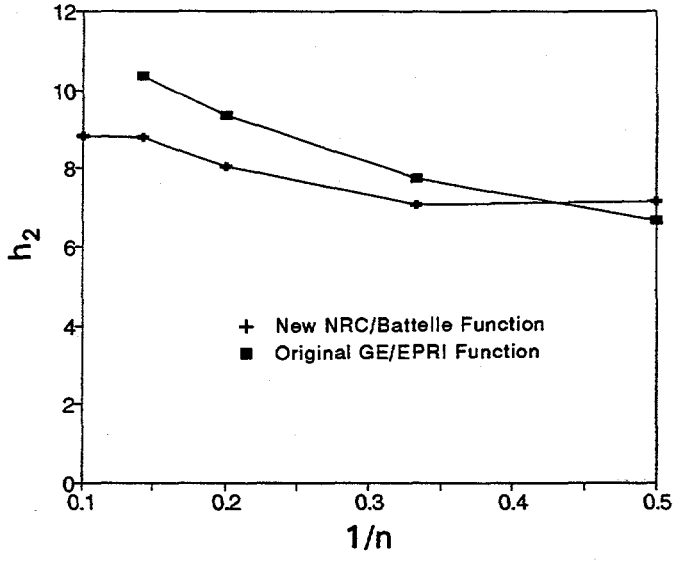

(c) $R_m/t = 20$, $\theta/\pi = 1/16$

Figure 2.6 Comparison of ABAQUS FEM results to past GE/EPRI solutions for h_2 fully plastic functions (h_2 relates fully plastic center-crack-opening displacement to moment)

T-6300-F2.6

2.5.5 Considerations of Hoop Stress in Pipes due to Pressure

The new GE/EPRI h-functions for combined bending and tension were calculated using two load steps. An axial tension (corresponding to internal pressure) was applied to the end of the pipe, and then the bending moment was increased. Hence, none of the influence functions computed in Reference 2.10 and the present study accounts for hoop (circumferential) stress in a pipe due to the internal pressure.

In order to evaluate the effects of hoop stress in a pipe, an additional analysis was performed. In this particular analysis, the load in the first step consisted of axial tension and internal pressure applied to all inside pipe elements. The second step was identical to the previous analysis, i.e., an increasing bending load was applied until fully plastic conditions were reached.

The analysis was performed for a short crack using Model 2 in Table 2.12 with $R_m/t = 10$, $\theta/\pi = 0.0625$, and $n = 5$. Table 2.16 shows the h-functions from this analysis and the corresponding results where no internal pressure was applied (i.e., only axial tension was applied). The comparisons of results suggest that the hoop stress due to pressure increases h_1, and hence, J. The mid-thickness crack-opening displacement (h_2) was also increased slightly. This may be due to local crack bulging. The load-point axial displacement (h_3) and the pipe rotation (h_4) were significantly affected due to stiffening of the pipes under additional hoop stresses.

Table 2.16 Tabulation of h-functions for through-wall-cracked pipes under combined bending and tension with and without hoop stresses due to internal pressure of 15.51 MPa (2,250 psi) [$R_m/t = 10$, $\theta/\pi = 0.0625$, and $n = 5$]

Plastic Function		Load	
		Axial Tension and Bending	Hoop Stress, Axial Tension, and Bending
h_1	(J)	7.157	7.605
h_2	(COD)	8.108	8.247
h_3	(load-point axial displacement)	2.264	0.549
h_4	(rotation)	3.199	1.952

2.6 Crack-Opening-Area Analysis of Complex-Cracked Pipes

A complex crack is a very long, internal surface crack in a pipe, which may penetrate the wall thickness, thereby creating a short through-wall crack in the same plane as the surface crack. Figures 2.7(a) and 2.7(b) show the idealized through-wall crack and internal surface crack in a pipe. When the surface crack encompasses the entire pipe circumference, under external load it may penetrate the pipe thickness, and hence may become a complex crack as exhibited in Figure 2.7(c). When subjected to further loading, the likelihood of pipe instability and/or crack arrest then requires understanding the structural behavior of complex-cracked pipe. Understanding the behavior of complex cracks, therefore, aids in performing leak-before-break analyses.

For accurately predicting the load-carrying capacity of complex-cracked pipes, an analysis based on fracture-mechanics methodologies is necessary. Since nuclear power-plant piping materials are generally tough and ductile, the fracture mechanics approach should also include elastic-plastic considerations. However, an elastic-plastic fracture mechanics analysis of a complex-cracked pipe in bending poses a formidable problem even with the three-dimensional finite element analysis. The main difficulty is in determining the crack-driving force, since attention must be given to both radial

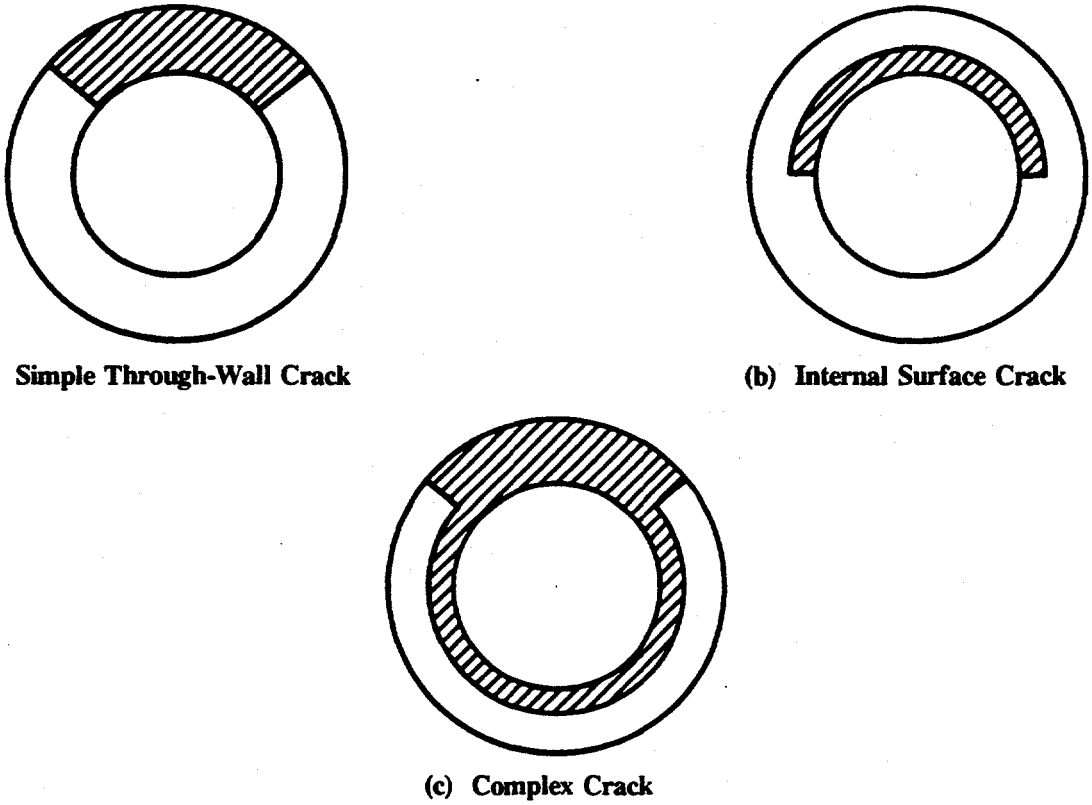

(a) Simple Through-Wall Crack

(b) Internal Surface Crack

(c) Complex Crack

Figure 2.7 Typical crack geometries in piping and piping welds

SC-SA-5/92-F7.1

and circumferential crack-growth directions. Another complicating factor is that the surface crack may close in the compressively stressed region of the pipe. This would necessitate the use of special techniques to model the resulting load transfer across the cracked surfaces.

A detailed numerical investigation of the complex-cracked pipe problem using three-dimensional finite element nonlinear analysis can be prohibitively expensive and was considered beyond the scope of the current effort. Instead, simple engineering estimation techniques, which can be predictive and generative, were considered. Predictive schemes usually require knowledge of the crack-growth resistance and plastic-flow behavior of the material. This information is used to predict the load-displacement behavior of the structure, including loads and displacements at crack initiation and at crack-growth instability. Generative schemes require knowledge of the experimentally applied load (or displacement) versus crack-growth data, and are used to calculate crack-growth resistance as a function of crack extension.

Strictly speaking, the precise estimation formulas to calculate J and COD for a complex-cracked pipe in bending have not yet been developed, primarily because the problem is too complicated to allow using the usual analyses employed in estimating J and COD for simpler problems. Here, it was assumed that the available estimation formulas for simple through-wall circumferentially cracked pipes that were discussed earlier could be applied to analyze complex-cracked pipes. This was done by adjusting the pipe radius and the thickness in the cracked plane to account for the presence of the surface crack. Thus, any radial crack-driving force contribution was ignored. Only growth of the through-wall crack in the circumferential direction was considered. Also, possible closure of the surface crack in the compressively stressed region of the crack plane was not included in the analysis, which can cause the loads to be underpredicted and the crack-opening to be overpredicted.

2.6.1 η-factor Analysis of Complex-Cracked Pipe

J-resistance curves for complex-cracked pipes are obtained using what is known as an η-factor approach (Ref. 2.39). In essence, this involves calculating the elastic component, J_e, and the plastic component, J_p, of the total energy release rate, J. Consider a complex-cracked pipe with mean radius, R_m and wall thickness, t. The depth of the 360-degree internal surface crack and the total angle of the through-wall crack are defined as d and 2θ, respectively. The pipe is subjected to a remote bending moment, M. Suppose that the crack driving force for the complex-cracked pipe can be approximated by considering a simple through-wall-cracked pipe that has an adjusted mean radius, $R_m^* = R_m + d/2$, adjusted wall thickness, $t^* = t - d$, and the same crack angle as the through-wall portion of the complex crack. The elastic and plastic components of the total energy release rate are given by

$$J_e = \frac{1}{E}\left[\sigma\sqrt{\pi R_m^* \theta}\; F_B\left(\theta/\pi, R_m^*/t^*\right)\right]^2 \qquad (2\text{-}51)$$

$$J_p = -\frac{F'(\theta)}{2\, R_m^* t^* F(\theta)} \int_0^{\Delta_p^c} F_v \, d\Delta_p^c \qquad (2\text{-}52)$$

in which $\sigma = M/\pi R_m^{*2} t^*$ is the far-field uniaxial tensile stress, $F(\theta) = \cos(\frac{1}{2}\theta) - \frac{1}{2}\sin(\theta)$, E is the modulus of elasticity, F_v is the total load in the four-point bending, and Δ_p^c is the plastic part of the load-point displacement in the presence of a crack, and F_B is a dimensionless geometry function of θ/π and R_m^*/t^*. The prime in Equation 2-52 denotes the symbol for ordinary differentiation with respect to the argument. Also in Equation 2-52, the plastic component of the J-resistance curve is based on Ernst's J_M (Modified J) parameter (Ref. 2.40) for analyzing data beyond J-controlled growth. No correction was made to account for crack growth as required in obtaining J_D (Deformation J). In this study, the J-resistance curve for complex-cracked pipe will be represented by the J_M-resistance curve defined above. On the basis of Equations 2-51 and 2-52, the J_M-resistance curves can be determined from a single pipe experiment once the simultaneous measurement of load, load-point displacement, and crack extension are provided.

2.6.2 J-Resistance Curves for Complex-Cracked Pipes

In common elastic-plastic fracture mechanics applications, J_M-resistance curves are obtained from small-specimen data. To determine whether these can be used to reliably and accurately predict the elastic-plastic crack growth behavior in nuclear power-plant pipes, it is worthwhile to assess how these J_M-resistance curves compare with those obtained from the complex-cracked pipes.

In Reference 2.41, a detailed study comparing the J_M-resistance curves from the C(T) specimens and pipe test data was conducted. For example, Figure 2.8 shows a plot of J_M versus crack extension Δa obtained from both η-factor analysis (generative estimation scheme) and C(T) specimen data for two TP304 stainless steel complex-cracked pipe experiments (Experiment 4113-1 and 4113-2) conducted in Reference 2.41. Results from these experiments along with others performed in the same reference and elsewhere consistently showed that the complex-cracked pipe resistance curves were significantly lower than the side-grooved C(T) specimen resistance curves. The quantitative aspects of the study in Reference 2.41 also indicated that the ratio of J_M-resistance obtained from complex-cracked pipe tests and C(T) specimens was strongly correlated with the pipe geometric parameter d/t, where d and t represent the depth of the surface crack and the thickness of the pipe, respectively. This ratio was also found to be invariant with respect to the crack length increment Δa at which it was evaluated. The above observations on J_M-resistance curves from the experiments performed in References 2.41, 2.42, and 2.43 suggest that it may be useful to establish a constraint factor C_F as a function of d/t. Consequently, the J-resistance curves for the simple through-wall-cracked pipes, which are typically represented by the compact tension specimen data, may then be used to predict the J-resistance curves for the complex-cracked pipes. For example, using the currently available data, one can find the points on a complex-crack J_M-resistance curve (J_M^{CC}) knowing the points on the corresponding through-wall-crack J_M-resistance (J_M^{TWC}) by using the following relation:

$$J_M^{CC} = C_F \, J_M^{TWC} \tag{2-53}$$

where the value of C_F as a function of d/t can be found from the database generated by the available pipe experiments. Figure 2.9 shows the plot of C_F versus d/t created from various pipe tests performed by David Taylor Naval Ship R&D Center (Ref. 2.43) and Battelle (Refs. 2.41 and 2.44).

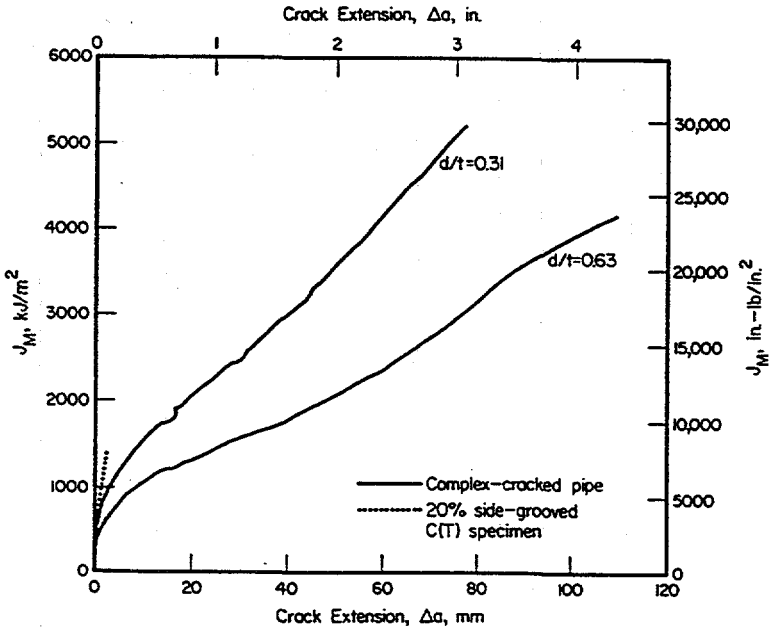

Figure 2.8 Comparison of J_M-resistance curves from complex-cracked TP304 pipe experiments and C(T) specimen data

SC-SA-5/92-F7.2

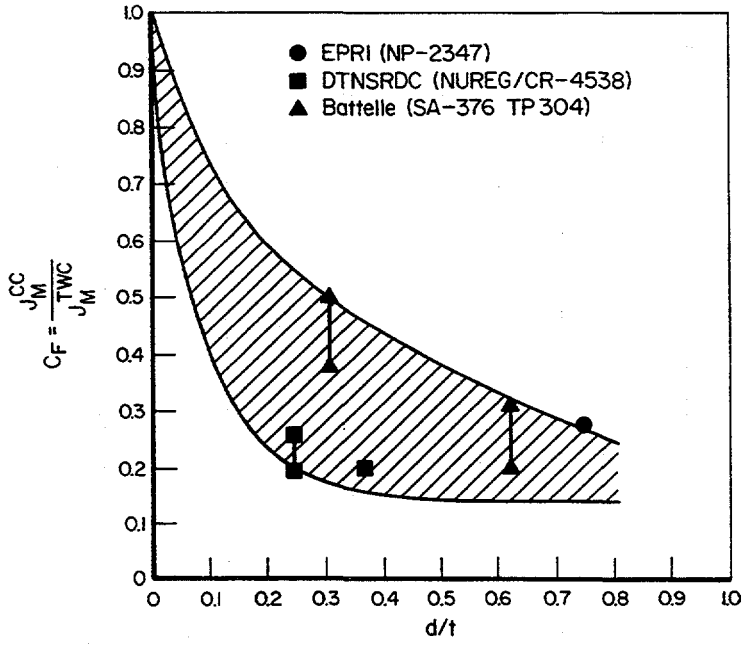

Figure 2.9 Complex-cracked pipe constraint factor as a function of d/t

T-6300-F2.9

2.6.3 Predictive Estimation Method for Complex-Cracked Pipes

As discussed earlier, the two types of estimation schemes are the generative and the predictive schemes. While generative schemes are used for determining the fracture resistance of the material, the predictive schemes are needed to obtain predictions of loads and displacements at crack initiation, during stable crack growth, and at instability, provided the fracture resistance of the material is known. Currently, available predictive estimation schemes applicable to cracked-pipe geometries include the GE/EPRI method, the Paris/Tada method, the LBB.NRC method, the LBB.ENG2 method, the LBB.ENG3 method, and others. These estimation schemes are, however, strictly developed for simple through-wall-cracked pipes for evaluating J and COD. To date, no specific estimation method exists to evaluate J and COD for complex-cracked pipes.

In this study, the LBB.ENG2 method was used to determine the crack-opening displacements for complex-cracked pipes. In performing analytical calculations, it was assumed that the estimation formulas (LBB.ENG2) for simple through-wall-cracked pipes can be applied to analyze complex-cracked pipes. This was accomplished by adjusting the pipe radius and the thickness in the cracked plane to account for the presence of the internal surface crack. Thus, any radial crack-driving force contribution was ignored. Only growth of the through-wall crack in the circumferential direction was considered. In addition, possible closure of the surface crack in the compressive region of the crack plane was not included in the analysis. The results of evaluations by the LBB.ENG2 method are given in Section 3 of this report.

2.7 References

2.1 Paul, D., Ahmad, J., Scott, P., Flanigan, L., and Wilkowski, G., "Evaluation and Refinement of Leak-Rate Estimation Models," NUREG/CR-5128, Rev. 1, U.S. Nuclear Regulatory Commission, Washington, D.C., June 1994.

2.2 Erdogan, F., "Fracture Analysis of Pipelines Containing Circumferential Flaws," Second Annual Report, U. S Department of Transportation, Contract No. DOT-RC-82007, June 198O.

2.3 Erdogan, F., and Delale, F., "Ductile Fracture of Pipes and Cylindrical Containers with a Circumferential Flaw," Trans. ASME, *Journal of Pressure Vessel Technology*, Vol. 103, pp 160-168, 1981.

2.4 Sanders, J. L., Jr., "Circumferential Through-Cracks in Cylindrical Shells Under Tension," *Journal of Applied Mechanics*, Vol. 49, pp. 103-107, March 1982.

2.5 Sanders, J. L., Jr., "Circumferential Through-Crack in a Cylindrical shell Under Combined Bending and Tension," *Journal of Applied Mechanics*, Vol. 50, p. 221, March 1983.

2.6 Yoo, S. H. and Pan, J., "Closed Form Displacement Solutions for Circumferentially Cracked Pipes in Bending and Tension," University of Michigan Report No. UM-MEAM-88-06, Ann Arbor, MI, October 1988.

2.7 Tada, H., Paris, P. C., and Irwin, G. R., *The Stress Analysis of Cracks Handbook*, Del Research Corp., Hellertown, 1973.

2.8 Wuthrich, C., "Crack Opening Areas in Pressure Vessels and Pipes," *Engineering Fracture Mechanics*, Vol. 18, No. 5, 1983.

2.9 Kumar, V., German, M., and Shih, C., "An Engineering Approach for Elastic-Plastic Fracture Analysis," EPRI Report NP-1931, Electric Power Research Institute, Palo Alto, CA, July 1981.

2.10 Kumar, V., German, M., Wilkening, W., Andrews, W., deLorenzi, H., and Mowbray, D., "Advances in Elastic-Plastic Fracture Analysis," EPRI Final Report NP-3607, Electric Power Research Institute, Palo Alto, CA, August 1984.

2.11 Kishida, K. and Zahoor, A., "Crack-Opening Area Calculations for Circumferential Through-Wall Pipe Cracks," EPRI Special Report NP-5959-SR, Electric Power Research Institute, Palo Alto, CA, August 1988.

2.12 Wilkowski, G. M., and others, "Short Cracks in Piping and Piping Program," Semiannual reports by Battelle, NUREG/CR-4599, Vols. 1 to 3, Nos. 1 and 2, U.S. Nuclear Regulatory Commission, Washington, D.C., 1991-1994.

2.13 Paris, P. C. and Tada, H., "The Application of Fracture Proof Design Methods Using Tearing Instability Theory to Nuclear Piping Postulating Circumferential Through-Wall Cracks," NUREG/CR-3464, U.S. Nuclear Regulatory Commission, Washington, D.C., September 1983.

2.14 Klecker, R., Brust, F., and Wilkowski, G., "NRC Leak-Before-Break (LBB.NRC) Analysis Method for Circumferentially Through-Wall-Cracked Pipes Under Axial Plus Bending Loads," NUREG/CR-4572, U.S. Nuclear Regulatory Commission, Washington, D.C., May 1986.

2.15 Brust, F. W., "Approximate Methods for Fracture Analyses of Through-Wall Cracked Pipes," NUREG/CR-4853, U.S. Nuclear Regulatory Commission, Washington, D.C., February 1987.

2.16 Gilles, P., and Brust, F., "Approximate Fracture Methods for Pipes - Part I: Theory," *Nuclear Engineering and Design*, Vol. 127, pp. 1-27, 1991.

2.17 Gilles, P., Chao, K. S., and Brust, F., "Approximate Fracture Methods for Pipes - Part II: Applications," *Nuclear Engineering and Design*, Vol. 127, pp. 13-31, 1991.

2.18 Rahman, S., Brust, F., Nakagaki, M., and Gilles, P., "An Approximate Method for Estimating Energy Release Rates of Through-Wall Cracked Pipe Weldments," *Fatigue, Fracture, and Risk*, PVP-Vol. 215, San Diego, California, 1991.

2.19 Rahman, S. and Brust, F., "An Estimation Method for Evaluating Energy Release Rates of Circumferential Through-Wall Cracked Pipe Welds," *Engineering Fracture Mechanics*, Vol. 43, No. 3, pp. 417-430, 1992.

2.20 Rahman, S. and Brust, F., "Elastic-Plastic Fracture of Circumferential Through-Wall Cracked Pipe Welds Subject to Bending," *Journal of Pressure Vessel Technology*, Vol. 114, No. 4, pp. 410-416, November 1992.

2.21 Rice, J. R., "A Path-Independent Integral and the Approximate Analysis of Strain Concentration by Notches and Cracks," Trans. ASME, *Journal of Applied Mechanics*, 35, pp. 376-386, 1968.

2.22 Rice, J. R. and Rosengren, G. F., "Plane Strain Deformation near a Crack-Tip in a Power-Law Hardening Material," *Journal of the Mechanics and the Physics of Solids*, 16, pp. 1-12, 1968.

2.23 Hutchinson, J. W., "Singular Behavior at the End of a Tensile Crack in a Hardening Material," *Journal of the Mechanics and the Physics of the Solids*, 16, pp. 13-31, 1968.

2.24 Hutchinson, J. W., "Fundamentals of the Phenomenological Theory of Nonlinear Fracture Mechanics," *Journal of Applied Mechanics*, 49, pp. 103-107, 1982.

2.25 Paris, P. C., Tada, H., Zahoor, A., and Ernst, H., "The Theory of Instability of the Tearing Mode of Elastic-Plastic Crack Growth," *ASTM STP 668, Elastic-Plastic Fracture*, pp. 5-36, 1979.

2.26 Shih, C. F., "J-Dominance Under Plane Strain Fully Plastic Conditions: The Edge Crack Panel Subject to Combined Tension and Bending," *International Journal of Fracture*, Vol. 29, pp. 73-84, 1985.

2.27 Shih, C. F., and Hutchinson, J. W., "Combined Loading of a Fully Plastic Ligament Ahead of an Edge Crack," *Journal of Applied Mechanics*, Vol. 53/271, June 1986.

2.28 Kaiser, S., "An Extension of Tearing Instability Theory to Multiple Loading Parameters," *International Journal of Fracture*, Vol. 29, pp. 85-99, 1985.

2.29 Sonnerlind, H., and Kaiser, S., "The J-Integral for a SEN Specimen Under Nonproportionally Applied Bending and Tension," *Engineering Fracture Mechanics*, Vol. 24, No. 5, pp. 637-646, 1986.

2.30 Brust, F. W., and Gilles, P., "Approximate Methods for Fracture Analysis of Tubular Members Subjected to Combined Tensile and Bending Loads," ASME *Journal of Offshore Mechanics and Arctic Engineering*, Vol. 116, pp 221-227, November 1994.

2.31 Shih, C. F., "J-Integral Estimates for Strain Hardening Materials in Antiplane Shear Using Fully Plastic Solutions," ASTM STP 590, pp. 3-22, 1976.

2.32 Bucci, R. J., Paris, P. C., Landes, J. D., and Rice, J. R., "J-Integral Estimation Procedures," ASTM STP 514, Part II, pp. 40-69, 1972.

2.33 Rice, J. R., Paris, P. C., Merkle, J. G., "Some Further Results of J-Integral Analysis and Estimates," ASTM STP 536, pp. 231-245, 1973.

2.34 Irwin, G. R., *Handbuch der Physik VI*, Flugge Ed., Springer, pp. 551-590, 1958.

2.35 Dugdale, D. S., "Yielding of Steel Sheets Containing Slits," *Journal of Mechanics and Physics of Solids*, Vol. 8, 1960.

2.36 Smith, E., "The Opening of Through-Wall Cracks in BWR Coolant Lines Due to the Application of Severe Overloads," NUREG/CP-0051, U.S. Nuclear Regulatory Commission, Washington, D.C., August 1984.

2.37 Brust, F., Rahman, S., and Ghadiali, N., "Elastic-Plastic Analysis of Small Cracks in Tubes," *Proceedings of the 11th International Conference on Offshore Mechanics and Arctic Engineering*, Calgary, Alberta, Canada, June 1992.

2.38 ABAQUS, User's Guide and Theoretical Manual, Version 5.3, Hibbitt, Karlsson, & Sorensen, Inc., Pawtucket, RI, 1993.

2.39 "The Development of a Plan for the Assessment of Degraded Nuclear Piping by Experimentation and Tearing Instability Analysis," Prepared for NRC by Battelle, Final Report, NUREG/CR-3142, U.S. Nuclear Regulatory Commission, Washington, D.C., June 1983.

2.40 Ernst, H. A., "Material Resistance and Instability Beyond J-Controlled Crack Growth," *Elastic-Plastic Fracture Second Symposium, Vol. I - Inelastic Crack Analysis*, ASTM STP 803, pp. I-191 through I-213, November 1983.

2.41 Kramer, G. and Papaspyropoulos, V., "An Assessment of Circumferentially Complex-Cracked Pipe Subjected to Bending," NUREG/CR-4687, U.S. Nuclear Regulatory Commission, Washington, D.C., October 1986.

2.42 Wilkowski, G. M., Pan, J., and Kanninen, K. F., "Effect of Flaw Shape on J-Resistance Curve of a Circumferentially Cracked Pipe," *Proceedings of the 4th ASME National Congress on Pressure Vessel and Piping Technology*, Portland, Oregon, June 1983.

2.43 Hays, R. A., Vassilaros, M. G., and Gudas, J. P., "Fracture Analysis of Welded Type 304 Stainless Steel Pipe," Prepared by David Taylor Naval Ship R&D Center (DTNSRDC) for NRC, NUREG/CR-4538, Vol. 1, U.S. Nuclear Regulatory Commission, Washington, D.C., May 1986.

2.44 Kanninen, M. F. and others, "Instability Predictions for Circumferentially Cracked Type 304 Stainless Steel Pipes Under Dynamic Loading," EPRI Report NP-2347, Electric Power Research Institute, Palo Alto, CA, April 1982.

3.0 VALIDATION OF ANALYTICAL MODELS

In this section, the accuracy of a number of crack-opening-area (COA) models discussed in Section 2 is evaluated by comparing their analytical predictions with the experimental pipe fracture data. The main focus is on evaluating engineering analysis procedures (estimation methods) as well as the ability of the finite element method (FEM) to predict crack-opening displacements (COD) and shapes in pipes with circumferential through-wall cracks. A wide variety of pipe fracture tests involving cracks in base metal, weld metal, and bimetallic weld metal were analyzed. Pipes containing both simple through-wall-cracks and complex-cracks were evaluated. A total of twenty-five pipe fracture experiments were analyzed to validate the predictive COA models for leak-before-break (LBB) applications. The pipe test data for these experiments were developed at Battelle during the Short Cracks in Piping and Piping Welds Program (Ref. 3.1), the Degraded Piping Program (Ref. 3.2), and the Second International Piping Integrity Research Group (IPIRG-2) Program.

3.1 Finite Element Analyses

3.1.1 Past Results

In the past, Battelle performed several elastic-plastic finite element analyses to determine crack-opening characteristics for circumferential through-wall-cracked (TWC) pipes under pure bending. The experimental data used for validation of finite element results were in the form of COD measurements made during two pipe fracture tests previously conducted at Battelle. One of these experiments, conducted on a 406-mm (16-inch) nominal diameter TP304 stainless steel unwelded pipe at room temperature (Experiment 8T), was part of an EPRI-funded effort (Ref. 3.3). The data for the other experiment, conducted on a 406-mm (16-inch) nominal diameter TP304 stainless steel welded pipe at 288 C (550 F) (Experiment 4141-3), was developed from an NRC-sponsored program (Ref. 3.2). The detailed information on these experiments and the related material property data can be found in References 3.2 and 3.3.

During Phase 1 of the IPIRG Program (Ref. 3.4), these two experiments were analyzed by elastic-plastic finite element analyses (Ref. 3.5). Figures 3.1 and 3.2, which were obtained from the original Reference 3.5, show the plots of crack-opening displacement as a function of distance from the crack tip for both experiment and finite element analysis for the two experiments described earlier. The applied loads were initiation load for Experiment 8T and maximum load for Experiment 4141-3. The results from these figures suggest that the elastic-plastic FEM can provide accurate estimates of crack-opening profile when compared with the corresponding experimental data. The results from an estimation model (original GE/EPRI method) with Ramberg-Osgood fit parameters in various strain regions are also shown in these figures. They will be discussed in further detail in the next section.

Figures 3.1 and 3.2 also show several crack-opening shapes (rectangle, ellipse, and diamond) from experimental values of center COD and crack length alone. The comparisons with strain gauge measurements as well as finite element results indicate that the elliptical shape with lengths of major axis and minor axis equal to crack length and center-crack-opening displacement, respectively, can be

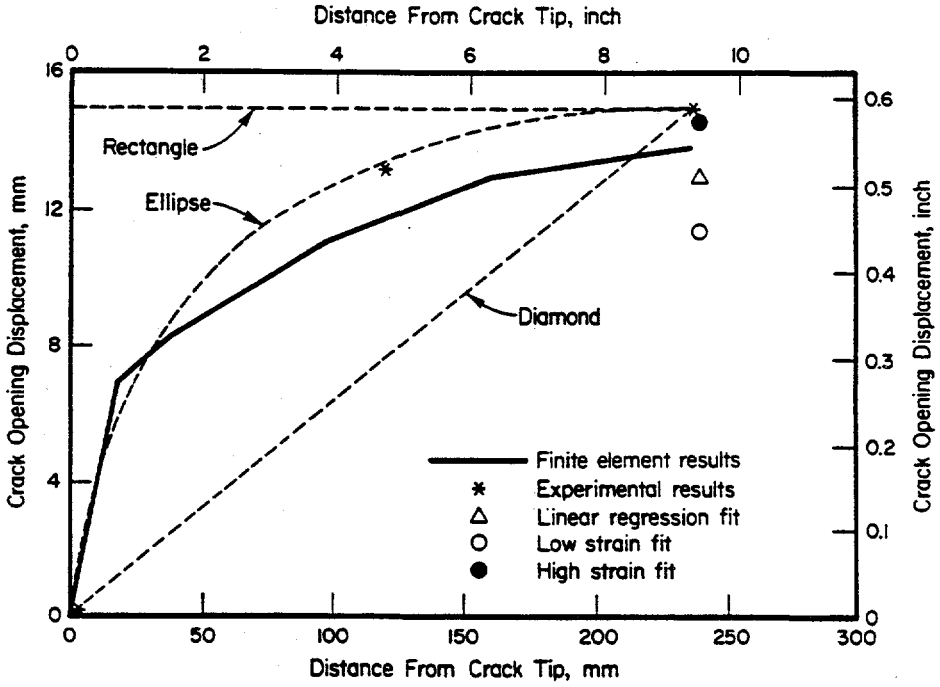

Figure 3.1 Crack-opening displacement at the load at crack initiation in Experiment 8T

T5128-F4.10

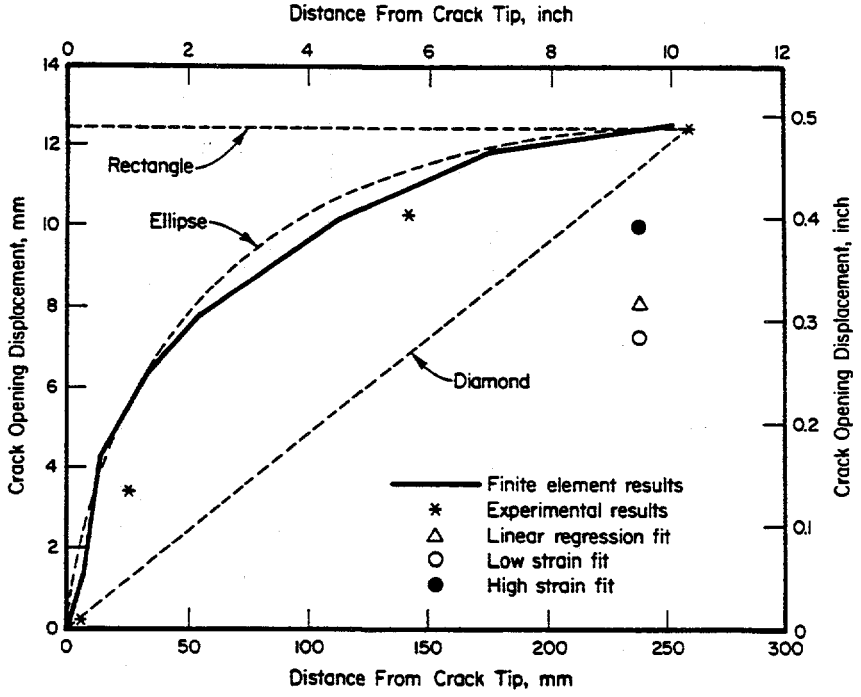

Figure 3.2 Crack-opening profile at maximum load in Experiment 4141-3

T5128-F4.15

used with reasonable accuracy to determine the crack-opening area for leak-rate evaluations. Further discussions on the validity of an elliptical-profile assumption are given Section 3.3 of this report.

3.1.2 New Thick-Walled Pipe Analysis

As part of the Short Cracks in Piping and Piping Welds Program, a full three-dimensional finite element analysis was conducted to predict crack-opening displacement in a through-wall-cracked pipe under pure bending loads. The data used to verify the finite element predictions were obtained from Experiment 1.1.1.21 and were also developed in the same program. This experiment was conducted on a 711.2-mm (28-inch) nominal diameter Schedule 60 A515 Grade 60 carbon steel unwelded pipe with a short circumferential through-wall crack which has length equal to 6.25-percent of the pipe circumference. Such crack lengths are typical in LBB applications for larger diameter pipes. Figure 3.3 shows the longitudinal dimensions of the pipe sections used to make up the specimen for Experiment 1.1.1.21. Figure 3.4 shows the cross-sectional geometry in the cracked section and instrumentation for collecting experimental data.

A three-dimensional elastic-plastic finite element model was developed for this pipe and is shown in Figure 3.5. The finite element model consisted of a 1/4 symmetric portion of the pipe with three different cross-sections. It consisted of 579 elements and 3,761 nodes. The number of elements through the thickness was one. The finite element analysis was performed under displacement control to a maximum load-line displacement of 160 mm (6.3 inches). Based on the experimental data, the crack initiated at a load-line displacement of 62.5 mm (2.46 inches).

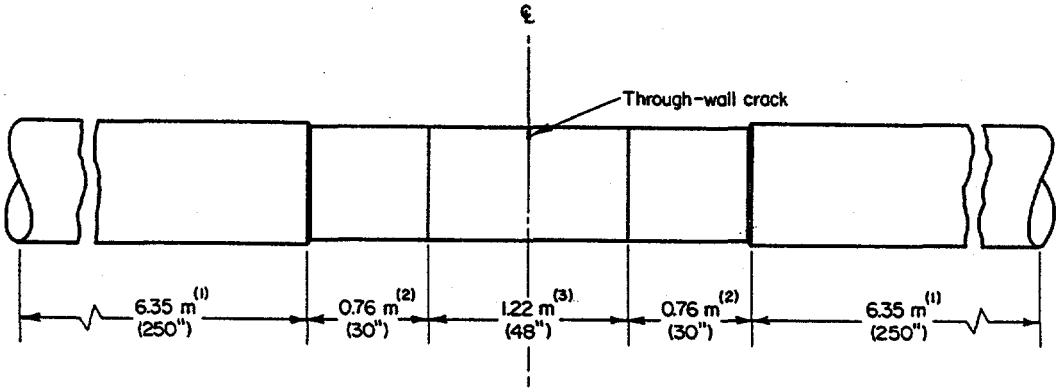

	(1)	(2)	(3)
Diameter	760 mm (30")	711 mm (28")	711 mm (28")
Wall Thickness	38.1 mm (1.5")	25.3 mm (0.995")	22.7 mm (0.893")
Ident. No.	IP-F5	DP2-F90	DP2-F26

Figure 3.3 Schematic of pipe used in Experiment 1.1.1.21

T-6300-F3.3

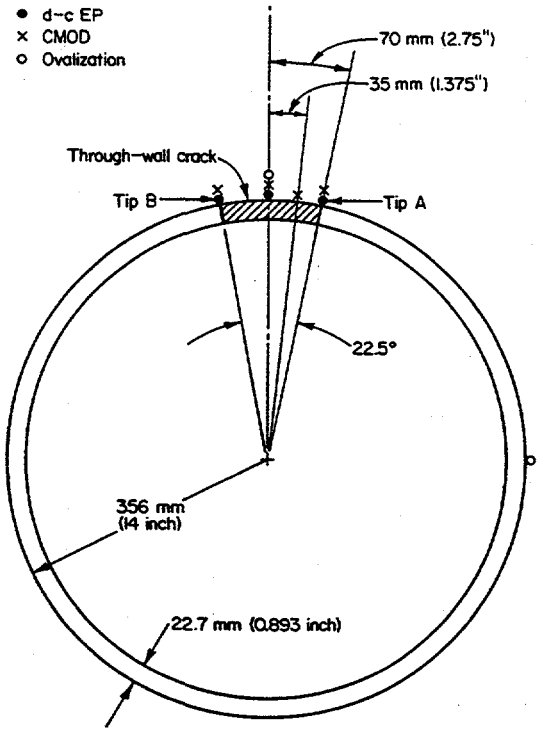

Figure 3.4 Schematic of crack geometry and instrumentation near the crack for Experiment 1.1.1.21

T-6300-F3.4

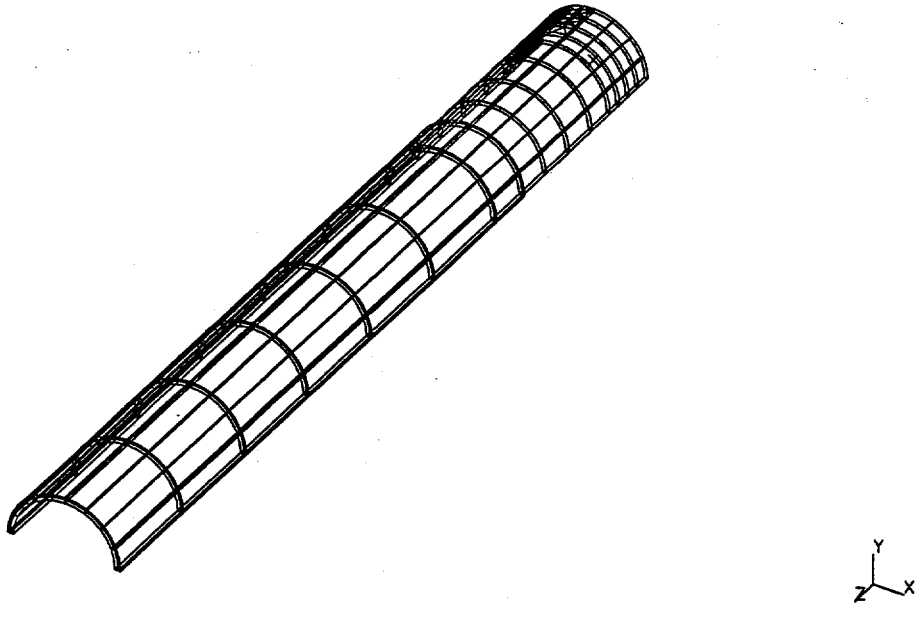

Figure 3.5 Finite element model for Experiment 1.1.1.21

T-6300-F3.5

Crack growth calculations were performed using the ABAQUS (Version 5.3) code (Ref. 3.6) with several load steps. The first load step was up to crack initiation. Subsequent steps consisted of releasing appropriate crack front nodes while simultaneously increasing the load-line displacement. The crack-growth and applied displacement data were obtained from the experimental record. Hence, the finite element predictions of crack-opening displacement following crack initiation were based on crack growth data from the test. As an alternative, the crack growth criteria based on J-integral evaluations could have been used, but were not adopted in this particular analysis. Table 3.1 shows the crack size, crack growth, and load-line displacement data for each load step in the finite element analysis.

Figure 3.6 shows the plots of total load versus pipe displacement at the load line from the experiment and the three-dimensional finite element calculations. The analysis results compare well with the experimental data. The center-crack-opening displacement as a function of pipe displacement at the load line is shown in Figure 3.7. Similar results of center-crack-opening displacement versus applied loads are also shown in Figure 3.8. The calculated center COD presented in these figures were obtained at the outer surface of the pipe. Once again, the agreement between the finite element results and the experimental data from the pipe fracture tests in Figures 3.7 and 3.8 is very good.

Table 3.1 Crack growth data for Experiment 1.1.1.21 used in finite element analysis

Step	Pipe Displacement at the Load-Line, mm (inch)	Crack Growth from One Crack Tip, mm (inch)
1*	62.5 (2.46)	0.0 (0.0)
2	73.4 (2.89)	12.2 (0.48)
3	90.4 (3.56)	24.5 (0.96)
4	110.5 (4.35)	36.7 (1.45)
5	130.8 (5.15)	49.0 (1.93)
6	139.9 (5.51)	61.4 (2.41)
7	149.1 (5.87)	73.7 (2.89)
8	153.7 (6.05)	85.9 (3.37)
9	159.7 (6.29)	98.2 (3.86)

* Crack Initiation

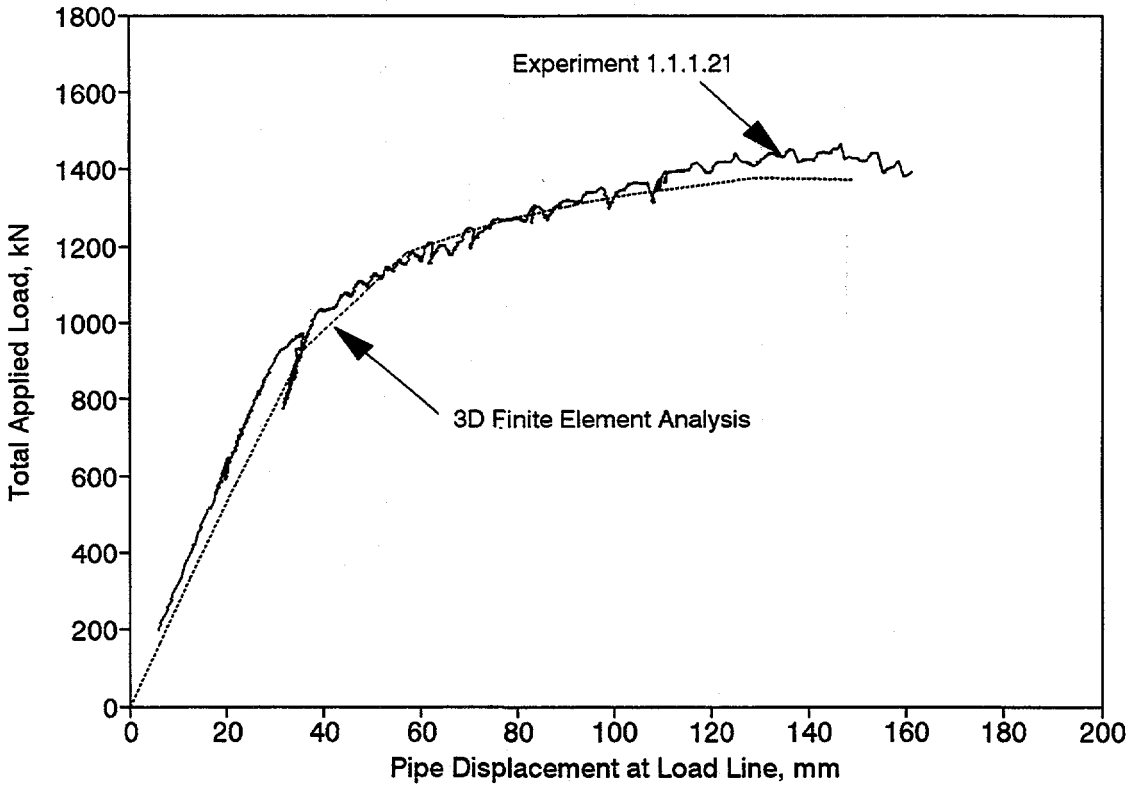

Figure 3.6 Load versus displacement comparison for Experiment 1.1.1.21

T-6300-F3.6

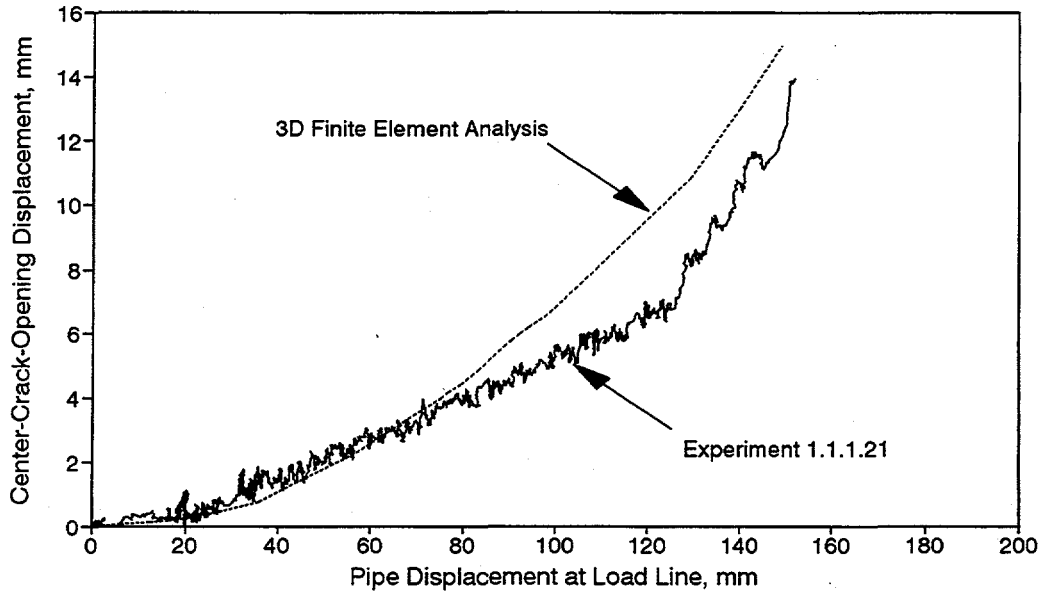

Figure 3.7 Center-crack-opening displacement comparison for Experiment 1.1.1.21

T-6300-F3.7

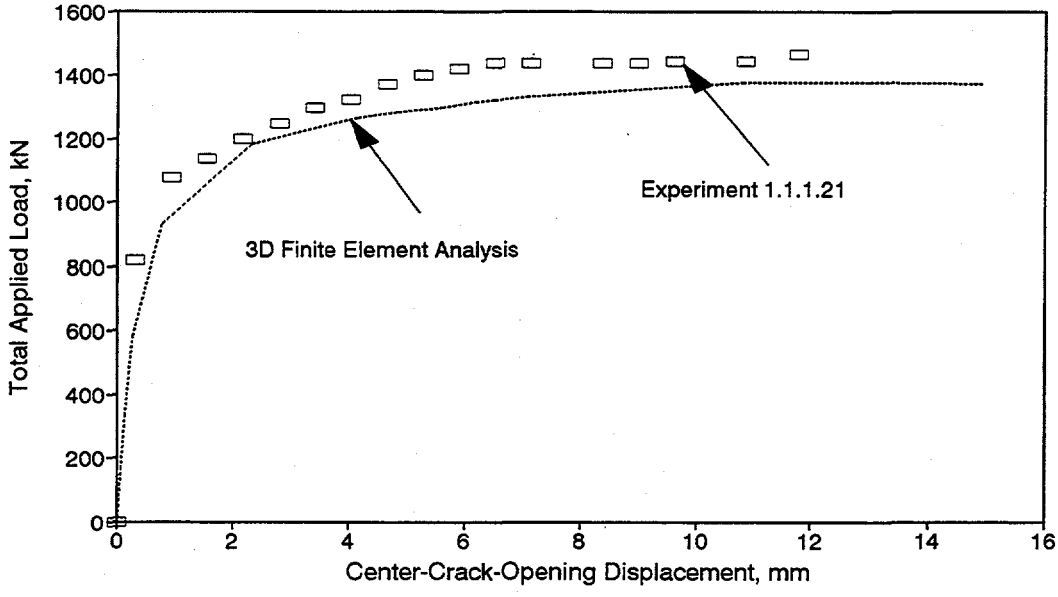

Figure 3.8 Comparison of predicted load versus center-crack-opening displacement for Experiment 1.1.1.21

T-6300-F3.8

3.2 Experimental Verification of Estimation Models

A total of twenty-five full-scale pipe fracture experiments were analyzed to determine the predictive capability of the COA estimation models discussed in Section 2. In all of these experiments, the pipes had circumferential through-wall cracks. Two cases of crack geometry were considered. One was a simple through-wall crack which has the same crack length on the inside and outside pipe diameter in terms of percentage of pipe circumference. The other was a complex-crack which consists of a 360-degree internal surface crack that penetrates the pipe thickness for a shorter through-wall-crack length. See Figure 3.9 for the definitions of these two crack geometries and the associated crack-size parameters.

The experiments involved both austenitic and ferritic steel piping with cracks located in the base metal, the weld metal, and the bimetallic weld. A wide range of pipe (outer) diameters from 114.3 mm (4.5 inches) to 1067 mm (42 inches) were considered. The initial through-wall crack lengths were both short and long and ranged between 6.25 and 38.6 percent of the pipe circumference. For the pipes with complex-crack geometry, the 360-degree internal surface cracks were both shallow and deep and the depths of these cracks varied from 32 to 64 percent of the pipe thickness. In all experiments, the cracks were placed in the center of the bending plane. For the welded pipe tests, the cracks were located in the center of the weld, except for the bimetallic pipe weld test in which case the crack was placed along the fusion line between the ferritic base metal and Inconel weld metal (see details in a forthcoming section). The test temperature varied from 7 C (45 F) to 288 C (550 F) with one experiment at 7 C (45 F), one experiment at room temperature, and the rest of the experiments at 288 C (550 F). The loading conditions were pure bending, pure tension, and combined bending and tension. Table 3.2 shows the summary of pipe fracture experiments analyzed in this study. Figure 3.10 shows a schematic of the experimental set-up for one of these full-scale pipe fracture tests conducted at Battelle.

In all of the above pipe experiments, the loading rates were quasi-static. Hence, all material property data used in the analyses were also based on quasi-static loading rates. The applied loads in the experiments were increased monotonically until the failure condition was reached.

3.2.1 Adequacy of Power Law Idealizations for Material Properties

In the estimation schemes for the COA analysis, the material model in Equation 2-1 is necessary since the formulations of crack-opening displacement and other fracture parameters are based on power-law idealization of the stress-strain curve. Unfortunately, there are actual material data for which it can be difficult to represent the complete range of actual stress-strain relation by a Ramberg-Osgood model. Reference 3.7 has some discussions on the limitation of this material model. It was indicated in this reference and Reference 3.5 that proper care must be taken in selecting the appropriate range of stress-strain data for a least-square fit by this power-law model. As shown in Figure 3.11, several possibilities exist in fitting the Ramberg-Osgood model to the test data and can correspondingly provide widely different values of model parameters, α and n. For typical LBB evaluations of large-diameter pipe, the fracture behavior of a cracked pipe is significantly elastic with little nonlinearity under normal operating conditions and hence, the estimations of crack-opening area and leak rate should be based on a power-law fit for low strain regions. However, for LBB applications (e.g., small-diameter pipes, higher operating stress, etc.) or general pipe flaw evaluations, if the magnitude

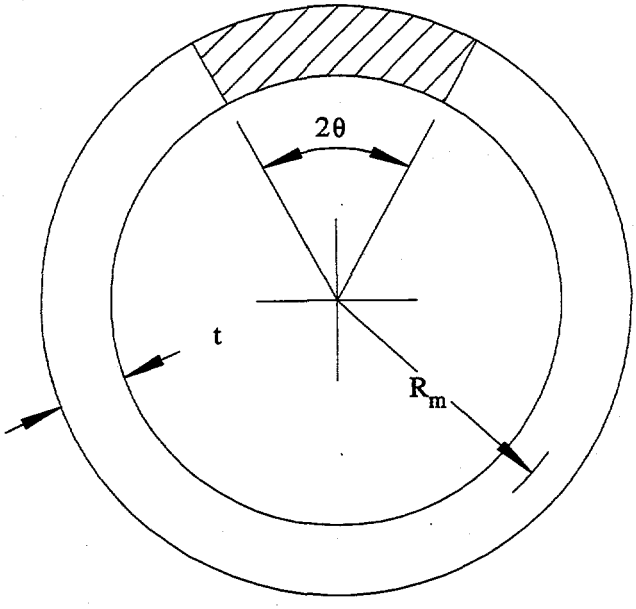

(a) Simple through-wall crack

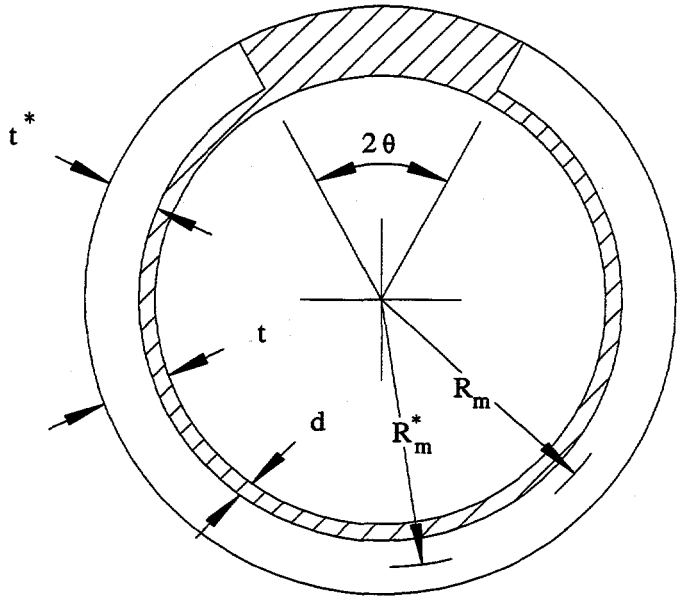

(b) Complex crack

Figure 3.9 Various through-wall-crack geometries and definitions of their parameters
T-6300-F3.9

Table 3.2 A list of 25 quasi-static pipe experiments for crack-opening-area analysis

Pipe Test No.	Outer Diameter, mm	Schedule	Material	Temperature, C	Flaw Shape[a]	$2a/\pi D_m$[b]	d/t[c]	Loading Condition[d]	Reference
			(a) Pipe Experiments with Base-Metal Cracks (19 Experiments)						
1.1.1.21	711	60	A515 Gr. 60	288	TWC	0.0625	0	B	3.1
1.1.1.26	106	160	TP316L	21	TWC	0.244	0	B	3.1
4111-1	114	80	A333 Gr. 6	288	TWC	0.370	0	B	3.2
4111-2	711	60	A515 Gr. 60	288	TWC	0.370	0	B	3.2
4111-3	1067	NA[e]	TP304	7	TWC	0.370	0	B	3.2
4121-1	168	120	TP304	288	TWC	0.386	0	T	3.2
4131-1	166	120	TP304	288	TWC	0.370	0	B+T	3.2
4131-3	274	100	A333 Gr. 6	288	TWC	0.370	0	B+T	3.2
1-8	399	100	A106 Gr. B	288	TWC	0.120	0	B+T	-[f]
4113-1	168	120	TP304	288	CC	0.370	0.32	B	3.2
4113-2	168	120	TP304	288	CC	0.370	0.63	B	3.2
4113-3	168	80	Inconel 600	288	CC	0.370	0.34	B	3.2
4113-4	168	80	Inconel 600	288	CC	0.370	0.61	B	3.2
4113-5	168	120	A106 Gr. B	288	CC	0.370	0.31	B	3.2
4113-6	168	120	A106 Gr. B	288	CC	0.370	0.64	B	3.2
4114-1	165	120	A106 Gr. B	288	CC	0.370	0.47	B	3.2
4114-2	166	120	TP304	288	CC	0.370	0.32	B	3.2
4114-3	413	100	TP304	288	CC	0.373	0.34	B	3.2
4114-4	413	100	TP304	288	CC	0.373	0.34	B	3.2
			(b) Welded Pipe Experiments (5 Experiments)[g]						
1.1.1.23	711	80	TP316L SAW	288	TWC	0.0625	0	B	3.1
1.1.1.24	612	80	A333 Gr. 6 SAW	288	TWC	0.079	0	B	3.1
4141-1	168	120	TP304 SAW	288	TWC	0.371	0	B	3.2
4141-5	168	120	TP304 SA-SAW	288	TWC	0.383	0	B	3.2
4111-5	720	80	TP316 SMAW	288	TWC	0.370	0	B	3.2
			(c) Bimetallic Pipe Weld Experiment (1 Experiment)[g]						
1.1.1.28	930	160	A516 Gr. 70/F316/ Inconel 182 SMAW	288	TWC	0.359	0	B	3.1

(a) TWC = simple through-wall crack; CC = complex crack
(b) 2a = through-wall crack length at mean pipe diameter; D_m = mean pipe diameter
(c) d = depth of 360-degree internal surface crack in a complex-cracked pipe; t = pipe wall thickness
(d) B = pure bending; T = pure tension (pressure); B+T = combined bending and tension (pressure)
(e) Not applicable
(f) Data were developed in the IPIRG-2 Program at Battelle
(g) SAW = submerged-arc weld; SMAW = shielded-metal arc weld; SA-SAW = solution-annealed submerged-arc weld

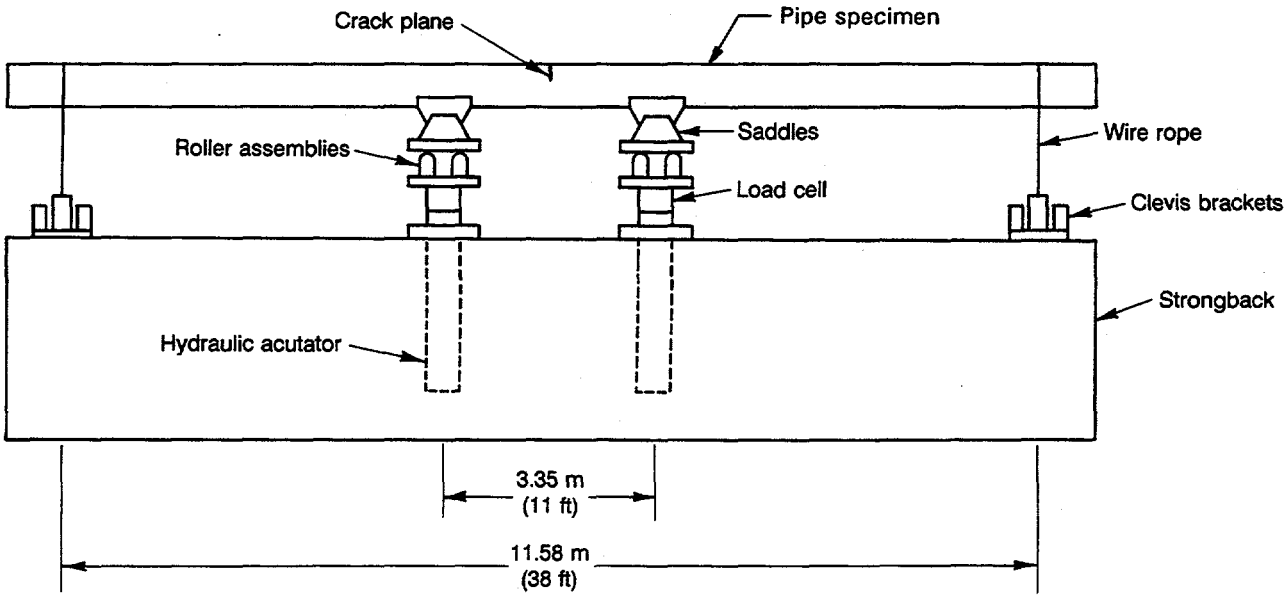

Figure 3.10 Schematic of experimental set-up for Experiment 1.1.1.23

T-6300-F3.10

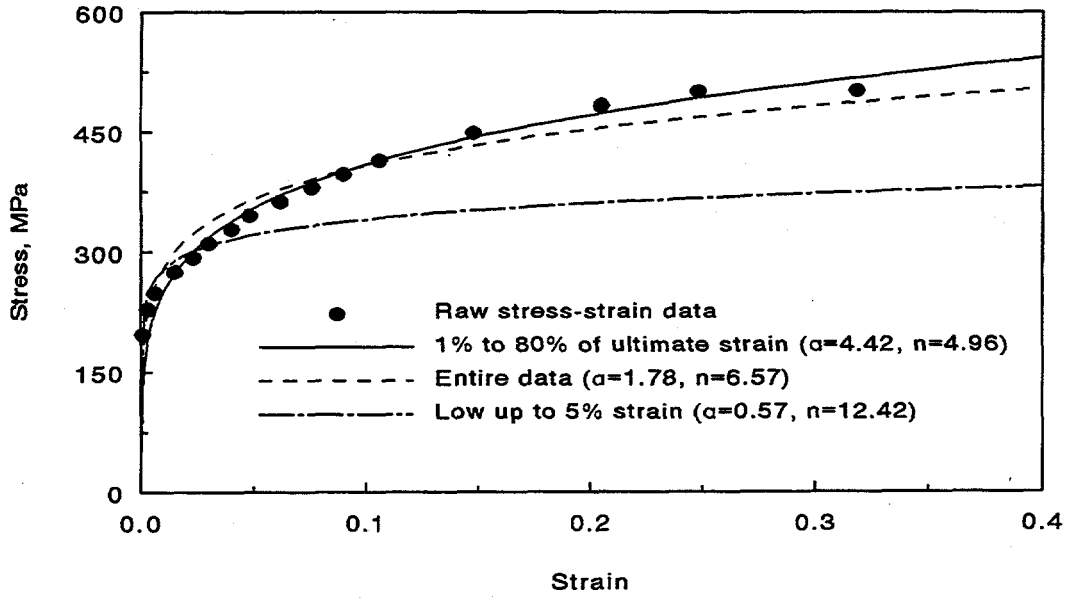

Figure 3.11 Ramberg-Osgood model for uniaxial stress-strain curves

T-6300-F3.11

of nonlinearity is high, the power-law fit to the high-strain region would be more appropriate. Since this study is focused on evaluating crack-opening characteristics up to initiation load or maximum load that are usually associated with large plastic strains, the Ramberg-Osgood fits in the high-strain region were used to determine the model parameters. From our past experience, we found that the range of raw stress-strain data between 1-percent strain and 80-percent of ultimate strain would provide the best representation by the Ramberg-Osgood model when analyzing pipe fracture experiments. All values of α and n presented in this study were computed in this strain range. Quantitative details on how α and n are affected by the choice of strain range and their impact on COA predictions are given in Section 4 of this report.

In characterizing the fracture toughness of materials, the ASTM Deformation J-resistance curve (the J_D-R curve) was used for pipes with simple through-wall cracks. For pipes with complex cracks, the Modified J-resistance curves (J_M-R curves) were used. For most of these cases, the J_D-R and J_M-R curves were extrapolated by either a power-law hardening model (i.e., Equation 2-2) and a linear model (i.e., a special case of Equation 2-2 with m = 1), respectively, for crack growth beyond 30-percent of the uncracked ligament in the C(T) specimens. Because, the C(T) specimens were small, large extrapolation of the data was necessary in order to predict crack growth in a pipe. Figure 3.12 shows that the power-law model of Equation 2-2 can represent fairly well the actual J_D-R data from C(T) specimens. Since, in many cases there were more than one set of experimental data for both stress-strain and J-R curves, the values of material property constants presented and used in the analyses represent their average values.

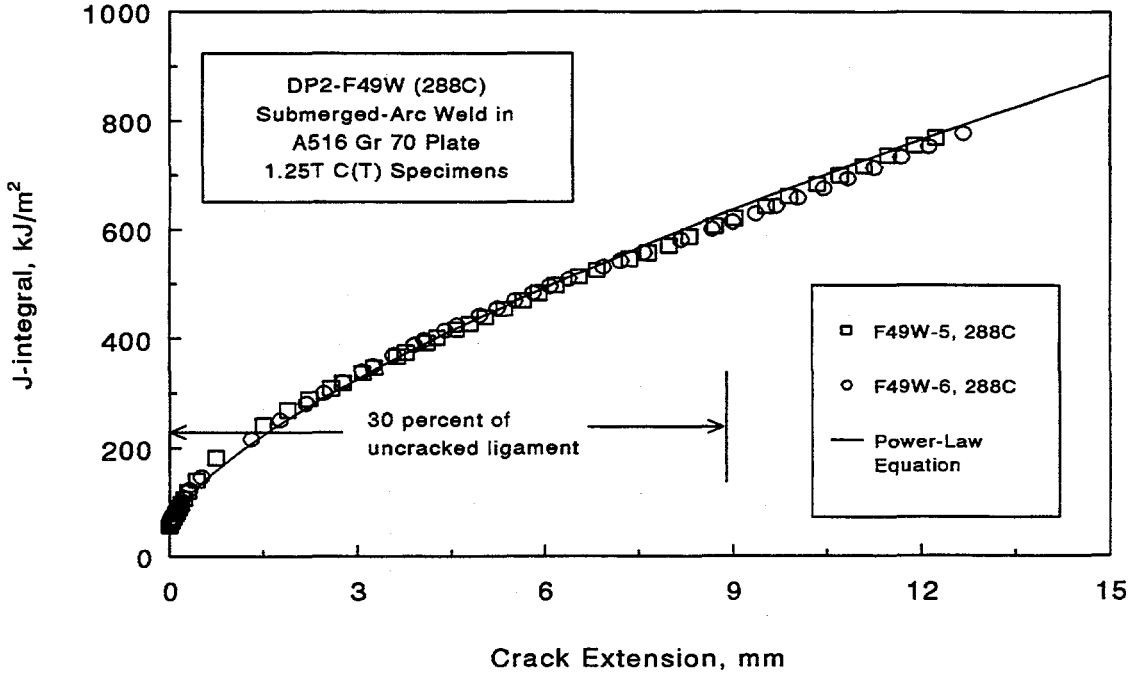

Figure 3.12 Power-law model for extrapolated J_D-R curves from compact tension specimens
T-6300-F3.12

3.2.2 The NRCPIPE Computer Program

The NRCPIPE computer code was developed to perform elastic-plastic fracture-mechanics analysis for establishing the fracture-failure conditions of a piping system in terms of sustainable load (or stress) or displacement (Refs. 3.1 and 3.2). For nuclear applications, engineering elastic-plastic fracture-mechanics techniques are based on the J-integral fracture parameter. To perform a fracture analysis, the user provides the input data describing the pipe and crack geometries, material stress-strain characteristics, and fracture resistance of the material (i.e., a J-R curve) as obtained from a laboratory test specimen. A wide variety of results for a pipe including crack-opening area predictions can be obtained.

The engineering treatment of elastic-plastic fracture mechanics to predict crack-opening is still in a state of development. Although a number of procedures have been proposed, many have not been validated by experimental data. For this reason, NRCPIPE was written to include numerous analysis procedures. At the user's option, NRCPIPE can perform an analysis using any of these procedures. In addition, the modular structure of NRCPIPE permits inclusion of new procedures as they are developed, because incomplete blocks of code have been reserved for just this purpose.

The NRCPIPE code was originally developed under the Degraded Piping Program (Ref. 3.2). A significant amount of development and numerous enhancements were made in the Short Cracks in Piping and Piping Welds Program (Ref. 3.1). Further details on these enhancements can be obtained from Reference 3.1.

The pipe fracture experiments listed in Table 3.2 were analyzed by various estimation methods described earlier. All of these methods are available in the current version of the NRCPIPE code (Version 2.0). All crack-opening results for the analyses of these experiments were generated using this program. The results are discussed in the forthcoming sections.

3.2.3 Analysis of Pipes with Base Metal Cracks

This section discusses the crack-opening-area analyses of nineteen pipe fracture experiments involving nine through-wall-cracked pipes and ten complex-cracked pipes. Five of these TWC pipe tests, such as Experiments 1.1.1.21, 1.1.1.26, 4111-1, 4111-2, 4111-3, were performed at pure bending load without any internal pressure. Experiment 4121-1 was conducted under pure tension load due to internal pipe pressure. The remaining three of the TWC pipe tests, such as Experiments 4131-1, 4131-3, and 1-8, were performed under combined bending and tension due to constant pipe pressure. On the other hand, all of the ten complex-cracked pipes tested in the Experiments 4113-1 to 4113-6 and 4114-1 to 4114-4 were subjected to pure bending without internal pressure. The fracture data for these experiments were developed at Battelle during the Short Cracks in Piping and Piping Welds Program (Ref. 3.1), the Degraded Piping Program (Ref. 3.2), and the Second International Piping Integrity Research Group (IPIRG-2) Program. Table 3.3 provides a summary of the pipe geometries and experimental results for these nineteen pipe fracture experiments. Material properties, including the power-law fit parameters for the stress-strain curves and the C(T) specimen J-R curves related to these experiments, are given in Table 3.4.

Table 3.3 Summary of pipe geometry and results for 19 pipe fracture experiments with base-metal cracks

Pipe Test No.	Outer Diameter, mm	Pipe Thickness, mm	Pipe Material	Internal Pressure, MPa	$2a/\pi D_m$ [(a)]	d/t [(b)]	Inner Span, m	Outer Span, m	Initiation Load, kN	Maximum Load, kN
				(a) Through-Wall-Cracked Pipes (9 Experiments)						
1.1.1.21	711	22.70	A515 Gr. 60	0	0.0625	0	3.35	11.58	1250	1470
1.1.1.26	106	8.31	TP316L	0	0.244	0	0.61	1.52	73	75
4111-1	114	8.89	A333 Gr. 6	0	0.370	0	0.81	1.52	73	88
4111-2	711	23.62	A515 Gr. 60	0	0.370	0	3.35	11.58	396	585
4111-3	1067	7.11	TP304	0	0.370	0	3.35	11.58	299	443
4121-1	168	12.88	TP304	-(c)	0.386	0	NA(d)	NA(d)	-(e)	-(f)
4131-1	166	13.41	TP304	17.24	0.370	0	1.22	3.2	31	40
4131-3	274	18.69	A333 Gr. 6	12.45	0.370	0	3.35	7.92	70	100
1-8	399	26.20	A106 Gr. B	15.51	0.120	0	3.35	11.58	302	504
				(b) Complex-Cracked Pipes (10 Experiments)						
4113-1	168	14.48	TP304	0	0.370	0.32	0.61	1.52	110	124
4113-2	168	14.48	TP304	0	0.370	0.63	0.61	1.52	76	81
4113-3	168	11.05	Inconel 600	0	0.370	0.34	0.61	1.52	106	118
4113-4	168	11.05	Inconel 600	0	0.370	0.61	0.61	1.52	79	87
4113-5	168	14.22	A106 Gr. B	0	0.370	0.31	0.61	1.52	118	147
4113-6	168	14.22	A106 Gr. B	0	0.370	0.64	0.61	1.52	55	89
4114-1	165	12.73	A106 Gr. B	0	0.370	0.47	1.22	2.34	68	83
4114-2	166	13.46	TP304	0	0.370	0.32	1.22	4.17	26	29
4114-3	413	26.16	TP304	0	0.373	0.34	3.35	11.58	146	158
4114-4	413	26.16	TP304	0	0.373	0.34	3.35	11.58	141	152

(a) 2a = through-wall crack length at mean pipe diameter; D_m = mean pipe diameter
(b) d = depth of 360-degree internal surface crack in a complex-cracked pipe; t = pipe wall thickness
(c) Pressure monotonically increased until failure
(d) Not applicable
(e) The initiation pressure was 26.9 MPa (3.9 ksi)
(f) The maximum pressure was 30.1 MPa (4.4 ksi)

Table 3.4 Tensile strength and fracture toughness properties of pipe materials for experiments with base-metal cracks

Pipe Test No.	Elastic Modulus (E), GPa	Yield Stress (σ_y), MPa	Ultimate Stress (σ_u), MPa	Ramberg-Osgood Coefficients[a] α	Ramberg-Osgood Coefficients[a] n	Extrapolated J-R Curve Parameters[b,c] J_{Ic}, kJ/m^2	Extrapolated J-R Curve Parameters[b,c] C, kJ/m^2	Extrapolated J-R Curve Parameters[b,c] m
(a) Through-Wall-Cracked Pipes								
1.1.1.21	179.3	231	544	1.10	5.50	207	166	0.483
1.1.1.26	157.5	254	532	5.50	4.76	879	779	0.974
4111-1	179.3	198	494	1.96	4.16	335	–[d]	–[d]
4111-2	179.3	231	544	1.10	5.50	207	166	0.483
4111-3	199.9	220	682	1.67	5.05	484	258	0.646
4121-1	179.3	139	450	4.91	3.88	1090	–[e]	–[e]
4131-1	179.3	139	450	4.91	3.88	1090	–[e]	–[e]
4131-3	179.3	239	527	3.77	3.84	298	–[e]	–[e]
1-8	193.1	217	508	174	4.66	72	140	0.72
(b) Complex-Cracked Pipes								
4113-1	183.8	139	450	5.33	3.80	1210	328	1
4113-2	183.8	139	450	5.33	3.80	1210	328	1
4113-3	221.4	197	610	5.35	3.90	1820	505	1
4113-4	221.4	197	610	5.35	3.90	1820	505	1
4113-5	198.4	320	621	1.20	5.90	100	107	1
4113-6	198.4	320	621	1.20	5.90	100	107	1
4114-1	198.4	320	621	1.20	5.90	100	107	1
4114-2	183.8	139	450	5.33	3.80	1210	328	1
4114-3	179.5	186	461	2.83	5.50	310	167	1
4114-4	179.5	186	461	2.83	5.50	310	167	1

(a) Stress-strain curve is represented by: $\epsilon/\epsilon_0 = \sigma/\sigma_0 + \alpha(\sigma/\sigma_0)^n$, where $\sigma_0 = \sigma_y$, $\epsilon_0 = \sigma_0/E$

(b) For through-wall-cracked pipe, J_D-R curve was used and was represented by: $J = J_{Ic} + C(\Delta a/r)^m$, where r = 1 mm and Δa is in mm

(c) For complex-cracked pipe, J_M-R curve was used and was represented by: $J = J_{Ic} + C\,\Delta a$, where Δa is in mm

(d) Crack growth data were not available

(e) Actual J_D-R data from C(T) specimens were used which were extrapolated linearly at the last two points

3.2.3.1 Simple Through-Wall-Cracked Pipes

Figures 3.13 through 3.21 show the plots of total applied load (in four-point bending) versus center-crack-opening displacement for the nine through-wall-cracked pipes with base-metal cracks from Experiments 1.1.1.21, 1.1.1.26, 4111-1, 4111-2, 4111-3, 4121-1, 4131-1, 4131-3, and 1-8, respectively. These plots were developed from both predictive formulas by several estimation models and experimental pipe fracture data mentioned previously.

Pure Bending. The results in Figures 3.13 to 3.17 involving only pure bending loads indicate that the LBB.ENG2 method provides excellent predictions of experimental COD. The only exception is Experiment 1.1.1.21. The crack size in Experiment 1.1.1.21 was very short ($2a/\pi D_m$ = 6.25 percent) and it appears that for this experiment, the GE/EPRI method using either the original or the Battelle-developed influence functions can predict COD with better accuracy than the other methods, at least up to crack initiation (Note, the measured initiation load for Experiment 1.1.1.21 was 1250 kN [281,013 lb]). In Experiments 1.1.1.21 and 1.1.1.26, both LBB.NRC and Paris/Tada methods underpredicted COD for applied loads that are less than the initiation load, although the results from the LBB.NRC method were closer to the experimental data. In Experiments 4111-1 to 4111-3, the CODs predicted by the LBB.ENG2 method and the GE/EPRI method (using original functions) were very similar and compared very well with the experimental data.

Pure Tension. Figure 3.18 shows the plots of both predicted and experimental results of applied pipe pressure as a function of center-crack-opening displacement in Experiment 4121-1 conducted under pure tension load (pressure induced). The GE/EPRI method (original functions) slightly overestimated both the experimental COD and the predicted COD by the LBB.ENG2 method. The agreement between the results from the LBB.ENG2 method and the experiment was excellent.

Combined Bending and Tension. For the pipe tests, Experiments 4131-1, 4131-3, and 1-8 that involved combined bending and tension (pressure induced), similar plots of load versus center COD were developed and are shown in Figures 3.19, 3.20, and 3.21, respectively. In these experiments, the measured COD values due to the initial pipe pressure were initialized before the application of additional bending loads. Hence, the center-crack-opening displacement plotted in these figures is equal to the center COD under combined bending and tension loads minus the center COD due to the pure tension load before the bending loads are applied.

For Experiment 4131-1 (see Figure 3.19), it is seen that all estimation methods underpredicted the COD for applied load before the crack growth initiated. (Note, the measured initiation load for Experiment 4131-1 was 31.00 kN [6,969 lb].) The Paris/Tada and LBB.NRC solutions gave the worst predictions, while the LBB.ENG2 and GE/EPRI methods predicted results closer to the experimental data. In Experiment 4131-3 (see Figure 3.20), the Paris/Tada and LBB.NRC methods underpredicted COD as in Experiment 4131-1, but the magnitude of underprediction by the LBB.NRC method was much smaller. In fact, for this particular experiment, the LBB.NRC method made better predictions of test data than any other methods.

Figure 3.21 shows the results of Experiment 1-8 that has a crack length of only 12 percent of the pipe circumference. For this experiment, the LBB.ENG2 method provided good predictions of COD for smaller loads, but also underpredicted COD significantly for larger loads. The trend curves for the

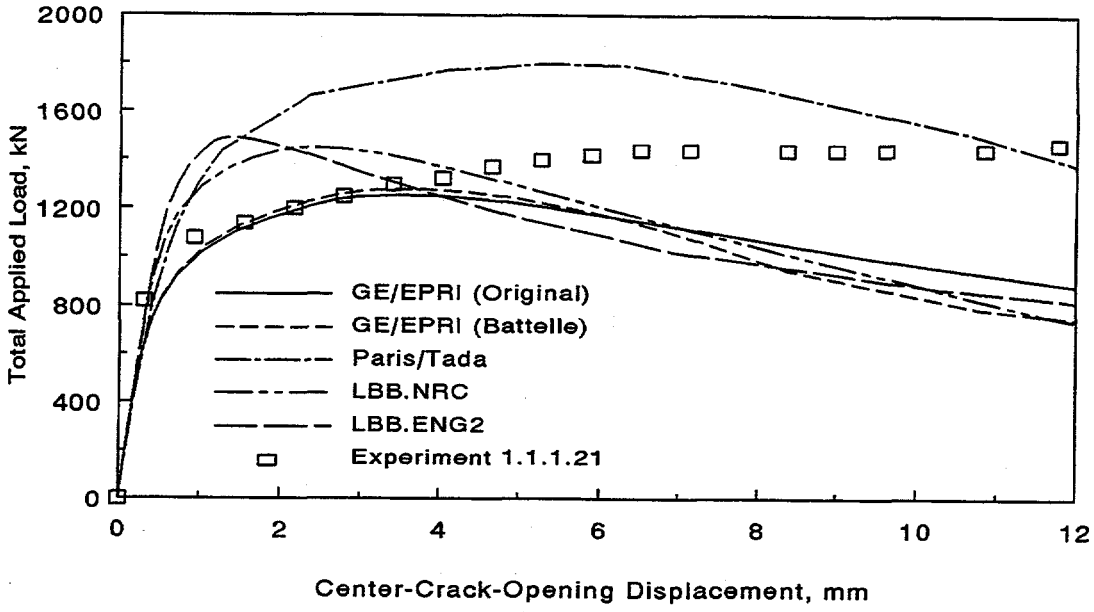

Figure 3.13 Load versus center-crack-opening displacement in Experiment 1.1.1.21
T-6300-F3.13

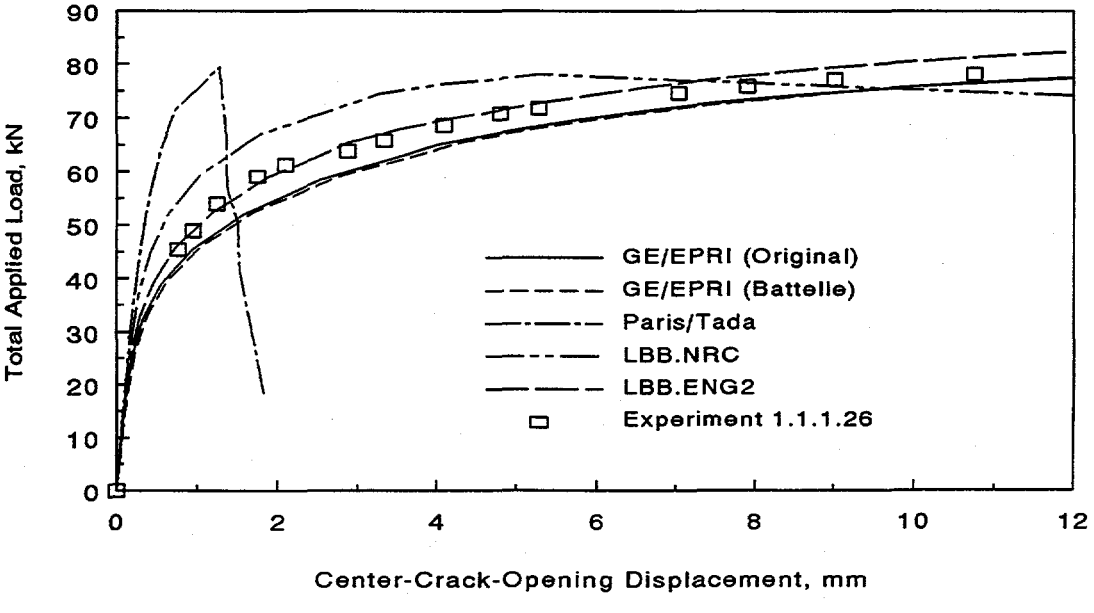

Figure 3.14 Load versus center-crack-opening displacement in Experiment 1.1.1.26
T-6300-F3.14

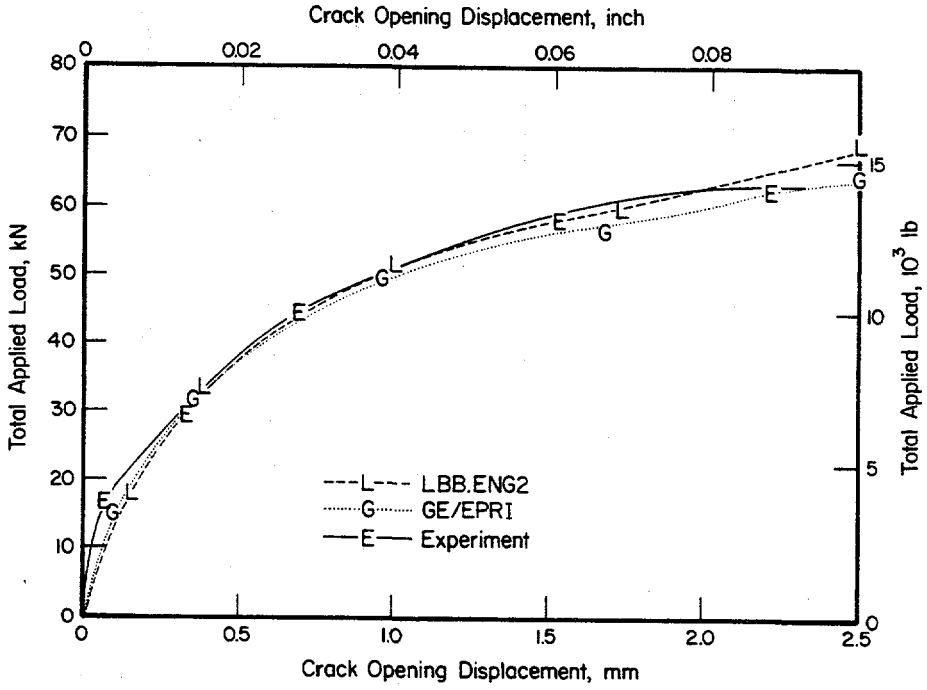

Figure 3.15 Load versus center-crack-opening displacement in Experiment 4111-1

SC-M-11/90/F2

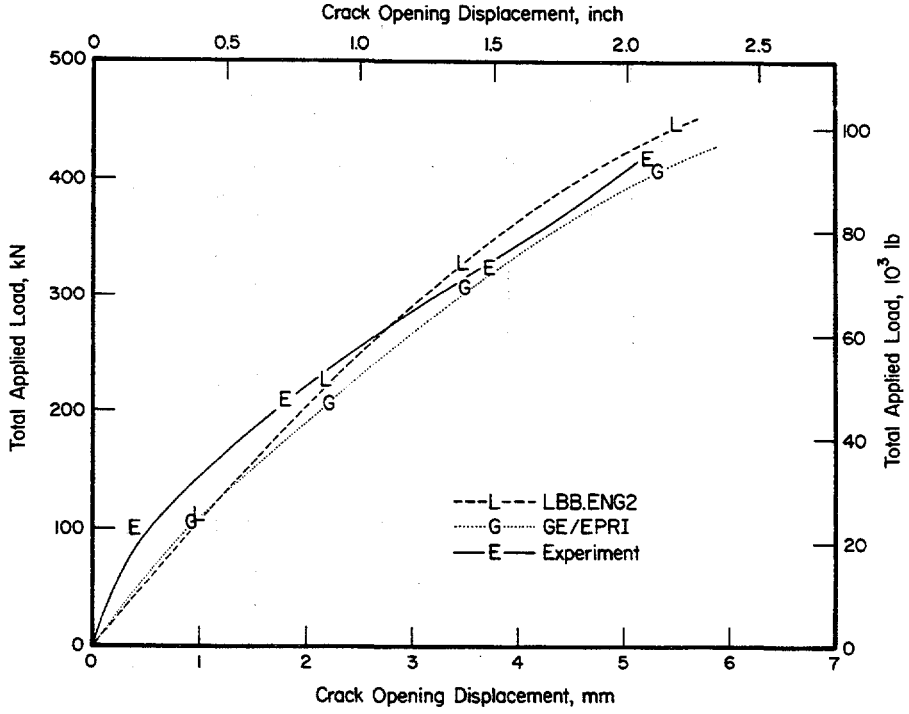

Figure 3.16 Load versus center-crack-opening displacement in Experiment 4111-2

SC-M-11/90-F3

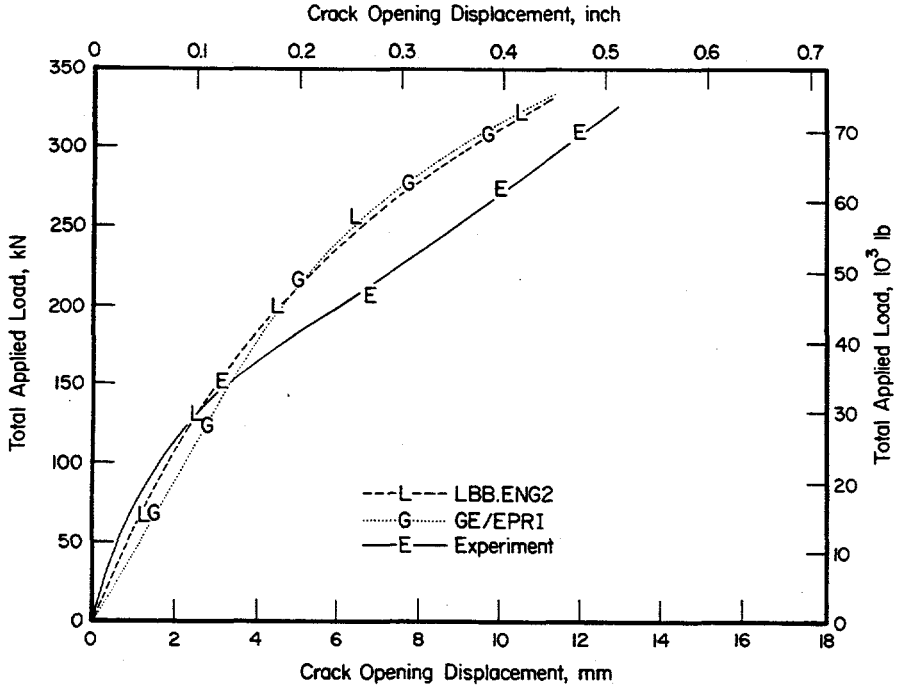

Figure 3.17 Load versus center-crack-opening displacement in Experiment 4111-3

SC-M-11/90-F4

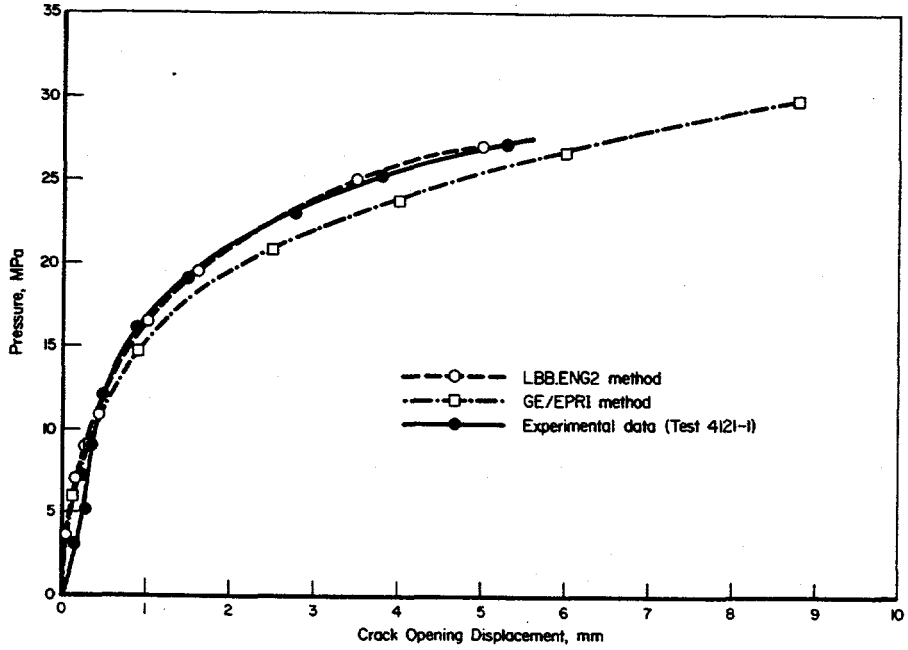

Figure 3.18 Pressure versus center-crack-opening displacement in Experiment 4121-1

SC-M-12/90-F6

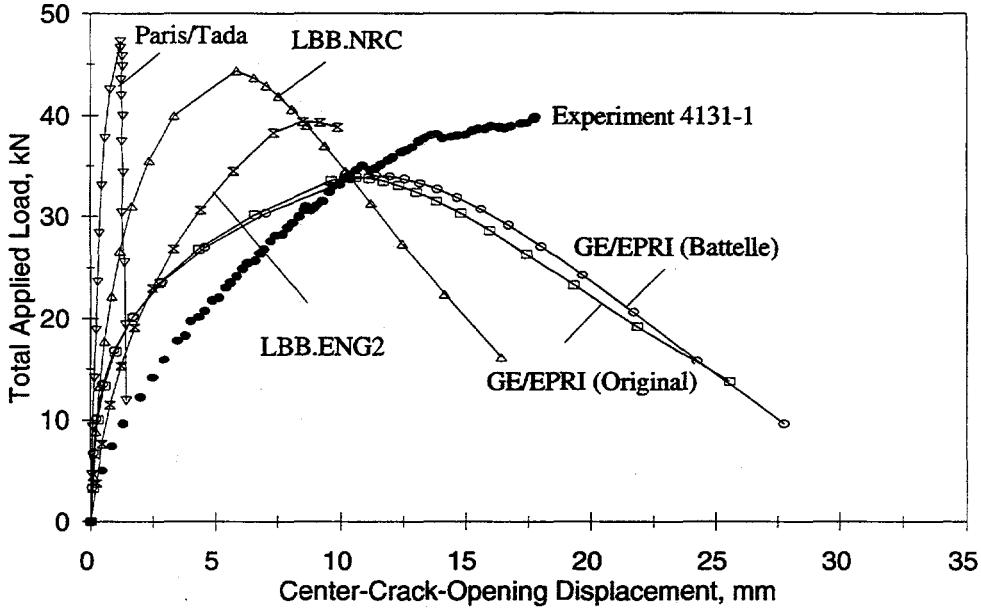

Figure 3.19 Load versus center-crack-opening displacement in Experiment 4131-1
T-6300-F3.19

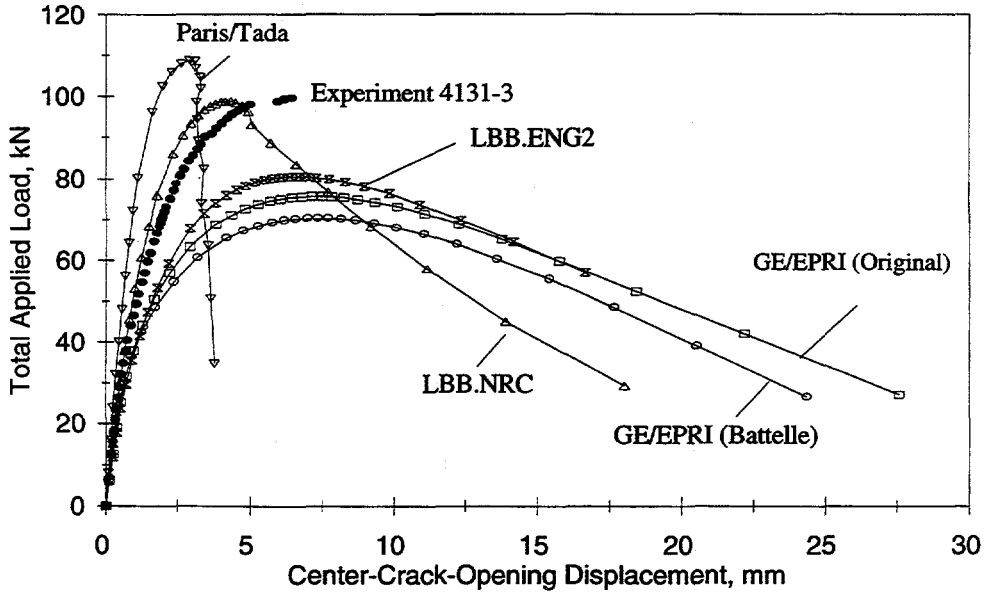

Figure 3.20 Load versus center-crack-opening displacement in Experiment 4131-3
T-6300-F3.20

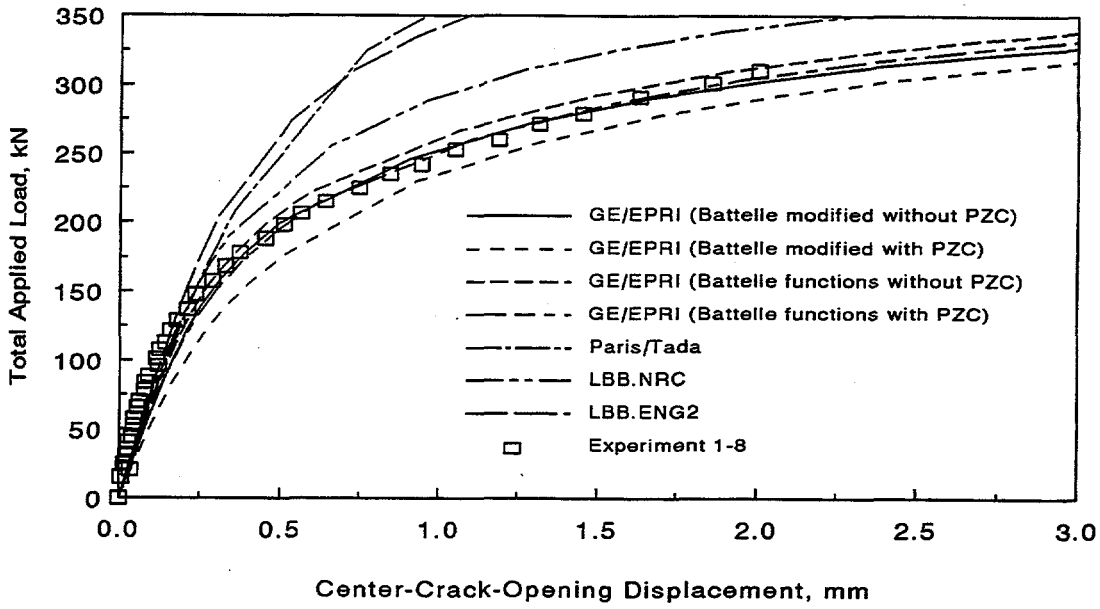

Figure 3.21 Load versus center-crack-opening displacement in Experiment 1-8
T-6300-F3.21

Paris/Tada and LBB.NRC methods showed similar behavior in predicting COD. Among all of these methods, the GE/EPRI method without plastic zone correction using either the original or the Battelle-developed influence functions provided the best results. Similar observations were also made for a pure bending pipe Experiment 1.1.1.21 with short cracks, see Figure 3.13.

3.2.3.2 Complex-Cracked Pipes

During the analyses of complex-cracked pipes, two cases of J-R curves based on the constraint factor, C_F, discussed in Section 2 were investigated. In the first case, the J_M-R curves obtained directly from the C(T) specimen data were used to represent the material's fracture toughness without any reduction (i.e., $C_F = 1$). In the second case, the J_M-R curves from C(T) specimens were multiplied by the relevant constraint factor which is a function of the d/t-ratio of the complex-cracked pipe (i.e., $C_F < 1$). The values of C_F for Experiments 4113-1 to 4113-6 and 4114-1 to 4114-4 were 0.5, 0.32, 0.5, 0.32, 0.5, 0.32, 0.4, 0.5, 0.5, and 0.5 respectively. They were obtained from the upper curve in Figure 2.9.

Figures 3.22 through 3.31 show the plots of total load versus center-crack-opening displacement for the ten complex-cracked pipes with base-metal cracks from Experiments 4113-1 to 4113-6 and 4114-1 to 4114-4, all of which were performed under four-point bending without any internal pressure. These plots contain results from the analyses by the LBB.ENG2 method with and without constraint factor and the corresponding experimental data. The results suggest that in most cases, the exceptions being Experiments 4113-5, 4114-1, and 4114-2, the estimation model (LBB.ENG2 method), with

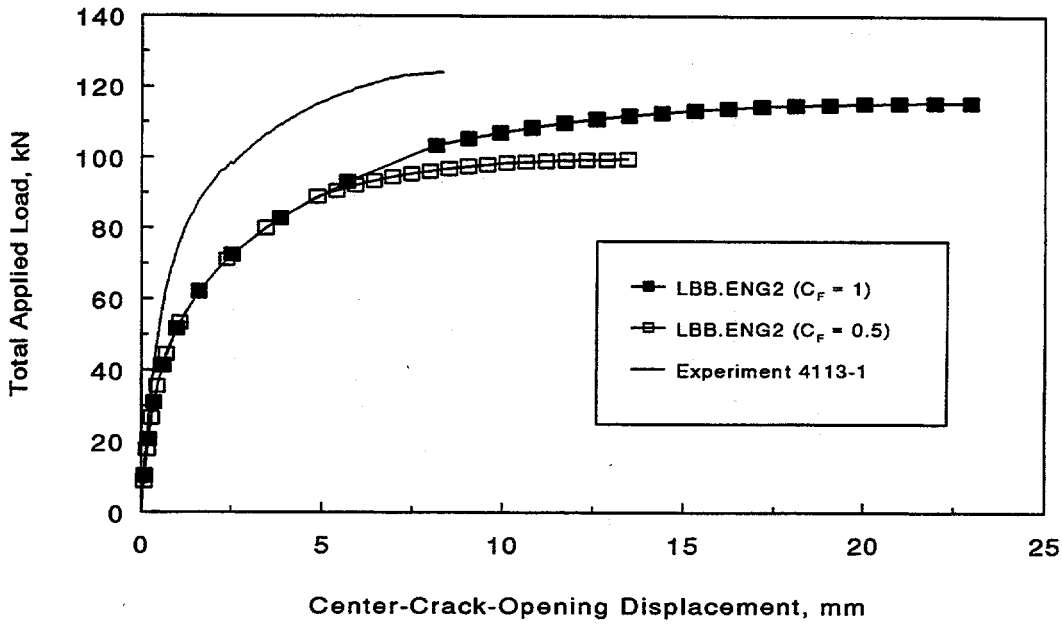

Figure 3.22 Load versus center-crack-opening displacement in Experiment 4113-1

T-6300-F3.22

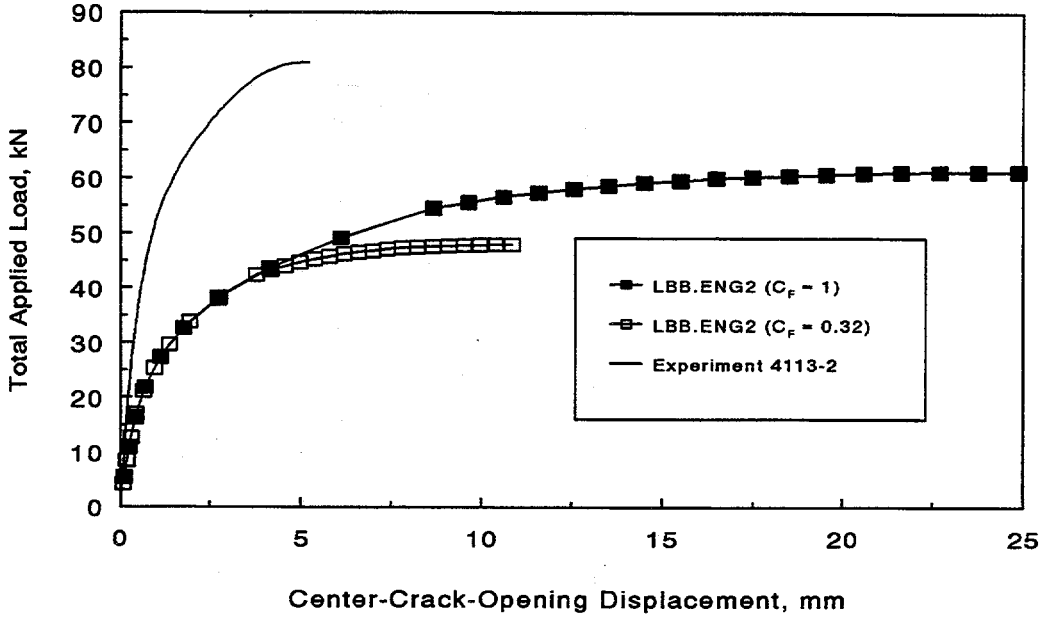

Figure 3.23 Load versus center-crack-opening displacement in Experiment 4113-2

T-6300-F3.23

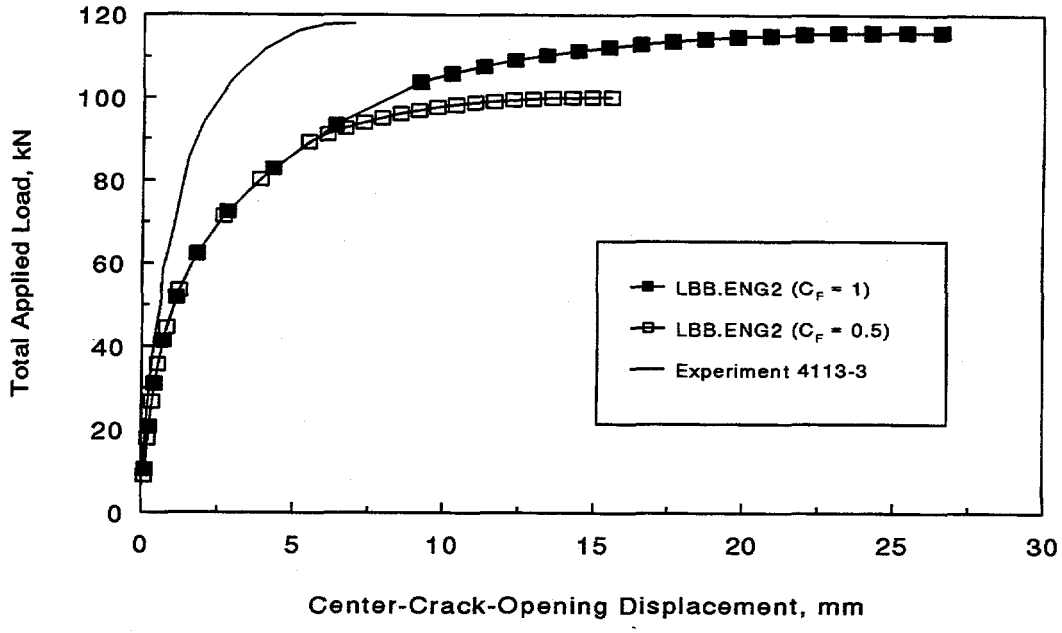

Figure 3.24 Load versus center-crack-opening displacement in Experiment 4113-3

T-6300-F3.24

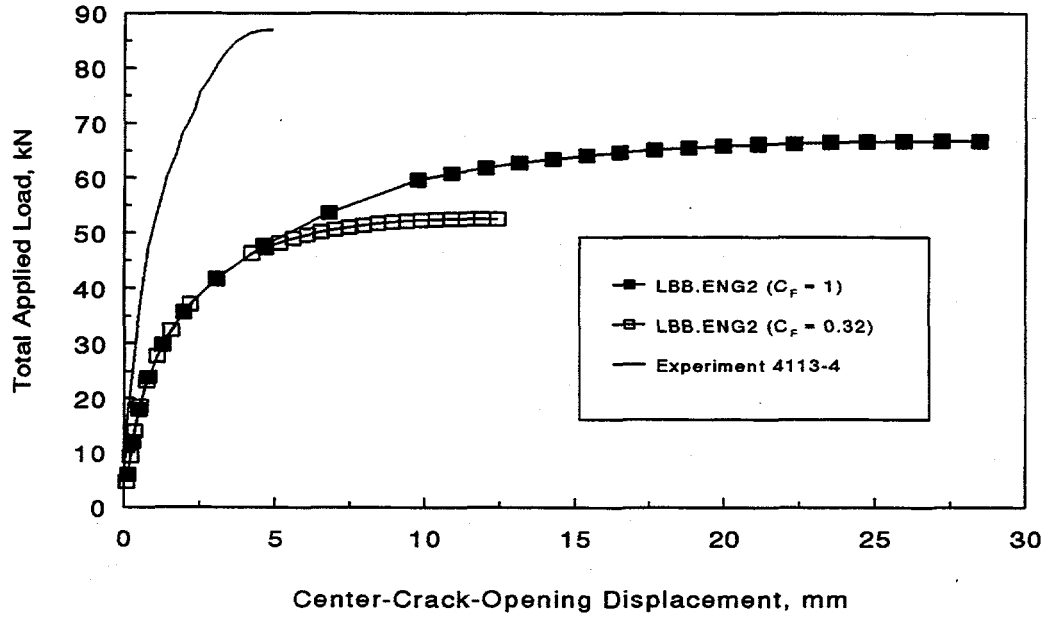

Figure 3.25 Load versus center-crack-opening displacement in Experiment 4113-4

T-6300-F3.25

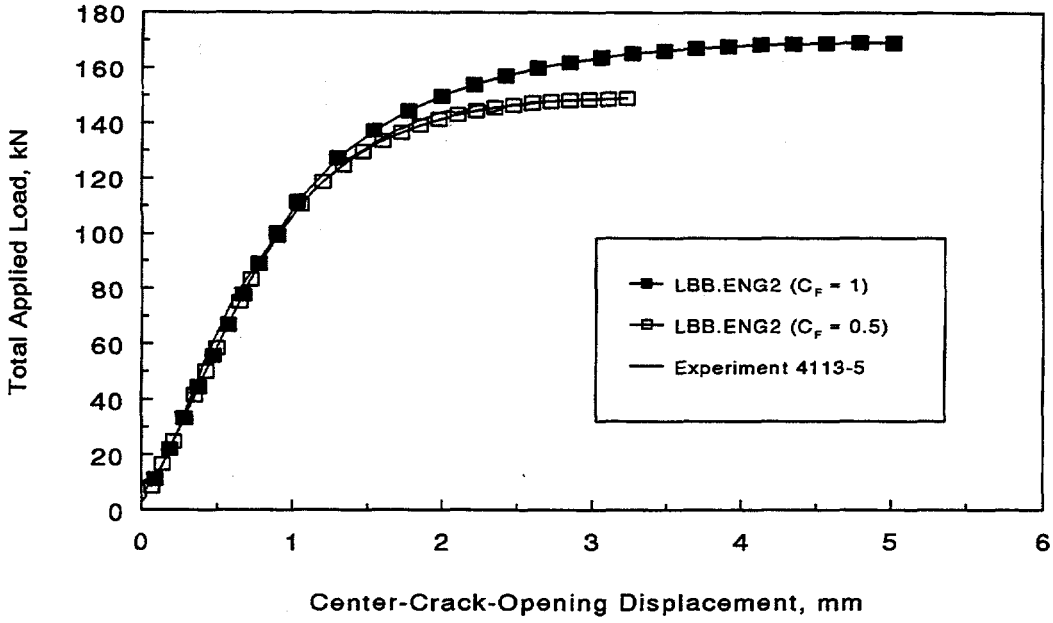

Figure 3.26 Load versus center-crack-opening displacement in Experiment 4113-5
T-6300-F3.26

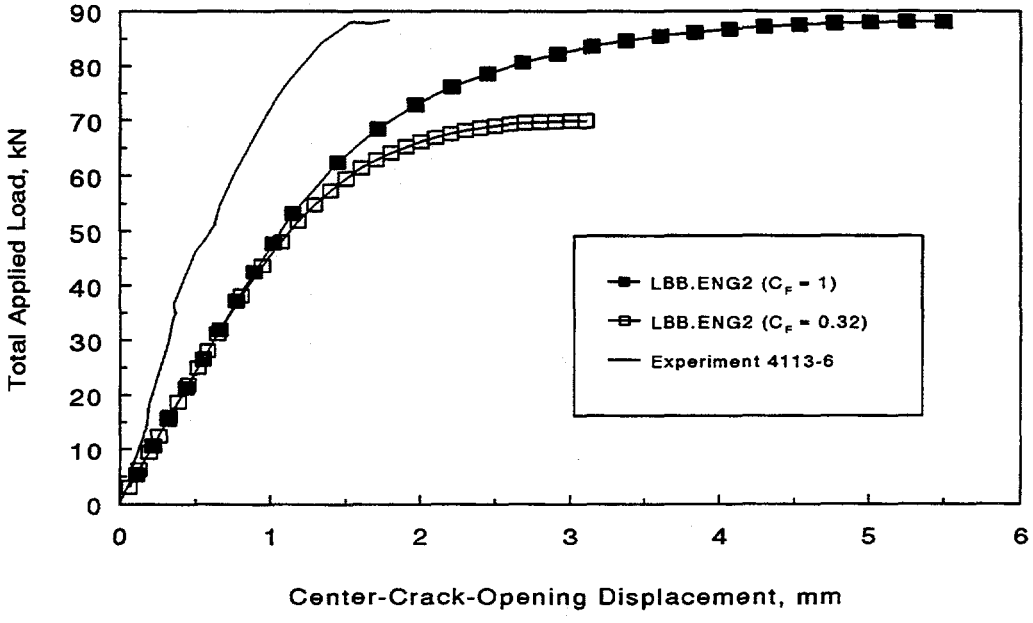

Figure 3.27 Load versus center-crack-opening displacement in Experiment 4113-6
T-6300-F3.27

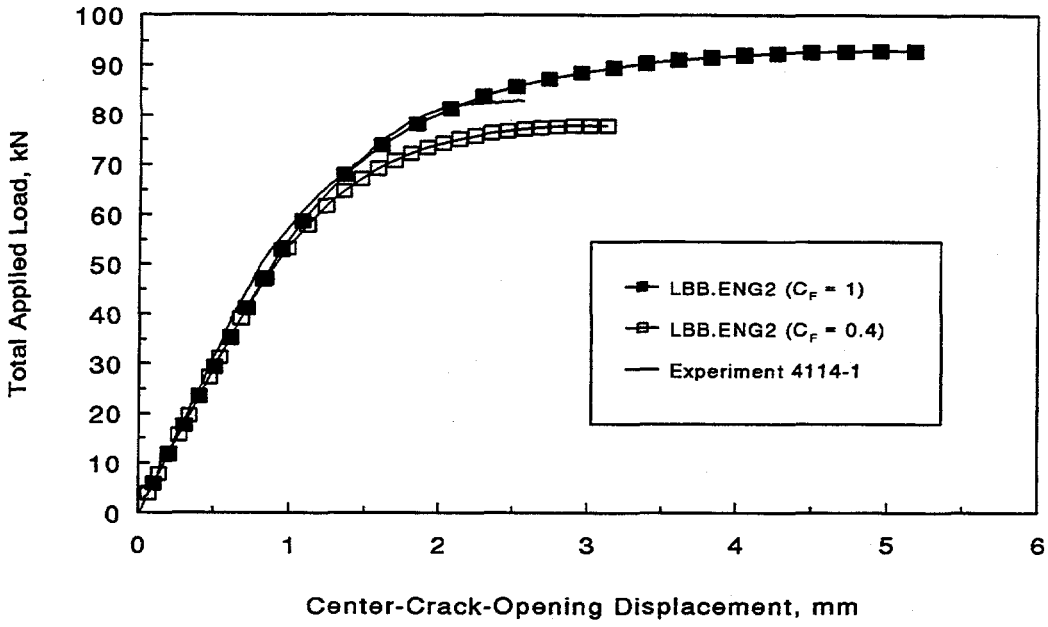

Figure 3.28 Load versus center-crack-opening displacement in Experiment 4114-1
T-6300-F3.28

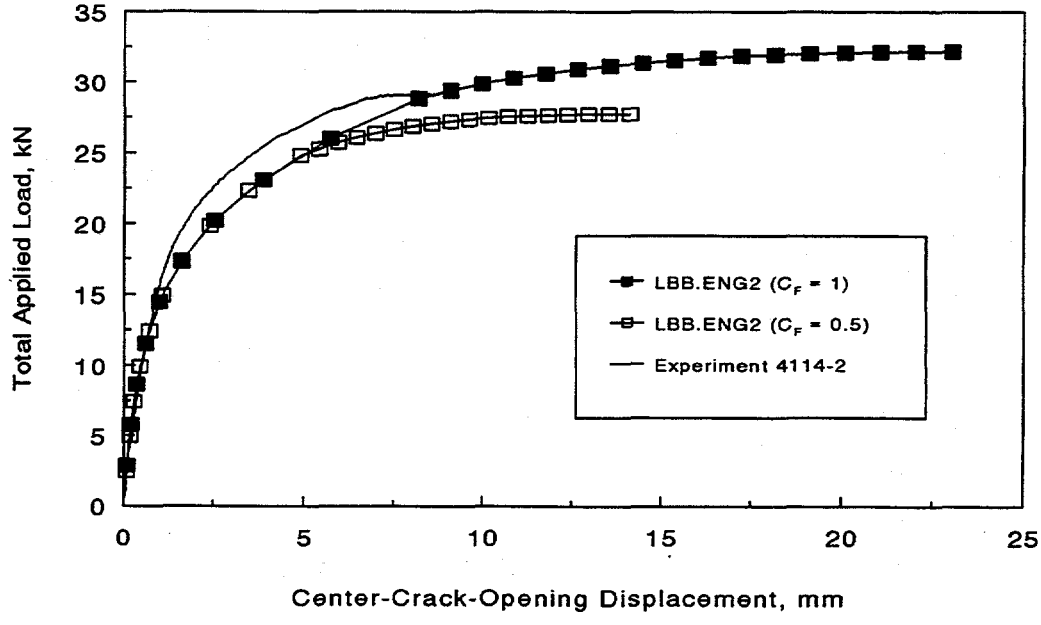

Figure 3.29 Load versus center-crack-opening displacement in Experiment 4114-2
T-6300-F3.29

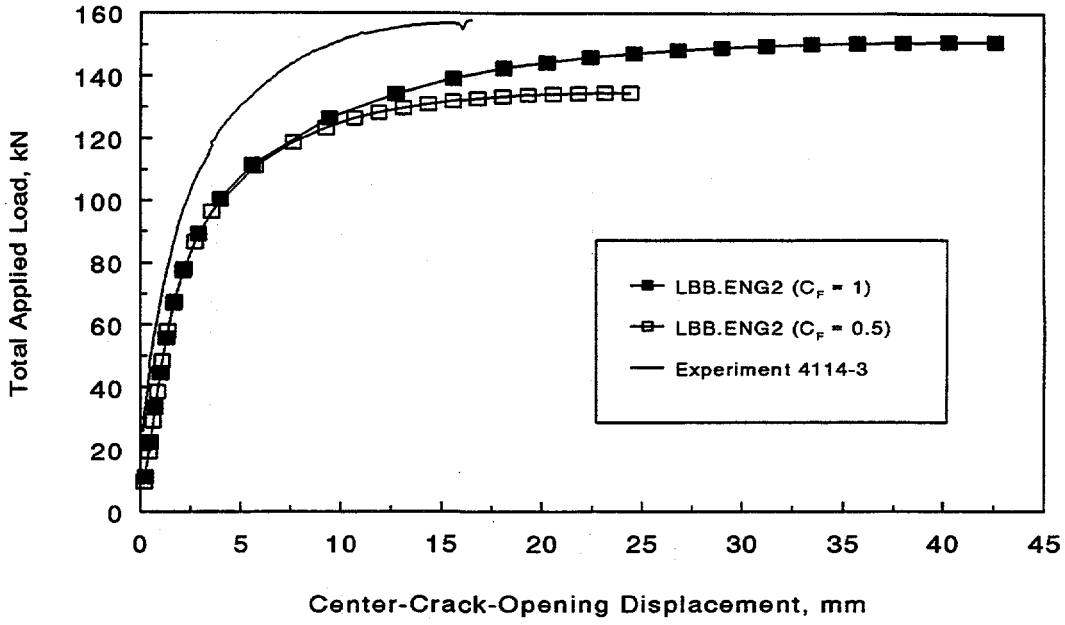

Figure 3.30 Load versus center-crack-opening displacement in Experiment 4114-3

T-6300-F3.30

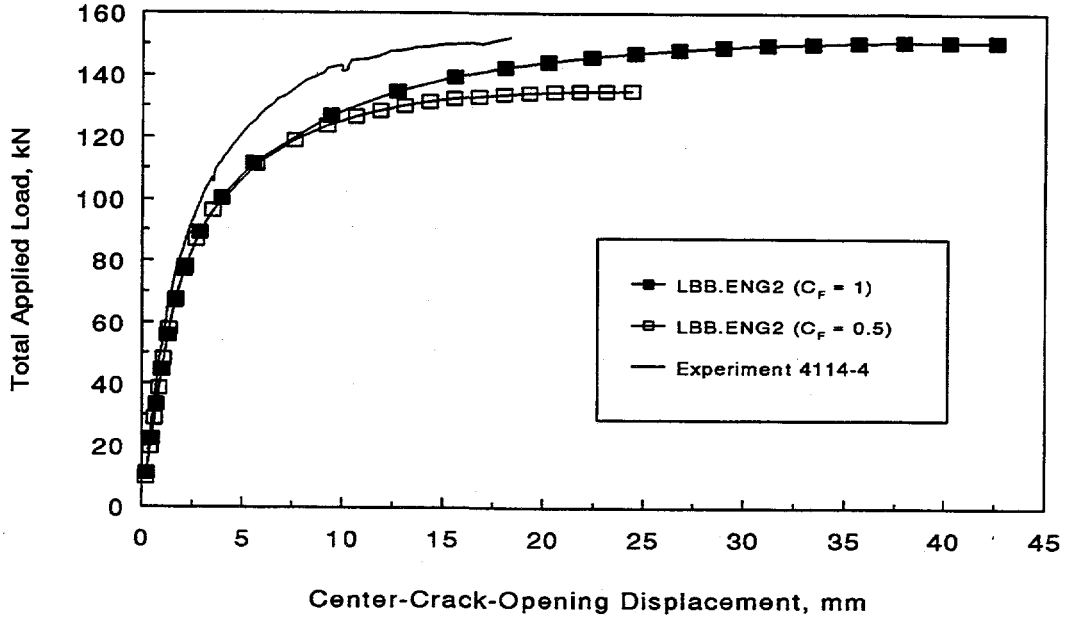

Figure 3.31 Load versus center-crack-opening displacement in Experiment 4114-4

T-6300-F3.31

either case of J_M-R curves, overestimates the COD at all load levels. This can be qualitatively explained by noting that for a complex-cracked pipe, an effective pipe thickness, $t^* = t - d$ was used in the estimation formulas for simple through-wall-cracked pipes. Consequently, the "equivalent" through-wall-cracked pipe assumed in an estimation model would have lower stiffness than the actual complex-cracked pipe. Hence, the predicted crack-opening displacements were larger than the experimental results. Obviously, when the surface cracks become deeper (e.g., Experiments 4113-2, 4113-4, and 4113-6), the magnitudes of these overestimates of the COD will also become larger and can be significantly different from the experimental results, as exhibited in Figures 3.23, 3.25, and 3.27. Again, this general loss of accuracy can be attributed to the over-simplification in the estimation formulas for through-wall-cracked pipes used for predicting the COD of complex-cracked pipes.

Figure 3.32 exhibits several plots of center COD at maximum load for various experiments considered in this study. As before, the results from the LBB.ENG2 method and the experimental data were compared. They all consistently show that the use of a J_M-R curve from C(T) specimens, reduced by a relevant constraint factor from Figure 2.9, results in a better prediction of experimental results than that based on J_M-R curve directly from the C(T) specimen tests.

3.2.4 Welded Pipe Analysis

In this section, the results of crack-opening-area analyses of five pipe fracture experiments on through-wall-cracked pipes with the cracks in welds are presented. The pipe tests are Experiments 1.1.1.23, 1.1.1.24, 4141-1, 4141-5, and 4111-5, all of which were performed at pure bending

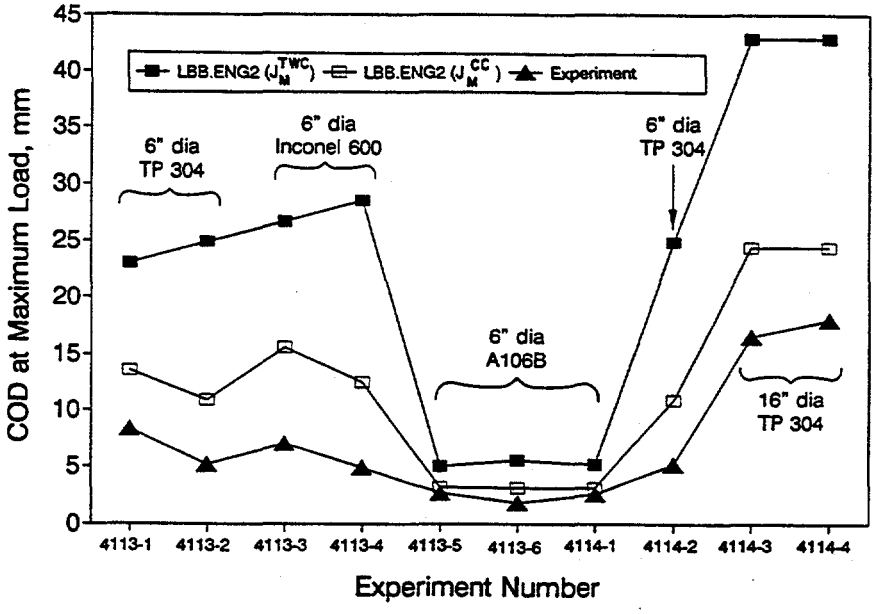

Figure 3.32 COD at maximum load for various complex-cracked pipe experiments

SC-SA-5/92-F7.14

without any internal pressure. The materials in the Experiments 1.1.1.23 and 1.1.1.24 were TP316L stainless steel submerged-arc weld and A333 Grade 6 submerged-arc weld, respectively. The crack lengths in Experiments 1.1.1.23 and 1.1.1.24 were short and were 6.25 and 7.9 percent of the pipe circumference, respectively. The fracture data for these two experiments were developed in the Short Cracks in Piping and Piping Welds Program (Ref. 3.1). In Experiments 4141-1 and 4141-5, the materials were TP304 stainless steel submerged-arc weld. However, the weld in Experiment 4141-5 was solution-annealed to eliminate residual stresses. The material for Experiment 4111-5 was TP316L shielded-metal arc weld. The crack lengths in Experiments 4141-1, 4141-5, and 4111-5 were long; 37.1, 38.3, and 37 percent of the pipe circumference, respectively. The fracture data for these three experiments were developed in the Degraded Piping Program (Ref. 3.2).

Table 3.5 shows a summary of the pipe geometries and test results for these five experiments on welded pipes. Tensile strength properties of the materials, including the power-law fit parameters for both base and weld metals, are provided in Table 3.6. The fracture toughness properties of the welds in terms of power-law parameters are given in Table 3.7.

Figures 3.33 through 3.37 show the comparisons of predicted load versus COD results with experimental data from the above pipe tests. A wide variety of estimation models were used to perform such comparisons. In Experiment 1.1.1.23 ($2a/\pi D_m$ = 6.25 percent), the Paris/Tada, the LBB.NRC, the LBB.ENG2, and the LBB.ENG3 methods underpredicted the experimental COD for most of the load ranges. The GE/EPRI methods with the original and the Battelle-modified influence functions overpredicted the COD significantly at both small and large load levels. In Experiment 1.1.1.24 ($2a/\pi D_m$ = 7.9 percent), all of the estimation methods, except the GE/EPRI method, underpredicted experimental results for most of the load ranges as also observed for Experiment 1.1.1.21 with a base-metal crack. However, for this experiment, the agreement between the predicted results from the GE/EPRI method and experimental data were very good up to initiation load. (Note, the measured initiation load for the Experiment 1.1.1.24 was 1,110 kN [249,500 lb]).

In Experiments 4141-1, 4141-5, 4111-5, all of which have long cracks, the comparisons of the predicted load versus COD relation with experimental data show mixed trends. The predicted results

Table 3.5 Summary of pipe geometry and results for 5 through-wall-cracked welded pipe experiments subjected to pure bending

Pipe Test No.	Outer Diameter, mm	Pipe Thickness, mm	Pipe Material	$2a/\pi D_m$[(a)]	Inner Span, m	Outer Span, m	Initiation Load, kN	Maximum Load, kN
1.1.1.23	711	30.2	TP316L SAW	0.0625	3.35	11.58	1274	1489
1.1.1.24	612	31.3	A333 Gr6 SAW	0.079	3.35	11.58	1110	1660
4141-1	168	14.3	TP304 SAW	0.371	1.20	3.25	58	74
4141-5	168	14.1	TP304 SA-SAW	0.383	1.20	3.25	46	61
4111-5	720	30.2	TP316 SMAW	0.370	3.35	11.58	471	611

(a) 2a = through-wall crack length at mean pipe diameter; D_m = mean pipe diameter

Table 3.6 Tensile strength properties of pipe materials for through-wall-cracked welded pipe experiments subjected to pure bending

	Base Metal Properties[a]					Weld Metal Properties[a]				
Pipe Test No.	Elastic Modulus (E), GPa	Yield Stress (σ_y), MPa	Ultimate Stress (σ_u), MPa	α	n	Elastic Modulus (E), GPa	Yield Stress (σ_y), MPa	Ultimate Stress (σ_u), MPa	α	n
1.1.1.23	183	143	427	8.71	3.26	183	366	503	1.63	10.94
1.1.1.24	200	229	525	2.14	4.36	200	412	578	1.41	9.65
4141-1	183	138	449	9.69	3.13	183	324	466	2.28	11.03
4141-5	183	138	449	9.69	3.13	183	194	465	3.42	4.84
4111-5	183	229	501	4.42	4.96	183	282	485	1.84	7.31

(a) Stress-strain curve is represented by: $\epsilon/\epsilon_0 = \sigma/\sigma_0 + \alpha(\sigma/\sigma_0)^n$, where $\sigma_0 = \sigma_y$, $\epsilon_0 = \sigma_0/E$

Table 3.7 Fracture toughness properties of pipe materials for through-wall-cracked welded pipe experiments subjected to pure bending

	Extrapolated Weld J-R Curve Parameters[a]		
Pipe Test No.	J_{Ic}, kJ/m^2	C, kJ/m^2	m
1.1.1.23	60	147.9	0.769
1.1.1.24	59	124.1	0.72
4141-1	99	164.1	0.703
4141-5	170	165.8	0.778
4111-5[b]	109	147.9	0.769

(a) J_D-R curve is represented by: $J = J_{Ic} + C(\Delta a/r)^m$, where r = 1 mm and Δa is in mm
(b) Only J_{Ic} was measured and available from the material characterization test. C and m are assumed to be the same as for Experiment 1.1.1.23.

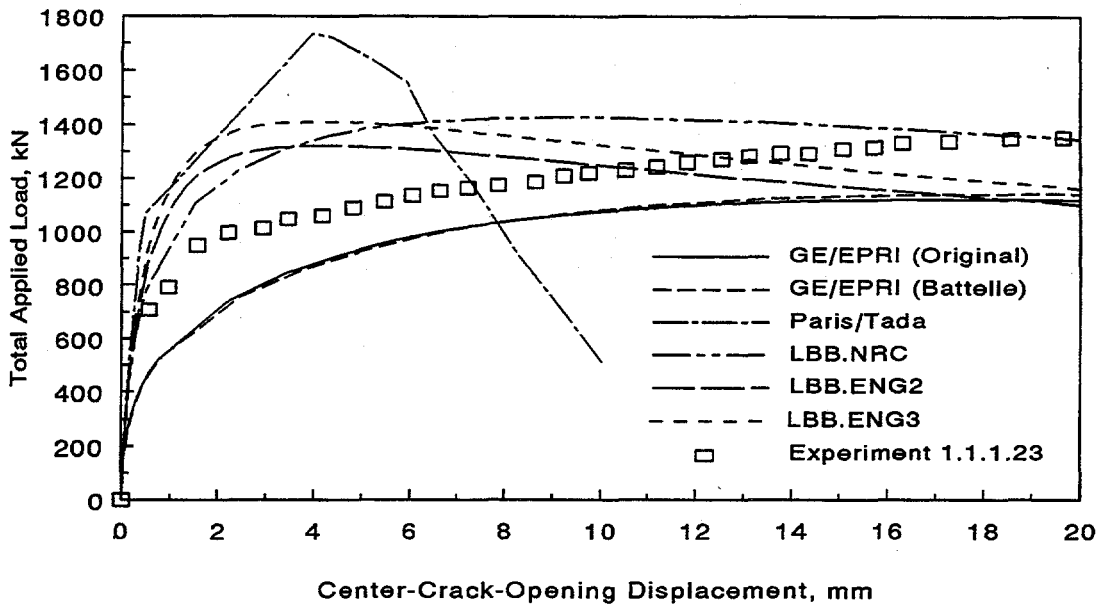

Figure 3.33 Load versus center-crack-opening displacement in Experiment 1.1.1.23
T-6300-F3.33

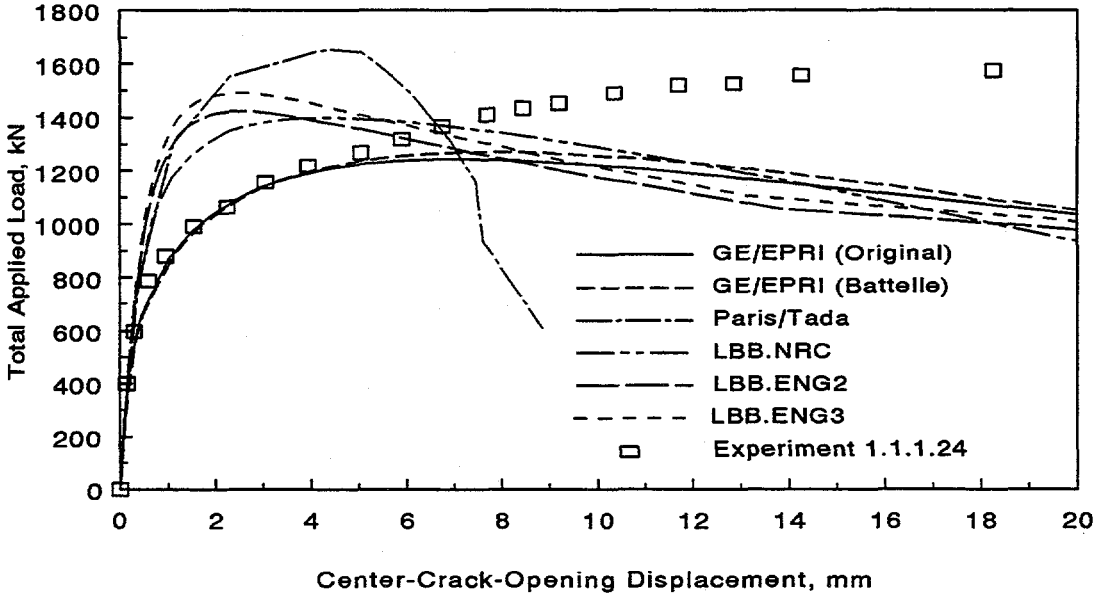

Figure 3.34 Load versus center-crack-opening displacement in Experiment 1.1.1.24
T-6300-F3.34

for Experiments 4141-1 and 4141-5 (see Figures 3.35 and 3.36) are consistent in the sense that most estimation methods overpredicted COD except the Paris/Tada method which exhibited almost linear (and stiff) behavior, thus significantly underpredicting crack-opening for a given load. For Experiment 4111-5 (see Figure 3.37), all methods underpredicted COD for most of the load ranges. Among the predictive schemes, the LBB.ENG2 and GE/EPRI methods produced results closer to the experimental data.

3.2.4.1 J_D-R Curves from Pipes and C(T) Specimens for Experiments 4141-1 and 4141-5

In order to explain why there was so much underprediction in loads for the Experiments 4141-1 and 4141-5, several η-factor analyses were conducted to generate pipe J_D-R curves using load-displacement records from the actual pipe experiments (Refs. 3.8 and 3.9). The objective was to determine the adequacy of J_D-R curves from 1T C(T) specimens. Further details on the η-factor analysis can be found in Reference 3.8.

Figure 3.38 shows the comparisons of both as-welded (Experiment 4141-1) and solution-annealed (Experiment 4141-5) SAW J-R curves obtained from 1T C(T) specimens and 152.4-mm (6-inch) diameter pipes via η-factor analyses. Two points are worthy of discussion regarding the SAW pipe data. First, the J_D-R curves from both pipe experiments were greater than those from the C(T) specimens. This is believed to be mainly due to the effects of the weld thickness and weld procedure. For instance, the 1T C(T) specimens were 25.4-mm (1-inch) thick. The 152.4-mm (6-inch) nominal diameter pipes, however, were 14.3-mm (0.562-inch) or 14.1-mm (0.555-inch) thick. The weld procedure involved depositing two layers using the TIG weld process, then depositing two layers

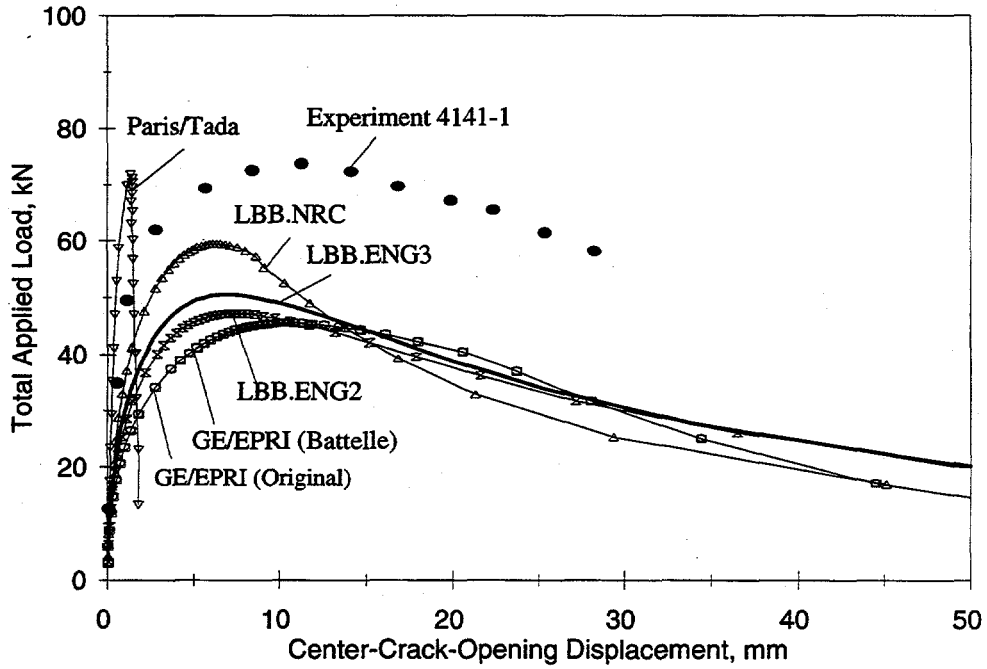

Figure 3.35 Load versus center-crack-opening displacement in Experiment 4141-1
T-6300-F3.35

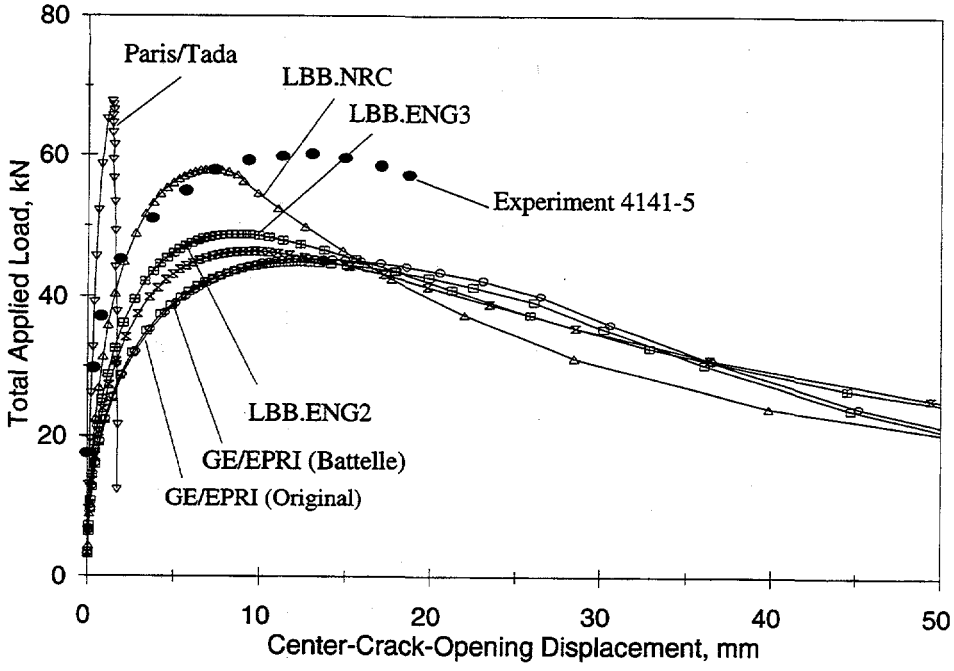

Figure 3.36 Load versus center-crack-opening displacement in Experiment 4141-5
T-6300-F3.36

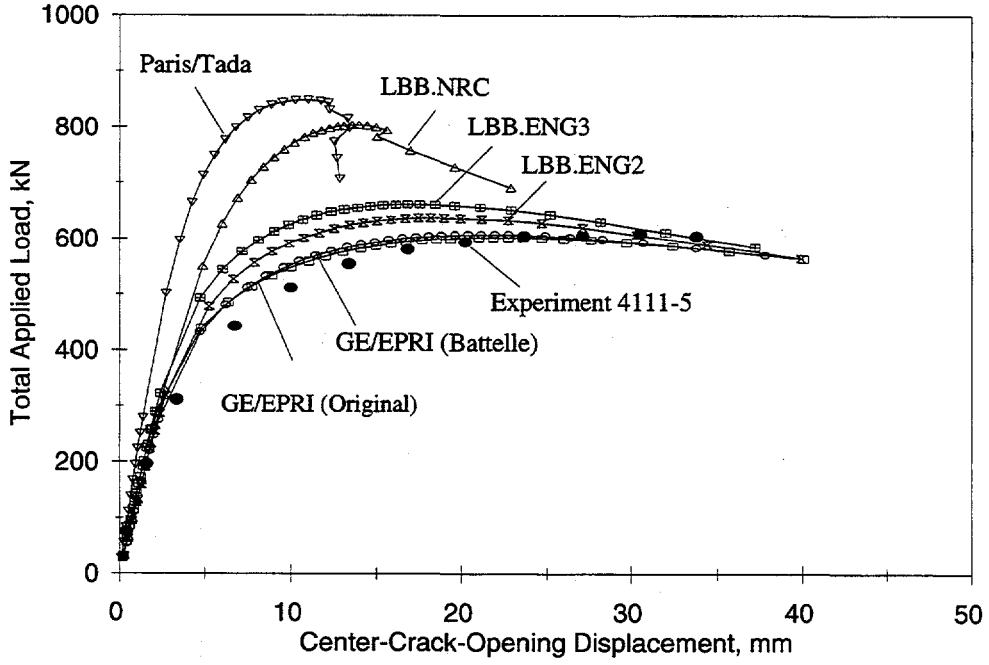

Figure 3.37 Load versus center-crack-opening displacement in Experiment 4111-5
T-6300-F3.37

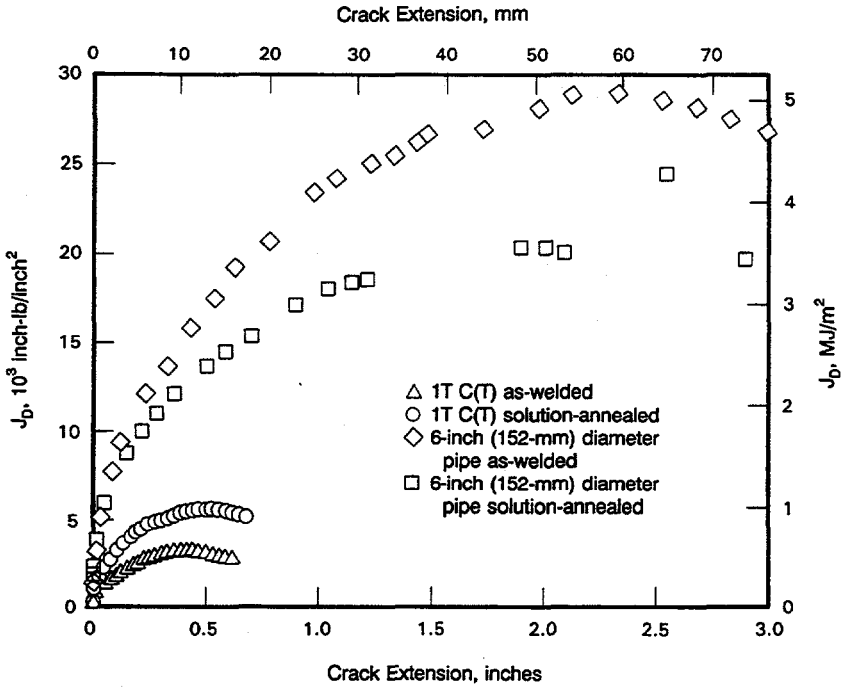

Figure 3.38 Comparisons between J-R curves from 1T C(T) specimens and 152.4-mm (6-inch) nominal diameter pipes via η-factor analysis

T-6300-F3.38

using the SMAW process, with the remainder of the weld joint filled using the SAW process. Hence with the thinner pipes, the amount of SAW metal was significantly less than in the 25.4-mm (1-inch) thick weldments of 1T C(T) specimens. Since the TIG weld metal is much higher in toughness (Ref. 3.8), the composite toughness of the 152.4-mm (6-inch) diameter pipes with 14.3-mm (0.562-inch) or 14.1-mm (0.555-inch) thickness was much higher. Perhaps this explains why the estimation schemes with the results shown in Figures 3.35 and 3.36 significantly underpredicted the loads and overpredicted the crack-opening.

The other point is that the J-R curve for the pipe with the SAW that was solution-annealed is lower than the as-welded SAW pipe J-R curve. This trend is the opposite to the C(T) specimen results (see Figure 3.38). For a typical η-factor analysis, the plastic component of the J-integral is proportional to the area under the load-displacement record. From Figure 3.39, showing the load versus load-point displacement records for the above two experiments, the area under the load-displacement record for as-welded pipe (Experiment 4141-1) is larger than that for solution-annealed pipe (Experiment 4141-5). Hence, the value of the J-integral, exhibited in pipe J_D-R curves, is higher for the as-welded pipe. Nevertheless, additional C(T) specimen data for various sizes and thicknesses would be helpful in clarifying this apparent anomaly.

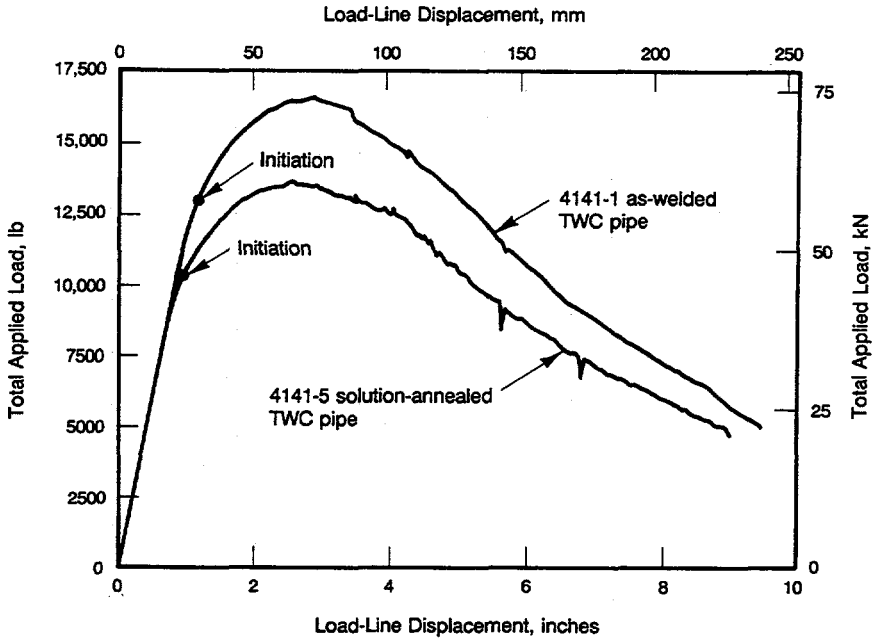

Figure 3.39 Total load versus load-line displacement record from Experiments 4141-1 and 4141-5 on the 152-mm (6-inch) nominal diameter TP304 stainless steel TWC as-welded and solution-annealed SAW pipes (Ref. 3.8)

T-6300-F3.39

3.2.4.2 Crack-Opening Predictions Using J_D-R Curves from Pipes

Following the comparisons between C(T) and pipe J-R curves, the estimation analyses were conducted again using the pipe J_D-R curves from Figure 3.38 to determine the crack-opening displacements for Experiments 4141-1 and 4141-5. The results are shown in Figures 3.40 and 3.41. Predictions made using the pipe J_D-R curves when compared with the experimental results appear to be much better than those using C(T) specimen J_D-R curves. Most estimation methods provided reasonably accurate predictions and among the five estimation methods considered here, LBB.ENG3 and LBB.NRC are the most accurate methods for computing crack-opening displacements of as-welded and solution-annealed pipes when the fracture toughness properties are generated from large-scale pipe tests. It appears that when the strength characteristics of weld metal are considered (e.g., in LBB.ENG3 method), the predictive capability of the LBB.ENG2 method can be improved.

3.2.5 Bimetallic Pipe Weld Analysis

The bimetallic pipe weld in Experiment 1.1.1.28 was part of a 930-mm (36.6-inch) outer diameter, cold-leg piping systems from a cancelled Combustion Engineering nuclear power plant. The welds joined the ferritic cold-leg pipe to stainless steel safe ends which were to be welded to stainless steel pump housings. The carbon steel pipe material was A516 Grade 70. The safe ends were fabricated from SA182 F316 stainless steel (forged TP316 stainless steel). The welds were fabricated by first

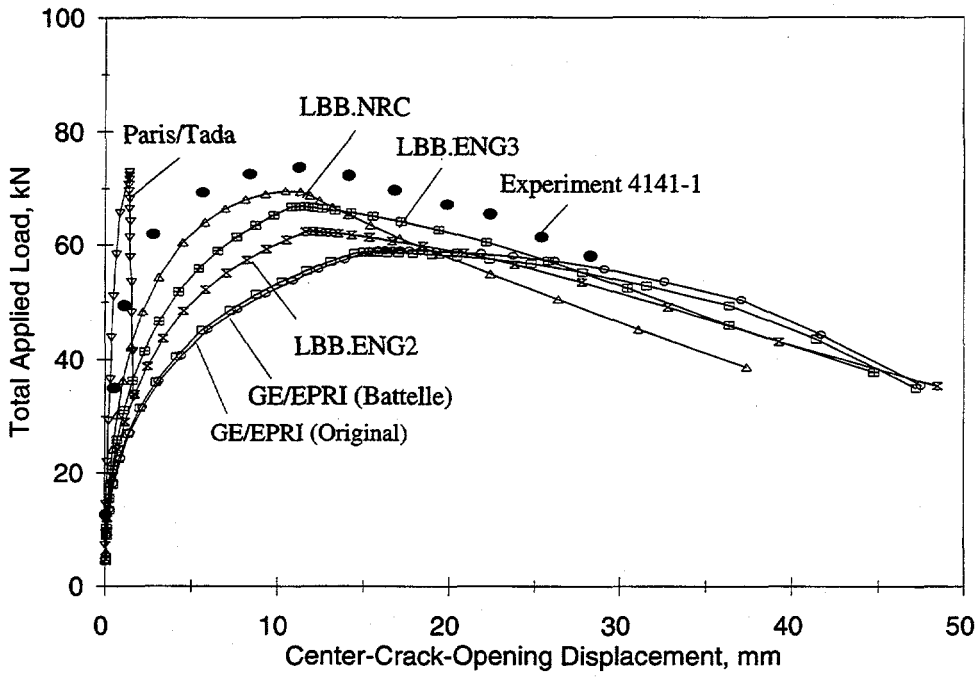

Figure 3.40 Load versus center-crack-opening displacement in Experiment 4141-1 using pipe J_D-R curve

T-6300-F3.40

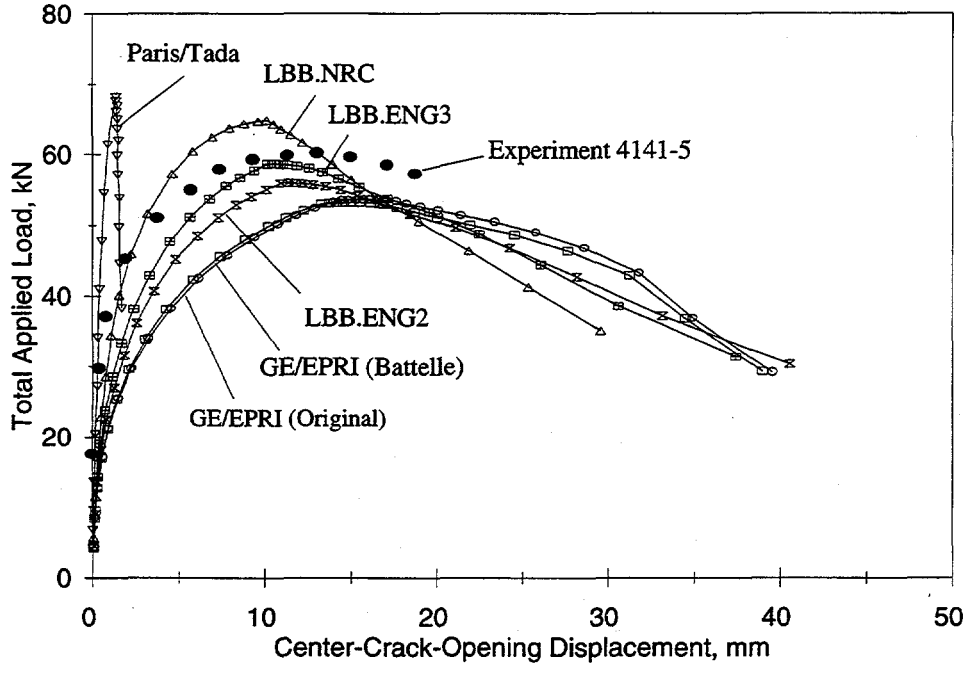

Figure 3.41 Load versus center-crack-opening displacement in Experiment 4141-5 using pipe J_D-R curve

T-6300-F3.41

buttering the beveled end of the carbon steel pipe with an ENiCrFe-3 (Inconel 182) electrode. The welds joining the buttered pipes and the stainless steel safe ends were then completed using a shielded-metal-arc weld process, using Inconel 182 weld rod.

The pipe in Experiment 1.1.1.28 had a wall thickness of 81.3 mm (3.20 inches). A through-wall-crack, with length 35.9 percent of pipe circumference, was placed at the interface between the buttered A516 Grade 70 carbon steel pipe and the Inconel 182 weld. Figure 3.42 shows the top and cross-sectional views of the through-wall-crack geometry in Experiment 1.1.1.28. The tensile properties for the A516 Grade 70 carbon steel, SA182 F316 stainless steel, and Inconel 182 weld are given in Table 3.8. The J-R curve properties for A516 Grade 70 carbon steel, SA182 F316 stainless steel, and A516 Grade 70/Inconel 182 fusion-line region are also given in Table 3.8.

To determine the crack-opening for the bimetallic weld specimen, three sets of analyses were conducted using the tensile properties of the A516 Grade 70 carbon steel pipe, the SA182 F316 stainless steel safe end, and the Inconel 182 weld. In each set of analyses, the same J-R curve of A516 Grade 70/Inconel 182 Weld fusion-line region was used. A total of five estimation methods were applied to predict the crack-opening displacement for Experiment 1.1.1.28. Figures 3.43, 3.44, and 3.45 show the comparisons of predicted results in terms of load versus center COD plots with the experimental data. The results from these figures suggest that the when the tensile properties of SA182 F316 stainless steel and Inconel 182 weld were used, the maximum load from the experiment would be underpredicted (except the Paris/Tada method) and overpredicted, respectively, by the estimation methods considered here. Correspondingly, using the tensile properties of these two

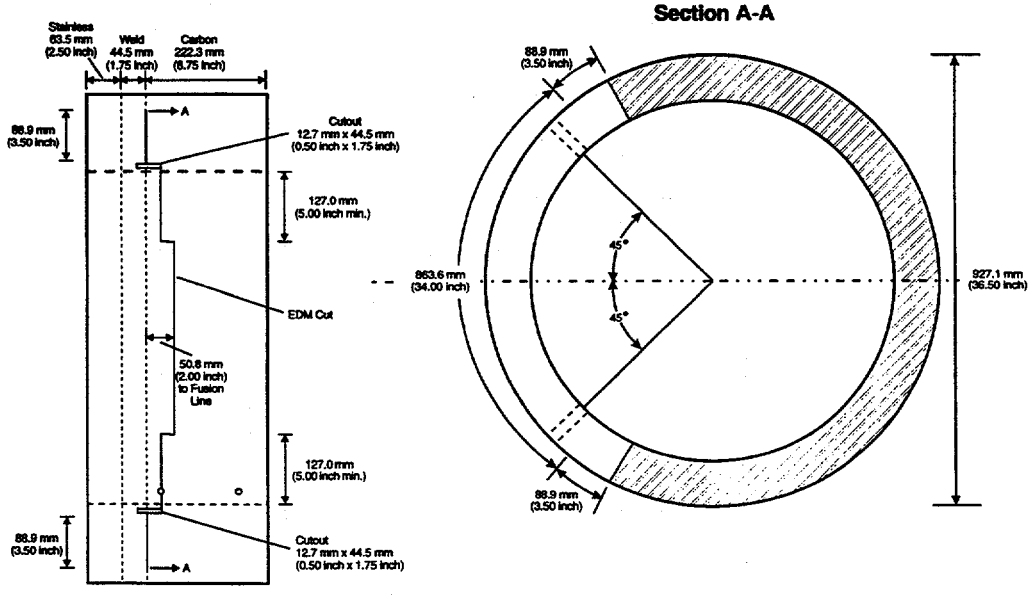

Figure 3.42 Sketch of through-wall-crack geometry used for bimetallic weld pipe Experiment 1.1.1.28

T-6300-F3.42

Table 3.8 Tensile strength and fracture toughness properties of pipe materials in a bimetallic pipe weld experiment subjected to pure bending

Pipe Material	Elastic Modulus (E), GPa	Yield Stress (σ_y), MPa	Ultimate Stress (σ_u), MPa	Ramberg-Osgood Coefficients[a]		Extrapolated J-R Curve Parameters[b]		
				α	n	J_{Ic}, kJ/m^2	C, kJ/m^2	m
A516 Gr. 70	200	235	496	2.07	5.20	185	-[c]	-[c]
F316	178	157	415	9.89	3.67	2,233	-[c]	-[c]
Inconel 182	178	372	599	3.11	8.47	ND[d]	ND[d]	ND[d]
A516 Gr.70/ Inconel 182	ND[d]	ND[d]	ND[d]	ND[d]	ND[d]	684	979.7	0.232

(a) Stress-strain curve is represented by: $\epsilon/\epsilon_0 = \sigma/\sigma_0 + \alpha(\sigma/\sigma_0)^n$, where $\sigma_0 = \sigma_y$, $\epsilon_0 = \sigma_0/E$.
(b) J_D-R curve is represented by: $J = J_{Ic}$ when $\Delta a = 0$; $J = C(\Delta a/r)^m$, when $\Delta a > 0$, where r = 1 mm and Δa is in mm.
(c) The power-law fit was not made for these materials.
(d) Not determined.

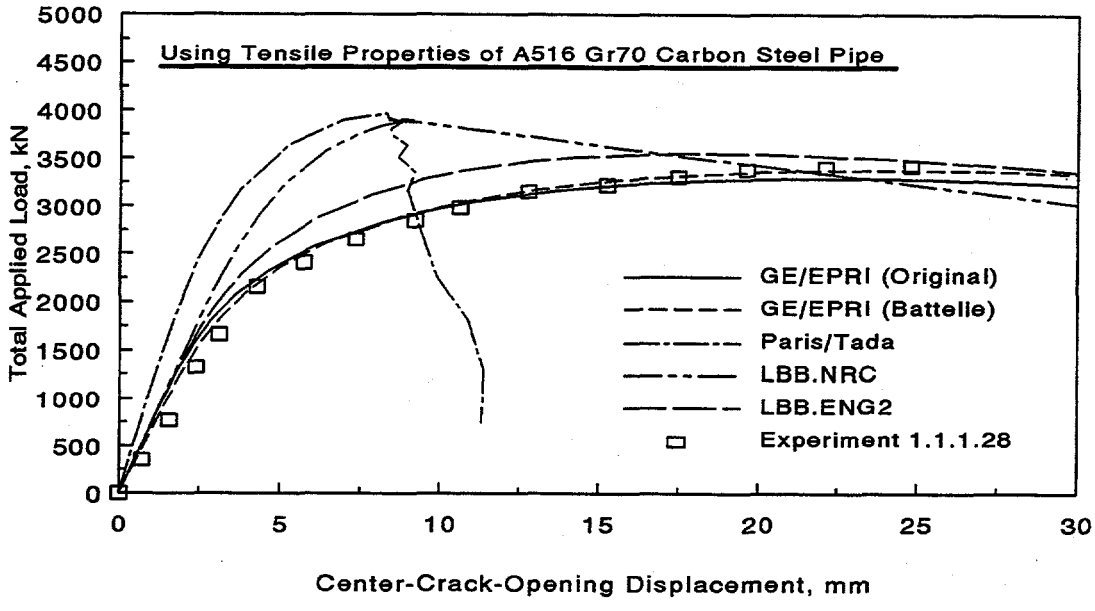

Figure 3.43 Load versus center-crack-opening displacement in Experiment 1.1.1.28 using tensile properties of A516 Grade 70 carbon steel pipe

T-6300-F3.43

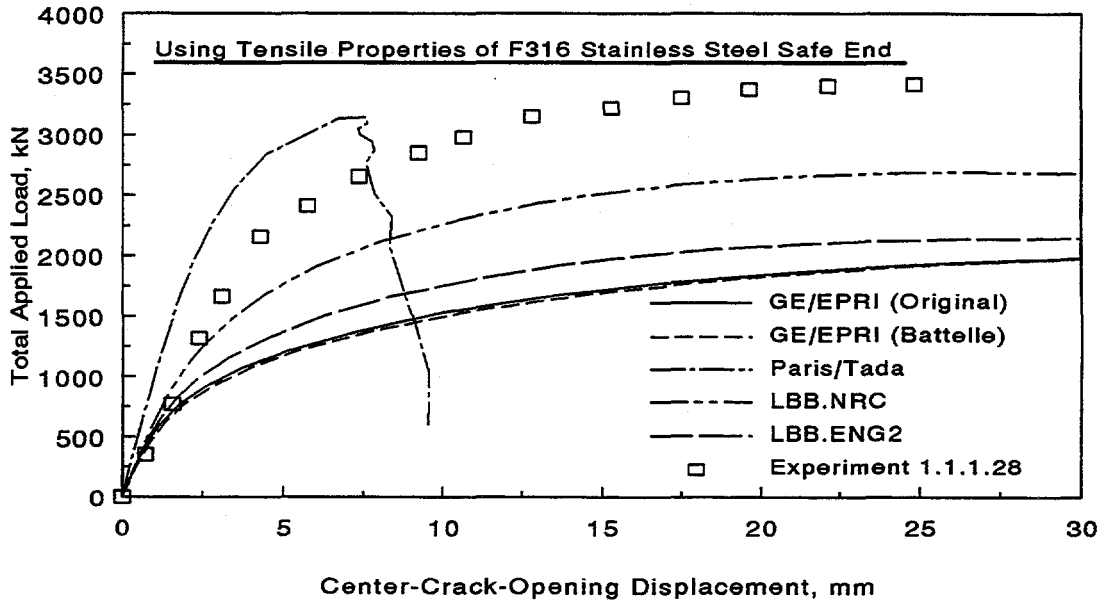

Figure 3.44 Load versus center-crack-opening displacement in Experiment 1.1.1.28 using tensile properties of F316 stainless steel safe end

T-6300-F3.44

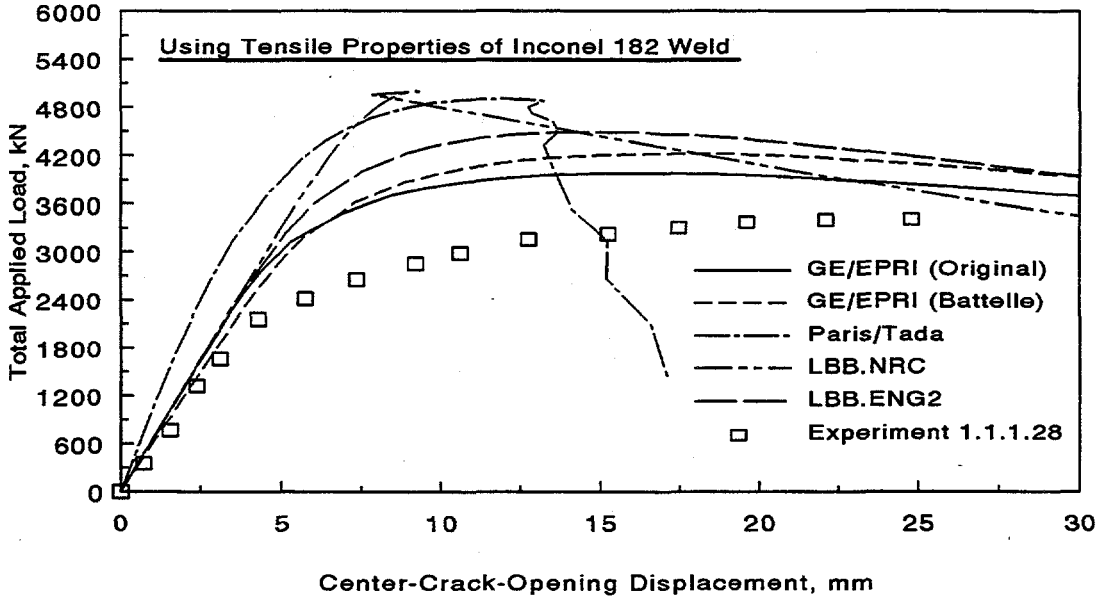

Figure 3.45 Load versus center-crack-opening displacement in Experiment 1.1.1.28 using tensile properties of Inconel 182 weld

T-6300-F3.45

materials, the experimental COD for a given applied load would be overpredicted (except the Paris/Tada method) and underpredicted, respectively. However, when the tensile properties of A516 Grade 70 were used, the predicted loads and COD by the estimation methods, particularly by the LBB.ENG2 and the GE/EPRI methods, were in good agreement with the corresponding experimental data. Further details on fracture analysis with explicit predictions of initiation and maximum loads including the ASME Section XI flaw evaluation for this bimetallic-weld pipe experiment are published in a separate topical report (NUREG/CR-6297).

3.2.6 Performance Evaluation of Predictive Analyses

3.2.6.1 Crack-Opening Predictions for Typical LBB Applications

In Sections 3.2.3 through 3.2.5, the experimental results were compared with the predicted center-crack-opening displacements by various methods in graphical form for loads up to initiation or maximum loads in many cases. In general, for LBB applications, one is more interested in the accuracy of the models in the elastic load range than at crack initiation load, maximum load, or beyond maximum load. Crack-opening predictions beyond crack initiation may be of interest to determine the jet forces or the decompression behavior. Such results were not quantified in this report other than the graphs supplied in Sections 3.2.3 to 3.2.5. However, it could be seen qualitatively that the Paris/Tada method did not work very well once the initiation or maximum loads were achieved. The reason for this behavior was not investigated.

Since stresses in LBB or leak-rate analyses for piping under normal operating loads are generally thought to be in the elastic range, we have statistically qualified the accuracy of the various methods in this region. To simplify this evaluation, we defined the linear-elastic region to occur when the applied load was 40 percent of the maximum experimental load or less. According to the ASTM guidelines for J-R curve testing, 40 and 50 percent of the limit load using yield strength as the collapse stress are currently used for fatigue precracking of C(T) and bend specimens (Ref. 3.10). Hence, at 40 percent of the maximum experimental load, the cracked pipes should experience primarily linear-elastic behavior with very little plasticity.

Figure 3.46 shows a schematic of load versus center-crack-opening displacement for a through-wall-cracked pipe. For LBB applications, it is generally desired that an analysis method would underpredict the maximum load slightly. It is also desirable to underpredict the COD in the elastic range. This is because, for a given leak rate, if the COD is underpredicted then the crack length for the crack stability analysis is overpredicted. Therefore, the final maximum load in the crack stability analysis will underpredict the actual maximum load.

In the analyses performed in Sections 3.2.3 to 3.2.5, the Ramberg-Osgood curve was fit to the stress-strain data using a fit of the engineering stress-strain curve from 1 percent strain to the strain at 80 percent of the ultimate strength. This was found to be a good fitting procedure for the prediction of crack initiation and maximum loads in a parallel study that is described in "Assessment of Short Through-Wall Circumferential Cracks in Pipes - Experiments and Analyses," NUREG/CR-6235. In work by others, the Ramberg-Osgood model is sometimes fitted in the low-strain regions for the purpose of leak-rate analyses. The sensitivity of crack-opening predictions to this fitting procedure is discussed further in Section 4 of this report.

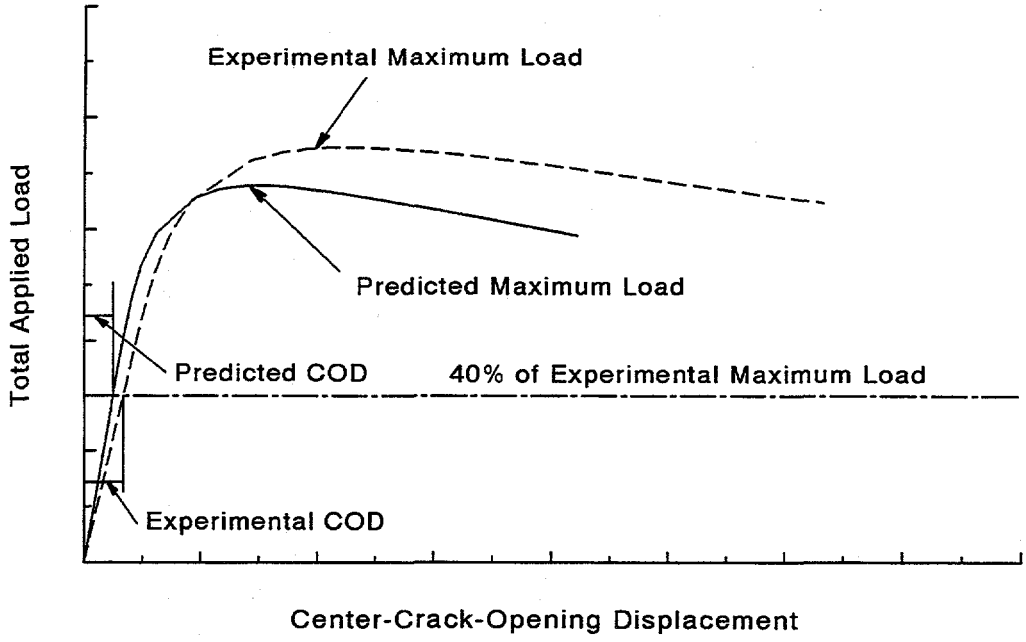

Figure 3.46 Schematic comparison of predicted and experimental load versus center-crack-opening displacement in a pipe (ideally COD and load are underpredicted for LBB analyses)

Finally, it should also be noted that in these comparisons of crack-opening displacements, the estimation methods predict the crack-opening at the mid-thickness, whereas the experimental data (except the IPIRG-2 Experiment 1-8) have the crack-opening measurements slightly above the outside diameter of the pipe. No corrections were made for this difference since that would involve considerable additional effort.

3.2.6.2 Statistics of Predicted Crack-Opening Ratio by Various Methods

Standard statistical analyses were performed to assess the accuracy of the predictive models in estimating the center-crack-opening displacement for pipes analyzed in this study. The statistics involved calculation of the mean and coefficient of variation (COV) [COV is equal to the ratio of standard deviation to the mean] of the ratio between the experimental and predicted values of the center-crack-opening displacement when the applied load is 40 percent of the experimental maximum load. This ratio is denoted as the predicted crack-opening ratio for further discussions in this report. It is desired to have this ratio greater than one to ensure smaller values of predicted crack-opening displacement than the experimental results. It should also be noted that a margin of 10 on leak-rate is generally applied in LBB analyses to account for various uncertainties including inaccuracy in crack-opening predictions (Ref. 3.11)

Simple Through-Wall-Cracked Pipes. Table 3.9 shows the mean and COV of the predicted crack-opening ratio for fifteen through-wall-cracked pipes subjected to various loading conditions. From the results of this table, when all TWC pipe experiments are considered, all of the predictive models

Table 3.9 Mean and coefficient of variation of the ratio between experimental and predicted values of center-crack-opening displacement by various methods for simple through-wall-cracked pipes under various loading conditions

	Ratio of Center-Crack-Opening Displacement[a]							
	All TWC Pipes (15 Tests)		TWC Pipes Under Pure Bending (11 Tests)		TWC Pipes Under Pure Tension (1 Test)		TWC Pipes Under Bending and Tension (3 Tests)	
Fracture Analysis Methods	Mean	Coefficient of Variation[b], percent	Mean	Coefficient of Variation[b], percent	Mean	Coefficient of Variation[b], percent	Mean	Coefficient of Variation[b], percent
GE/EPRI (Original)	1.01	72.8	0.84	51.7	0.75	-[c]	1.70	69.9
GE/EPRI (NRC/Battelle)	1.02	86.5	0.74	59.5	-[d]	-[c]	1.78	69.8
Paris/Tada	2.96	146	1.60	39.2	-[d]	-[c]	6.59	107
LBB.NRC	1.61	90.9	1.16	47.6	-[d]	-[c]	2.82	79.4
LBB.ENG2	1.16	47.0	1.07	45.5	1.0	-[c]	1.57	41.4
LBB.ENG3	1.18	45.7	1.10	44.1	1.0	-[c]	1.57	41.4

(a) Ratio of center-crack-opening displacement = experimental center COD/predicted center COD; the CODs were measured and calculated at 40 percent of experimental maximum load
(b) Coefficient of variation = (standard deviation/mean) × 100
(c) Not applicable
(d) Not determined

underpredicted the mean value of the COD. The GE/EPRI methods (with the original and newly developed influence functions from this report) predicted experimental COD with very good accuracy in terms of the mean value of the crack-opening ratio, but their predicted COVs were much higher. The differences between the statistics for the GE/EPRI method based on the original influence functions and the present study were not significant. The LBB.ENG2 and LBB.ENG3 methods slightly underpredicted the mean experimental COD with much lower COVs. The LBB.NRC method underpredicted the COD more than the LBB.ENG2 or LBB.ENG3 methods with higher values of COV. Among all methods, the Paris/Tada method underpredicted COD by the largest margin in terms of both mean and COV of the predicted crack-opening ratio.

Table 3.9 provides a further breakdown of statistics for three different loading conditions involving pure bending, pure tension, and combined bending and tension. For pipes under pure bending loads, the LBB.ENG2 and LBB.ENG3 methods slightly underpredicted the experimental COD when the mean values were compared. The LBB.NRC and Paris/Tada methods also underpredicted the COD with the Paris/Tada method underpredicting the most. It is interesting to note that the GE/EPRI methods overpredicted the mean COD for this loading condition.

For a pipe under pure tension from pressure loading, similar trends were exhibited by the GE/EPRI, LBB.ENG2, and LBB.ENG3 methods. The comparisons of the COD predictions by the LBB.ENG2 and LBB.ENG3 methods with the experimental data were excellent.

For pipes under combined bending and tension, all methods considered in this study underpredicted the experimental COD. The qualitative behavior is similar to that exhibited for the results of all pipe experiments discussed earlier. On a quantitative scale, however, the magnitudes of underprediction were much higher regardless of the methods used. Once again, the Paris/Tada method significantly underpredicted the COD.

Table 3.10 shows the statistics of the predicted crack-opening ratio for pipes with short cracks ($\theta/\pi \leq$ 12 percent) and pipes with cracks in the girth welds. The mean results indicate that for pipes with short cracks, the crack-opening would be underpredicted by the Paris/Tada, LBB.NRC, LBB.ENG2, and LBB.ENG3 methods and overpredicted by the GE/EPRI method. A similar trend was found for pipes under pure bending. The results for pipes with cracks in girth welds also reveal a similar qualitative behavior. For the girth weld cracks, the LBB.ENG2 and LBB.ENG3 methods predicted crack-opening displacement with reasonable accuracy with mean ratios close to one.

Complex-Cracked Pipes. Table 3.11 shows the mean and COV of the predicted crack-opening ratio for ten complex-cracked pipes under pure bending. These statistics were developed only for the LBB.ENG2 method with two cases of J-R curves: one using the J-R curve from C(T) specimens and the other using the C(T) specimen J-R curve multiplied by a constraint factor, C_F. As explained in Section 2, the constraint factor (C_F) denotes the ratio of the J-R curve from a complex-cracked pipes to that from a simple through-wall-cracked pipes. This was determined from a suitable database of complex-cracked pipe experiments for a given value of depth-to-thickness (d/t) ratio. The results in Table 3.11 suggest that regardless of the these two J-R curves, the LBB.ENG2 method would overpredict (in terms of the mean value) crack-opening displacement for pipes with complex cracks. This is clearly opposite to the behavior exhibited by this method in analyzing simple through-wall-cracked pipes. Further breakdown of the statistics for shallow cracks ($d/t \leq 0.5$) and deep cracks

Table 3.10 Mean and coefficient of variation of the ratio between experimental and predicted values of center-crack-opening displacement by various methods for simple through-wall-cracked pipes with short cracks and cracks in girth welds

Fracture Analysis Methods	Ratio of Center-Crack-Opening Displacement[a]			
	TWC Pipes with Short Cracks ($\theta/\pi \leq 0.12$) (4 Tests)		TWC Pipes with Cracks in Girth Welds (6 Tests)	
	Mean	Coefficient of Variation[b], percent	Mean	Coefficient of Variation[b], percent
GE/EPRI (Original)	0.74	31.0	0.67	70.4
GE/EPRI (NRC/Battelle)	0.76	36.0	0.62	67.0
Paris/Tada	1.42	37.2	1.61	33.5
LBB.NRC	1.30	21.4	1.04	45.1
LBB.ENG2	1.45	26.8	1.01	58.3
LBB.ENG3	1.47	27.3	1.06	55.3

(a) Ratio of center-crack-opening displacement = experimental center COD/predicted center COD; the CODs were measured and calculated at 40 percent of experimental maximum load

(b) Coefficient of variation = (standard deviation/mean) × 100

Table 3.11 Mean and coefficient of variation of the ratio between experimental and predicted values of center-crack-opening displacement by the LBB.ENG2 method for complex-cracked pipes with shallow and deep surface cracks

	Ratio of Center-Crack-Opening Displacement[a]					
	All CC Pipes (10 Tests)		CC Pipes with Shallow Cracks (d/t ≤ 0.5) (7 Tests)		CC Pipes with Deep Cracks (d/t ≥ 0.5) (3 Tests)	
Fracture Analysis Methods	Mean	Coefficient of Variation[b], percent	Mean	Coefficient of Variation[b], percent	Mean	Coefficient of Variation[b], percent
LBB.ENG2 (Using J_M^{TWC})	0.63	41.5	0.77	24.7	0.33	36.5
LBB.ENG2 (Using J_M^{CC})	0.64	41.7	0.77	25.0	0.33	36.5

(a) Ratio of center-crack-opening displacement = experimental center COD/predicted center COD; the CODs were measured and calculated at 40 percent of experimental maximum load

(b) Coefficient of variation = (standard deviation/mean) × 100

(d/t ≥ 0.5), also shown in Table 3.11, reveals that the estimation method provides better predictions of the experimental COD if the depth of the 360-degree surface crack is smaller. Nevertheless, the LBB.ENG2 predictions for complex-cracked pipes were much larger than the experimental values of the COD. As mentioned before, this overprediction of the LBB.ENG2 method is due to the over-simplification in the estimation formulas for TWC pipes used for predicting COD of complex-cracked pipes. Hence, further developments are necessary to improve crack-opening models for complex-cracked pipes.

In analyzing pipes with a leaking crack that may potentially be a complex crack, it may not be always possible to estimate accurately the depth of the internal surface crack unless detailed nondestructive examination is performed. For such a crack, if the depth of the surface crack is overestimated, the current analysis methods would overpredict crack-opening. Hence, for a given leak rate, this will cause the crack length to be underestimated resulting overprediction of the pipe's maximum load-carrying capacity. On the other hand, if the depth of the surface crack is underestimated or ignored, the predictive methods would underestimate crack-opening, and hence, also underestimate the load-carrying capacity of the pipe.

3.3 Finite Element Evaluations of Crack-Opening Shapes

During this study, several finite-element analyses were performed to evaluate the adequacy of the elliptical representation of a crack-opening profile. Two pipes, one with large diameter containing a short crack and the other with small diameter containing a long crack, were analyzed. The crack

sizes are typical of leakage size flaws in LBB applications for nuclear piping systems. For the large-diameter pipe, there was one elastic analysis under pure bending. For the small-diameter pipe, there were two elastic-plastic analyses, one for pure bending and the other for combined bending and tension. They are explained below.

3.3.1 Large-Diameter Pipes with Short Cracks

In this analysis, the pipe had outer diameter, D_o = 406.4 mm (16 inches), wall thickness, t = 26.19 mm (1.031 inches), crack size, θ/π = 12 percent, and a single applied bending moment, M = 522.61 kN-m (4,626 inch-kip). The elastic modulus, E, was 193.06 GPa (28,000 ksi) and Poisson's ratio, ν, was 0.3. The loading was assumed to be linear-elastic with no plasticity or crack growth. Hence, the results of this analysis can be scaled for any other moments, if needed. The finite element analysis was performed by the ABAQUS code (Ref. 3.6) with twenty-noded three-dimensional solid elements. The total number of elements and nodal points were 1,260 and 9,030, respectively. Only one element through the thickness was used.

Figure 3.47 shows the results of finite element analysis in terms of COD plotted as a function of normalized angle from the crack tip ($\xi/2\theta$). In this figure, two plots are shown, one for the crack-opening profile at the outer surface and the other for the crack-opening profile at the inner surface of the pipe. For each case, the continuous line indicates the crack-opening shape assuming an elliptical representation with the center COD estimated by FEM analysis. The points indicate explicit calculations by FEM as a function of $\xi/2\theta$. It appears that both outer and inner crack-opening profiles can be accurately modeled by an elliptical shape.

3.3.2 Small-Diameter Pipes with Long Cracks

To understand the crack-opening characteristics for long cracks in small-diameter pipes, similar finite element computations were also conducted in this study. In this case, the pipe had mean diameter, D_m = 101.6 (4 inches), wall thickness, t = 8.56 mm (0.337 inch), and crack size, θ/π = 37 percent. Two loading cases were studied: (1) pure bending and (2) combined bending and tension. For each loading case, the results due to several load intensities were investigated. They were:

1. Pure Bending Case (p = 0)

   M = 6.97 kN-m (61.7 inch-kip)
   M = 9.57 kN-m (84.7 inch-kip)
   M = 12.3 kN-m (108.9 inch-kip)

2. Combined Bending and Tension Case (p = 15.51 MPa [2,250 psi])

   M = 1.50 kN-m (13.3 inch-kip)
   M = 4.32 kN-m (38.2 inch-kip)
   M = 10.64 kN-m (94.2 inch-kip)
   M = 15.0 kN-m (132.8 inch-kip)

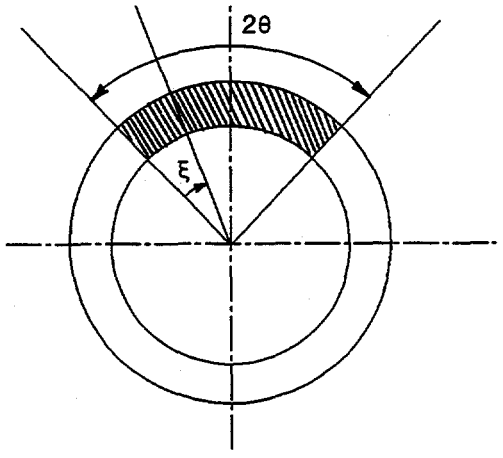

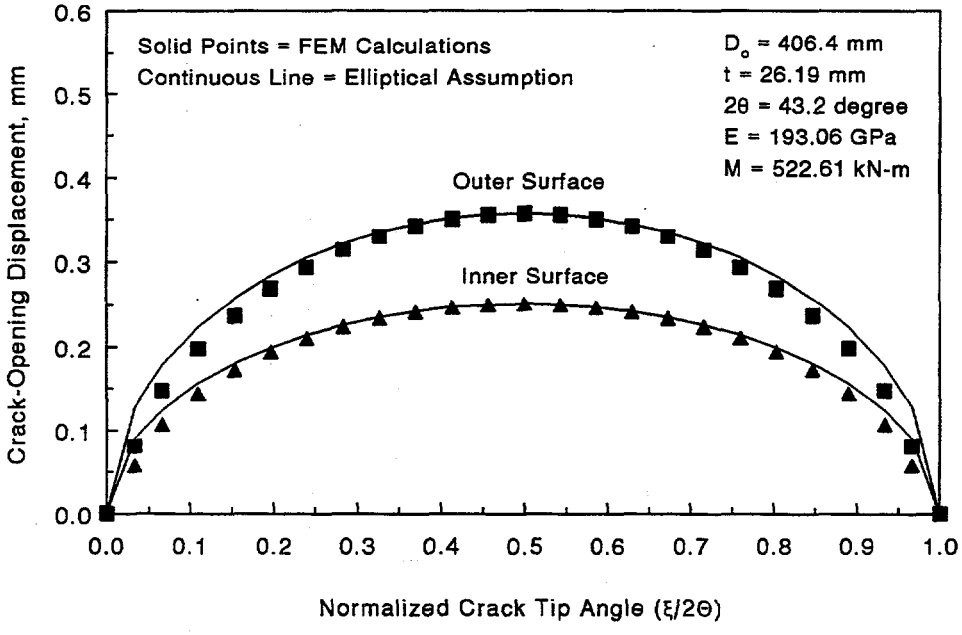

Figure 3.47 Crack-opening shape for a large-diameter pipe with a short crack under pure bending (elastic analysis)

T-6300-F3.46

The internal pressure in the pipe was simulated by applying the axial (tension) force only. No hoop stress or crack-face pressure were modeled.

The elastic modulus and Poisson's ratio were 193.06 GPa (28,000 ksi) and 0.29, respectively. The analyses were elastic-plastic and, therefore, a nonlinear stress-strain curve for the pipe material needs to be specified as well. In this regard, the Ramberg-Osgood model (see Equation 2-1) was chosen to represent the tensile properties with the parameters: σ_0 = 210 MPa (30.5 ksi), α = 2.6, and n = 4.06. No crack growth was assumed for any of the applied loads defined above.

The finite element analyses were performed by the ABAQUS code (Ref. 3.6) with twenty-noded three-dimensional solid elements. The total number of elements and nodal points were 949 and 4,984, respectively. There were four elements through the thickness. The size (length along the cracked plane) of the smallest element near the crack tip was 0.051 mm (0.002 inch).

The crack-opening displacements calculated by the FEM at the mid-thickness level of the pipe are given in Figures 3.48 and 3.49. Figure 3.48 shows several plots of crack-opening displacement as a function of the normalized crack angle from the crack tip ($\xi/2\theta$) for several bending moments without any internal pressure. Similar results are plotted in Figure 3.49 for the pipe under combined bending and tension with four different moments. For each loading case and applied moment, the crack-opening shapes based on elliptical representations with crack length as the major axis and the center COD as the minor axis are also shown. The comparisons between finite element results (points) and the elliptical equation (lines) suggest that, indeed, the crack-opening profile can be modeled by an elliptical shape, regardless of load intensity and hence, the amount of plasticity in the cracked pipe.

For very large moments, the crack-driving force (applied J) was much higher than typical fracture initiation toughness (J_{Ic}) of austenitic or ferritic materials. This explains why there were slight crack-tip blunting in the finite element calculations in which no crack growth was allowed.

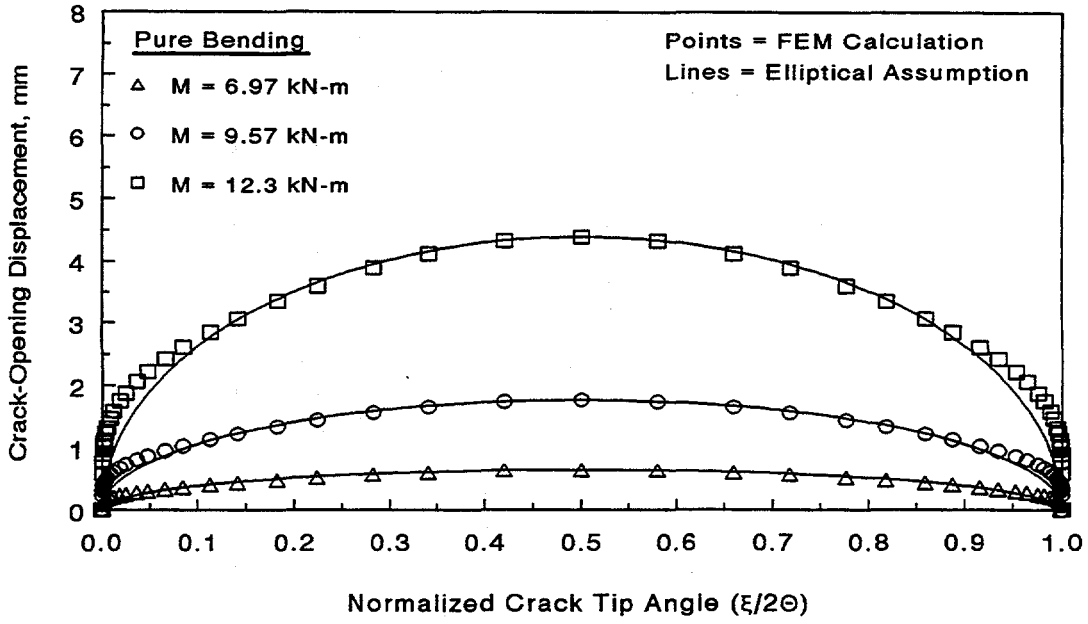

Figure 3.48 Crack-opening shape for a small-diameter pipe with a long crack under pure bending (elastic-plastic analysis)

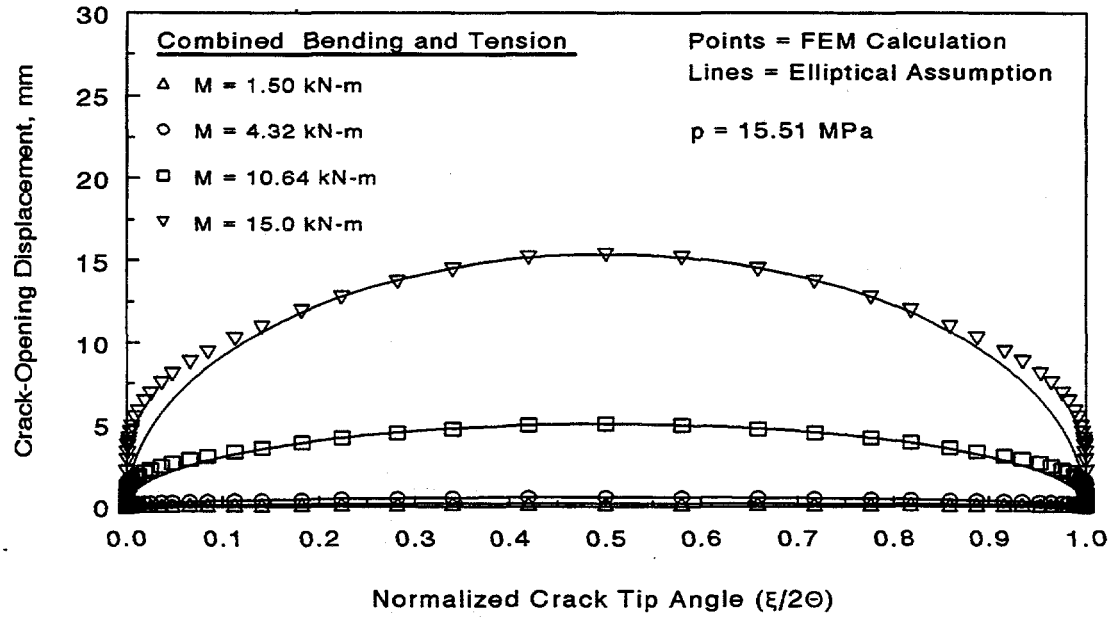

Figure 3.49 Crack-opening shape for a small-diameter pipe with a long crack under combined bending and tension (elastic-plastic analysis)

T-6300-F3.48

3.4 References

3.1 Wilkowski, G. M., and others, "Short Cracks in Piping and Piping Program," Semiannual reports by Battelle, NUREG/CR-4599, Vols. 1 to 3, Nos. 1 and 2, U.S. Nuclear Regulatory Commission, Washington, D.C., 1991-1994.

3.2 Wilkowski, G. M., Ahmad, J., Barnes, C. R., Brust, F., Ghadiali, N., Guerrieri, D., Jones, D., Kramer, G., Landow, M., Marschall, C. W., Olson, R., Papaspyropoulos, V., Pasupathi, V., Rosenfeld, M., Scott. P., and Vieth, P., "Degraded Piping Program - Phase II: Summary of Technical Results and Their Significance to Leak-Before-Break and In-Service Flaw Acceptance Criteria, March 1984 - January 1989," NUREG/CR-4082, Vol. 8, U.S. Nuclear Regulatory Commission, Washington, D.C., March 1989.

3.3 Kanninen, M. F. and others, "Instability Predictions for Circumferentially Cracked Type-304 Stainless Steel Pipes Under Dynamic Loading - Volume 2: Appendices," EPRI Report NP-2347, Volume 2, Electric Power Research Institute, Palo Alto, CA, April 1982.

3.4 Schmidt, R. A., Wilkowski, G. M., and Mayfield, M. E., "The International Piping Integrity Research Group (IPIRG) Program: An Overview," *Transactions of the 11th International Conference on Structural Mechanics in Reactor Technology, Vol. G2: Fracture Mechanics and Non-Destructive Evaluation - 2*, Edited by H. Shibata, Tokyo, Japan, Paper No. G23/1, pp. 177-188, August 1991.

3.5 Paul, D., Ahmad, J., Scott, P., Flanigan, L., and Wilkowski, G., "Evaluation and Refinement of Leak-Rate Estimation Models," NUREG/CR-5128, Rev. 1, U.S. Nuclear Regulatory Commission, Washington, D.C., June 1994.

3.6 ABAQUS, User's Guide and Theoretical Manual, Version 5.3, Hibbitt, Karlsson, & Sorensen, Inc., Pawtucket, RI, 1993.

3.7 Brust, F. W., "Approximate Methods for Fracture Analyses of Through-Wall Cracked Pipes," NUREG/CR-4853, U.S. Nuclear Regulatory Commission, Washington, D.C., February 1987.

3.8 Wilkowski, G., Ahmad, J., Brust, F., Guerrieri, D., Kramer, G., Kulhowvick, G., Landow, M., Marschall, C., Nakagaki, M., Papaspyropoulos, V., and Scott, P., "Analysis of Experiments on Stainless Steel Flux Welds," NUREG/CR-4878, U.S. Nuclear Regulatory Commission, Washington, D.C., April 1987.

3.9 Rahman, S., Wilkowski, G., and Brust, F., "Analysis of Full-Scale Pipe Fracture Experiments on Stainless Steel Flux Welds," Fatigue, Flaw Evaluation, and Leak-Before-Break Assessments - 1994, ASME Special Publication, Edited by G. Wilkowski, PVP-Vol. 280, June 1994.

3.10 ASTM Standard E1152-87, "Standard Test Method for Determining J-R Curve," *Annual Book of ASTM Standards*, Volume 03.01, 1991.

3.11 "Report to the U.S. Nuclear Regulatory Commission Piping Review Committee," Prepared by the Pipe Break Task Group, NUREG/CR-1061, Vol. 3, U.S. Nuclear Regulatory Commission, Washington, D.C., November 1984.

4.0 SENSITIVITY ANALYSES

4.1 Introduction

In conducting crack-opening-area (COA) evaluations for a through-wall-cracked (TWC) pipe, uncertainties arise due to incomplete knowledge of several key factors and parameters. Some of these factors include: (1) crack-face pressure for a pipe under pure pressure or combined bending and pressure and its effects on crack-opening predictions, (2) the range of stress-strain curve one should use for the Ramberg-Osgood idealization of material constitutive equations, and (3) probable error in the elastic modulus from material handbook calculations.

Sample calculations were made to perform a sensitivity study for these parameters. Experimental pipe fracture results were used whenever available to evaluate the effects of these parameters on the COA predictions. This section discusses the results from these sensitivity analyses to determine if these parameters are important and quantify their impact on the COA evaluations.

4.2 Crack-Face Pressure

4.2.1 Approximate Crack-Opening Evaluations for Crack-Face Pressure

In conducting fracture analyses for a TWC pipe under either combined bending and pressure or pure pressure, the axial tensile force due to the pressure is typically the only driving force for fracture assessments and crack-opening. The pressure on the cracked face is seldom used to determine the crack-opening displacement. In this section, the effects of crack-face pressure are discussed in the light of COA calculations.

For this analysis, a TWC pipe was analyzed with a mean radius, R_m, wall thickness, t, and a crack angle, 2θ, centered in the plane of bending. The pipe is subjected to a remote bending moment, M, and an internal pressure, p. Let p_c denote the pressure on the cracked surface of the pipe. Obviously, the crack-face pressure, p_c, is related to the internal pipe pressure. The determination of p_c and its possible variation (radial) through the pipe thickness requires thermal-hydraulics analysis. For a pipe with a known crack-opening geometry and crack-morphology parameters (e.g., surface roughness, number of turns, discharge coefficients, etc.), the thermal-hydraulic analysis can be conducted to determine the leak rate and pressures at the entrance and exit planes. These entrance (inner diameter) and exit (outer diameter) pressures provide a profile of the pressure on the crack face. Hence, the evaluation of the effects of crack-face pressure on crack-opening is an iterative process that may require both fracture-mechanics and thermal-hydraulic analyses.

In this study, a much simpler representation of the crack-face pressure was assumed to estimate its effects on crack-opening. It was assumed that p_c is uniformly distributed on the crack face both radially and circumferentially. Ideally, when the COD is very large, the fluid flow through the crack is primarily single-phase and hence, p_c is almost equal to p. However, when the COD is very small, the fluid experiences two-phase flow and hence, p_c can be much smaller than p. For this reason, several magnitudes of p_c as percentages of internal pressure (e.g., 25, 50, and 100 percent of p) were

considered. For a given p_c, the effects of crack-face pressure can be approximately accounted for by considering the additional bending moment, M_{CP} that is given by

$$M_{CP} = F_{CP}(r_t + r_b) \tag{4-1}$$

where $F_{CP} = 2R_m t\theta p_c$ is the resultant force due to uniform pressure p_c on the cracked area, r_t is the distance between the centroid of the cracked area and the centroidal axis of the uncracked pipe cross-section that can be obtained from

$$r_t = \frac{\int_{\pi/2-\theta}^{\pi/2+\theta} R_m^2 t \sin\zeta d\zeta}{\int_{\pi/2-\theta}^{\pi/2+\theta} R_m t d\zeta} = \frac{R_m \sin\theta}{\theta} \tag{4-2}$$

and r_b is the distance between the centroidal axis of the uncracked pipe cross-section and an axis A-A shown in Figure 4.1. For a linear-elastic analysis, axis A-A represents the elastic neutral axis of a cracked pipe (i.e., the centroidal axis of the uncracked area of the cracked pipe section), while for a rigid-plastic analysis, axis A-A represents the plastic neutral axis of a cracked pipe (i.e., the equal area axis for the uncracked area of the cracked pipe section). Based on these two definitions of axis A-A, the following are the explicit expressions of r_b (Refs. 4.1 and 4.2):

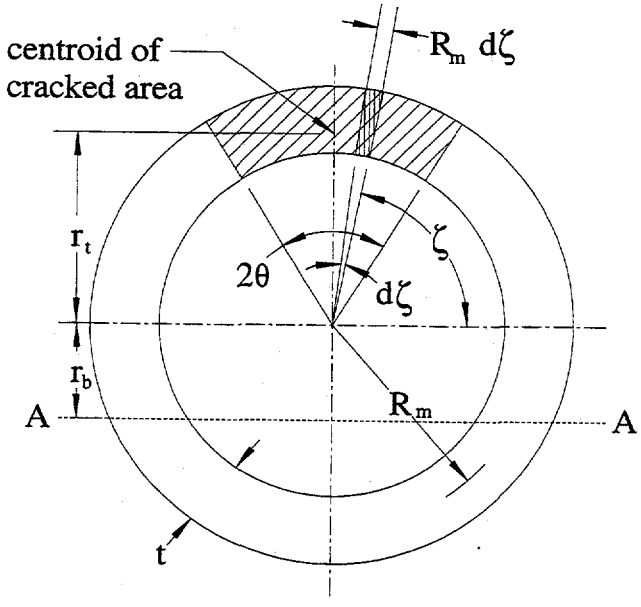

Figure 4.1 Schematic for calculating equivalent moment due to crack-face pressure in a pipe

T-6300-F4.1

(1) Elastic Neutral Axis (Pure Bending)

$$r_b = \frac{R_m \sin(\pi-\theta)}{\pi-\theta} \tag{4-3}$$

(2) Plastic Neutral Axis

$$r_b = R_m \cos\left[\frac{\pi-\theta}{2} - \frac{\pi R_i^2 p}{4t\sigma_f R_m}\right] \tag{4-4}$$

where R_i is the inside radius of the pipe and σ_f is the flow stress of the material. Note that Equations 4-2, 4-3, and 4-4 are strictly valid for thin-walled pipe only.

4.2.2 Numerical Examples

For numerical applications, two pipes were considered with one representing a Boiling Water Reactor (BWR) pipe and the other representing a Pressurized Water Reactor (PWR) pipe. The BWR pipe had outer diameter, D_o = 711.2 mm (28 inches), wall thickness, t = 33.87 mm (1.33 inches), and an internal pressure, p = 7.24 MPa (1,050 psi). The PWR pipe had outer diameter, D_o = 711.2 mm (28 inches), wall thickness, t = 67.74 mm (2.67 inches), and an internal pressure, p = 15.51 MPa (2,250 psi). In both pipes, two crack sizes, one with θ/π = 1/16 (short crack) and the other with θ/π = 1/4 (long crack), were considered. The crack-face pressure was varied from 25 to 100 percent of the internal pressure.

The analysis was assumed to be linear-elastic. Hence, according to the GE/EPRI method, the center-crack-opening displacement under combined bending and pressure, without considering crack-face pressure, is (Refs. 4.3 to 4.6)

$$\delta_1 = 4a\frac{R_m}{I}V_1^B(a/b, R_m/t)\frac{M}{E} + \frac{2a}{\pi R_m t}V_1^T(a/b, R_m/t)\frac{P}{E} \tag{4-5}$$

in which all of the variables were defined in Section 2. When the crack-face pressure is accounted for, the equation for the center-crack-opening displacement becomes

$$\delta_2 = 4a\frac{R_m}{I}V_1^B(a/b, R_m/t)\frac{M+M_{CP}}{E} + \frac{2a}{\pi R_m t}V_1^T(a/b, R_m/t)\frac{P}{E} \tag{4-6}$$

where the crack-face contribution to the additional moment, M_{CP}, can be obtained from Equation 4-1. Although this is a linear-elastic analysis, both Equations 4-3 and 4-4 were used to calculate r_b and

M_{CP}. In conducting the estimation analyses, the elastic influence functions $V_1^T(a/b,R_m/t)$ and $V_1^B(a/b,R_m/t)$ were obtained from References 4.4 and 4.6, respectively.

Using the plastic neutral axis, Figure 4.2 shows the plots of normalized center-crack-opening displacement (δ_2/δ_1) for the BWR pipe as a function of the applied remote moment also normalized by the Net-Section-Collapse moment (M_{nsc}) under combined bending and pressure. The results are presented for two crack sizes (θ/π = 1/16 and 1/4) and three magnitudes of crack-face pressure (p_c/p = 1/4, 1/2, and 1). In general, the crack-face pressure will increase the amount crack-opening. The amount of increase in COD, however, diminishes with the increasing values of applied (remote) moment. This is because at a smaller load level the moment due to the crack-face pressure can be compared to the applied moment. As M increases, the relative magnitude of M_{CP} also decreases and hence, the trend exhibited in Figure 4.2. Also, in this figure, the results show that for a given crack-face pressure (or crack size), when the crack size (or the crack-face pressure) is larger, the effects of crack-face pressure on the crack-opening is also larger. These are expected. Figure 4.3 shows similar trends of results for the PWR pipe. However, since the pressure in the PWR pipe was much higher than that in the BWR pipe, the effects of crack-face pressure were also higher in the PWR pipe.

Finally, Figures 4.4 and 4.5 show the corresponding results for these two pipes using the elastic neutral axis (pure bending) to compute r_b and M_{CP}. The trends are identical to those in Figures 4.2 and 4.3, although the effects on the crack-opening are slightly lower due to the smaller values of r_b and M_{CP}.

The results in Figure 4.3 suggest that the ratio of δ_2/δ_1 can be as large as 1.38 when the crack-face pressure is equal to the internal pressure of the pipe and the applied moment approaches zero. However, it should be borne in mind that for a load range that small, the crack-opening is much smaller. Hence, the effective pressure on the crack face is also much smaller than the internal pressure. In consequence, the values of δ_2/δ_1 could drop from 1.38 to 1.10 for p_c/p = 1/4 or even smaller. Hence, it appears that the crack-face pressure has a minor effect on the crack-opening for the pipe and pressure cases considered here.

4.3 Stress-Strain Region for Ramberg-Osgood Idealization

4.3.1 The Ramberg-Osgood Model

In conducting general fracture evaluations, the Ramberg-Osgood model, which is a two-parameter model (for fixed elastic modulus), is frequently used for an idealization of a uniaxial stress-strain curve of a pipe material (see Equation 2-1). Since there are only two parameters in this model, the Ramberg-Osgood representation allows evaluations of fracture response and crack-opening in a much simpler way than using the multilinear stress-strain curve from the tensile data. However, due to the small number of parameters in the Ramberg-Osgood model, there are many cases of actual data (particularly for stainless steel) for which it cannot adequately represent material constitutive behavior in the complete range of the stress-strain curve. In those cases, proper care must be taken in deciding the appropriate range of the stress-strain curve to use to fit this model. Frequently, confusions

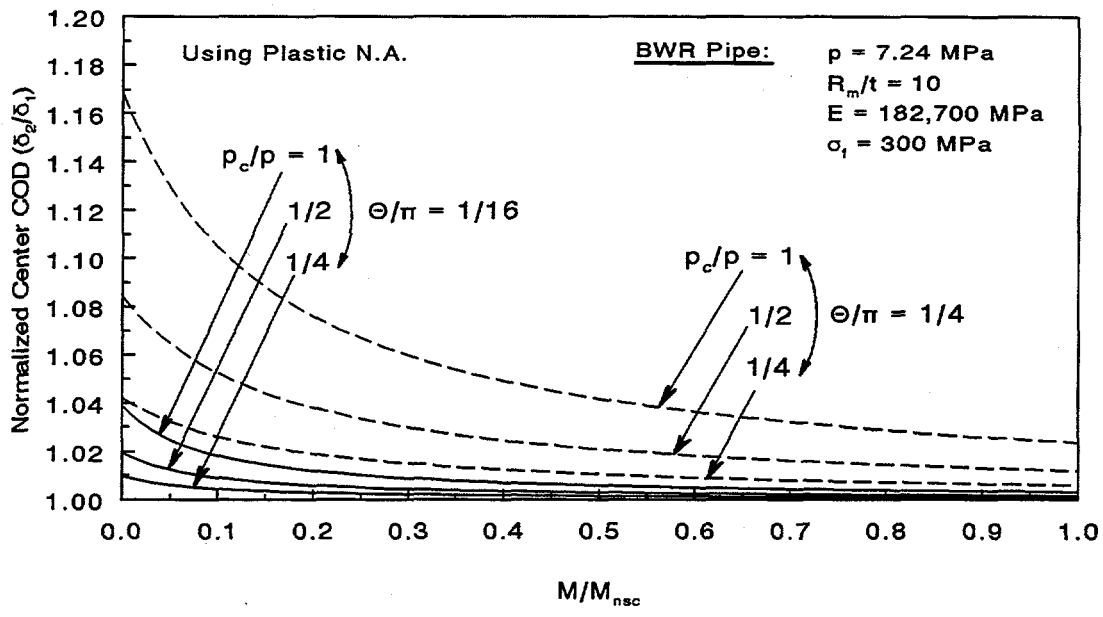

Figure 4.2 Normalized center-crack-opening displacement for a BWR pipe showing the effects of crack-face pressure (using plastic neutral axis)

T-6300-F4.2

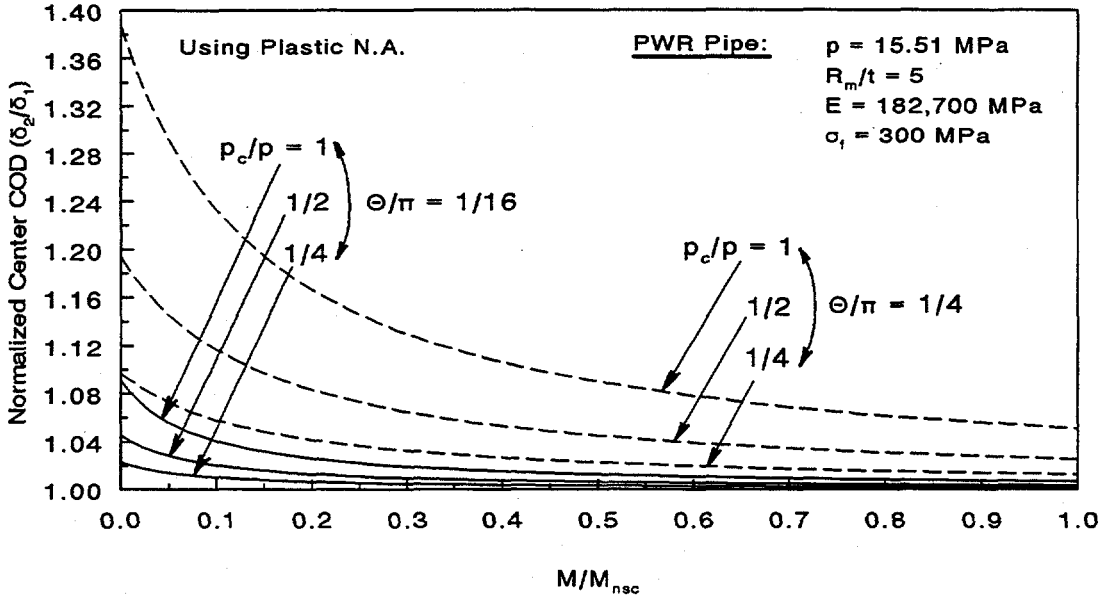

Figure 4.3 Normalized center-crack-opening displacement for a PWR pipe showing the effects of crack-face pressure (using plastic neutral axis)

T-6300-F4.3

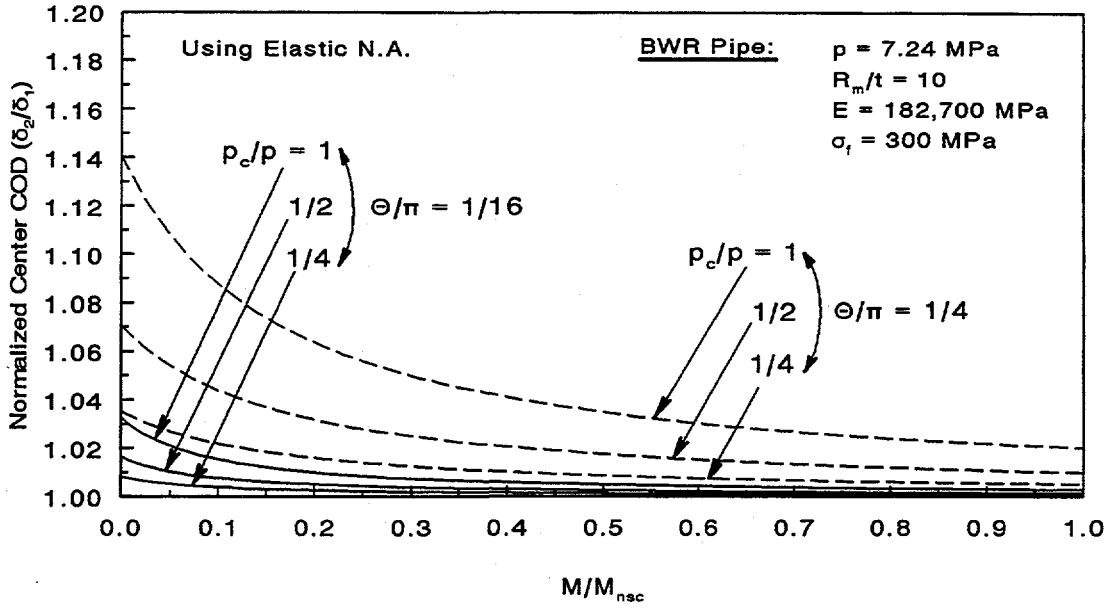

Figure 4.4 Normalized center-crack-opening displacement for a BWR pipe showing the effects of crack-face pressure (using elastic neutral axis)

T-6300-F4.4

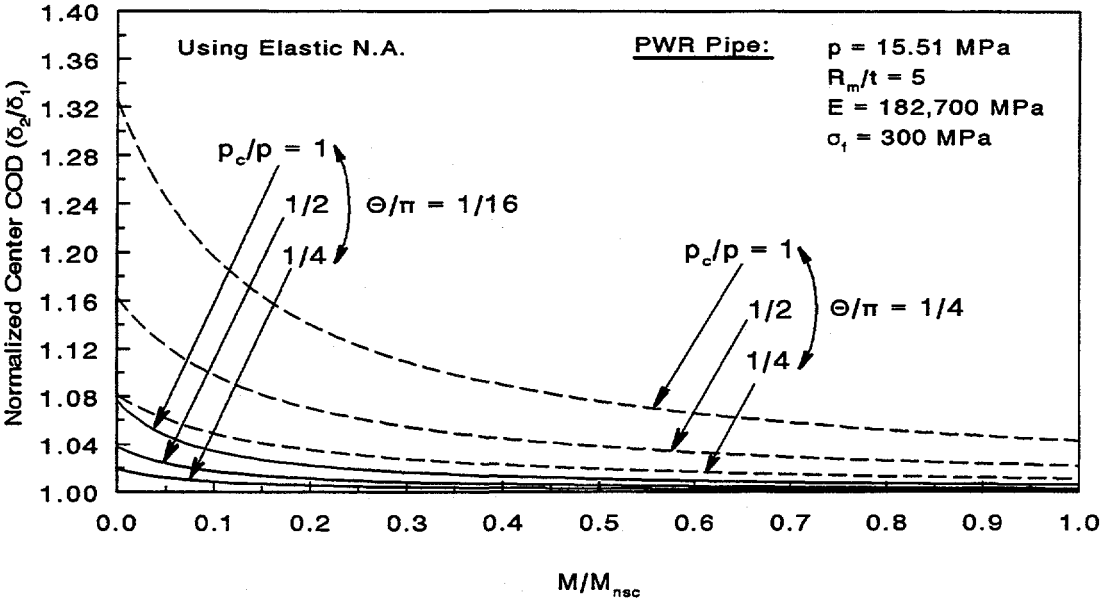

Figure 4.5 Normalized center-crack-opening displacement for a PWR pipe showing the effects of crack-face pressure (using elastic neutral axis)

T-6300-F4.5

arise in obtaining different values of Ramberg-Osgood parameters when the strain region of interest is not properly defined.

In this study, sensitivity calculations were made to determine the effects on Ramberg-Osgood parameters that were calculated by fitting various regions of several stress-strain curves. Data from two pipe fracture experiments conducted in the Short Cracks in Piping and Piping Welds Program (Ref. 4.7) were used to evaluate the crack-opening predictions. The tests involved Experiments 1.1.1.21 and 1.1.1.26 that were conducted on a 711.2-mm (28-inch) nominal diameter Schedule 60 A515 Grade 60 carbon steel pipe and a 101.6-mm (4-inch) nominal diameter, Schedule 160 pipe of French TP316L stainless steel (French designation Z3 CND 18-12) pipe, respectively. The geometries, crack sizes, and material properties for these two pipes are already described in Section 3 of this report.

4.3.2 Sensitivity Analysis

During the sensitivity analysis, four different stress-strain (σ-ϵ) regions were considered. They were:

(1) $0 \leq \epsilon \leq 0.01$,
(2) $0 \leq \epsilon \leq 0.05$,
(3) $0 \leq \epsilon \leq 0.15$, and
(4) $0 \leq \epsilon \leq 0.30$.

In each of the pipe experiments, there were two specimens for which tensile test data were available. Table 4.1 shows the values of α and n obtained by a least-square fit of these data corresponding to each of the four strain ranges considered. Figures 4.6 and 4.7 show the plots of the Ramberg-Osgood equation using the values of α and n from this table for the pipe material (F26-5 and F26-6) in Experiment 1.1.1.21. The corresponding tensile data are also included in these figures for comparisons. Similar plots and comparisons with the tensile data for pipe (IP-A2-1 and IP-A2-2) in Experiment 1.1.1.26 are shown in Figures 4.8 and 4.9. The results suggest that there are, indeed, differences in the values of the Ramberg-Osgood parameters, particularly when they are calculated from fitting the data in a low strain region (e.g., $0 \leq \epsilon \leq 0.01$) and a high strain region (e.g., $0 \leq \epsilon \leq 0.30$). However, they were not very sensitive when compared in the intermediate to high strain regions.

Table 4.1 Ramberg-Osgood parameters for various strain ranges

	Experiment 1.1.1.21				Experiment 1.1.1.26			
	F26-5		F26-6		IP-A2-1		IP-A2-2	
Strain Range	α	n	α	n	α	n	α	n
$0\% \leq \epsilon \leq 1\%$	1.01	10.1	1.06	9.29	1.75	4.41	1.32	3.6
$0\% \leq \epsilon \leq 5\%$	1.12	5.99	1.04	6.36	2.75	5.94	4.26	5.98
$0\% \leq \epsilon \leq 15\%$	1.34	5.18	1.31	5.12	2.89	5.92	4.43	5.68
$0\% \leq \epsilon \leq 30\%$	1.02	5.99	0.91	6.23	3.02	5.56	4.85	5.19

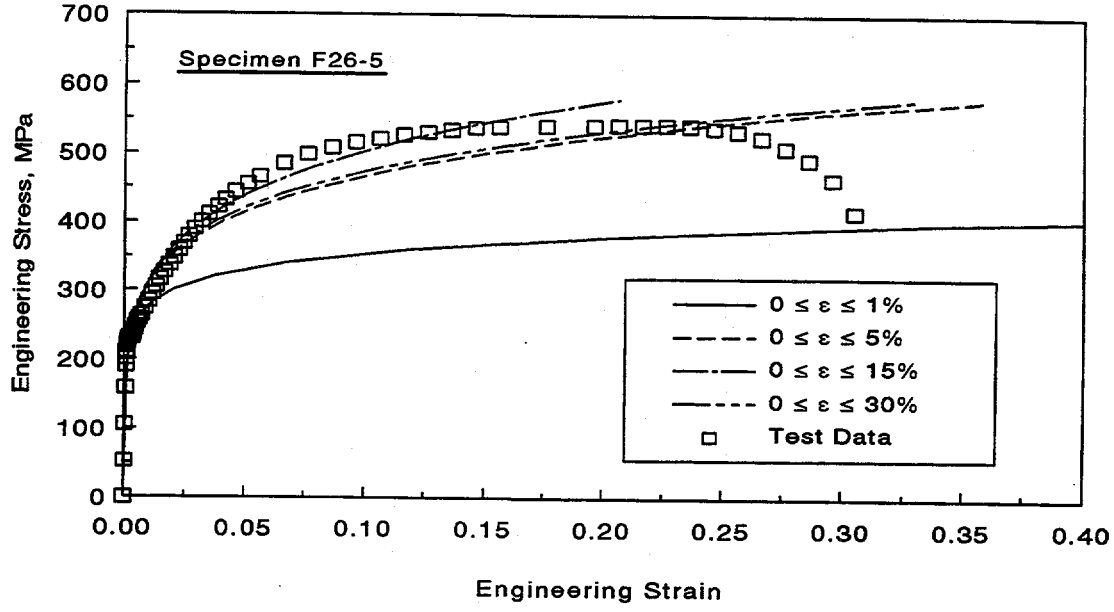

Figure 4.6 Comparisons of Ramberg-Osgood equations for various strain regions with actual test data from tensile Specimen F26-5

T-6300-F4.6

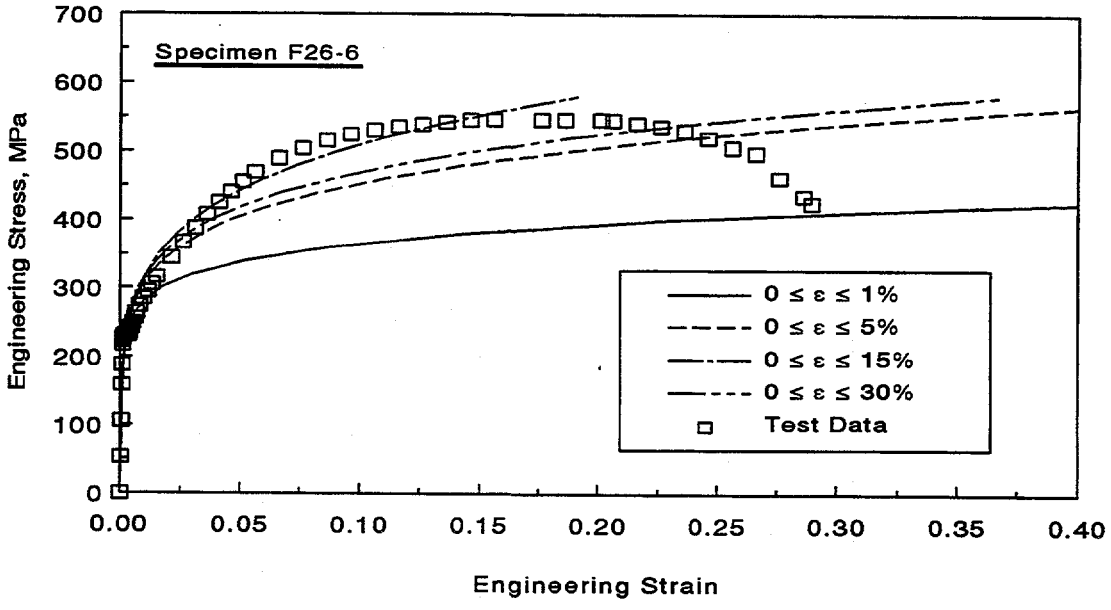

Figure 4.7 Comparisons of Ramberg-Osgood equations for various strain regions with actual test data from tensile Specimen F26-6

T-6300-F4.7

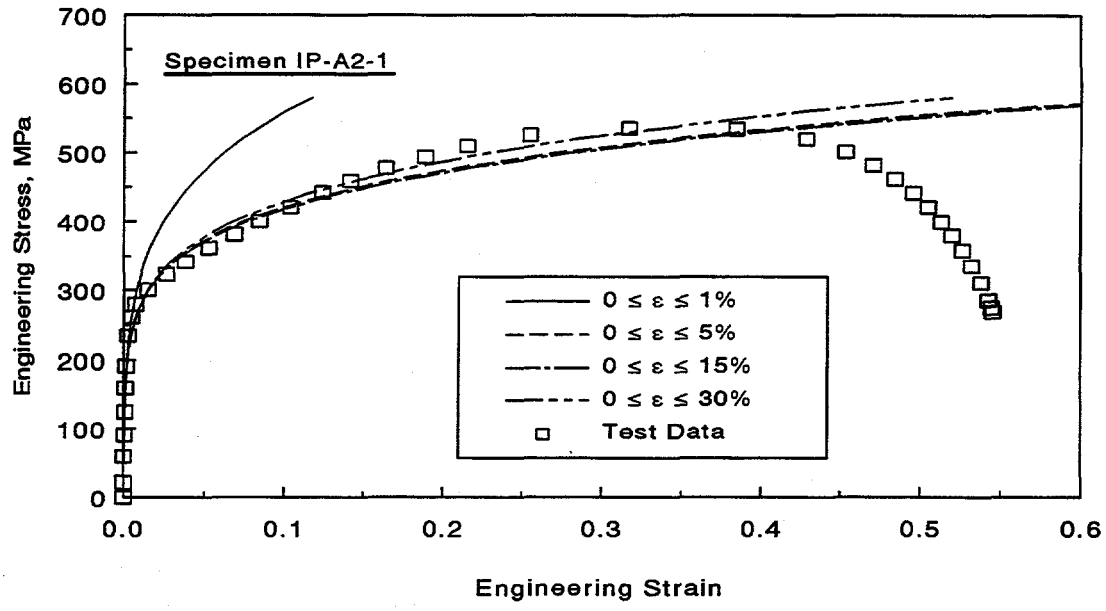

Figure 4.8 Comparisons of Ramberg-Osgood equations for various strain regions with actual test data from tensile Specimen IP-A2-1

T-6300-F4.8

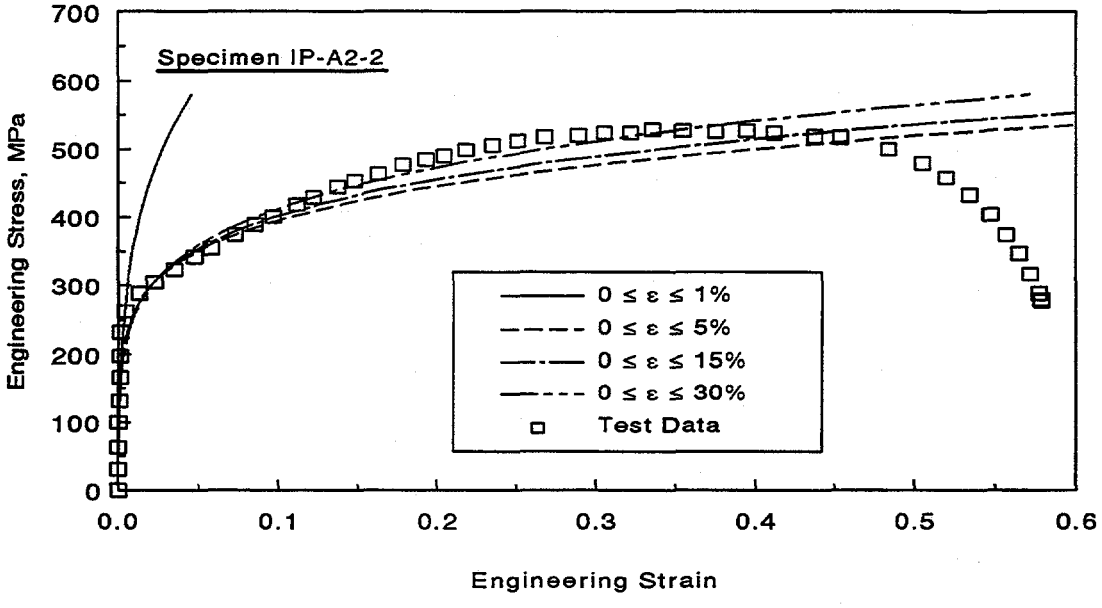

Figure 4.9 Comparisons of Ramberg-Osgood equations for various strain regions with actual test data from tensile Specimen IP-A2-2

T-6300-F4.9

In addition, the model parameters in the low strain range ($0 \leq \epsilon \leq 0.01$) for the pipe materials in these two experiments showed opposite trends, see Figures 4.6 through 4.9. For the ferritic pipe F26, the low-strain fit provided the largest value of n, whereas for Pipe IP-A2, which was an austenitic material, it predicted the smallest value of n (see also Table 4.1). It is, however, not clear whether these are the generic trends for ferritic and austenitic materials.

Figures 4.10 and 4.11 show the crack-opening predictions by the GE/EPRI method (Refs. 4.3 and 4.4) using original influence functions and no plastic-zone corrections in terms of applied load versus center-crack-opening displacement for pipes in Experiments 1.1.1.21 and 1.1.1.26, respectively. The comparisons with the experimental data, also included in these two figures, suggest that the differences in the Ramberg-Osgood parameters obtained from various strain regions can affect the predictions of crack-opening displacement. This is particularly true for the austenitic pipe (Experiment 1.1.1.26) in which case the prediction based on a low-strain fit significantly underpredicted COD when compared with the test data and predictions based on a Ramberg-Osgood fit of other regions of the stress-strain curve. For the ferritic pipe (Experiment 1.1.1.21), there is less difference in the predictions based on low-strain or high-strain fit. However, for large loads, the results based on low-strain fit overpredicted the experimental values of crack-opening.

It appears that a Ramberg-Osgood fit in the intermediate to high strain region would provide the best prediction of results in a pipe fracture experiment. This is consistent with past studies at Battelle. However, when the applied load is smaller, in which case the structural behavior is primarily elastic or slightly elastic-plastic (small plastic strains), the Ramberg-Osgood parameters based on a low strain fit can be used. This was clearly shown for the ferritic pipe (see Figure 4.10).

4.4 Errors in Elastic Modulus

The Ramberg-Osgood model defined by Equation 2-1 and discussed above has actually three independent parameters, such as E, α, and n. However, since E has a strong physical interpretation representing the well known Young's modulus in linear elasticity, it is typically chosen either from the material handbook or measured from an experiment. Hence, by fixing E to a certain value, only α and n remain to be calculated from a least-square fit of a given tensile data set. Frequently, it is assumed that the value of E varies from 179.27 GPa (26×10^6 psi) to 182.7 GPa (26.5×10^6 psi) for stainless steel and 193.1 GPa (28×10^6 psi) to 199.96 GPa (29×10^6 psi) for carbon steel materials. However, in a recent pipe experiment conducted on a 101.6-mm (4-inch) nominal diameter, Schedule 160 pipe of French TP316L stainless steel (French designation Z3 CND 18-12), Battelle found the elastic modulus for this pipe material to be only 157.5 GPa (22.84×10^6 psi). Similar low values of elastic modulus were initially reported by Electricité de France (EDF). Later, Battelle conducted a test in a Magniflux Type FM-500 Elastomat to verify EDF's findings.

Since the elastic crack-opening displacement is inversely proportional to the elastic modulus, the evaluation of the effects due to any error in E is straightforward. In this particular experiment (Experiment 1.1.1.26), the elastic COD will be underpredicted by 13.8 percent and 16 percent when the elastic modulus is approximated by 179.27 GPa (26×10^6 psi) and 182.7 GPa (26.5×10^6 psi), respectively. Hence, accurate estimates of E are somewhat important for COA calculations when

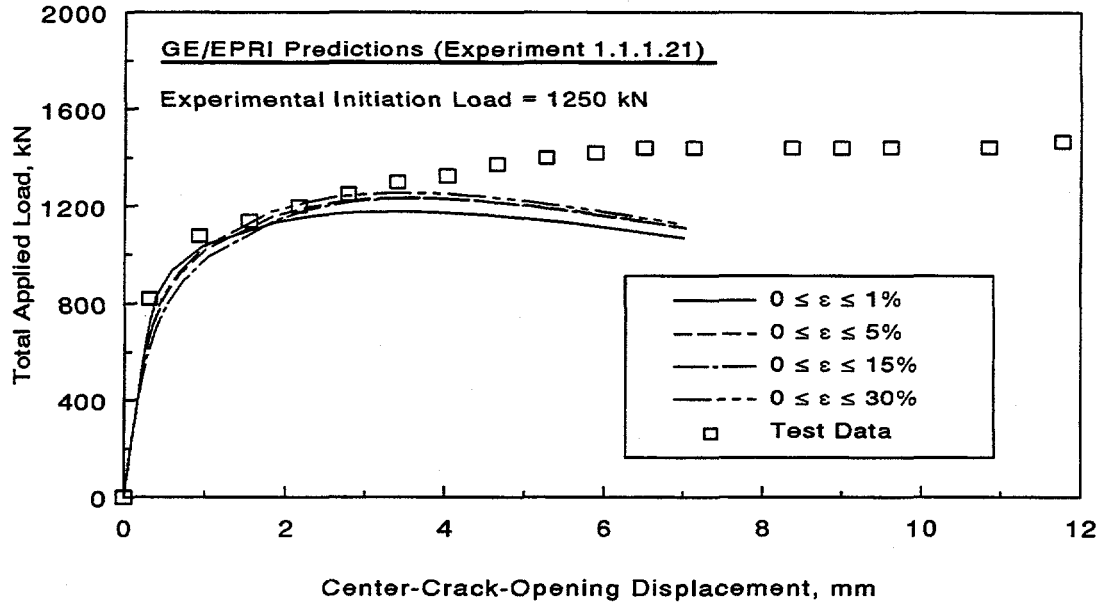

Figure 4.10 Comparisons of crack-opening predictions using various strain regions for Ramberg-Osgood fit with test data in Experiment 1.1.1.21

T-6300-F4.10

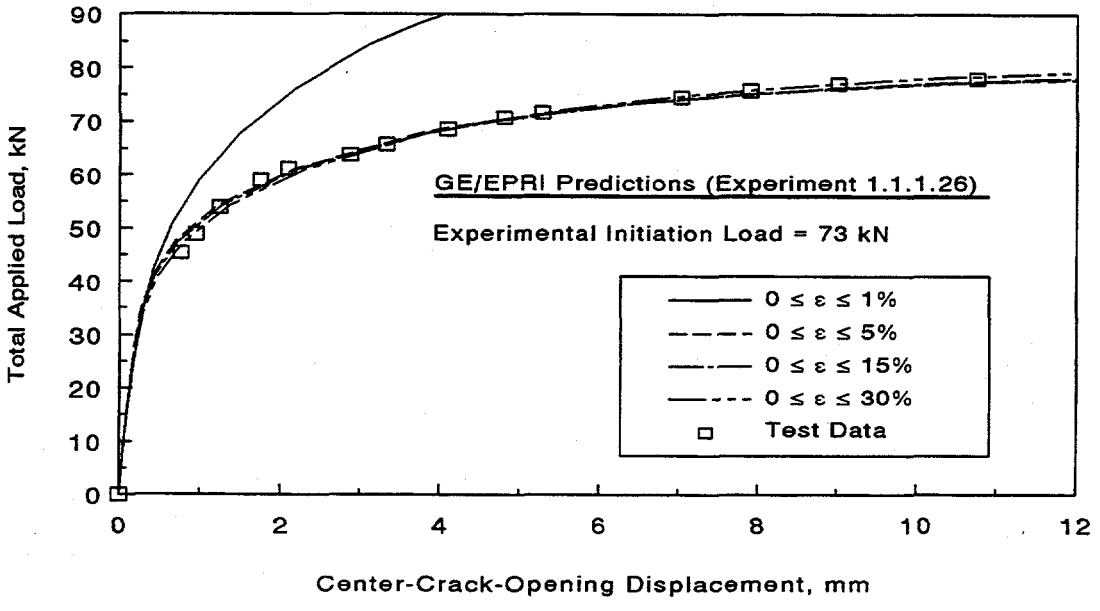

Figure 4.11 Comparisons of crack-opening predictions using various strain regions for Ramberg-Osgood fit with test data in Experiment 1.1.1.26

T-6300-F4.11

the analysis is linear-elastic. However, if a pipe experiences significant plasticity, e.g., in a typical pipe experiment in which loading continues until failure, such an error in E would be of much lesser importance.

4.5 References

4.1 Kanninen, M. F., Broek, D., Marschall, C. W., Rybicki, E. F., Sampath, S. G., Simonen, F. A., and Wilkowski, G. M., "Mechanical Fracture Predictions for Sensitized Stainless Steel Piping with Circumferential Cracks," Final Report, EPRI Report NP-192, Electric Power Research Institute, Palo Alto, CA, September 1976.

4.2 Kanninen, M. F. and others, "Instability Predictions for Circumferentially Cracked Type 304 Stainless Steel Pipes Under Dynamic Loading," EPRI Report NP-2347, Electric Power Research Institute, Palo Alto, CA, April 1982.

4.3 Kumar, V., German, M., and Shih, C., "An Engineering Approach for Elastic-Plastic Fracture Analysis," EPRI Report NP-1931, Electric Power Research Institute, Palo Alto, CA, July 1981.

4.4 Kumar, V., German, M., Wilkening, W., Andrews, W., deLorenzi, H., and Mowbray, D., "Advances in Elastic-Plastic Fracture Analysis," EPRI Final Report NP-3607, Electric Power Research Institute, Palo Alto, CA, August 1984.

4.5 Kishida, K. and Zahoor, A., "Crack-Opening Area Calculations for Circumferential Through-Wall Pipe Cracks," EPRI Special Report NP-5959-SR, Electric Power Research Institute, Palo Alto, CA, August 1988.

4.6 Brust, F., Rahman, S., and Ghadiali, N., "Elastic-Plastic Analysis of Small Cracks in Tubes," *Proceedings of the 11th International Conference on Offshore Mechanics and Arctic Engineering*, Calgary, Alberta, Canada, June 1992.

4.7 Wilkowski, G. M., and others, "Short Cracks in Piping and Piping Program," Semiannual reports by Battelle, NUREG/CR-4599, Vols. 1 to 3, Nos. 1 and 2, U.S. Nuclear Regulatory Commission, Washington, D.C., 1991-1994.

5.0 OFF-CENTER CRACKS

5.1 Introduction

In conducting both leak-rate and flaw stability analyses, a postulated through-wall-crack size (leakage flaw) is often calculated based on its symmetric placement with respect to the bending plane of the pipe, see Figure 2.1. This is usually justified with the reasoning that the tensile stress due to bending is largest at the center of this symmetric crack. However, fabrication imperfections will occur randomly around the pipe circumference. Additionally, during the normal operating condition of a plant, the stress component due to pressure is more significant than that due to bending. As such, the postulated leakage flaw may be off-centered and can thus be located anywhere around the pipe circumference, see Figure 5.1. Furthermore, a symmetric bending plane under normal operating stresses may be different than the plane under normal plus safe-shutdown earthquake stresses, due to the uncertainty in seismic ground motion. As a consequence, there are two major effects on pipe fracture evaluations:

(1) for a given leak rate and identically applied load, the detectable flaw size for the off-centered crack will be larger (due to smaller crack-opening area) than that for the symmetrically centered crack (detrimental effects); and

(2) for the same crack length, the load-carrying capacity of the pipe with an off-centered crack will be higher than that with a symmetrically centered crack (beneficial effects).

Since these are two opposing effects, pipe-specific calculations are needed to determine the resultant effect on pipe flaw evaluations. This study examines numerical pipe fracture results to quantify the effects of off-centered cracks on the crack-opening-area (COA) analysis of pipes. Both finite element method (FEM) and a simple estimation scheme were employed to compute the center-crack-opening displacement and crack-opening shapes. Recommendations are made on how an off-centered crack can be analyzed based on the analysis of a centered crack and some additional assumptions. Numerical examples are presented to illustrate and support the findings of this study.

5.2 Crack-Opening-Area Analysis of an Off-Centered Crack

In this analysis, a through-wall-cracked (TWC) pipe was considered with mean pipe radius, R_m, wall thickness, t, and through-wall-crack angle, 2θ. The crack was off-centered by an angle, ψ. The pipe and crack geometric properties are defined in Figure 5.1. The pipe was subjected to a pure bending moment, M, without any internal pressure. The stress analysis was linear-elastic, and both plasticity and crack-growth effects were ignored. This is justified since the normal operating stress for a typical nuclear piping is well below the yield stress of the material and the relatively short crack being considered should not experience significant crack tip plasticity.

In assessing the crack-opening for an off-centered crack, both finite element and estimation analyses were conducted in this study. They are described below.

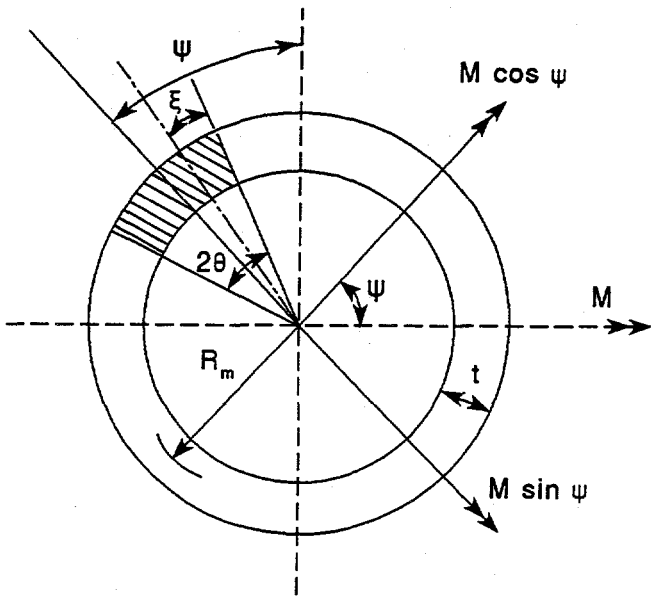

Figure 5.1 Pipe cross-section with an off-centered through-wall crack

T-6300-F5.1

5.2.1 Finite Element Analysis

Standard three-dimensional, linear-elastic, finite element analyses (FEA) were conducted to determine the crack-opening displacement (COD) and the crack-opening shape for a pipe with an off-centered crack. Due to symmetry about loading, only half of the pipe was modeled (Note, symmetry with respect to the crack geometry is violated by the off-centered crack). Since this is a direct method, no further approximations or assumptions are required to evaluate crack-opening characteristics. This is referred to as Method-1 in this report.

When the crack-opening results are needed for several values of ψ (i.e., for several off-centered cracks), conducting FEA for each of them is not efficient. In this regard, one standard finite element analysis was performed to determine the center-crack-opening-displacement, $\delta(0)$, for a symmetrically centered crack (i.e., when $\psi = 0$) under bending moment, M. Then, the center COD, $\delta(\psi)$, under a bending moment M, for an off-centered crack with angle ψ, was estimated from

$$\delta(\psi) = \delta(0)\cos\psi \tag{5-1}$$

by resolving the applied moment into its components as shown in Figure 5.1. (Note, this is possible due to linear-elastic assumptions). This method will be referred to as Method-2 in this report. Since

no explicit finite element analysis was conducted for an off-centered crack, exact determination of the crack-opening profile, and hence crack-opening area and leak rate, could not be made by Method-2. In Method-2, it was assumed that the crack-opening shape is elliptical to allow for the computation of the crack-opening area. The justification came from past studies at Battelle (Refs. 5.1 to 5.3) and also from the results of the present study (see Section 3) which showed that the crack-opening shape for a symmetrically centered crack would approximately follow an elliptical profile. It would be interesting to see how much the crack-opening shape for an off-centered crack would deviate from the ideal elliptical profile. The elliptical assumption will be evaluated when numerical examples are presented in Section 5.3.

5.2.2 Estimation Analysis

For routine fracture calculations, when the finite element analysis cannot be performed or is not needed, the estimation methods discussed in this report (see Sections 2 and 3) can also be applied to determine the crack-opening for off-centered cracks. The applications of these methods are similar to Method-2 of the finite element analysis except that the center-crack-opening-displacement, $\delta(0)$, for a symmetrically centered crack is calculated by a suitable estimation scheme. These estimation schemes may include the GE/EPRI method (Refs. 5.4 to 5.6), the LBB.NRC method (Ref. 5.7), the Paris/Tada method (Ref. 5.8), the LBB.ENG2 method (Ref. 5.9), the LBB.ENG3 method (Refs. 5.10 and 5.11), and others (Ref. 5.12). For example, using the GE/EPRI method, the elastic solution of $\delta(0)$ can be obtained from (Refs. 5.4 to 5.6)

$$\delta(0) = \frac{4R_m^2\theta}{I} V_1^B(\theta/\pi, R_m/t) \frac{M}{E} \qquad (5\text{-}2)$$

where I is the moment of inertia of the uncracked pipe cross-section and $V_1^B(\theta/\pi, R_m/t)$ is the influence (elastic) function tabulated in References 5.4 to 5.6 for several combinations of θ/π and R_m/t. Note that $\delta(0)$ given above by the GE/EPRI method (and also by other estimation methods) denotes the center COD only at the mid-thickness level, because the elastic V_1 functions, compiled in References 5.4 to 5.6, were derived at the mid-thickness of the pipe. See References 5.4, 5.5, 5.6, and 5.12 for further details. Similar to Method-2 in FEA, the crack-opening area by the GE/EPRI method can also be approximated by assuming an elliptical crack-opening profile.

5.3 Numerical Results

For a numerical example, consider a pipe with outer diameter (D_o) of 406.4 mm (16 inches), wall thickness (t) of 26.19 mm (1.031 inch), and crack angle ratio (θ/π) of 0.12. The crack is off-centered by an angle (ψ). It is assumed that the crack length is the same on the inside and outside surfaces in terms of percent of pipe circumference. The pipe is subject to a remote bending moment, M = 522.6 kN-m (4,626 inch-kip) without any internal pressure. The material behavior is assumed to be linear-elastic. The elastic modulus, E = 193.06 GPa (28,000 ksi) and Poisson's ratio, ν = 0.3 were used.

Linear-elastic finite element analyses were performed for this pipe using the structural analysis code, ABAQUS (Ref. 5.13). A total of seven analyses were conducted corresponding to the off-centered

angles, ψ = 0, 15, 30, 45, 60, 75, and 90 degrees. In all cases, twenty-noded three-dimensional solid elements were used in the FEA. The total number of elements and nodes were 1,260 and 9,030, respectively. The number of elements through the thickness was one. Due to symmetry, only half of the pipe was modeled. Figure 5.2 shows the finite element mesh for a pipe with an off-centered crack.

Figures 5.3 and 5.4 show the plots of COD versus the normalized coordinate angle, $\xi/2\theta$, representing detailed crack-opening shapes in the inner and outer surfaces of the pipe, respectively, for values of ψ = 0, 15, 30, 45, 60, 75, and 90 degrees. The angle ξ represents the crack front location from a crack tip and is defined in Figure 5.1. The results in Figures 5.3 and 5.4 were generated by the direct FEM (i.e., Method-1) described earlier. From Figures 5.3 and 5.4, it appears that the maximum COD shifts from the center when the cracks become off-centered. Also, the values of COD for an off-centered crack can become much lower than those for a symmetrically centered crack. Consequently, the crack-opening area (and hence, leak rate) can also be much lower. Hence, idealizing an off-centered crack by a centered crack will yield a smaller crack length for a given leak-rate. The comparison of the results between Figures 5.3 and 5.4 show that the COD at the outer surface is larger than that at the inner surface regardless of the value of ψ.

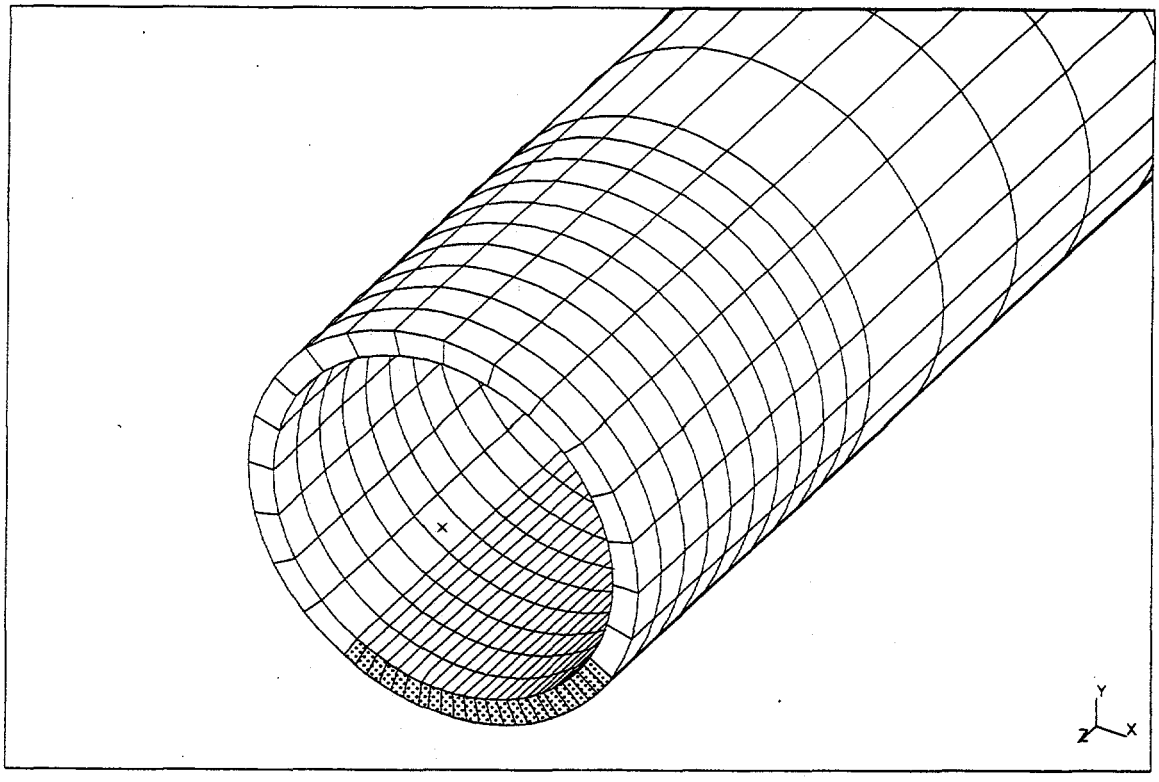

Figure 5.2 Finite element model for a pipe with an off-centered crack (θ/π = 12 percent)
T-6300-F5.2

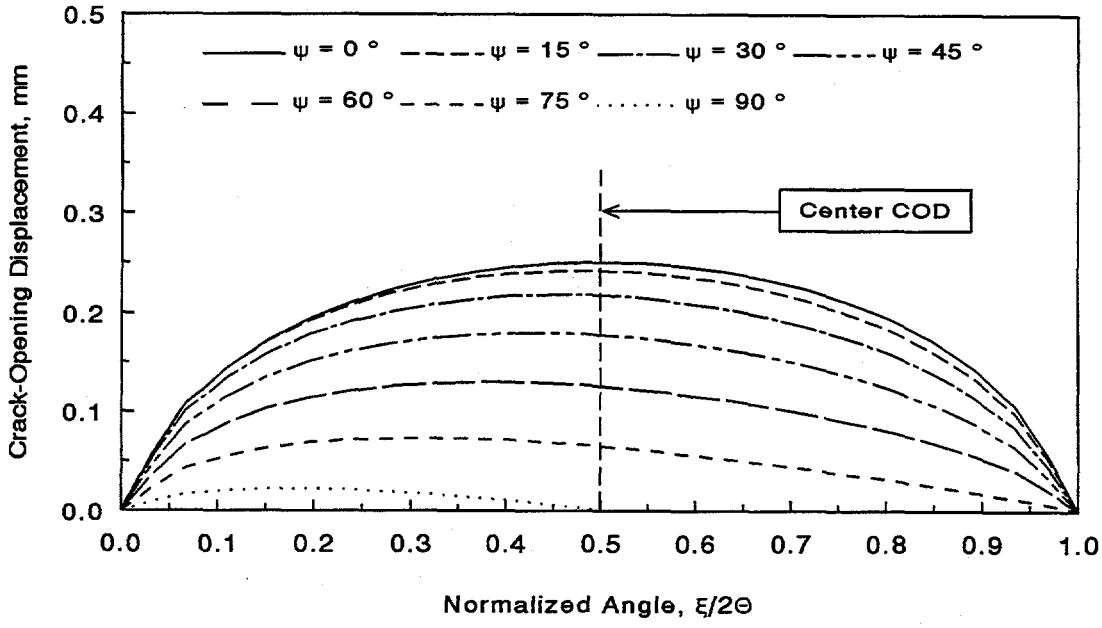

Figure 5.3 Predicted crack-opening displacements for various off-centered cracks as a function of $\xi/2\theta$ (inside surface)

T-6300-F5.3

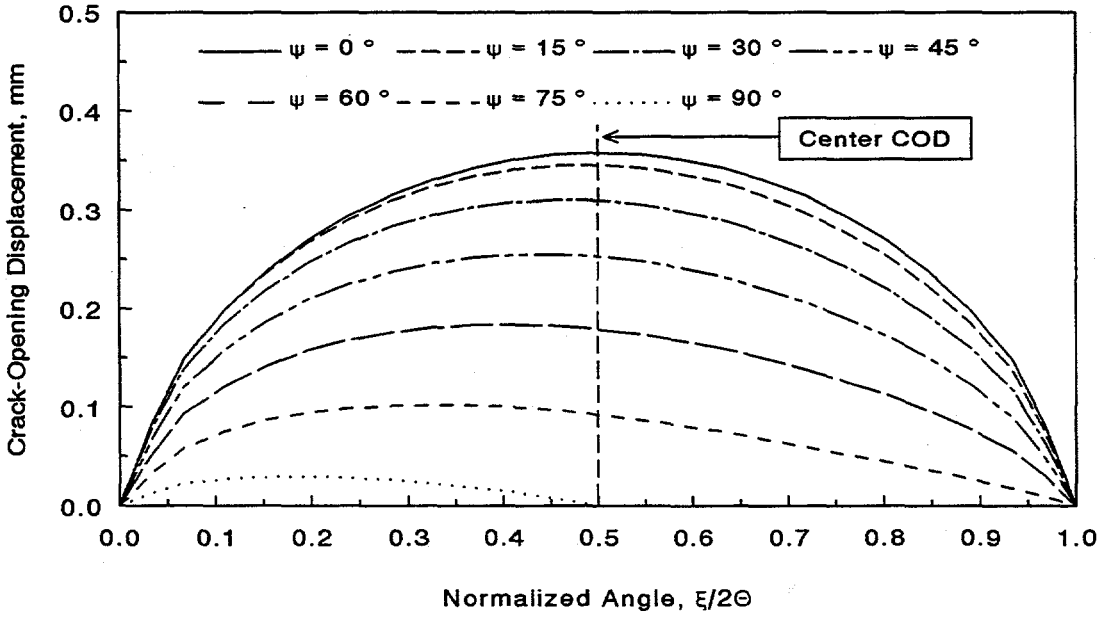

Figure 5.4 Predicted crack-opening displacements for various off-centered cracks as a function of $\xi/2\theta$ (outside surface)

T-6300-F5.4

Similar results predicting various crack-opening characteristics computed by Method-2 of FEA are shown in Figures 5.5 to 5.8. For comparison, the results from Method-1 are also presented. It appears that the center COD predicted by Method-2 compares extremely well with the corresponding Method-1 solutions. However, the elliptical shape assumed by Method-2 underpredicted the COD for one-half of the crack length and overpredicted the COD for the other half of the crack length (see Figures 5.5 and 5.6). But, the comparisons of crack-opening area, which are shown in Figure 5.8, reveal that it can be predicted with good accuracy with an elliptical opening profile, i.e., by Method-2. This is an important finding since for leak-rate calculations, accuracy in the prediction of crack-opening area is more significant than that of entire crack-opening shape. This justifies the use of Method-2 in FEA for analyzing off-centered cracks in pipe fracture evaluations.

For routine pipe flaw evaluation, when finite element analysis cannot be performed, a suitable estimation method, such as the GE/EPRI method described earlier (see Equation 5-2), can also be used. Using Equations 5-1 and 5-2, the predicted center-crack-opening displacements by this estimation method are also shown with the finite element results in Figure 5.7. The results of FEM in Figure 5.7 are given at the inner, middle, and outer surfaces of the pipe in which the mid-thickness COD was calculated from the average COD values at the inside and the outside surfaces. In the same figure, the estimation results were calculated at the mid-thickness level. The COD solutions by the estimation method compare very well with those from more accurate finite element methods. The comparisons of crack-opening area, shown in Figure 5.8, also indicate reasonably accurate predictions by the GE/EPRI estimation method.

5.4 Status of Crack-Opening Methodology

From the numerical results presented in this section, the effects of an off-centered crack were determined considering only crack-opening area on pipe fracture evaluations. Their effects on the load-carrying capacity and the fracture stability of a leaking crack have not been assessed yet. From a qualitative viewpoint, one can, however, argue that when a crack is off-centered, the crack-driving force, be it stress-intensity factor in linear-elastic fracture or J-integral in elastic-plastic fracture, will be lower than that for a centered crack assuming that the bending plane is the same for normal moments and seismic moments. However, it is more likely that these bending planes will differ. Hence, an off-centered crack, which may increase the length of the leakage flaw due to reduced crack-opening, can have positive effects on the maximum load-carrying capacity of pipes. In this report, the explicit effects on crack-opening area have been quantified. It would be interesting to see how they would be countered by the positive effects related to the structural integrity of the pipes.

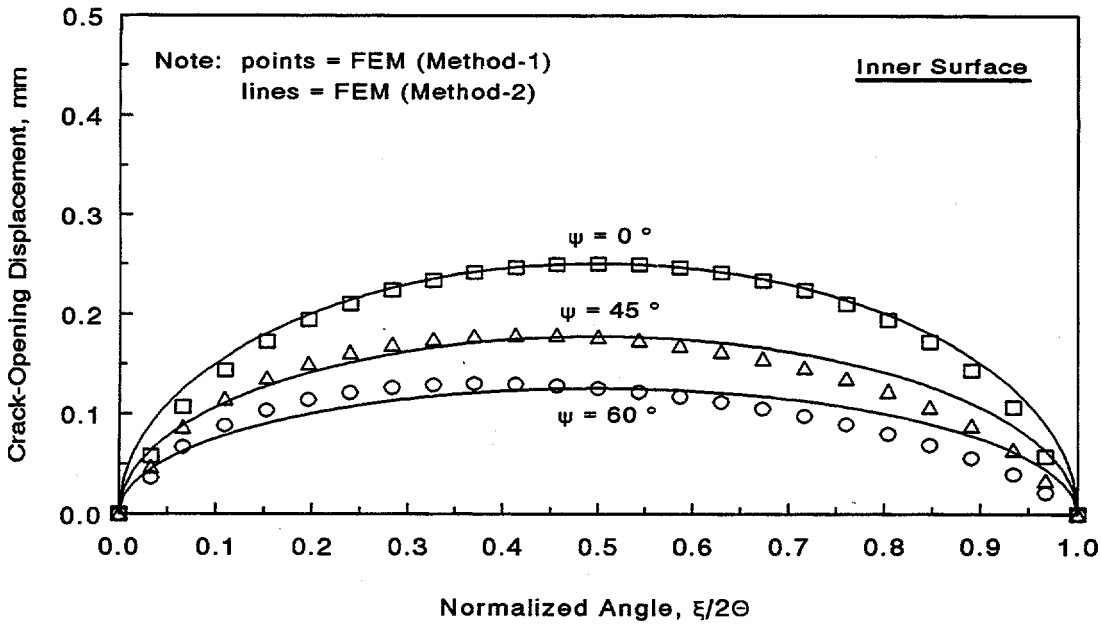

Figure 5.5 Comparisons of two finite element solutions for predicting crack-opening displacements for off-centered cracks as a function of $\xi/2\theta$ (inside surface)

T-6300-F5.5

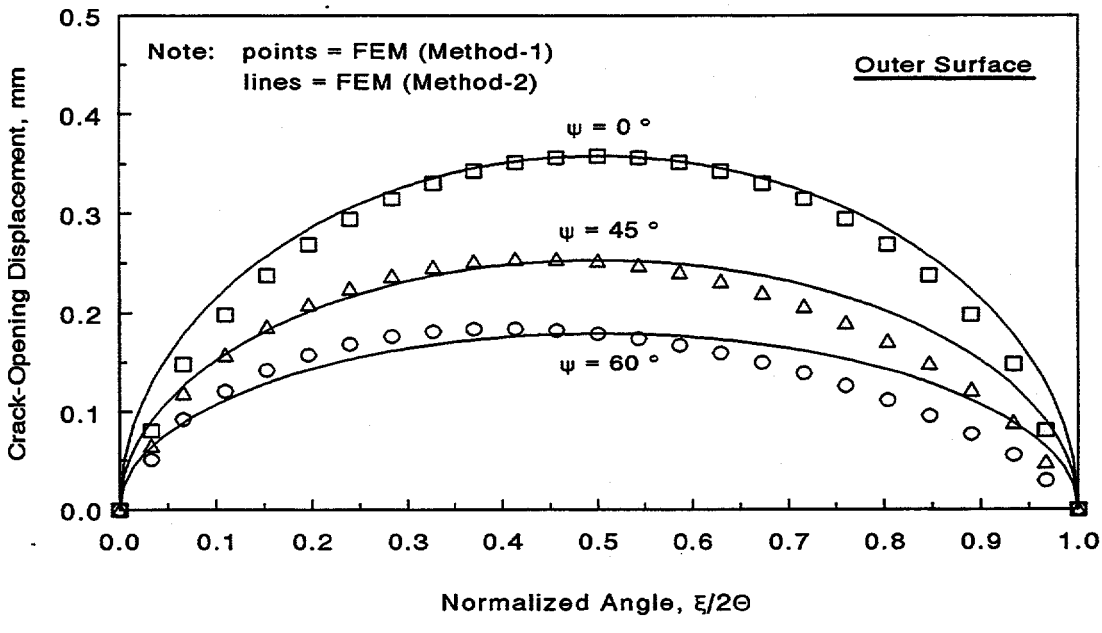

Figure 5.6 Comparisons of two finite element solutions for predicting crack-opening displacements for off-centered cracks as a function of $\xi/2\theta$ (outside surface)

T-6300-F5.6

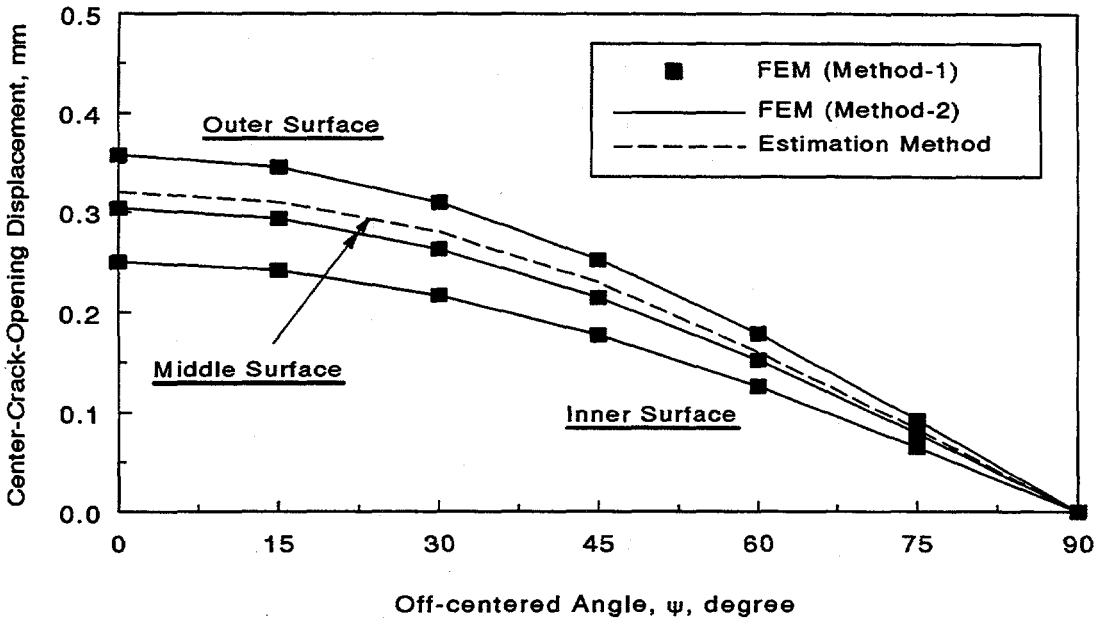

Figure 5.7 Predicted center-crack-opening displacements for off-centered cracks by finite element and GE/EPRI estimation methods

T-6300-F5.7

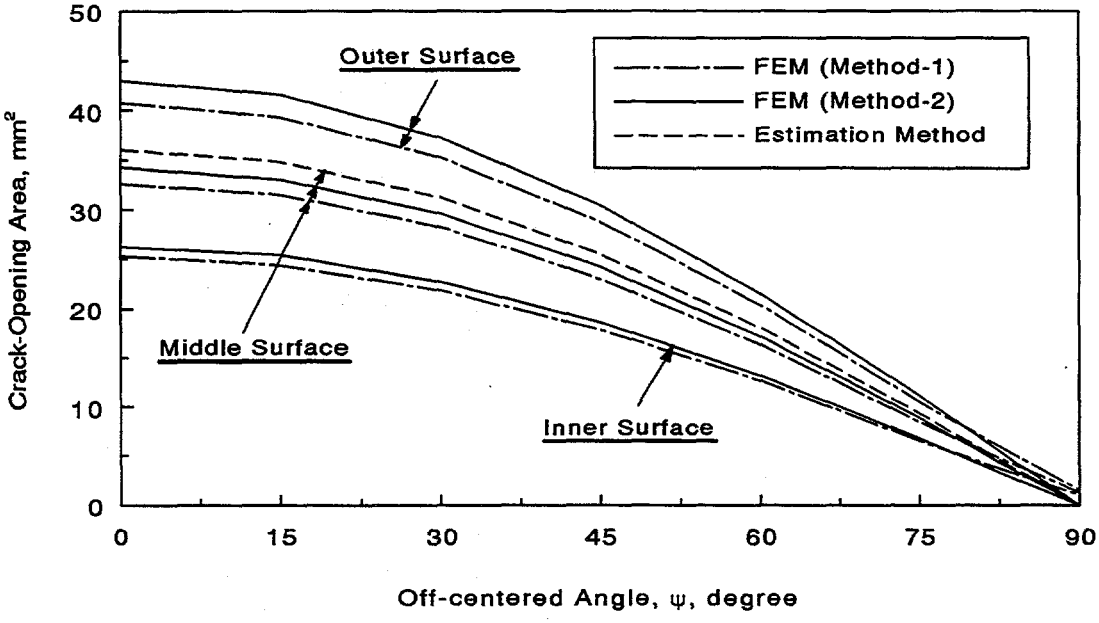

Figure 5.8 Predicted crack-opening areas for off-centered cracks by finite element and GE/EPRI estimation methods

T-6300-F5.8

5.5 References

5.1 Wilkowski, G. M., Ahmad, J., Barnes, C. R., Brust, F., Ghadiali, N., Guerrieri, D., Jones, D., Kramer, G., Landow, M., Marschall, C. W., Olson, R., Papaspyropoulos, V., Pasupathi, V., Rosenfeld, M., Scott. P., and Vieth, P., "Degraded Piping Program - Phase II: Summary of Technical Results and Their Significance to Leak-Before-Break and In-Service Flaw Acceptance Criteria, March 1984 - January 1989," NUREG/CR-4082, Vol. 8, U.S. Nuclear Regulatory Commission, Washington, D.C., March 1989.

5.2 Paul, D., Ahmad, J., Scott, P. M., Flanigan, L. F., and Wilkowski, G., "Evaluation and Refinement of Leak-Rate Estimation Models," NUREG/CR-5128, Rev. 1, U.S. Nuclear Regulatory Commission, Washington, D.C., June 1994.

5.3 Wilkowski, G., Rahman, S., Paul, D., and N. Ghadiali, "Pipe Fracture Evaluations for Leak-Rate Detection: Deterministic Models," PVP-Vol. 266, *Creep, Fatigue Evaluation, and Leak-Before-Break Assessment*, pp. 243-254, 1993.

5.4 Kumar, V., German, M., and Shih, C., "An Engineering Approach for Elastic-Plastic Fracture Analysis," EPRI Report NP-1931, Electric Power Research Institute, Palo Alto, CA, July 1981.

5.5 Kumar, V., German, M., Wilkening, W., Andrews, W., deLorenzi, H., and Mowbray, D., "Advances in Elastic-Plastic Fracture Analysis," EPRI Final Report NP-3607, Electric Power Research Institute, Palo Alto, CA, August 1984.

5.6 Brust, F., Rahman, S., and Ghadiali, N., "Elastic-Plastic Analysis of Small Cracks in Tubes," *Proceedings of the 11th International Conference on Offshore Mechanics and Arctic Engineering*, Calgary, Alberta, Canada, June 1992.

5.7 Klecker, R., Brust, F., and Wilkowski, G., "NRC Leak-Before-Break (LBB.NRC) Analysis Method for Circumferentially Through-Wall-Cracked Pipes Under Axial Plus Bending Loads," NUREG/CR-4572, U.S. Nuclear Regulatory Commission, Washington, D.C., May 1986.

5.8 Paris, P. C. and Tada, H., "The Application of Fracture Proof Design Methods Using Tearing Instability Theory to Nuclear Piping Postulating Circumferential Through-Wall Cracks," NUREG/CR-3464, U.S. Nuclear Regulatory Commission, Washington, D.C., September 1983.

5.9 Brust, F. W., "Approximate Methods for Fracture Analyses of Through-Wall Cracked Pipes," NUREG/CR-4853, U.S. Nuclear Regulatory Commission, Washington, D.C., February 1987.

5.10 Rahman, S. and Brust, F., "An Estimation Method for Evaluating Energy Release Rates of Circumferential Through-Wall Cracked Pipe Welds," *Engineering Fracture Mechanics*, Vol. 43, No. 3, pp. 417-430, 1992.

5.11 Rahman, S. and Brust, F., "Elastic-Plastic Fracture of Circumferential Through-Wall Cracked Pipe Welds Subject to Bending," *Journal of Pressure Vessel Technology*, Vol. 114, No. 4, pp. 410-416, November 1992.

5.12 Wilkowski, G. M., Brust, F., Francini, R., Ghadiali, N., Kilinski, T., Krishnaswamy, P., Landow, M., Marschall, C. W., Rahman, S., and Scott, P., "Short Cracks in Piping and Piping Welds," Semi-Annual Reports, Volumes 1, 2, and 3, Nos. 1 and 2, NUREG/CR-4599, U.S. Nuclear Regulatory Commission, Washington, D.C., 1990-1992.

5.13 ABAQUS, User's Guide and Theoretical Manual, Version 5.3, Hibbitt, Karlsson, & Sorensen, Inc., Pawtucket, RI, 1993.

6.0 RESTRAINT OF BENDING FROM PRESSURE CONTRIBUTION IN A PIPE SYSTEM

6.1 Introduction

Current structural analyses for through-wall-cracked (TWC) pipes subjected to axial tension loads (generally pressure induced) or combined bending and tension loads assume that the pipe is free to rotate. The restraint of the rotation increases the failure stresses (Refs. 6.1 and 6.2), but can decrease the crack-opening at a given load. If the pipe system restrains the bending, for example from cracks being close to a nozzle or restraint from the rest of the piping system, then the leak rate will be less than the leak rate calculated by using analyses that assume that the pipe is free to rotate. This will cause the actual leakage crack size to be larger than that calculated by the current analysis methods for the same leak rate. Since stress due to internal pressure is a significant component of the total stress, this could have a significant effect on the leak-before-break (LBB) analysis and pipe flaw evaluations. Some scoping calculations were performed to assess the magnitude of the trends.

6.2 Analysis for Restraint of Axial Tension (Pressure) Induced Bending

Figure 6.1 illustrates a TWC pipe with mean radius, R_m, wall thickness, t, and an initial through-wall crack angle, 2θ. The pipe is subjected to an axial tension load, P, (due to internal pressure) with full restraint of axial tension (pressure) induced bending at a distance, L_R, on either side of the cracked plane. Linear-elastic analyses by the finite element method were performed to examine the effects of restraint due to axial tension-induced bending in a piping system when the pressure load was applied. The results of crack-opening displacement (COD) as a function of "restraint length" were investigated. The restraint length (L_R) defined here simply represents the location of the restrained pipe cross-sections from the cracked plane and is shown in Figure 6.1.

The following steps were undertaken to determine the effects of restraint of induced bending due to axial tension from internal pressure:

Step 1: Create a finite element model of a cracked pipe with thickness, t, mean pipe diameter, D_m, initial crack angle, 2θ, and total pipe length, $2L_R$, where L_R is the restraint length discussed previously.

Step 2: Apply an arbitrary positive (tensile) displacement loading, Δ, in the longitudinal direction of the pipe to all the nodes in cross-section A-A located (see Figure 6.1) at a distance L_R from the cracked plane (i.e., the pipe ends in this case). In this way, the complete restraint of induced bending from tension is simulated symmetrically about the crack. (A nonsymmetric restraint analyses would require a more sophisticated model and was not warranted in this initial investigation.)

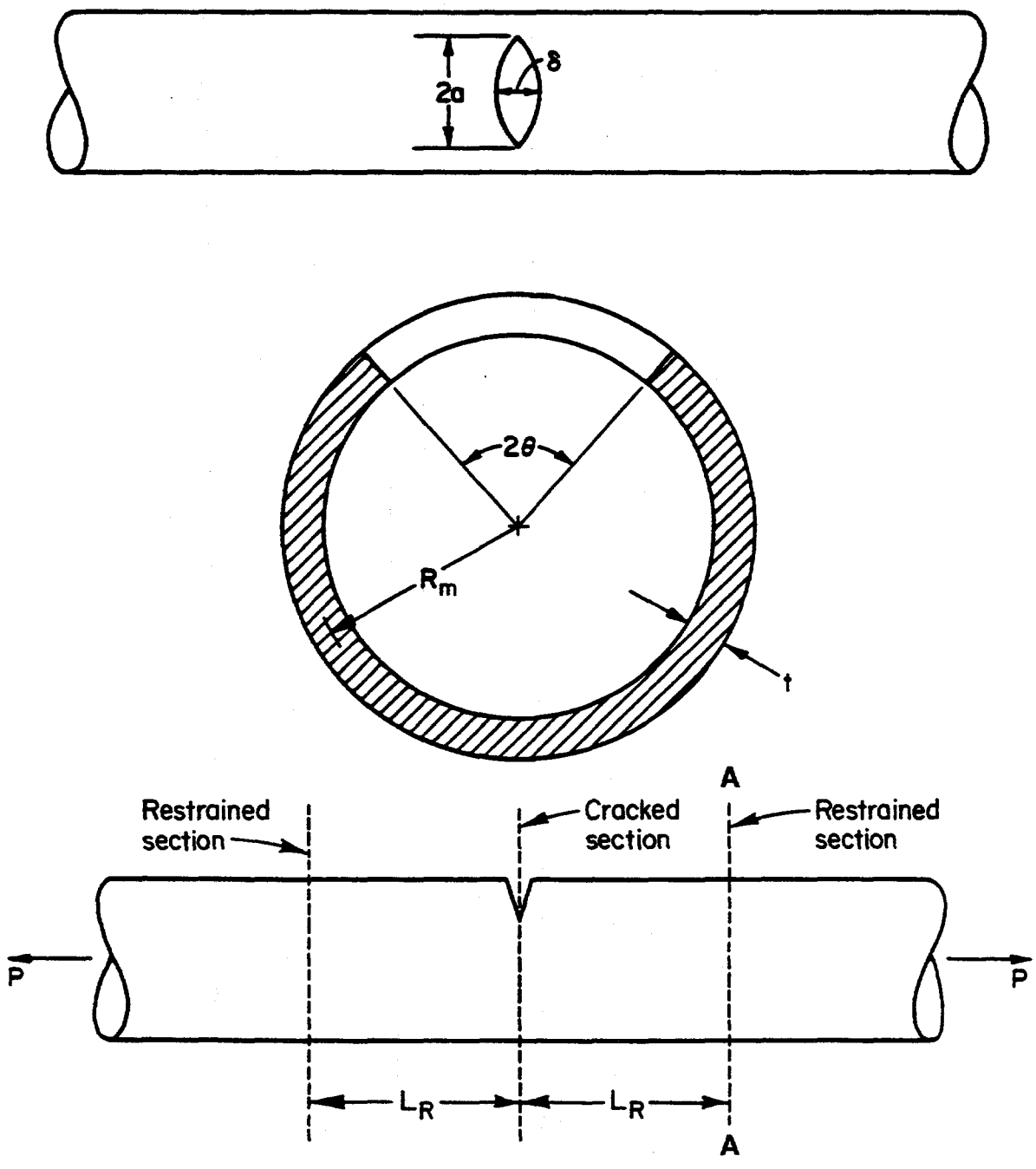

Figure 6.1 Schematic of a through-wall-cracked pipe under pure tension (restrained locations prevent rotation and ovalization)

T-6300-F6.1

Step 3: Conduct a finite element analysis and determine the COD resulting from the remote displacement, Δ. The stresses at the cross-section A-A are not uniform and can be decomposed into a bending component with a linear variation and a tensile component. Denote the COD (unscaled) and the tension stress by δ_{uns} and σ_{ten}, respectively.

Step 4: Compute the scaled COD, $\delta_s = \delta_{uns} \times (\sigma_{ref}/\sigma_{ten})$, where σ_{ref} is any arbitrarily defined reference tensile stress. The COD due to a reactive tensile stress, σ_{ref}, with complete restraint of induced bending at cross-sections L_R away from the cracked plane is represented by δ_s. This scaling is permissible due to the linear-elastic stress analysis.

Step 5: In the same finite element model apply a tension stress loading of magnitude σ_{ref} but allowing free rotation. Denote the resultant COD by δ_∞ which now represents the reference crack-opening displacement due to an axial tensile stress, σ_{ref}, when there are no external bending restraints present in the pipe, i.e., when the restraint length, L_R, approaches infinity.

Step 6: Divide the scaled COD, δ_s, by the reference COD, δ_∞, to get the normalized COD, $\delta_{NOR} = \delta_s/\delta_\infty$. The restrained COD normalized by the unrestrained COD is represented by δ_{NOR}.

Step 7: For a given crack geometry, repeat Steps 1 - 6 for several values of L_R. Develop a plot of δ_{NOR} versus L_R/D_m and hence, determine the effects of the normalized restraint length, L_R/D_m, on the crack-opening displacement.

6.3 Numerical Applications

As a numerical example, consider a TWC pipe with a mean radius of 355.6 mm (14 inches), thickness of 35.56 mm (1.4 inches), R_m/t of 10, and two distinct cases of initial total crack angles of 2θ where for the two cases $\theta/\pi = 1/8$ and $\theta/\pi = 1/4$ ("small" and "large" cracks). For material properties, it was assumed that the modulus of elasticity, E, was 200 GPa (29,000 ksi) and Poisson's ratio, ν, was 0.3. The pipe was subjected to remote pressure with the resultant force applied at the centroid of the uncracked pipe cross-section. Linear-elastic analyses by the finite element method were performed using twenty-noded three-dimensional solid brick elements in the structural analysis code ABAQUS (Ref. 6.3). The total number of elements and nodes were 172 and 1,252, respectively. The number of elements through the thickness was one. Due to symmetry, only a quarter of the pipe was modeled. Figure 6.2 shows a typical mesh representing the finite element discretization.

Tables 6.1 and 6.2 show the calculated values of various crack-opening displacements for both "small" ($\theta/\pi = 1/8$) and "large" ($\theta/\pi = 1/4$) cracks, respectively. These were obtained following the steps described earlier. Several values of restraint length, L_R, were considered and are also tabulated. For these calculations, the arbitrary applied displacement, Δ, was set equal to 2.54 mm

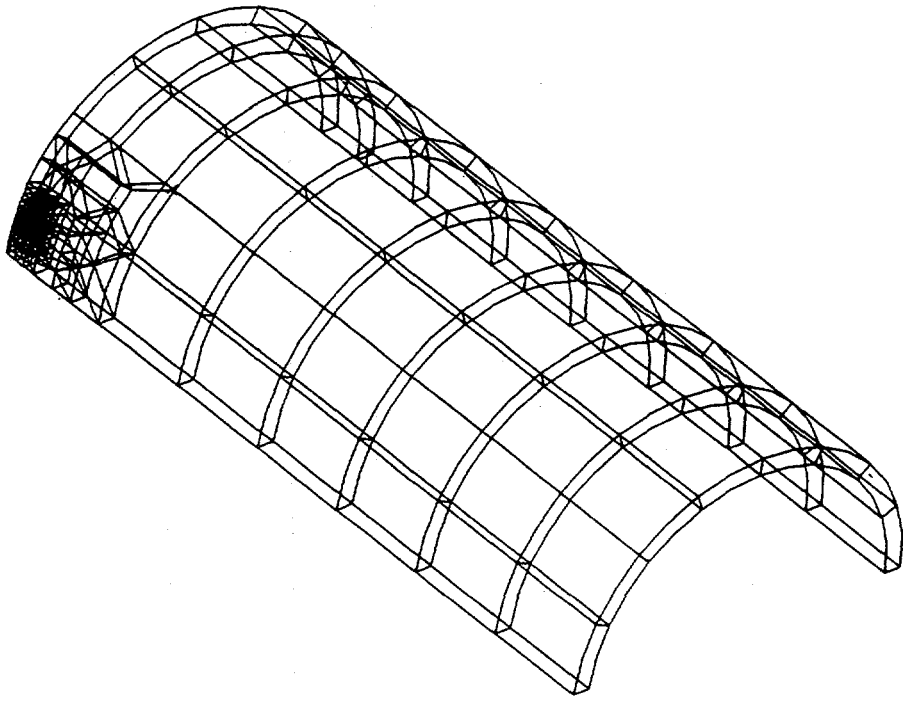

Figure 6.2 Finite element mesh for linear-elastic restraint of crack-opening displacement

T-6300-F6.2

Table 6.1 Elastic crack-opening displacements for TWC pipe (θ/π = 1/8)

L_R/D_m	Unscaled COD (δ_{uns}), mm	Tensile Stress (σ_{ten}), MPa	Scaled COD (δ_s), mm	Normalized COD (δ_{NOR})
1	2.460	849.12	2.460	0.9573
5	0.547	182.47	2.546	0.9909
10	0.290	95.83	2.569	1.000

Table 6.2 Elastic crack-opening displacements for TWC pipe (θ/π = 1/4)

L_R/D_m	Unscaled COD (δ_{uns}), mm	Tensile Stress (σ_{ten}), MPa	Scaled COD (δ_s), mm	Normalized COD (δ_{NOR})
1	4.873	650.97	4.873	0.5606
5	1.624	174.35	6.065	0.6977
10	0.870	75.84	7.469	0.8593
20	0.474	36.54	8.445	0.9716

(0.1 inch) (Step 2). The arbitrary elastic reference tensile stresses, σ_{ref}, were assumed to be 849.12 MPa (123.15 ksi) and 650.97 MPa (94.41 ksi) for θ/π = 1/8 and θ/π = 1/4, respectively (Steps 4 and 5). From the finite element analysis, the corresponding values of reference COD, δ_∞, were computed to be 2.569 mm (0.101 inch) and 8.692 mm (0.342 inch), respectively (Step 5).

Figure 6.3 presents the results of the calculations for normalized crack-opening displacement (δ_{NOR}) as a function of normalized restraint length, L_R/D_m, in which $D_m = 2R_m$ represents the mean pipe diameter. As mentioned before, the COD values are normalized with reference to the crack-opening displacement when there are no external constraints present in the pipe (i.e., when the restraint length becomes infinity), allowing free rotation and ovalization. The results suggest that when the crack angle is small (θ/π=1/8), the restraint effects are also small and may be neglected. However, for larger crack angles (θ/π=1/4), the restrained COD can be significantly different than the unrestrained COD, and hence, should not be ignored in the crack-opening-area analysis for leak-rate quantification. This is especially true for small-diameter pipes in which the leaking crack size for LBB analysis can be large. It is interesting to note that a significant input parameter like the "restraint length" is not currently considered in either of the thermal-hydraulic codes SQUIRT (Ref. 6.4) or PICEP (Ref. 6.5) or in any other leak-rate analyses.

6.4 Status of Crack-Opening Methodology

From the numerical results presented in this report, the potential reduction of crack-opening area due to the restraint of pressure-induced bending has been evaluated for some specific cases. It is recognized that for a pipe which restrains bending from pressure loads, the load-carrying capacity of the pipe will tend to increase. However, it could be argued that since the normal operating plus seismic loads have a higher percentage of bending than axial membrane loads, the beneficial effects on the fracture loads may not be as great. Nevertheless, the restraint of pressure-induced bending, which may have unfavorable effects on calculating leakage flaw size, can have positive effects on the maximum load-carrying capacity of pipes. In this report, the effects on crack-opening area have been quantified. It would be useful to also quantify the possible increase in the failure loads and then

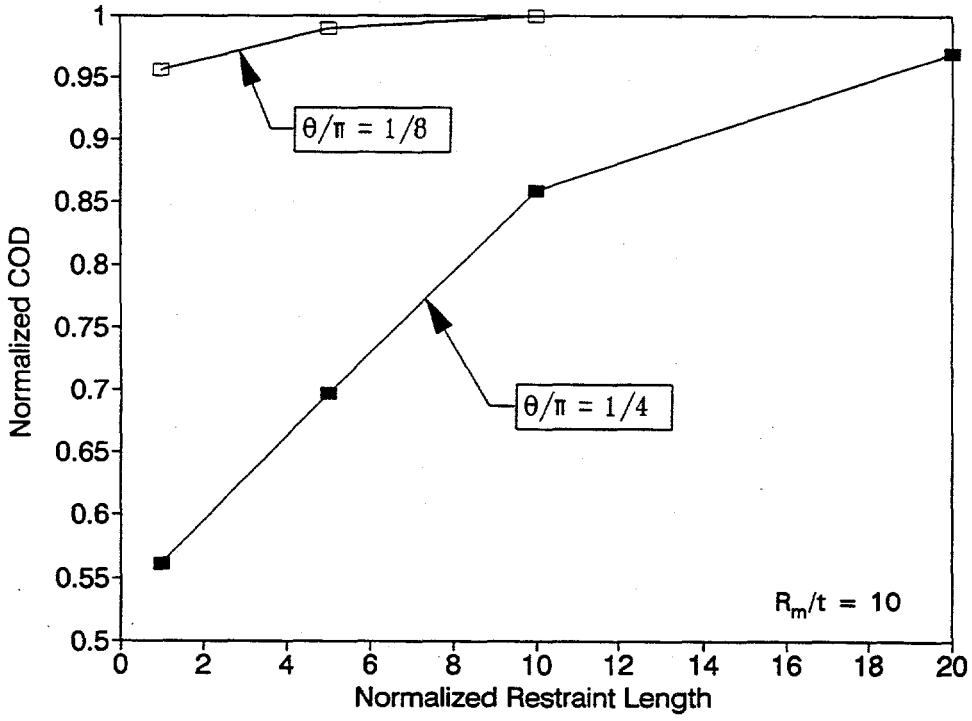

Figure 6.3 Effects of fully restrained bending conditions from crack location on COD normalized by the unrestrained COD

T-6300-F6.3

evaluate how it would counter the effects of crack-opening-area reduction. Hence, further studies and developments are needed to assess quantitatively their resultant effects.

In regard to the effect of restrained bending on failure loads, the following experimental data exists. From one pipe system experiment in the International Piping Integrity Research Group Program (Phase 1), it was experimentally determined that a guillotine break did not occur until the growing through-wall crack was 95 percent around the circumference (Ref. 6.2). From the pressure loads alone, it was expected that a double-ended guillotine break would occur once the crack reached 65 percent of the circumference. The 95-percent crack length corresponded to the pressure-induced failure if the induced bending was restrained. This crack was located 3.4 pipe diameters from an elbow. This is strong evidence of the effect of pressure-induced bending restraint on increasing load-carrying capacity in a pipe system, even if only at the instability crack length.

6.5 References

6.1 Wilkowski, G. M. and others, "Degraded Piping Program - Phase II," Semiannual Report, October 1984 - March 1985, NUREG/CR-4082, Vol. 2, U.S. Nuclear Regulatory Commission, Washington, D.C., July 1985.

6.2 Schmidt, R. A., Wilkowski, G. M., and Mayfield, M. E., "The International Piping Integrity Research Group (IPIRG) Program: An Overview," *Transactions of the 11th International Conference on Structural Mechanics in Reactor Technology, Vol. G2: Fracture Mechanics and Non-Destructive Evaluation - 2*, Edited by H. Shibata, Tokyo, Japan, Paper No. G23/1, pp. 177-188, August 1991.

6.3 ABAQUS, User's Guide and Theoretical Manuals, Version 4.8, Hibbitt, Karlsson, & Sorensen, Inc., Pawtucket, RI, 1989.

6.4 Paul, D., Ahmad, J., Scott, P., Flanigan, L., and Wilkowski, G., "Evaluation and Refinement of Leak-Rate Estimation Models," NUREG/CR-5128, Rev. 1, U.S. Nuclear Regulatory Commission, Washington, D.C., June 1994.

6.5 Norris, D. and others, "PICEP: Pipe Crack Evaluation Program," EPRI Report NP-3596-SR, Electric Power Research Institute, Palo Alto, CA, 1984.

7.0 CIRCUMFERENTIAL CRACK AT A THICKNESS TRANSITION

7.1 Introduction

A practical problem in leak-rate analysis involves evaluating the effects of thickness transition on the crack-opening-area (COA) analysis of a circumferential crack. Thickness transition effects can occur, for example, when a crack develops in a girth weld at a nozzle with a thickness taper on both sides with the same or differential gradients. Currently, there are no engineering models for calculating crack-opening displacements (COD) for such a girth weld nozzle crack.

This section discusses the analytical efforts undertaken to assess the effects of a typical thickness transition and geometric constraint associated with heavy, integrally reinforced nozzles on the crack-opening displacements for a circumferential through-wall crack in a carbon steel nozzle. This study was conducted to obtain a better understanding of the crack-opening characteristics for circumferential cracks at a thickness transition.

7.2 A Girth Weld Crack at a Nozzle with a Thickness Taper

Figure 7.1 shows a typical carbon steel nozzle between a 423.6-mm (16.7-inch) diameter cold-leg pipe and a 333.2-mm (13.1-inch) safety injection line. The outer diameter of the nozzle varies from 534.92 mm (21.1 inches) to 333.2 mm (13.1 inches) with the corresponding wall thickness varying from 124.0 mm (4.88 inches) to 23.1 mm (0.910 inch). There is thickness gradient on each side of Section D-D as shown in Figure 7.1. On one side of Section D-D, the thickness decreases gradually with a constant gradient from 124.0 mm (4.88 inches) to 46.7 mm (1.84 inches). The gradient becomes smaller for the other side of Section D-D in which case, the thickness varies from 46.7 mm (1.84 inches) to 23.1 mm (0.91 inch). The thicknesses for the cold-leg pipe and the safety injection line are constant and are equal to 85.1 mm (3.35 inches) and 34.8 mm (1.37 inches), respectively. The geometric properties defining lengths for each of these pipes are given in Figure 7.1.

A circumferential through-wall crack was placed in the welded section of the nozzle (i.e., at Section D-D of Figure 7.1) with thickness gradient on both sides. The crack length was 12.5 percent of the pipe circumference measured at Section D-D. It was assumed that the crack length on the inside diameter is the same as on the outside diameter in terms of percent of pipe circumference (i.e., the crack tips are radial). The crack was placed in the center of the bending plane of the pipe (i.e., no off-center crack). The crack was assumed to be stationary.

The material properties of the carbon steel nozzle at 288 C (550 F) are given in Table 7.1. The values in Table 7.1 represent the base metal properties of carbon steel. The plastic behavior was represented by the standard Ramberg-Osgood equation (see Equation 2-1). No weld metal properties were used in the finite element analysis. Also, the material properties of the cold-leg pipe and safety injection line were not used in the analyses.

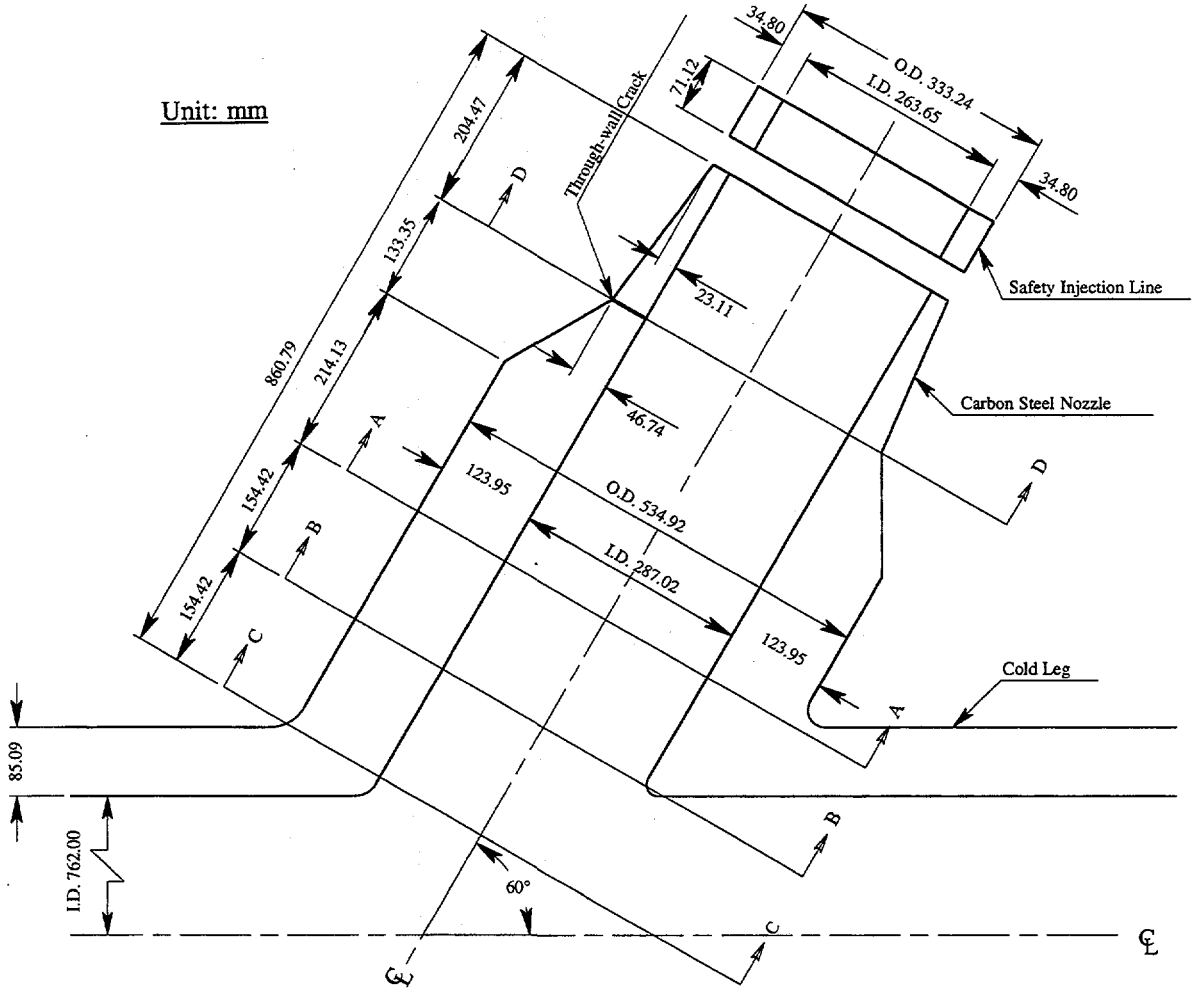

Figure 7.1 Geometric details of a carbon steel nozzle with a through-wall crack at thickness transition, dimensions in mm

T-6300-F7.1

Table 7.1 Material properties of carbon steel nozzle at 288 C (550 F) for crack-opening analysis

Material Properties	Values
Elastic Modulus (E), GPa (ksi)	193.1 (28,000)
Poisson's Ratio (ν)	0.3
Yield Strength (σ_y), MPa (ksi)	237 (34.4)
Ultimate Strength (σ_u), MPa (ksi)	610 (88.5)
Ramberg-Osgood Coefficient (α)[a]	2.157
Ramberg-Osgood Exponent (n)[a]	4.042

(a) The stress-strain (σ-ϵ) curve is represented by: $\epsilon/\epsilon_0 = \sigma/\sigma_0 + \alpha(\sigma/\sigma_0)^n$, where $\sigma_0 = \sigma_y$, $\epsilon_0 = \sigma_0/E$

7.3 Loading Conditions

The nozzle was pressurized with an internal pressure of 15.51 MPa (2,250 psi) at 288 C (550 F) representing typical operating condition of a PWR. Four different bending moments in addition to the pressure were applied at the free end of the nozzle. The applied bending moments were:

Load Case 1: M = 0 kN-m (0 inch-kip),

Load Case 2: M = 200 kN-m (1,770 inch-kip),

Load Case 3: M = 600 kN-m (5,311 inch-kip), and

Load Case 4: M = 1,000 kN-m (8,851 inch-kip).

For Load Case 1, the pipe is under pure tension, whereas for Load Cases 2 to 4, the pipe is under combined bending and tension with increasing values of moment shown above.

7.4 Finite Element Analysis

7.4.1 Idealized Nozzle Geometry

According to Figure 7.1, the nozzle has a slanted configuration which makes a full three-dimensional finite element analysis difficult. In addition, modeling the slanted geometry would require large computer resources. In order to simplify the analysis, an idealized nozzle geometry was chosen and is shown in Figure 7.2. The nozzle in Figure 7.2 has the same geometric parameters as in Figure 7.1

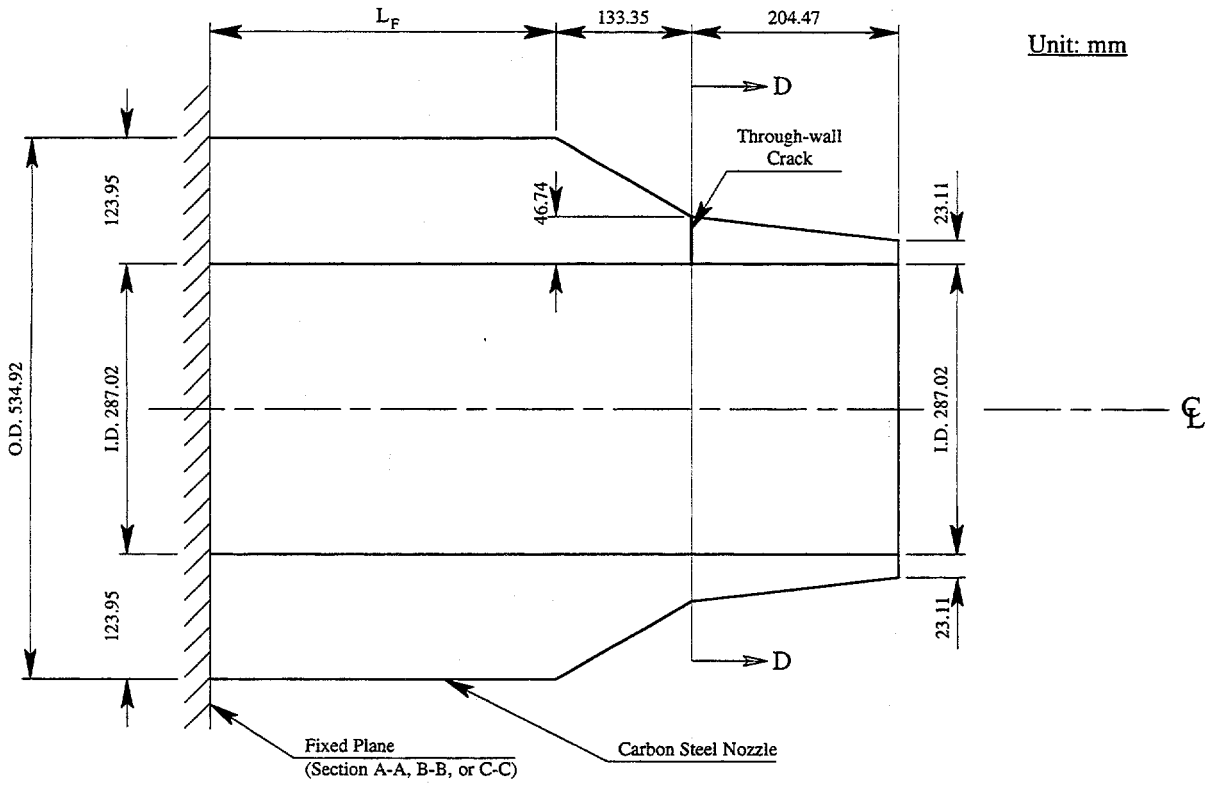

Case 1	L_F= 214.13 mm
Case 2	L_F= 368.55 mm
Case 3	L_F= 522.97 mm

Figure 7.2 Idealized nozzle geometry with fixed boundary condition, dimensions in mm

T-6300-F7.2

except that one end of the nozzle is completely fixed. The distance between the fixed plane and the nozzle section with largest wall thickness (or outer diameter) is denoted by L_F and is shown in Figure 7.2. Due to the uncertainty in the location of this fixed plane, three distinct locations denoted by Sections A-A, B-B, and C-C, and shown in Figure 7.1, were considered. Based on the geometric details given in Figure 7.1, the values of L_F corresponding to the fixed boundary conditions were:

Case 1 Boundary Condition (Section A-A): L_F = 214.13 mm (8.43 inches)

Case 2 Boundary Condition (Section B-B): L_F = 368.55 mm (14.51 inches)

Case 3 Boundary Condition (Section C-C): L_F = 522.97 mm (20.59 inches)

All three boundary conditions were used in the finite element analyses to determine the effects of L_F on the crack-opening area as opposed to full three-dimensional analysis of the nozzle and the cold-leg pipe. For the analyses, the moments were applied at the free-end of the idealized nozzle in Figure 7.2.

7.4.2 Finite Element Modeling

Standard three-dimensional, elastic-plastic, finite element analyses were performed for the nozzle pipe in Figure 7.2 using the structural analysis code ABAQUS (Ref. 7.1). A total of twelve finite element analyses were conducted for four different loading conditions and three different boundary conditions defined earlier. In all cases, twenty-noded, three-dimensional solid elements were used in the finite element model. Due to symmetry, only half of the pipe was needed to be modeled. The total number of elements and nodes were 260 and 2,093, respectively. The number of elements through the thickness was three. Figure 7.3 shows a finite element mesh for half of the nozzle (undeformed configuration) with a crack at the thickness transition.

The ABAQUS analyses were performed using two load steps. The first load step consisted of an internal pressure of 15.514 MPa (2,250 psi) applied directly to the inside of the pipe and also an equivalent tension load due to pressure at the end was applied. In this way, both the axial and circumferential (hoop) stress in the pipe due to internal pressure were simulated. The second load step consisted of bending moments applied in several substeps up to a maximum of 1.00 MN-m (8,851 inch-kip).

7.4.3 Results of Analysis

Figure 7.4 shows the sensitivity of the finite element results to the fixed locations defined by the Sections A-A, B-B, and C-C. From this figure, the center-crack-opening displacements calculated at the inner and the outer surfaces of the pipe subjected to two extreme loadings (one was pure pressure and other was combined pressure and bending of 1.00 MN-m [8,851 inch-kip]) do not appear to be dependent on length, L_F, which defines the location of the fixed plane. Clearly, the crack-opening results are not affected by the choice of the boundary conditions defined earlier. This also implies that the analysis of an idealized nozzle geometry shown in Figure 7.2, instead of modeling

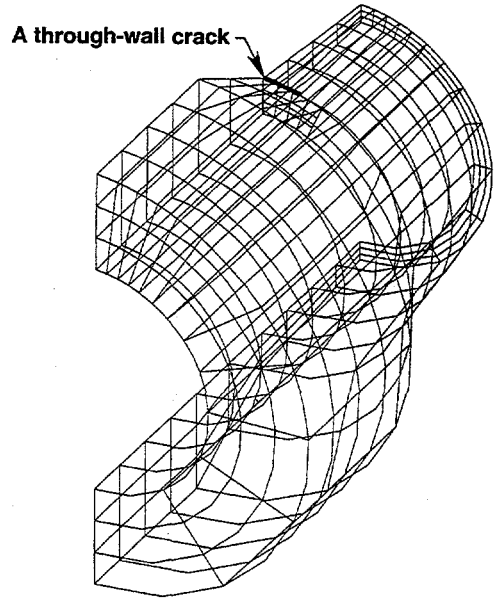

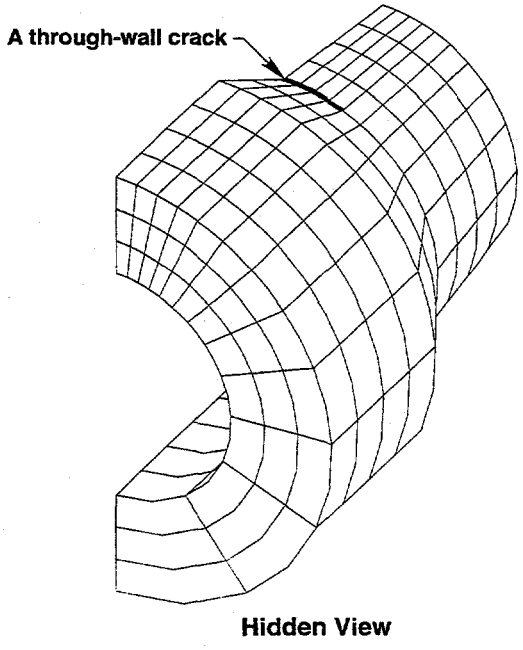

Figure 7.3 Finite element model of a carbon steel nozzle with a through-wall crack

T-6300-F7.3

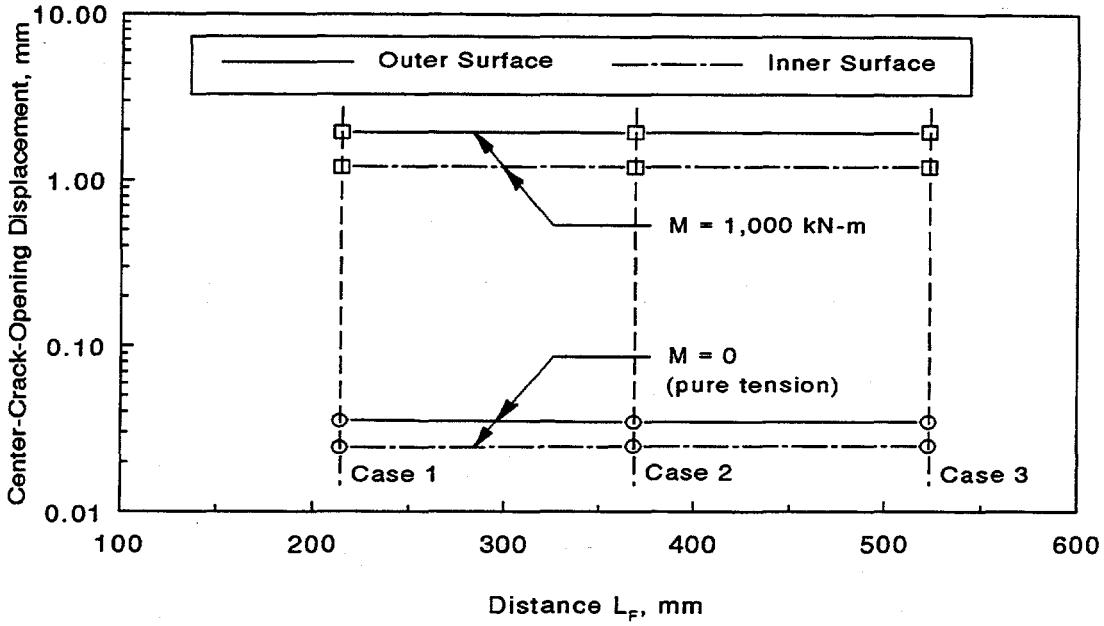

Figure 7.4 Center-crack-opening displacement versus location of fixed plane for various applied moments

T-6300-F7.4

the combined nozzle and cold-leg pipe of Figure 7.1 is a useful simplification for crack-opening-area analyses.

Figures 7.5 through 7.8 provide detailed plots of crack-opening displacement versus normalized distance from the crack-tip for four different load cases showing the crack-opening profiles of the nozzle crack. For better understanding of the problem, the components of the COD in the direction of both thinner and thicker sides of the cracked section are shown. The "zero" horizontal lines in Figures 7.5 to 7.8 simply denote a straight line joining two crack tips at the deformed configuration of the pipe. A positive value of the COD denotes the component of COD in the thinner side of the crack, whereas a negative value of the COD denotes the component of COD in the thicker side of the crack. Both components of the COD were calculated at the inner and outer surfaces of the pipe from the finite element analyses and are presented in Figures 7.5 to 7.8. The results indicate that due to thickness gradient on both sides of the crack, the component of COD in the thinner side is much larger than that in the thicker side, thereby breaking the symmetry of the crack-opening profile about the crack length. The differences in these COD components can be significant when the applied moment is large, e.g., when M = 1.00 MN-m (8,851 inch-kip) in this study (see Figure 7.8).

Finally, Figure 7.9 shows the variations of center-crack-opening displacement as a function of the applied moment which are calculated at both inner and outer surfaces of the pipe. The results suggest that the crack-opening behavior is still linear at M = 600 kN-m (5,311 inch-kip), but can be significantly nonlinear after that moment is exceeded. This strong nonlinearity is clearly exhibited

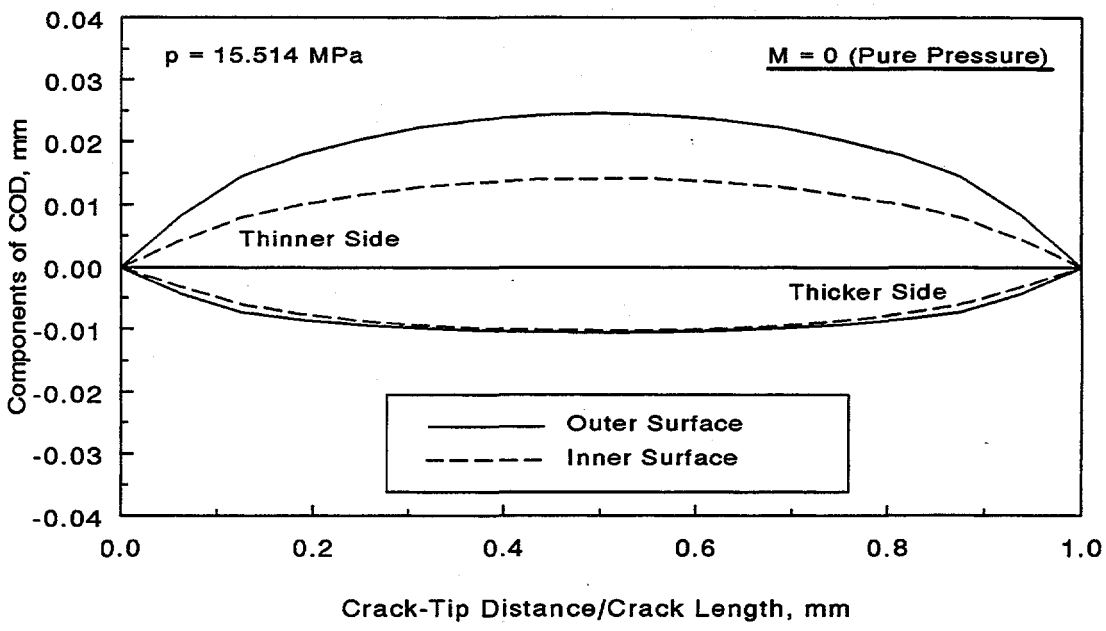

Figure 7.5 Crack-opening profiles under pure tension (M = 0)

T-6300-F7.5

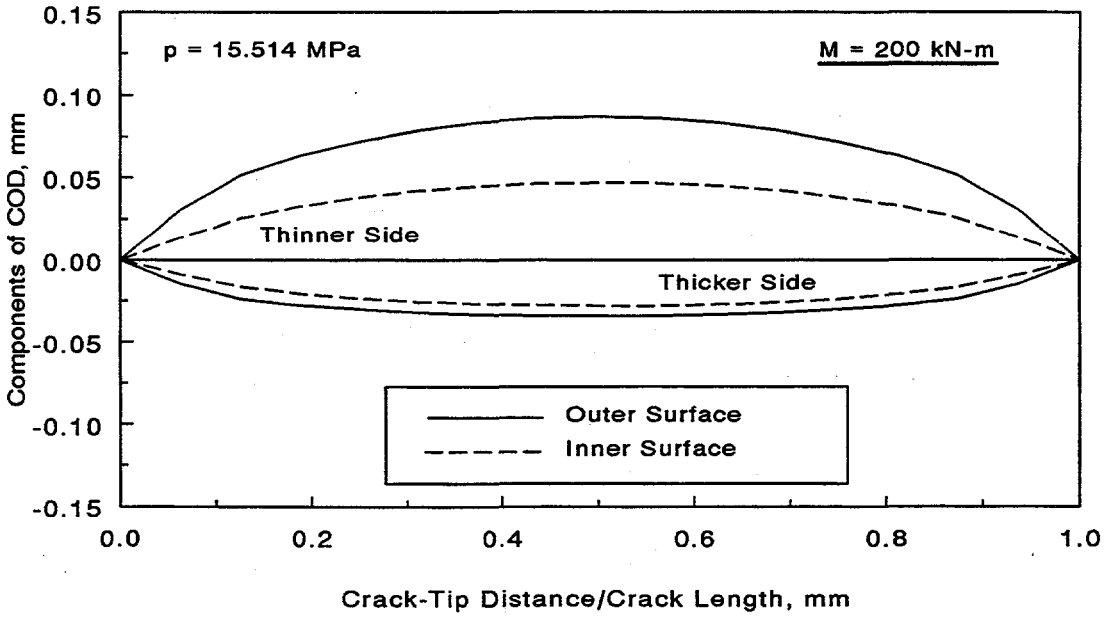

Figure 7.6 Crack-opening profiles under combined bending and tension (M = 200 kN-m)

T-6300-F7.6

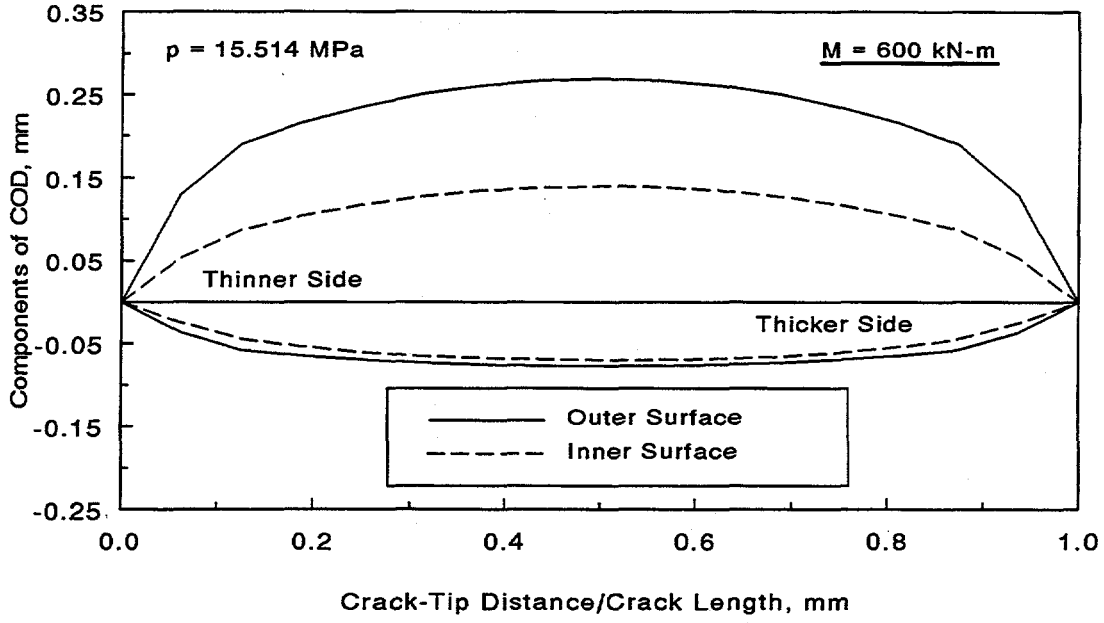

Figure 7.7 Crack-opening profiles under combined bending and tension (M = 600 kN-m)

T-6300-F7.7

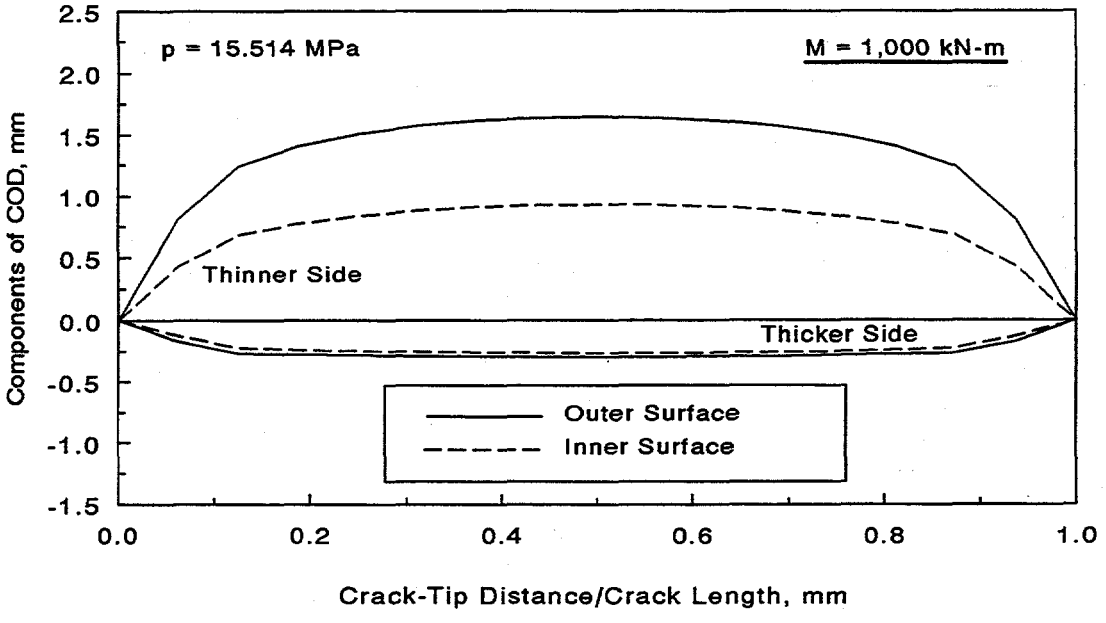

Figure 7.8 Crack-opening profiles under combined bending and tension (M = 1.00 MN-m)

T-6300-F7.8

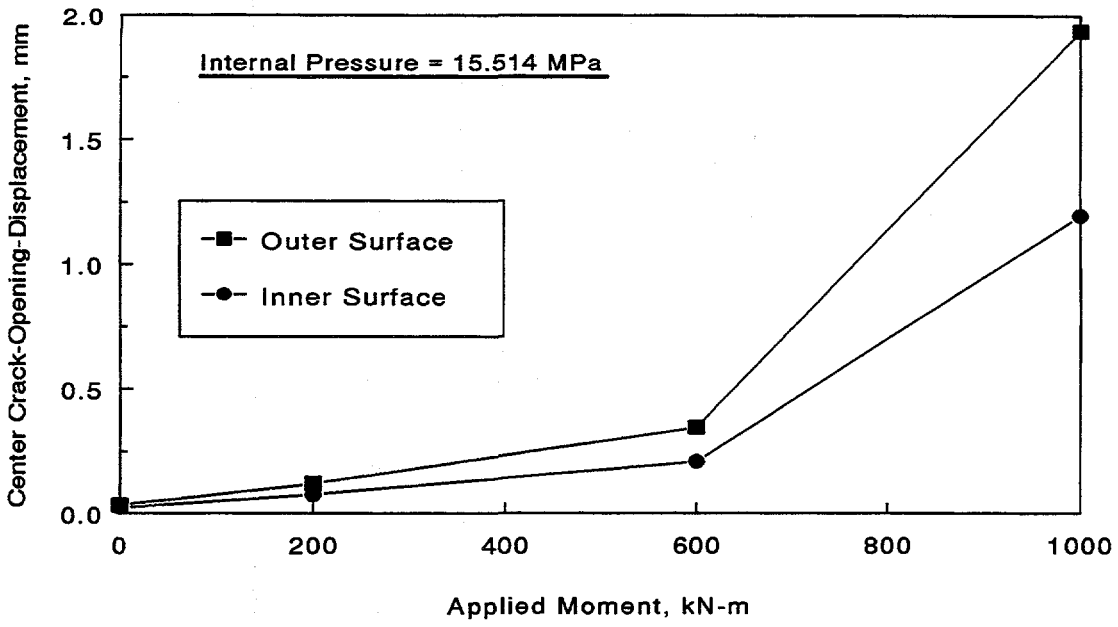

Figure 7.9 Center-crack-opening displacement as a function of applied bending moment

T-6300-F7.9

when M = 1.00 MN-m (8,851 inch-kip). The results in Figure 7.9 also reveal that there are significant differences in the center CODs at the inner and outer surfaces of the pipe, particularly when the applied moment is large. Similar trends were also found for the overall crack-opening shapes which are shown in Figures 7.5 to 7.8.

Figure 7.10 shows a plot of center-crack-opening displacement (half) versus wall thickness for a straight pipe without any thickness gradient which has the identical crack size, material properties, and inside diameter of the carbon steel nozzle defined earlier. This plot was developed by performing simple linear-elastic analyses by the GE/EPRI method (Refs. 7.2 to 7.4) for this pipe that was subjected to a bending moment of 200 kN-m (1,770 inch-kip) and an internal pressure of 15.51 MPa (2,250 psi) for several values of wall thickness. The elastic influence functions in the GE/EPRI method were obtained from Reference 7.3 According to the results in Figure 7.6, the components of center COD (average) in the directions of thinner and thicker sides are 0.067 mm and 0.031 mm, respectively. Using these finite element results in Figure 7.10, the equivalent thicknesses of a pipe without any taper would have to be 44.8 mm (1.76 inches) and 84.0 mm (3.31 inches) to match the components of the center-crack-opening displacement at the thinner and thicker sides of the carbon steel nozzle, respectively. The corresponding ratio of the effective thickness of a constant thickness pipe to the thickness of the nozzle at cracked plane would be 0.96 and 1.8, respectively. Using these ratios, one can then determine the crack-opening for a nozzle crack by conducting simple estimation analyses of a straight pipe without any thickness gradient. However, for general nozzle analysis (elastic), these ratios depend on the angle of taper on either side of the crack, crack size, and

possibly, the R_m/t ratio at the cracked plane. To determine the functional relationship between these ratios and the above geometric parameters quantitatively, one would require several finite element analyses by varying these parameters.

The next logical question to be addressed is whether the nozzle crack case can be analyzed using simple constant thickness pipe estimation methods, rather than having to conduct finite element analyses. This was addressed by comparing the finite element results of center-crack-opening displacements with the effective thicknesses of the pipe with the same inside diameter of the nozzle.

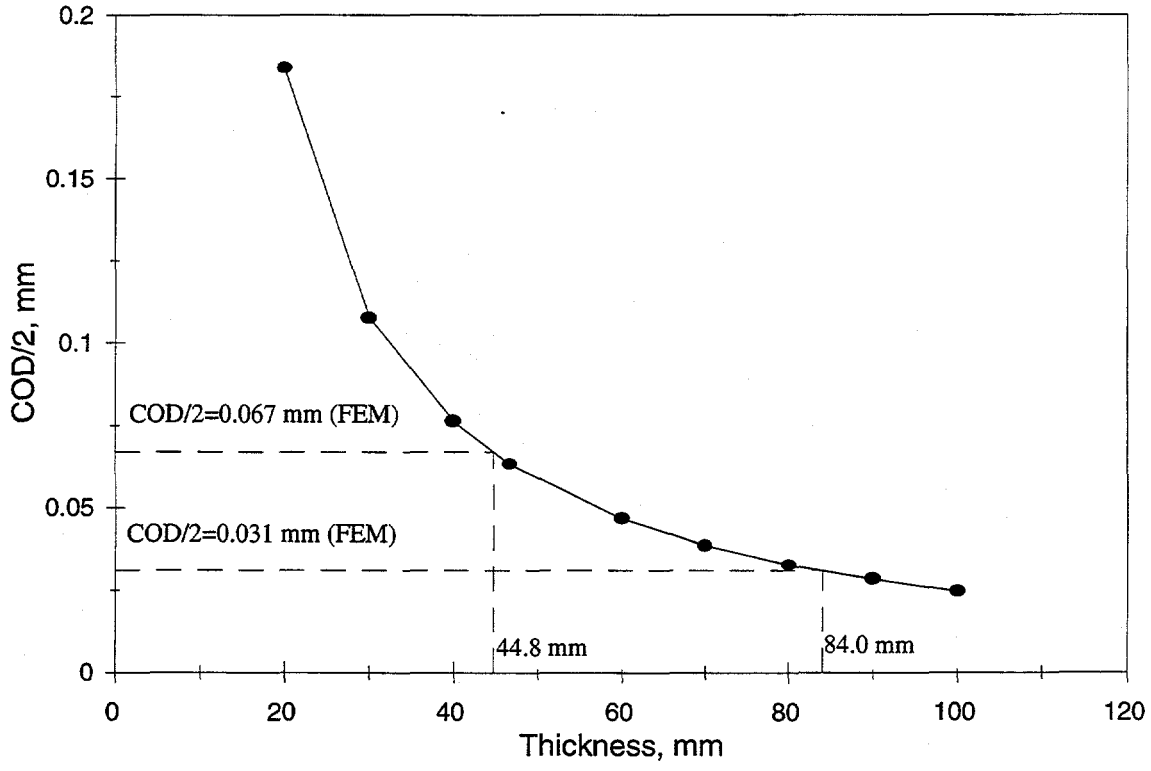

Figure 7.10 Crack-opening displacement for a pipe with constant thickness and same inside diameter of nozzle

7.5 References

7.1 ABAQUS, User's Guide and Theoretical Manual, Version 5.3, Hibbitt, Karlsson, & Sorensen, Inc., Pawtucket, RI, 1993.

7.2 Kumar, V., German, M., and Shih, C., "An Engineering Approach for Elastic-Plastic Fracture Analysis," EPRI Report NP-1931, Electric Power Research Institute, Palo Alto, CA, July 1981.

7.3 Kumar, V., German, M., Wilkening, W., Andrews, W., deLorenzi, H., and Mowbray, D., "Advances in Elastic-Plastic Fracture Analysis," EPRI Final Report NP-3607, Electric Power Research Institute, Palo Alto, CA, August 1984.

7.4 Brust, F., Rahman, S., and Ghadiali, N., "Elastic-Plastic Analysis of Small Cracks in Tubes," *Proceedings of the 11th International Conference on Offshore Mechanics and Arctic Engineering*, Calgary, Alberta, Canada, June 1992.

8.0 EFFECTS OF RESIDUAL STRESSES ON CRACK-OPENING AREA

8.1 Introduction

The effect of residual stress on crack-opening displacement (COD) in leak-rate analyses is not well understood. There are no simple analyses to account for those effects, and, therefore, they are frequently neglected. The objective of the work reported in this section was to assess the magnitude of the residual stress effects on the crack-opening displacement. The effects of residual stresses are most pronounced on the crack-opening variations through the thickness. The thermal-hydraulic models can account for the effects on leak-rates due to the differences in COD on the inside and outside surfaces of the pipe (Ref. 8.1). The leak-rate aspects of these differences are discussed in Reference 8.1. In this study, standard linear-elastic, finite element analyses were conducted to compute the crack-opening displacement for a pipe with and without residual stresses.

8.2 Simulation of Residual Stresses

Attempts to understand the effects of weld parameters on residual stresses have been made through experimentation by various researchers at Battelle (Refs. 8.2 to 8.6), General Electric (Ref. 8.7), Argonne National Laboratories (Refs. 8.8 to 8.10) and many others (Refs. 8.11 to 8.17). A computational model for predicting residual stresses due to girth welding of pipes has also been developed (Refs. 8.2 to 8.6). This model, verified with past experimental data, usually involves two parts: (1) a temperature model and (2) a thermal stress model. The temperature analysis is based on the steady-state heat flow due to a point source moving at a constant speed in an infinite solid. The thermal stress model is an axisymmetric finite element analysis which allows temperature-dependent material properties and elastic unloading. The output from the thermal analysis consists of the temperature versus time histories in each finite element for each individual pass. These temperature histories then provide the input for the finite element analysis to compute stresses and strains in the body. In this way, the weld residual stresses in a pipe can be accurately simulated.

The computational approach, defined above, involves comprehensive numerical modeling for both temperature analysis and thermo-elastic or thermo-plastic analysis. While it is possible to perform a full-scale, three-dimensional finite element analysis of the welding problem, the computational cost can be enormous. As an alternative, the residual stress field can be specified directly from a suitable experimental database. The database, which might have been developed for a set of specific conditions, is sometimes difficult to apply because of the need to extrapolate to other cases of interest. Nevertheless, this approach can be valuable for prescribing weld residual stresses. It is discussed in the next section.

8.3 Residual Stress Field in a Pipe Weld

There is significant residual stress variation from weldment-to-weldment even for large-diameter pipes. Substantial effort has been made in the past to calculate and/or experimentally measure the magnitude and distribution of residual stresses in austenitic pipe welds (Refs. 8.8 to 8.14).

Figure 8.1 shows the available experimental data for the axial residual stress in large diameter pipes as a function of radial distance into the pipe wall from the inside surface (Refs. 8.9 and 8.15). Few experimental measurements of circumferential through-wall residual stress distributions have been reported. Figure 8.2 shows the data available for circumferential, inside surface residual stress as a function of pipe diameter. Inside surface measurements on 101.6-mm (4-inch) to 304.8-mm (12-inch) pipe weldments with smaller wall thicknesses show that the circumferential residual stresses are tensile and are similar in magnitude to the axial residual stresses (Refs. 8.8 and 8.16). The data in Figure 8.2 and finite element calculations presented in References 8.10 and 8.12, suggest that the circumferential stresses on the inner surface of large-diameter (diameter $\geq$ 405.4 mm [16 inch]) pipe-to-pipe weldments that are thicker can become compressive, although this may depend on the heat input during fabrication.

Finite element calculations (Refs. 8.10 and 8.12), supported by limited experimental measurements (Refs. 8.8 and 8.9), suggest that there are significant differences in through-wall residual stress distributions between thinner-wall small-diameter (i.e., less than 102 mm [4.0 inch]) and thicker-wall large-diameter (i.e., greater than 406 mm [16 inch]) pipe weldments. The calculations also suggest that the form of the stress distributions in intermediate thickness and diameter (254-mm [10-inch] to 305-mm [12-inch]) weldments depends strongly on the weld heat input (Ref. 8.12). The residual stress differences are due primarily to the increased heat capacity of thicker-wall pipe and are only coincidentally associated with the diameter. Consequently, the recommended residual stresses are given in terms of wall thickness with a transition chosen somewhat arbitrarily at 25.4 mm (1 inch).

Based on the available data and finite element computations, the axial and circumferential through-wall residual stress distributions recommended by the Task Group on Piping Flaw Evaluation of ASME Section XI are presented in Table 8.1 (Ref. 8.17). Because there is a lack of data, through-thickness uniform axisymmetric distributions were recommended for the circumferential through-wall residual stresses.

Pipe-to-pipe welds represent only a portion of the welds in nuclear power plants. Few experimental data are available for other configurations. However, finite element calculations have been carried out for a variety of weld geometries (Ref. 8.12), including a 304.8-mm (12-inch) pipe-to-sweepolet weld, a 304.8-mm (12-inch) pipe-to-reducer weld, and a 558.8-mm (22-inch) pipe-to-valve weld. In all three cases the weld induced axial stresses are compressive, and an upper bound of stress distribution is shown in Table 8.1. The stress field given in Table 8.1 was used in this study to evaluate the effects of the residual stresses on the crack-opening-area (COA) analysis.

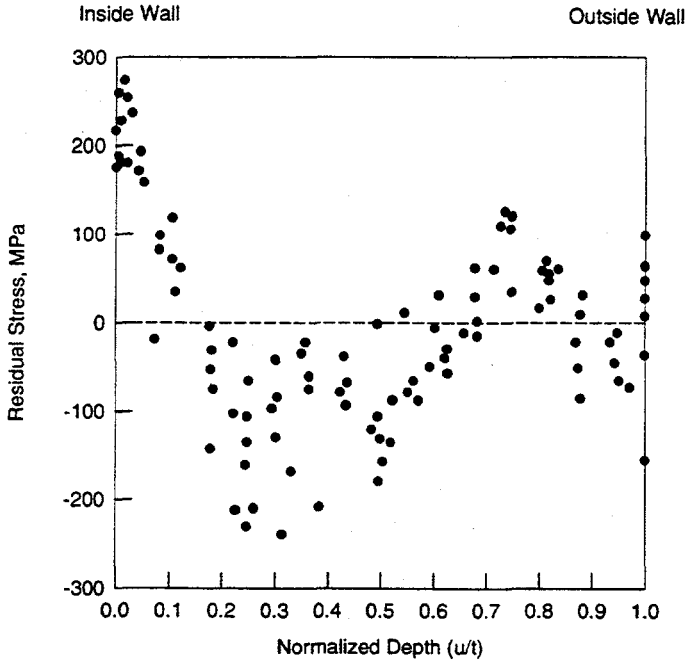

Figure 8.1 Measured axial through-wall residual stress as a function of radial distance through the pipe wall for austenitic stainless steel pipe welds

T-6300-F8.1

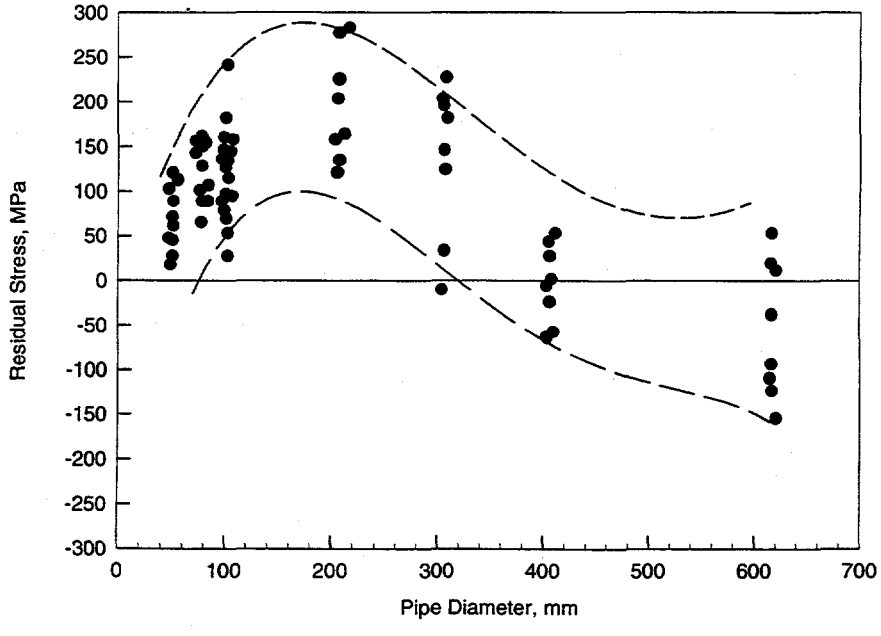

Figure 8.2 Circumferential residual weld stress in heat-affected zone at the inside surface of the pipe as a function of diameter of Schedule 80 pipe

T-6300-F8.2

Table 8.1 Prescribed residual stress field from ASME Section XI IWB-3640 analyses

Wall Thickness	Through-Wall Residual Stress[1]	
	Circumferential	Axial
t = 8.9 mm	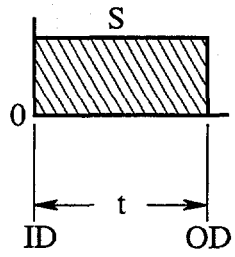	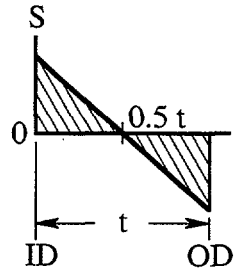
t = 26.41 mm	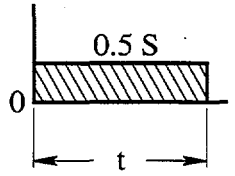	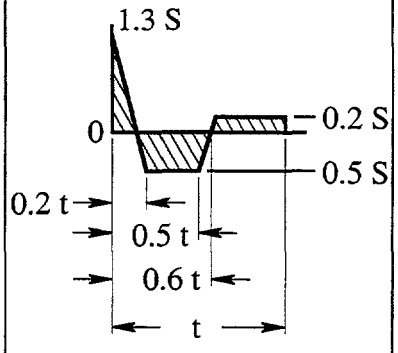

[1] S = 207 MPa (30 ksi)

8.4 Applications of Residual Stresses for COA Analysis

Once the residual stress field is calculated from a numerical analysis, or defined from an experimental database, the pipe flaw evaluation can be performed to study the effects of residual stress on crack-opening characteristics. Ideally, one can apply the residual stresses as "initial" locked-in stresses and then introduce a through-wall-crack to conduct crack-opening-area analysis. In this way, the redistribution of stresses that occurs due to the presence of the crack can be automatically accounted for in the subsequent finite element analysis.

In this study, a simpler alternative approach was undertaken. In this approach, the residual stresses were applied as crack face pressure since the superposition principle is applicable for linear-elastic stress analysis (Ref. 8.18). The stresses were applied as force-controlled as for a very long pipe far from restraints. The superposition principle implies that the state of stress due to two or more loads acting together is equal to the sum of the stresses due to each load acting separately. The redistribution of stresses that occurs due to the presence of the crack, growing or non-growing, does not imply that the superposition principle is invalid. This fact has been pointed out by Parker (Ref. 8.19) for fatigue crack growth and demonstrated by Quinones and Reaugh (Ref. 8.20) for stress corrosion crack growth.

In the present work, no circumferential residual stresses were applied for the circumferential crack since they would have negligible effects in a linear-elastic analysis (Ref. 8.18).

8.5 The Pipe Crack Problem

In this analysis a through-wall-cracked pipe was used with outer diameter, D_o, and wall thickness, t. Two pipes were chosen; one with large diameter and thickness, i.e., D_o = 402.6 mm (15.85 inches) and t = 26.41 mm (1.04 inches); the other with small diameter and thickness, i.e., D_o = 102.0 mm (4.02 inches) and t = 8.9 mm (0.35 inch). The pipe has a circumferential through-wall crack with total crack angle, 2θ. The pipe and crack geometries are defined in Table 8.2. The crack sizes were

Table 8.2 Geometric details and applied bending moments for large and small diameter pipes used in finite element analysis

Pipe	Outer Diameter, mm (inch)	Wall Thickness, mm (inch)	θ/π, percent	Bending Moment, kN-m
Thicker-Wall Large-Diameter Pipe	402.6 (15.85)	26.41 (1.04)	12	522.07[(a)]
Thinner-Wall Small-Diameter Pipe	102.0 (4.02)	8.9 (0.35)	20	8.83[(b)]

(a) The corresponding elastic stress = 189.4 MPa (1.08 × ASME Service Level A limit)
(b) The corresponding elastic stress = 158.23 MPa (0.9 × ASME Service Level A limit)

small enough to be representative of typical situations encountered in leak-before-break analyses. In both pipes, the cracks are symmetrically located on the bending plane and have the same length on the inside diameter and the outside diameter in terms of percent of pipe circumference.

In both pipes, the material was TP304 stainless steel at 288 C (550 F). The modulus of elasticity and Poisson's ratio were assumed to be 193.06 GPa (28,000 ksi) and 0.3, respectively. The design stress intensity, S_m, defined by the Section II of the ASME Code (Ref. 8.21) is 116.9 MPa (16.95 ksi) at 288 C (550 F). However, since this is an elastic analysis, the results should be applicable to ferritic welds, assuming they have a similar residual stress field. The residual stress distributions in Table 8.1 came from experimental work on stainless steel welds, as mentioned previously.

For this study, both pipes were unpressurized and were subjected to pure bending moments applied at the remote ends. The moments were 522.07 kN-m (4,620.9 inch-kip) and 8.83 kN-m (78.16 inch-kip) for the thicker-wall large-diameter and thinner-wall small-diameter pipes, respectively, see Table 8.2. These moments correspond to elastic bending stresses (at the outer fiber of uncracked pipe cross-section) of 189.4 MPa (27.47 ksi) and 158.23 (22.95 ksi) for the thicker-wall large-diameter and thinner-wall small-diameter pipes, respectively. These stresses were larger than typical normal operating stresses (axial plus bending combined) in a nuclear plant piping. Comparisons with the ASME Service Level A stress limit, which is defined as $1.5S_m$, show that the above stresses correspond to 1.08 and 0.9 times the Service Level A stresses, respectively. However, since the analysis is linear-elastic, the COD results can be linearly scaled for any given applied moment or stress. They are discussed in a forthcoming section.

For the crack-opening-area analyses, two different load cases were considered. In the first case, the above bending load was applied without any residual stresses. In the second case, the bending load was applied with the residual stresses prescribed in Table 8.1. In both cases, the loadings were assumed to be elastic, so there was no plasticity and/or crack growth. This was justified since normal operating stresses associated with a leaking crack are typically elastic.

8.6 Finite Element Analysis

8.6.1 Results of Analysis

Linear-elastic finite element analyses were conducted to determine the crack-opening for each pipe with the two load cases defined above. The general-purpose commercial code ABAQUS (Ref. 8.22) was used in the analyses. The finite element idealizations involved 3,200 twenty-noded three-dimensional solid elements. The number of elements through the thickness was ten. Due to symmetry in both the longitudinal and circumferential directions, only a quarter of the pipe was modeled. Figure 8.3 shows the original (undeformed) finite element mesh for one of the pipes. Figure 8.4 shows the blown up view of the same undeformed mesh with details of mesh refinement around the crack tip.

Figures 8.5 and 8.6 show the deformed configurations of the large diameter (D_o = 402.6 mm [15.85 inches]) and the small diameter (D_o = 102.0 mm [4.02 inches]) pipes, respectively. In both pipes, deformed shapes calculated with and without residual stresses are shown. Detailed results from the

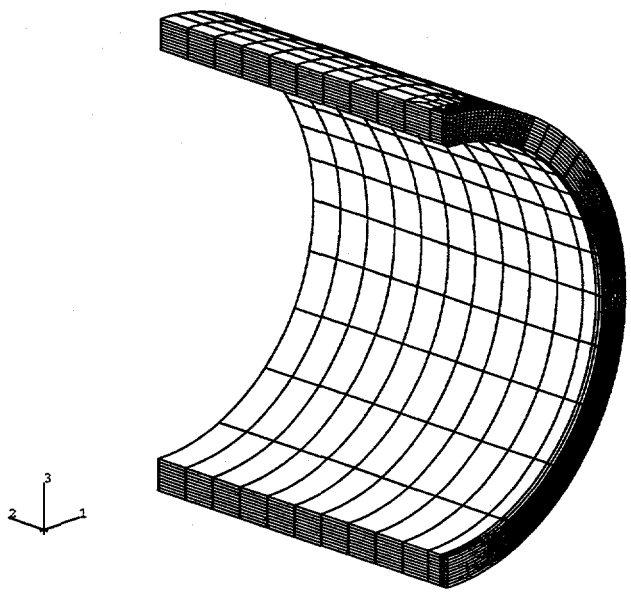

Figure 8.3 Original finite element mesh for a quarter pipe (undeformed)

T-6300-F8.3

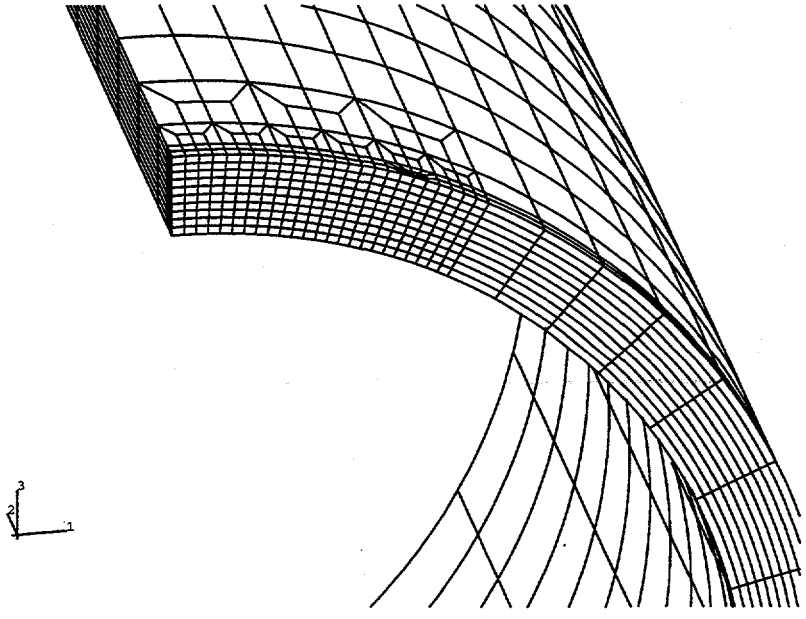

Figure 8.4 Amplified view of undeformed mesh showing refinement around the crack tip

T-6300-F8.4

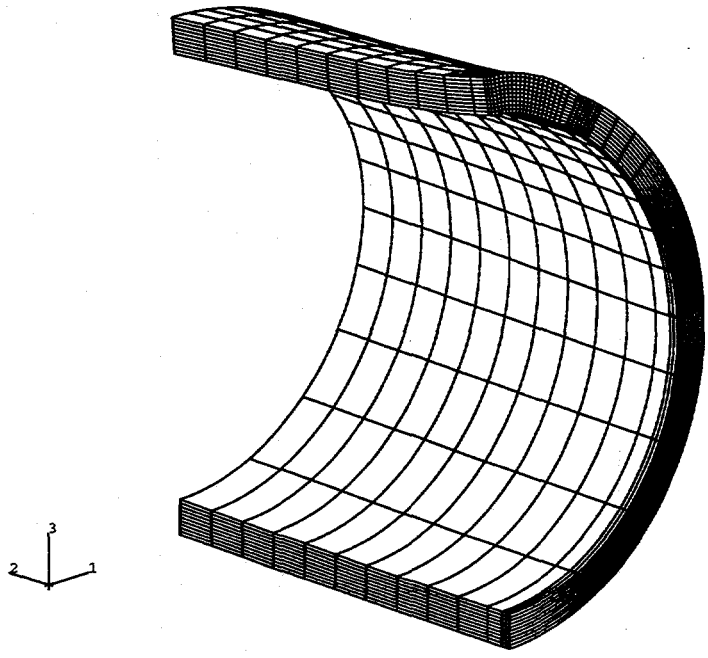

(a) Bending moment only

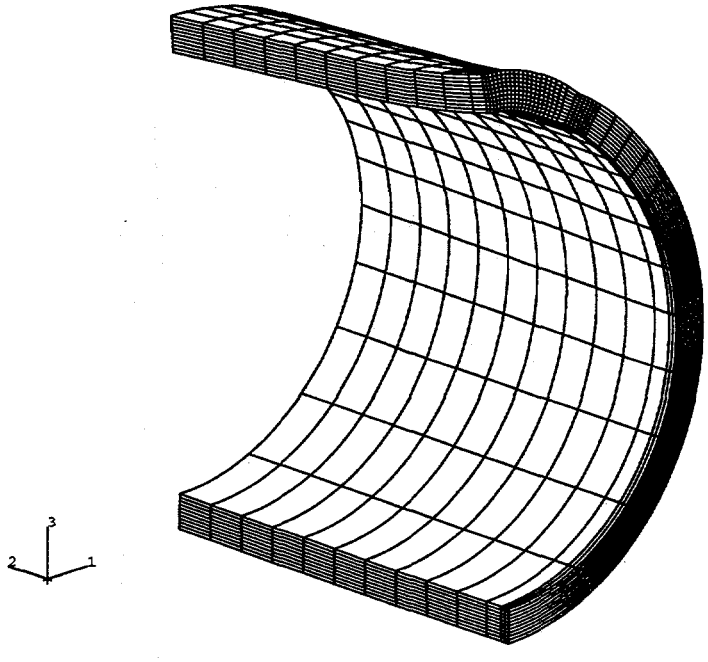

(b) Bending moment and residual stress

Figure 8.5 Deformed finite element mesh for the large-diameter pipe (D_o = 402.6 mm)

T-6300-F8.5

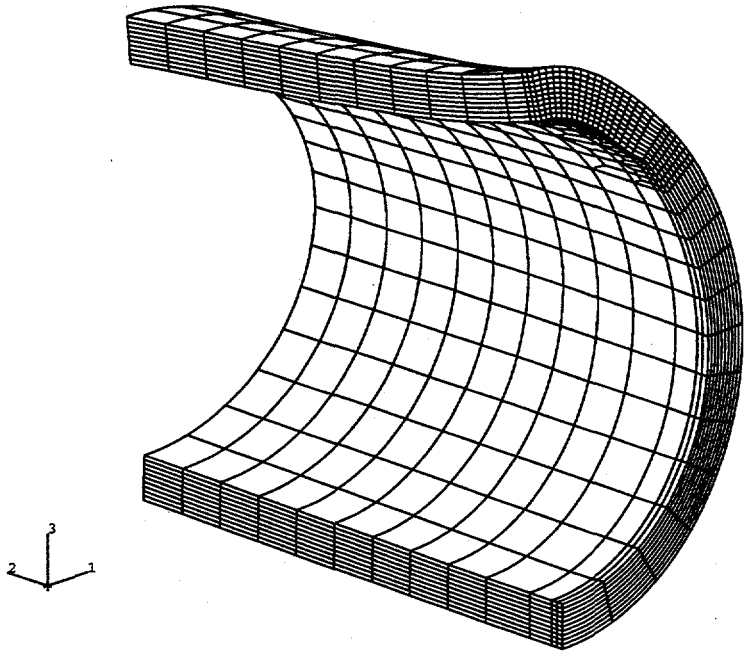

(a) Bending moment only

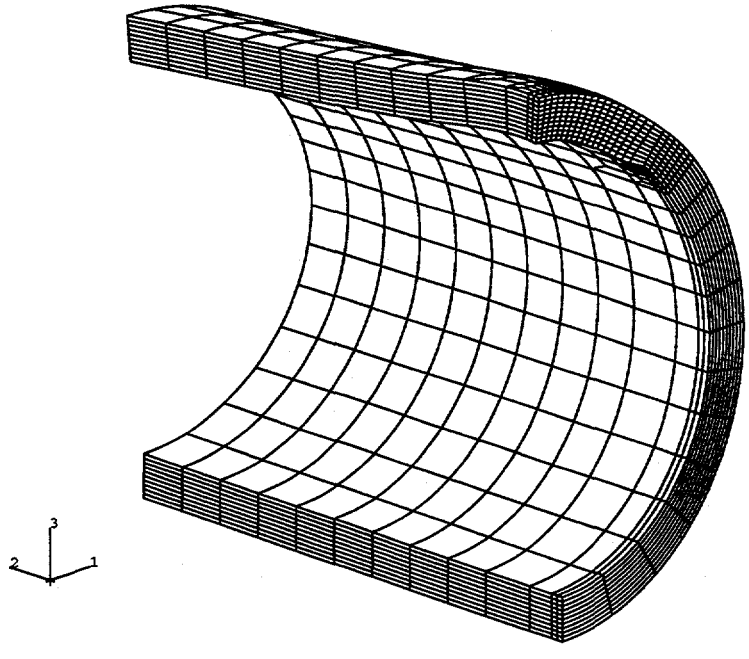

(b) Bending moment and residual stress

Figure 8.6 Deformed finite element mesh for the small-diameter pipe (D_o = 102 mm)

T-6300-F8.6

finite element analysis reveal that the center-crack-opening-displacement at the inside and the outside surfaces could be increased or decreased due to the inclusion of residual stresses. Table 8.3 shows the predicted values of center COD at the inside, middle, and outside surfaces calculated with and without residual stresses. It appears that the prescribed residual stress field, defined by Table 8.1, did not significantly affect the crack-opening for the large-diameter pipe (D_o = 402.6 mm [15.85 inch]), but could seriously affect the crack-opening for small-diameter pipe (D_o = 102.0 mm [4.02 inch]). More specifically, for the large-diameter pipe, when the residual stresses were considered, the center-crack-opening displacement increased by 4.4 percent at the inside surface, decreased by 2.4 percent at the middle surface, and increased by 3.3 percent at the outer surface of the pipe. For the small-diameter pipe, when the residual stresses were included, the center COD at the inside, middle, and outside surfaces increased by 17.1 percent, decreased by 11.7 percent, and decreased by 31.7 percent, respectively.

More detailed results related to the effects of the above residual stresses are provided in Figures 8.7 and 8.8, which show the plots of center-crack-opening displacement as a function of a normalized distance, u/t, where u is the coordinate distance (radial) from the inside surface of the pipe and t is the pipe wall thickness. The functional variation of center COD with respect to u/t was calculated with and without residual stresses for both the thicker-wall large-diameter pipe and the thinner-wall small-diameter pipe and are shown in Figures 8.7 and 8.8, respectively. The analyses indicate that the effects of residual stresses for the thinner-wall pipe are significantly greater than those for the thicker-wall pipe.

Table 8.3 Center-crack-opening displacements calculated with and without residual stresses from finite element analysis

Pipe	Outer Diameter, mm	Load Case	Center-Crack-Opening Displacement, mm		
			Inside Surface	Middle Surface	Outside Surface
Thicker-Wall Large-Diameter Pipe	402.6	Bending Moment[a] Only	0.274	0.334	0.395
		Bending Moment[a] and Residual Stress	0.286 (+4.4)[b]	0.326 (-2.4)[b]	0.408 (+3.3)[b]
Thinner-Wall Small-Diameter Pipe	102.0	Bending Moment[c] Only	0.111	0.137	0.164
		Bending Moment[c] and Residual Stress	0.130 (+17.1)[b]	0.121 (-11.7)[b]	0.112 (-31.7)[b]

(a) Moment = 522.07 kN-m with corresponding elastic stress = 189.4 MPa (1.08 × ASME Service Level A limit)
(b) Percent change relative to center COD calculated without residual stress (+ = increase; - = decrease)
(c) Moment = 8.83 kN-m with corresponding elastic stress = 158.23 MPa (0.9 × ASME Service Level A limit)

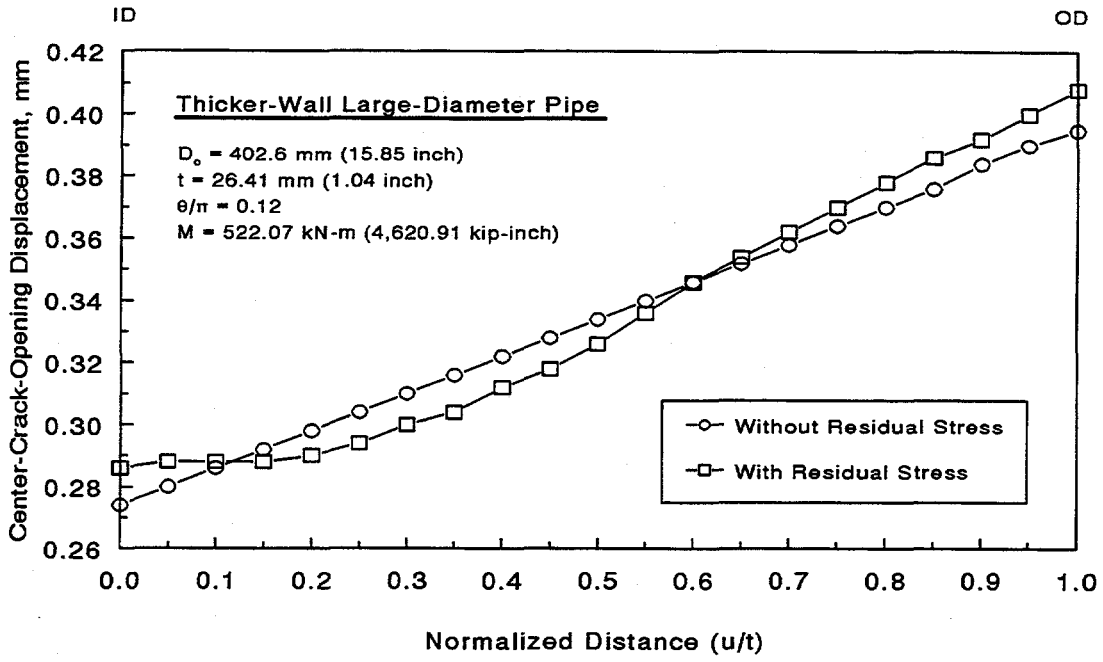

Figure 8.7 Effects of residual stresses on the through-the-thickness variation of center-crack-opening displacement for the thick-walled large-diameter pipe

T-6300-F8.7

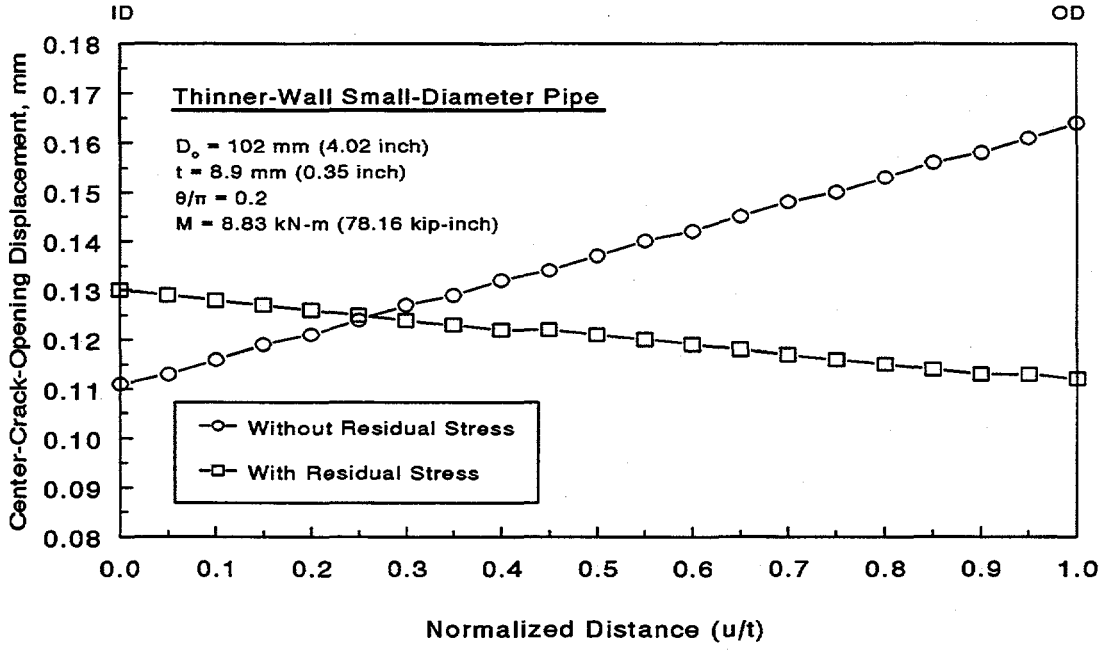

Figure 8.8 Effects of residual stresses on the through-the-thickness variation of center-crack-opening displacement for the thin-walled small-diameter pipe

T-6300-F8.8

8.6.2 Effects of Residual Stresses for Various Applied Loads

At more typical normal operating stresses, which can be much smaller than the applied stresses used in these analyses, the effects of residual stresses on crack-opening can be much higher. Since the analyses performed in this study are linear-elastic, the effects of residual stresses for pipes with any other applied loads can also be evaluated. This is because the results of finite element analyses conducted for the applied moments in Table 8.2, can be scaled linearly for any other moments or stresses.

Based on linear scaling, Figures 8.9 and 8.10 show the percent change in center COD due to the inclusion of residual stresses for both thicker-wall large-diameter and thinner-wall small-diameter pipes, respectively. In both figures, the horizontal axis defines the applied moment that corresponds to an applied elastic stress as a percentage of ASME Service Level A stress limits. The vertical axis represents the difference of the calculated center COD with residual stresses (δ_{M+RS}) and without residual stresses (δ_M) normalized by the center COD without residual stresses. In general, the effects of residual stresses are significant when the normal operating stresses are lower. For example, when the applied stress is equal to 50-percent of ASME Service Level A stress, the center COD for the thick-walled large diameter pipe will increase by 9.46 and 7.11 percent at the inside and outside surfaces, respectively, and decrease by 5.17 percent at the mid-thickness level. Correspondingly, the center COD for the thin-walled small-diameter pipe will increase by 30.9 percent at the inner surface and decrease by 57.2 and 21.1 percent at the outer and middle surfaces of the pipe, respectively. Relative comparisons of the crack-opening results in Figures 8.9 and 8.10 indicate that at any given applied load the residual stress effects are more severe for the thin-walled small-diameter pipe than for the thick-walled large-diameter pipe.

According to Figure 8.9, for the thick-walled large-diameter pipe, the calculated CODs which account for residual stresses are always larger than those estimated without residual stresses at both inner and outer surfaces of the pipe. However, the COD at the mid-thickness level can be smaller when the residual stresses are considered. For the thin-walled small-diameter pipe, the results for which are shown in Figure 8.10, the calculated COD with residual stresses are higher at the inner surface and lower at the outer or middle surfaces than those without residual stresses. Consequently, the crack-opening area and the subsequent leak-rate calculations can be affected by the residual stresses in those pipes. In particular, when the values of δ_{M+RS} and δ_M are such that $(\delta_{M+RS} - \delta_M)\times 100/\delta_M$ (the variable in the vertical axis) reaches a value of -100, the calculated COD with residual stresses becomes zero. Hence, there would be no leakage even for a pipe containing a through-wall crack, which clearly demonstrates how important the residual stresses are for the leak-rate calculations. This is especially true for the thin-walled small-diameter pipe in which case the results in Figure 8.10 predict that due to the residual stress, the outer surface of the pipe will close (thus preventing any leakage) when the applied load is equal to 28.6 percent of the ASME Service Level A stress limit. Similar calculations can also be made for the middle surface of both pipes, but the trend curves in Figures 8.9 and 8.10 suggest that for closure to occur, the applied stresses would have to be very small, i.e., 2.60 and 10.5 percent of the ASME Service Level A stress limit for the thicker-wall large-diameter and thinner-wall small-diameter pipes, respectively.

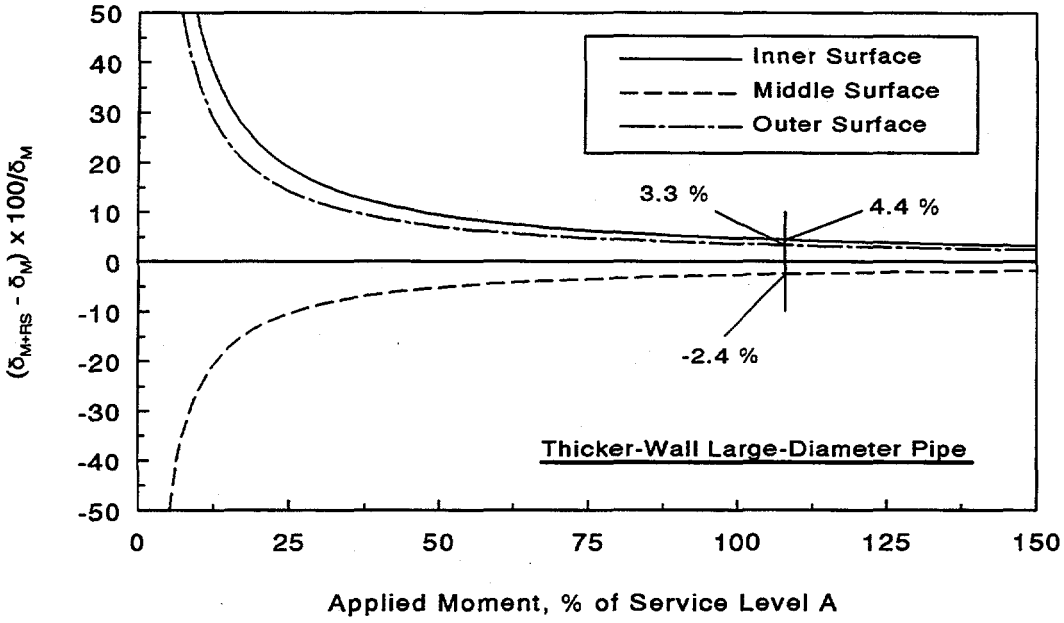

Figure 8.9 Percentage change in calculated COD due to residual stress as a function of applied moment for the thick-walled large-diameter pipe

T-6300-F8.9

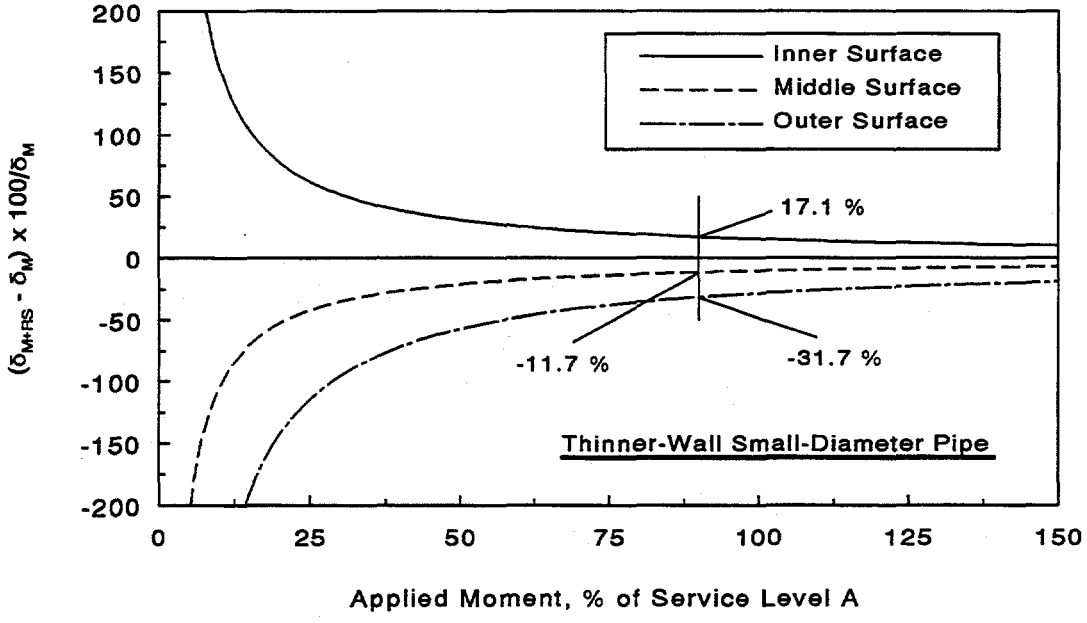

Figure 8.10 Percentage change in calculated COD due to residual stress as a function of applied moment for the thin-walled small-diameter pipe

T-6300-F8.10

Finally, the above results of COD should be viewed as the preliminary estimates for the residual stress effects. No efforts were undertaken to determine the accuracy of this approximate finite element analysis compared with more rigorous thermo-plastic finite element analysis, where the residual stress field is numerically simulated. One major difference between these two approaches, is that modeling the residual stress field as a crack-face pressure, imposes a load-controlled stress field, whereas, the actual residual stresses are a local displacement-controlled stress field. The load-controlled crack-face-pressure modeling should produce a larger effect on the COD, than the thermo-plastic modeling of the residual stresses (with unpinning of the nodes to determine the COD). Considering these aspects, the results from this analysis should overemphasize predictions of the crack-opening displacements due to residual stresses. Nevertheless, the conclusion that the residual stress effects on the COD for thinner-wall small-diameter pipe are more severe than the thicker-wall large-diameter pipe, is an important result.

8.7 References

8.1 Paul. D., Ahmad, J., Scott, P. M., Flanigan, L. F., and Wilkowski, G. M., "Evaluation and Refinement of Leak-Rate Estimation Models," NUREG/CR-5128, Rev. 1, U.S. Nuclear Regulatory Commission, Washington, D.C., June 1994.

8.2 Barber, T. E., Brust, F. W., Mishler, H. W., and Kanninen, M. F., "Controlling Residual Stresses by Heat Sink Welding," EPRI Report NP-2159-LD, Electric Power Research Institute, Palo Alto, CA, December 1981.

8.3 Kanninen, M. F., Brust, F. W., Ahmad, J., and Abou-Sayed, I. S., "The Numerical Simulation of Crack Growth in Weld-Induced Residual Stress Fields," *Residual Stress and Stress Relaxation*, Edited by E. Kula and V. Weiss, in *Proceedings of 28th Army Sagamore Research Conference*, Lake Placid, NY, pp. 227-248, July 1981

8.4 Brust, F. W. and Rybicki, E. F., "A Computational Model of Backlay Welding for Controlling Residual Stresses in Welded Pipes," *Journal of Pressure Vessel Technology*, Vol. 103, pp. 226-232, August 1981.

8.5 Brust, F. W. and Kanninen, M. F., "Analysis of Residual Stresses in Girth Welded Type 304 Stainless Steel Pipes," *Journal of Materials for Energy Systems*, Vol. 3, No. 3, pp. 56-62, December 1981.

8.6 Iwamura, Y. and Rybicki, E. F., "A Transient Elastic-Plastic Thermal Stress Analysis of Flame Forming," *ASME Transactions Journal of Engineering for Industry*, February 1973.

8.7 Klepzer, H. and others, "Investigation of Cause of Cracking in Austenitic Stainless Steel Piping," General Electric Report No. NEDO-21000-1, July 1975.

8.8 W. J. Shack, W. A. Ellington, and L. Pahis, "Measurement of Residual Stress in Type 304 Stainless Steel Piping Butt Weldments," EPRI Report NP-1413, Electric Power Research Institute, Palo Alto, CA, 1980.

8.9 W. J. Shack, "Measurement of Through-wall Residual Stresses in Large Diameter Type 304 Stainless Steel Piping Butt Weldments," Report ANL-82-15, Argonne National Laboratory, Argonne, IL, 1982.

8.10 W. J. Shack et al., "Environmentally Assisted Cracking in Light Water Reactors," Annual Report, October 1981 to September 1982, NUREG/CR-3292, U.S. Nuclear Regulatory Commission, Washington, D.C.,

8.11 E. F. Rybicki, et al., "Residual Stresses at Girth-Butt Welds in Pipes and Pressure Vessels," NUREG-0376, U.S. Nuclear Regulatory Commission, Washington, D.C., 1977.

8.12 E. F. Rybicki et al., "Computational Residual Stress Analysis for Induction Heating of Welded BWR Pipes," EPRI Report NP-2662-LD, Electric Power Research Institute, Palo Alto, CA, 1982.

8.13 W. J. Shack et al., "Environmentally Assisted Cracking in Light Water Reactors," Annual Report, October 1983 to September 1984, NUREG/CR-4287, U.S. Nuclear Regulatory Commission, Washington, D.C., 1985.

8.14 D. O. Harris, "The Influence of Crack Growth Kinetics and Inspection on the Integrity of Sensitized BWR Piping Welds," EPRI Report NP-1163, Electric Power Research Institute, Palo Alto, CA, 1979.

8.15 Horn, R. M., "The Growth and Stability of Stress Corrosion Cracks in Large Diameter BWR Piping," EPRI Report, NP-2472, Vols. 1 and 2, Electric Power Research Institute, Palo Alto, CA, July 1982.

8.16 R. Sasaki et al., "Mitigation of Inside Surface Residual Stress of Type 304 Stainless Steel Pipe Welds by Inside Water Cooling Method," in *Proceedings: Seminar on Countermeasures for Pipe Cracking in BWRs*, EPRI WS-79-174, Vol. I, Electric Power Research Institute, Palo Alto, CA, 1980.

8.17 "Evaluation of Flaws in Austenitic Steel Piping," (Technical basis document for ASME IWB-3640 analysis procedure), prepared by Section XI Task Group for Piping Flaw Evaluation, EPRI Report NP-4690-SR, Electric Power Research Institute, Palo Alto, CA, July 1986.

8.18 Bergman, M. and Brickstad, B., "A New Computerized Procedure to Analyze LBB in Pipes with Complex Crack Shapes," *Proceedings of the 20th MPA-Seminar*, Stuttgart, Germany, October 1994.

8.19 Parker, A. P., "LEFM and Fatigue Crack Growth - Residual Stress Effects," *Residual Stress and Stress Relaxation*, edited by E. Kula, Plenum Publication Corporation, pp. 249-271, 1982.

8.20 Quinones, D. F. and Reaugh, J. E., "Weld Residual Stress Distribution Near Growing Cracks," EPRI Report NP-2694, Electric Power Research Institute, Palo Alto, CA, 1983.

8.21 1992 ASME Boiler & Pressure Vessel Code - Section II, Materials: Part D - Properties.

8.22 ABAQUS, User's Guide and Theoretical Manual, Version 5.3, Hibbitt, Karlsson, & Sorensen, Inc., Pawtucket, RI, 1993.

9.0 IMPROVED MODELS FOR CRACK-MORPHOLOGY PARAMETERS

9.1 Introduction

The key crack-morphology variables considered in past leak-rate analyses were surface roughness, number of turns in the leakage path, and entrance loss coefficients (Refs. 9.1 and 9.2). However, the examination of service cracks also shows that the cracks frequently do not grow radially through the pipe thickness. Hence, a fourth parameter, "actual crack path/thickness," representing deviation from straightness can also play an important role in the calculation of leak rates. Traditionally, this parameter has been ignored.

In addition, current leak-rate calculations do not explicitly account for the effects of crack-opening on the crack-morphology parameters. Examination of service cracks in pipes as well as theoretical considerations suggest that these variables should depend on the magnitude of crack-opening. But, currently, there are no engineering models that would allow for these crack-morphology variables to be functionally dependent on the crack-opening characteristics of a pipe (Ref. 9.3).

In this study, simple linear models were developed based on local and global definitions of the crack-morphology variables which can be measured from current service data. Standard statistical analyses of these data were conducted to determine the probabilistic characteristics (e.g., mean and standard deviation) of the crack-morphology parameters for several types of cracking mechanisms and pipe materials. Using these statistics, one can evaluate the effects of crack-morphology variability on the leak rate or leakage-size flaw for leak-before-break (LBB) or other applications.

9.2 Improved Definitions of Crack-Morphology Parameters

9.2.1 Surface Roughness

This input parameter defines the peak-to-peak roughness of the crack-face surface to be used in the calculation of the friction factor and pressure loss due to friction for fluid flow through a crack in a pipe. In the past, the surface roughness was assumed to be invariant with respect to COD. For example, the constant numerical values, such as 0.0062 mm and 0.04 mm, were used to quantify surface roughness of intergranular stress-corrosion cracks and fatigue cracks, respectively (Ref. 9.1). However, a careful examination of Figure 9.1 suggests that the appropriate surface roughness could be large (global) or small (local) depending on whether the COD is large or small, respectively. In this study, the dependence of surface roughness, μ, was achieved by assuming a piecewise linear function given by

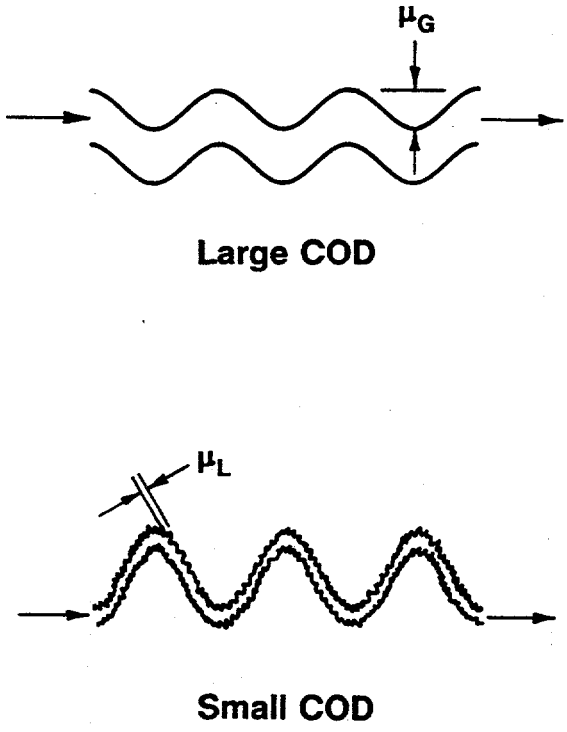

Figure 9.1 Local and global surface roughness and number of turns

T-6300-F9.1

$$\mu = \begin{cases} \mu_L, & 0.0 \le \dfrac{\delta}{\mu_G} < 0.1 \\ \mu_L + \dfrac{\mu_G - \mu_L}{9.9}\left[\dfrac{\delta}{\mu_G} - 0.1\right], & 0.1 \le \dfrac{\delta}{\mu_G} \le 10 \\ \mu_G, & \dfrac{\delta}{\mu_G} > 10 \end{cases} \qquad (9\text{-}1)$$

where μ_L is the local surface roughness, μ_G is the global surface roughness, and δ is the center-crack-opening-displacement. Figure 9.2 shows the schematic variation of μ with respect to δ.

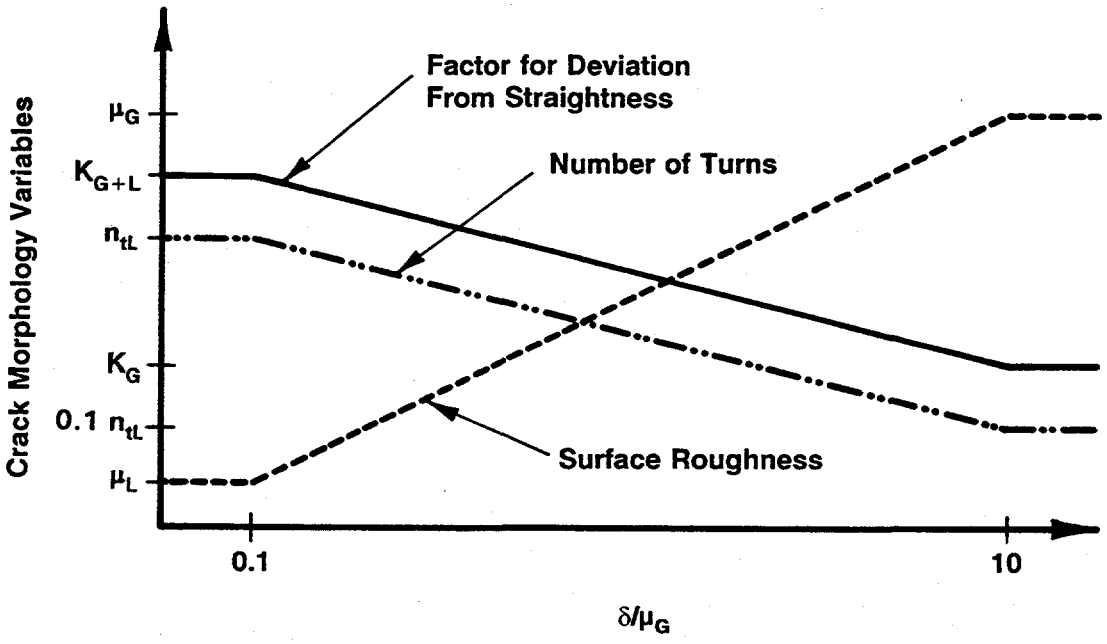

Figure 9.2 Crack-morphology variables versus normalized COD

T-6300-F9.2

9.2.2 Number of Turns

This input parameter defines the number of turns that the fluid must make when flowing through the crack. In fatigue and stress-corrosion cracks, the number and severity of the bends can in some circumstances account for upwards of one-half the total pressure loss of the fluid when flowing through the crack. Typically, a 45- or a 90-degree angle change in flow direction results in about a 0.4 and 1.0 velocity head loss, respectively. Norris et al. (Ref. 9.2) have shown this parameter to be of importance for stress-corrosion cracks. In the past, this parameter was thought to be of lesser importance for fatigue cracks because fatigue cracks generally break through in a fairly flat plane. However, the experimental results shown in Reference 9.1 indicate that the number of bends in the flow path can be significant even for fatigue cracks. This occurs when the variations in the contours of the relatively flat plane of a fatigue crack are large compared with the COD. Therefore, even though the fracture faces of a fatigue crack appear to be fairly flat to the naked eye, the fatigue cracks contain many flow path bends when the crack is tight.

Following similar considerations given above for the surface roughness, the appropriate number of turns, n_t, also depends on the COD. Once again, a piece-wise linear function was assumed, i.e.,

$$n_t = \begin{cases} n_{tL}, & 0.0 \le \dfrac{\delta}{\mu_G} < 0.1 \\ n_{tL} - \dfrac{n_{tL}}{11}\left[\dfrac{\delta}{\mu_G} - 0.1\right], & 0.1 \le \dfrac{\delta}{\mu_G} \le 10 \\ 0.1 n_{tL}, & \dfrac{\delta}{\mu_G} > 10 \end{cases} \tag{9-2}$$

where n_{tL} is the local number of turns. A schematic plot of Equation 9-2 is also shown in Figure 9.2.

9.2.3 Discharge Coefficient

The discharge coefficient is the ratio of the flow areas associated with the *vena contracta* to the flow area at the crack entrance. For sharp-edged crack entrances, a typical discharge coefficient would be a value of 0.60. For round or smooth-edged crack entrances, a typical discharge coefficient would be close to 0.95.

9.2.4 Actual Crack Path/Thickness

This parameter represents the deviation of flow path from straightness. Depending on the COD (see Fig. 9.3), it can be defined as

$$\frac{L_a}{t} = \begin{cases} K_{G+L}, & 0.0 \le \dfrac{\delta}{\mu_G} < 0.1 \\ K_{G+L} - \dfrac{K_{G+L} - K_G}{9.9}\left[\dfrac{\delta}{\mu_G} - 0.1\right], & 0.1 \le \dfrac{\delta}{\mu_G} \le 10 \\ K_G, & \dfrac{\delta}{\mu_G} > 10 \end{cases} \tag{9-3}$$

where L_a is the actual length of the flow path, K_G is the correction factor for global path deviations for straightness (e.g., a crack following the fusion line of the weld), and K_{G+L} is the correction factor for global plus local path deviations for straightness (e.g., a crack following the grain boundaries for IGSCC). A schematic plot of Equation 9-3 is also shown in Figure 9.2.

Note that the piecewise linear variation of the above crack morphology variables is a first attempt to simulate their dependency on COD. The numerical constants in Equations 9-1 to 9-3 are based on a review of cracks found in service and expert opinion at Battelle. Additional studies are needed to evaluate these linear models.

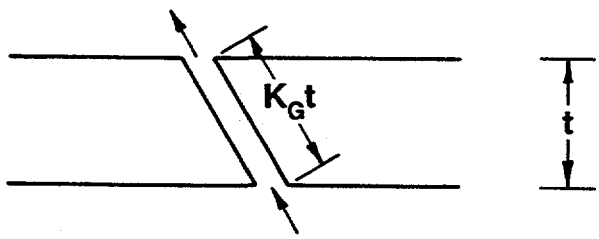

Large COD

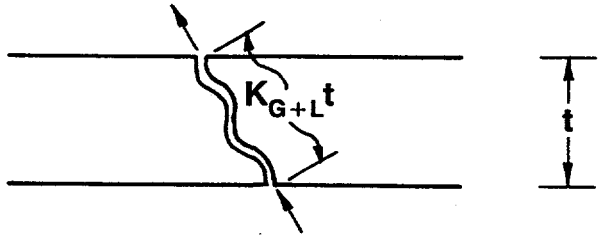

Small COD

Figure 9.3 Global-plus-local and global path deviations from straightness

T-6300-F9.3

9.3 Statistical Characterization of Crack Morphology Parameters

9.3.1 Surface Roughness

Some peak-to-peak roughness values for cracks found in pipes removed from service are summarized below. The statistics are listed in Tables 9.1 and 9.2 for stainless steel and carbon steel pipes, respectively, with various cracking mechanisms.

9.3.1.1 Stainless Steel - IGSCC

Surface roughness values for an IGSCC crack from the Battelle/EPRI Phase II pipe leak rate experiments (Ref. 9.4) were measured to be 5.10 μm (200 microinches). (Note: The authors expressed doubt about the accuracy of this measurement in the paper.) Furthermore, the crack was

Table 9.1 Summary of surface roughness measurements in stainless steel pipes[a]

Mechanism	Source	Roughness, μm (μinch) Local	Roughness, μm (μinch) Global
	(a) Stainless steel pipes - IGSCC		
IGSCC	NP-2472 Vol. 2 (see Figure I-1)	2.03 (80)	101 (3,990)
IGSCC	NP-2472 Vol. 2 (see Figure H-9)	--	107 (4,230)
IGSCC	NP-3684SR, Vol. 3 (Paper 4, Figure 11)	7.37 (290)	74.4 (2,930)
IGSCC	NP-3684SR, Vol. 3 (Paper 4, Figure 5)	10.5 (412)	41.9 (1,650)
IGSCC	NP-3684SR, Vol. 2 (Paper 5, Figure 21)	0.635 to 6.35 (25.0 to 250)	127 (5,000)
IGSCC	NP-3684SR, Vol. 2 (Paper 19, Figure 12)	1.40 (55)	27.9 (1,100)
Average		4.699 (185)	80.010 (3,150)
Standard Deviation		3.937 (155)	39.014 (1,536)
Range		0.635 to 10.5 (25 to 412)	27.94 to 127 (1,100 to 5,000)
Number of Samples		6	6
	(b) Stainless steel pipes - fatigue in air		
Fatigue (air)	Hitachi, (NED, Vol. 128, 1991, pp 24)	8.05 (317)	33.8 1,330

(a) Original measurements made in U.S. customary units and converted to SI units.

Table 9.2 Summary of surface roughness measurements in carbon steel pipes[a]

Mechanism	Source	Roughness, μm (μinch) Local	Global
	(a) Ferritic Steels - fatigue in air		
Fatigue (air)	NUREG/CR-5128 (girth weld)	3.02 (119)	--
Fatigue (air)	NUREG/CP-0051 Mayfield, pp 365 (A106B)	8.53 (336)	--
Fatigue (air)	Hitachi, NED, Vol. 128 1991, pp. 24 (STS 42)	8.05 (317)	33.8 (1,330)
Average		6.528 (257)	33.8 (1,300)
Standard Deviation		3.048 (120)	--
Range		3.02 to 8.53 (119 to 336)	--
Number of Samples		3	1
	(b) Ferritic Steels - corrosion fatigue in feedwater line		
Corrosion fatigue (Point Beach plant feedwater line)	NUREG/CR-1603, Figure 3.13	8.64 (340)	44.4 (1,750)
Corrosion fatigue (D.C. Cook plant feedwater line)	NUREG/CR-1603, Figure 3.17	3.05 (120)	20.1 (790)
Corrosion fatigue (Beaver Valley plant feedwater line)	NUREG/CR-1603, Figure 3.15	9.14 (360)	38.1 (1,500)
Corrosion fatigue (Palisades plant feedwater line)	NUREG/CR-1603, Figure 3.11	10.7 (420)	61.0 (2,400)
Corrosion fatigue (Ginna plant feedwater line)	NUREG/CR-1603, Figure 3.8	10.4 (410)	58.4 (2,300)
Corrosion fatigue (Salem plant feedwater line	NUREG/CR-1603, Figure 3.16	10.9 (430)	21.1 (830)
Average		8.814 (347)	40.513 (1,595)
Standard Deviation		2.972 (117)	17.653 (695)
Range		3.05 to 10.9 (120 to 430)	(20.1 to 61.0) (790 to 2,400)
Number of Samples		6	6

(a) Original measurements made in U.S. customary units and converted to SI units.

thought to grow at a 10 to 15 degree angle from the straight crack through the thickness, which would increase the global flow path by 1.5 to 3.5 percent.

From a typical stainless steel used in Ref. 9.5 (see Figure I-1 of Ref. 9.5), the global surface roughness that includes the peak-to-peak heights for intergranular crack growth was 101 μm (3,990 microinches). The roughness along the grain boundary was estimated to be 2.03 μm (80 microinches).

Using Figure H-9 in Reference 9.5, a global roughness for an IGSCC crack was estimated to be 107 μm (4,230 microinches).

From a paper by Christer Jansson on Swedish IGSCC studies (Ref. 9.6), Figure 11 of Reference 9.6 shows the typical global surface roughness for an IGSCC crack to be 74.5 μm (2,930 microinches), and Figure 5 of Reference 9.6 shows a global roughness of 41.9 μm (1,650 microinches). The roughness along a grain boundary could be up to 7.37 μm (290 microinches) in Figure 11 of Reference 9.6 and 10.5 μm (412 microinches) in Figure 5 of Reference 9.6.

From the paper by Olson et al. (Ref. 9.7) on large pipe IGSCC experiments at Battelle Pacific Northwest Laboratory (PNL), Figure 21 of Reference 9.7 shows that the typical global surface roughness of IGSCC cracks was 127.0 μm (5,000 microinches). The roughness along a grain boundary could be up to 6.4 μm (250 microinches) in some areas and perhaps a factor of 10 less in other areas (0.64 μm [25 microinches]).

From the paper by Kurtz (Ref. 9.8) on effects of sulfides on IGSCC at PNL, Figure 12 of Reference 9.8 shows the typical global surface roughness for an IGSCC crack to be 27.9 μm mm (1,100 microinches). The roughness along a grain boundary was 1.40 μm (55 microinches) in some relatively smooth areas.

9.3.1.2 Stainless Steel - Fatigue (Air)

Hitachi fatigue cracked pipe results showed a smaller or local surface roughness superimposed on a larger or global surface roughness (Ref. 9.9). The average value of the global roughness may correspond to the waviness of the fatigue crack, 33.8 μm (1,330 microinches). The average value of the local roughness was 8.05 μm (317 microinches). The results were very similar for their ferritic and stainless steel pipes.

9.3.1.3 Carbon Steel - Corrosion Fatigue

From an investigation on thermal fatigue cracks in a feedwater line from the Point Beach plant in the 1978 time period (Ref. 9.10), Figure 3.13 of Reference 9.10 showed a local surface roughness of 8.64 μm (340 microinches) and a global surface roughness of 44.4 μm (1,750 microinches).

From the same investigation (Ref. 9.10), a thermal fatigue crack in a feedwater line from the D.C. Cook plant in the 1978 time period, Figure 3.17 of Reference 9.10 showed a local surface roughness of 3.05 μm (120 microinches) and a global surface roughness of 20.1 μm (790 microinches).

From the same investigation (Ref. 9.10), a thermal fatigue crack in a feedwater line from the Beaver Valley plant in the 1978 time period, Figure 3.15 of Reference 9.10 showed a local surface roughness of 9.14 μm (360 microinches) and a global surface roughness of 38.1 μm (1,500 microinches).

From the same investigation (Ref. 9.10), a thermal fatigue crack in a feedwater line from the Palisades plant in the 1978 time period, Figure 3.11 of Reference 9.10 showed a local surface roughness of 10.7 μm (420 microinches) and a global surface roughness of 61.0 μm (2,400 microinches).

From the same investigation (Ref. 9.10), a thermal fatigue crack in a feedwater line from the Ginna plant in the 1978 time period, Figure 3.8 of Reference 9.10 showed a local surface roughness of 10.4 μm (410 microinches) and a global surface roughness of 58.4 μm (2,300 microinches).

9.3.1.4 Carbon Steel - Fatigue (Air)

In Reference 9.1, results on a carbon steel weld fatigue crack showed a roughness of 3.02 μm (119 microinches).

Measurements of a carbon steel base metal fatigue crack in air from the NRC Cold-Leg program showed a roughness of 8.53 μm (336 microinches). These are obtained from a technical paper authored by Mayfield and Collier (Ref. 9.11).

Hitachi fatigue cracked pipe results showed a local surface roughness superimposed on a global surface roughness (Ref. 9.9). The average value of the global roughness may correspond to the waviness of the fatigue crack, 33.8 μm (1,330 microinches). The average value of the local roughness was 8.05 μm (317 microinches). The results were very similar for their ferritic and stainless steel pipes.

9.3.2 Number of Turns per Unit Thickness

From the examinations of photomicrographs in References 9.8 to 9.12, Tables 9.3 and 9.4 show the number of 90-degree turns per inch of thickness for stainless steel and carbon steel pipes, respectively. For IGSCC cracks in stainless steels this can be a much larger number than for a corrosion fatigue crack, and can also vary significantly since the grain size may vary.

9.3.3 Entrance Loss Coefficient (C_D)

If entrance edges have a radius of 1/6 of the COD or larger, then they are considered to be rounded and $C_D = 0.62$. Consequently, for IGSCC with sharp edges (no pitting corrosion to smooth the edges), $C_D = 0.95$ for small COD values, i.e., COD < 0.006 inch. For Fatigue and corrosion fatigue typically at small pits with some surface corrosion to round the edges, $C_D = 0.62$ for all COD values of interest. These values were obtained from Reference 9.1.

Table 9.3 Summary of measurements of the number of 90-degree turns in stainless steel pipes[a]

Mechanism	Source	Number of 90-degree Turns per Unit Distance, mm^{-1} ($inch^{-1}$)
	(a) Stainless steel pipes - IGSCC	
IGSCC	NP-2472, Vol. 2 (see Figure I-1)	57.1 (1,450)
IGSCC	NP-3684SR, Vol. 3 (Paper 4, Figure 11)	13.9 (352)
IGSCC	NP-3684SR, Vol. 3 (Paper 4, Figure 5)	34.4 (873)
IGSCC	NP-3684SR, Vol. 2 (Paper 5, Figure 21)	9.45 (240)
IGSCC	NP-3684SR, Vol. 2 (Paper 19, Figure 12)	26.4 (670)
Average		28.23 (717)
Standard Deviation		18.94 (481)
Range		9.45 to 57.1 (240 to 1,450)
Number of Samples		5
	(b) Stainless steel pipes - fatigue in air	
Fatigue (air)	Hitachi (NED, Vol. 128, 1991, pp. 24)	2.52 (64)

(a) Original measurements made in U.S. customary units and converted to SI units.

Table 9.4 Summary of measurements of the number of 90-degree turns in carbon steel pipes[a]

Mechanism	Source	Number of 90-degree Turns per Unit Distance, mm^{-1} ($inch^{-1}$)
	(a) Ferritic steels -- fatigue in air	
Fatigue (air)	Hitachi, NED, Vol. 128 1991, pp. 24 (STS 42)	2.0 (51)
	(b) Ferritic steels - corrosion fatigue in feedwater lines	
Corrosion fatigue (Point Beach plant feedwater line)	NUREG/CR-1603, Figure 3.13	2.4 (61)
Corrosion fatigue (D.C. Cook plant feedwater line)	NUREG/CR-1603, Figure 3.17c	20.0 (507)
Corrosion fatigue (Beaver Valley plant feedwater line)	NUREG/CR-1603, Figure 3.15	2.3 (58)
Corrosion fatigue (Palisades plant feedwater line)	NUREG/CR-1603, Figure 3.11	13.7 (349)
Corrosion fatigue (Ginna plant feedwater line)	NUREG/CR-1603, Figure 3.8	1.42 (36.0)
Corrosion fatigue (Salem plant feedwater line)	NUREG/CR-1603, Figure 3.16	0.63 (16)
Average		6.73 (171)
Standard deviation		8.07 (205)
Range		1.42 to 20.0 (16 to 507)
Number of Samples		6

(a) Original measurements made in U.S. customary units and converted to SI units.

9.3.4 Actual Crack Path/Thickness

Most leak-rate analyses assume that a crack grows straight through the thickness. This is not true for real cracks. In the first type of example, a crack could follow a weld. Here the length of the crack along a typical 37-degree weld bevel is 1/[cos (37 degrees)] or 1.25 times the thickness. Reference 9.12 shows an example of such a service crack. Another example for angular crack growth of thermal fatigue cracks in feedwater piping, where from metallographic sections in Reference 9.10 showed that the flow path length was 1.05 times the thickness. These changes in the flow path length would effect the leak rate for small or large crack-opening displacements. We termed this effect the global flow path correction, K_G.

Additionally, many leak-rate analyses account for the pressure drop from a turn in the flow path, but do not account for the flow path being longer because of these turns. For instance, these small turns can occur along grain boundaries for an IGSCC. This local waviness is termed K_{G+L}, because of the way it was measured included the K_G effects. If the COD is small compared with the global roughness, then the local waviness will cause an increase in the flow path length. If the COD is small compared with the global roughness, then the local surface roughness should be used with this local plus global waviness flow-path multiplication factor, K_{G+L}, as well as the pressure drop from the number of turns.

Measured values of K_G and K_{G+L} from typical cracks for stainless steel and carbon steel, are presented in Tables 9.5 and 9.6. In general, these values are larger for IGSCC cracks in stainless steels than for corrosion fatigue cracks in carbon steels.

A separate evaluation was also made to assess the crack morphology parameters for a thermal fatigue crack in cast stainless steel. Photographs of fracture surfaces from Reference 9.13 were examined. Only a few cases were sufficiently documented for the level of detail needed in this work. Of these, the crack morphology parameters fell in the range of the carbon steel corrosion-fatigue cracks. Hence, the carbon steel crack morphology variables could be used for the cast stainless steel thermal fatigue-crack morphology. Further details on the statistical characterization of crack-morphology parameters are available in References 9.14 and 9.15.

Table 9.7 shows the summary of results in terms of statistics of the crack morphology variables. In general, it was found that the global surface roughness, local number of turns, and the path deviation factors for IGSCC in stainless steel are larger than those for corrosion fatigue in carbon steel. But, when the local surface roughness is considered, it was found to be larger for the corrosion fatigue type of cracking mechanism. However, note that the statistical properties presented in Table 9.7 were based on a small number of samples. Hence, these results should be viewed as preliminary estimates. Further studies are needed to verify these results.

Table 9.5 Crack flow-path-length to pipe thickness ratios for stainless steel pipes

Mechanism	Source	K_{G+L}	K_G
	(a) Stainless steel pipes - IGSCC		
IGSCC	NP-2472, Vol. 2 (See Figure G-14)	1.47	1.25
IGSCC	NP-3684SR, Vol. 3 (Paper 4, Figure 11, 75x)	1.35	1.02
IGSCC	NP-3684SR, Vol. 3 (Paper 4, Figure 5, 100x)	1.53	1.06
IGSCC	NP-3684SR, Vol. 2 (Paper 5, Figure 21)	1.15	1.02
IGSCC	NP-3684SR, Vol. 2 (Paper 19, Figure 12, 200x)	1.15	1.01
Average		1.33	1.07
Standard Deviation		0.17	0.10
Range		1.15 to 1.53	1.01 to 1.25
Number of Samples		5	5

Table 9.6 Crack flow-path-length to pipe thickness ratios for carbon steel pipes

Mechanism	Source	K_{G+L}	K_G
	(a) Ferritic Steels - Corrosion fatigue in feedwater lines		
Corrosion fatigue (Point Beach plant feedwater line)	NUREG/CR-1603, Figure 3.13	1.10	1.035
Corrosion fatigue (D.C. Cook plant feedwater line)	NUREG/CR-1603, Figure 3.17c	1.03	1.001
Corrosion fatigue (Beaver Valley plant feedwater line)	NUREG/CR-1603, Figure 3.15	1.08	1.03
Corrosion fatigue (Palisades plant feedwater line	NUREG/CR-1603, Figure 3.11	1.04	1.004
Corrosion fatigue (Ginna plant feedwater line)	NUREG/CR-1603, Figure 3.8	1.07	1.03
Corrosion fatigue (Salem plant feedwater line)	NUREG/CR-1603, Figure 3.16	1.02	1.001
Average		1.06	1.017
Standard Deviation		0.03	0.0163
Range		1.02 to 1.10	1.001 to 1.035
Number of Samples		6	6

Table 9.7 Mean and standard deviation of crack morphology parameters

Crack Morphology Variable	IGSCC		Corrosion Fatigue	
	Mean	Standard Deviation	Mean	Standard Deviation
μ_L, μm	4.70	3.94	8.81	2.97
μ_G, μm	80.0	39.0	40.5	17.7
n_{tL}, mm^{-1}	28.2	18.9	6.73	8.07
K_G	1.07	0.10	1.02	0.016
K_{G+L}	1.33	0.17	1.06	0.03

9.4 Implications of Crack Morphology Variables

The statistical properties of crack-morphology variables developed in this work can be used to calculate the probabilistic characteristics of the leak rate and leakage flaw size for LBB applications. Calculations of this kind are routine in performing LBB evaluations. Based on the statistics, both deterministic and probabilistic evaluations can be made.

Battelle recently conducted a probabilistic study using these statistics to compute the probability distribution of crack size for given leak-rate detection capability.[(a)] In that study, a stainless steel pipe with a probable IGSCC cracking mechanism was analyzed. Assuming that the associated crack-morphology variables are lognormally distributed, 100 independent samples of these variable were generated from the statistical properties in Table 9.7. An example calculation is shown here to see the effect of the crack morphology variables on calculating a flaw size for a given leak rate.

For each set of these crack morphology parameters, standard (deterministic) thermal-hydraulic and fracture-mechanics analyses were performed to compute the crack size for a leak rate of 3.785 l/min (1 gpm). This was done for a 711-mm (28-inch) diameter Schedule 80 stainless steel pipe assuming an IGSCC mechanism. The same deterministic analyses were repeated for each of the 100 sample sets of crack-morphology variables to generate the corresponding samples of the leakage flaw size. Following standard statistical analysis of these replicated samples, Figures 9.4 and 9.5 show the histogram and cumulative probability of leakage flaw size in this pipe. Comparisons with the theoretical distributions suggest that the flaw size can also be modeled as a lognormal variable.

Examples of this kind show how the uncertainties in the crack-morphology input can be accounted for in characterizing leakage flaw size for LBB evaluations. Further details on these calculations can be found in a topical report NUREG/CR-6004. The report also contains subsequent probabilistic pipe fracture evaluations for a wide variety of nuclear piping systems in BWR and PWR plants.

(a) Further details can be found in "Probabilistic Pipe Fracture Evaluations for Leak-Rate-Detection Applications," by S. Rahman, N. Ghadiali, D. Paul, and G. Wilkowski, NUREG/CR-6004, to be published in 1995.

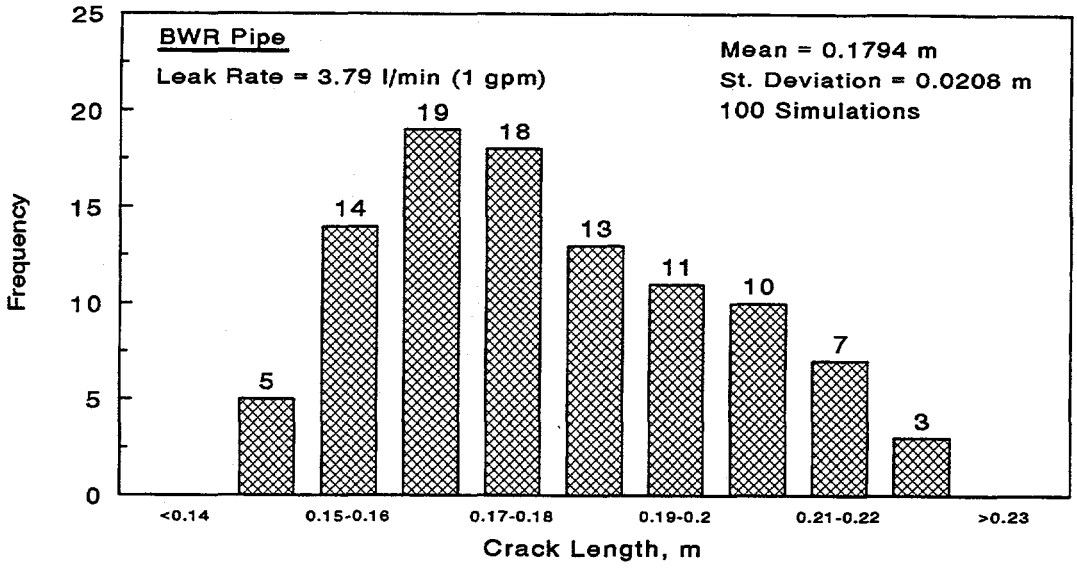

Figure 9.4 Histogram of leakage flaw size in a pipe for 3.785 l/min (1 gpm) leak rate and 50 percent of ASME Service Level A stress limit

T-6300-F9.4

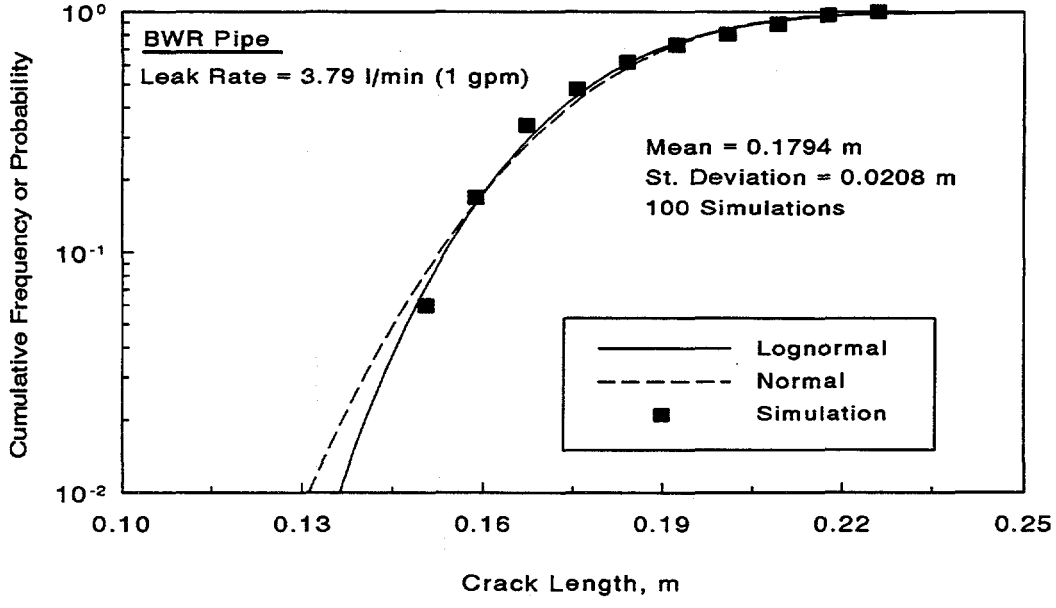

Figure 9.5 Probability distribution of leakage flaw size in a pipe for 3.785 l/min (1 gpm) leak rate and 50 percent of ASME Service Level A stress limit

T-6300-F9.5

9.5 References

9.1 Paul, D., Ahmad, J., Scott, P., Flanigan, L., and Wilkowski, G., "Evaluation and Refinement of Leak-Rate Estimation Models," NUREG/CR-5128, Rev. 1, U.S. Nuclear Regulatory Commission, Washington, D.C., June 1994.

9.2 Norris, D. et al., "PICEP: Pipe Crack Evaluation Program," EPRI Report, NP-3596-SR, Electric Power Research Institute, Palo Alto, CA,1984.

9.3 Wilkowski, G., Rahman, S., Paul. D., and Ghadiali, N., "Pipe Fracture Evaluations for Leak-Rate Detection: Deterministic Models," PVP-Vol. 266, *Creep, Fatigue Evaluation, and Leak-Before-Break Assessment*, Edited by Y. Garud, pp. 243-254, July 1993.

9.4 Collier, R. P., Stulen, F. B., Mayfield, M. E., Pape, D. B., and Scott, P. M., "Two-Phase Flow Through Intergranular Stress Corrosion Cracks and Resulting Acoustic Emission," EPRI Report NP-3540-LD, Electric Power Research Institute, Palo Alto, CA, 1984.

9.5 Hale, D. A., and others, "The Growth and Stability of Stress Corrosion Cracks in Large-Diameter BWR Piping," EPRI NP-2472, Vol. 2., Final Report, Electric Power Research Institute, Palo Alto, CA, July 1982.

9.6 Jansson, C., and others, "BWR Pipe Repairs in Sweden," Paper 4 in *Proceedings: Second Seminar on Countermeasures for Piping Cracks in BWRs*, EPRI NP-3684-SR, Vol. 3, Special Report, Electric Power Research Institute, Palo Alto, CA, September 1984.

9.7 Olson, N. H., and others, "Crack Growth Rates and Effectiveness of LPHSW Remedy in Large-Diameter Type 304 Stainless Steel BWR Pipe," Paper 5 in *Proceedings: Second Seminar on Countermeasures for Piping Cracks in BWRs*, EPRI NP-3684-SR, Vol. 2, Special Report, Electric Power Research Institute, Palo Alto, CA, September 1984.

9.8 Kurtz, R. J., "Effect of Sulfate and Chloride Intrusions on Cracking of Stainless Steel at 288°C," Paper 19 in *Proceedings: Second Seminar on Countermeasures for Piping Cracks in BWRs*, EPRI NP-3684-SR, Vol. 2, Special Report, Electric Power Research Institute, Palo Alto, CA, September 1984.

9.9 Matsumoto, K., Nakamura, S., Gotoh, N., Narabayashi, T., Tanaka, Y., and Horimizu, Y., "Study on Coolant Leak Rates Through Pipe Cracks," ASME PVP - Vol. 165, pp. 121-127, 1989.

9.10 Goldberg, A., Streit, R. D., and Scott, R. G., "Evaluation of Cracking in Feedwater Piping Adjacent to the Steam Generators in Nine Pressurized Water Reactor Plants," NUREG/CR-1603, U.S. Nuclear Regulatory Commission, Washington, D.C., October 1980.

9.11 Mayfield, M. E. and Collier, R. P., "Leak-Before-Break Due to Fatigue in the Cold Leg Piping System," *Proceedings of the CSNI Specialist Meeting on Leak-Before-Break in Nuclear Reactor Piping*, NUREG/CP-0051, U.S. Nuclear Regulatory Commission, Washington, D.C., September 1983.

9.12 "Ultrasonic Sizing Capability of IGSCC and Its Relation to Flaw Evaluation Procedures," prepared by EPRI NDE Center and EPRI Staff, August 4, 1983.

9.13 Bates, D. J., Doctor, S. R., Heasler, P. G., and Burck, E., "Stainless Steel Round Robin Test Centrifugally Cast Stainless Steel Screening Phase," NUREG/CR-4970, U.S. Nuclear Regulatory Commission, Washington, D.C., October 1987.

9.14 Rahman, S., Wilkowski, G., and Ghadiali, N., "Pipe Fracture Evaluations for Leak-Rate Detection: Probabilistic Models," PVP-Vol. 266, *Creep, Fatigue Evaluation, and Leak-Before-Break Assessment*, Edited by Y. Garud, pp. 255-267, July 1993.

9.15 Wilkowski. G. M., and others, "Short Cracks in Piping and Piping Welds," NUREG/CR-4599, U.S. Nuclear Regulatory Commission, Washington, D.C., Vol. 2., No. 2, May 1993.

10.0 UPDATES AND MODIFICATIONS TO THE SQUIRT CODE

10.1 Introduction

The development of a leak-rate estimation methodology was initiated in response to intergranular-stress-corrosion cracking in Boiling Water Reactor piping. Further interest in this area was stimulated by investigations into the application of a leak-before-break (LBB) philosophy to piping integrity safety analyses instead of assuming a double-ended guillotine break. Adoption of an LBB philosophy requires reliable leak-detection systems and verified leak-rate estimation techniques. Accurate leak-rate prediction requires correlation of crack size and shape, and is necessary to evaluate the ability of normal makeup systems to handle potential leakage. The development of a verifiable leakage-rate assessment methodology is an essential part in LBB evaluations. Regulatory implications include the elimination of pipe whip restraints and jet impingement shields, as well as changing requirements for equipment qualification for the case of steam released from a break.

SQUIRT, which stands for **S**eepage **Q**uantification of **U**psets **I**n **R**eactor **T**ubes, is a deterministic computer program that predicts the leakage rate and area of crack-opening for cracked pipes in nuclear power plants (Ref. 10.1). In all cases, the fluid in the piping system is assumed to be water at either subcooled or saturated conditions. The development of the SQUIRT computer model enables licensing authorities and industry users to conduct the leak-rate evaluations for leak-before-break applications in a more efficient manner. The SQUIRT code also includes technical advances that are not available in other computer codes currently used for leak-rate estimation.

The SQUIRT code (Version 1.0) was originally developed in 1990 during the First International Piping Integrity Research Group Program [IPIRG-1] (Ref. 10.2). Since then, various modifications and enhancements were pursued in the NRC's Short Cracks in Piping and Piping Welds Program (Ref. 10.3). This section briefly describes the SQUIRT code and provides an update on the modified versions of SQUIRT.

10.2 Thermal-Hydraulic and Fracture-Mechanics Models in SQUIRT

10.2.1 Thermal-Hydraulic Analysis by SQUIRT

The two-phase critical flow of water through cracks in piping systems is a highly complex physical phenomenon that has been widely studied during the last 40 years. What makes this problem so difficult is the existence of the two phases in the flow system (i.e., crack path), which can interact in a variety of ways. For instance, a two-phase flow system can exist with either vapor bubbles dispersed in a continuous liquid phase or as liquid droplets dispersed in a continuous vapor phase. The physics of each of these situations is vastly different, yet each represents a two-phase flow condition. Further complications arise when the two-phase mixture is experiencing critical flow. In this case, the time required for the fluid to reach thermodynamic equilibrium when moving into regions of lower pressure is comparable to the time that the fluid is flowing in the crack. This leads to nonequilibrium vapor generation rates for two-phase critical flows. To account for nonequilibrium effects between the phases, Henry and Fauske (Refs. 10.4 to 10.6) proposed a simple model for the

nonequilibrium vapor generation rate. In this model, it is assumed that the mixture quality relaxes in an exponential manner toward the equilibrium quality that would be obtained in a long tube. The relaxation coefficient was calculated based on their experiments with the critical flow of a two-phase water mixture in long tubes ($L_a/D_i > 100$ where L_a is the flow-path length and D_i is the inside diameter of the pipe). The Henry-Fauske model is the one that is chosen in SQUIRT to model the two-phase critical flow of water through cracks in piping systems.

10.2.2 Fracture-Mechanics Analysis by SQUIRT

The fracture-mechanics part of SQUIRT is based on the estimation methods available in the current literature to conduct crack-opening-area (COA) analyses for a pipe with circumferential through-wall cracks. Using these estimation methods, which are discussed in the earlier sections of this report, the crack-opening displacement for a cracked pipe can be predicted when the pipe geometry, crack size, pipe material properties, and applied loads are prescribed. In the original version of the SQUIRT code (Version 1.0), only the GE/EPRI method (Ref. 10.7) could be used to perform the COA analysis. In the new version of SQUIRT (Version 2.3), the LBB.ENG2 method (Ref. 10.8) in addition to the GE/EPRI method are available for fracture-mechanics analyses. In either of the two methods, elastic-plastic fracture-mechanics equations are invoked to calculate the crack-opening displacement for both stationary and growing (J-controlled) cracks. Further details on the crack-opening model in SQUIRT can be obtained from Reference 10.1.

In using SQUIRT, several options exist in modeling crack-opening profiles. The options for crack-opening shapes available in SQUIRT are: elliptical, diamond-shaped, and rectangular. The comparisons with experimental data as well as finite element results reported in Reference 10.1 and also examined in this report suggest that the ellipse may provide the best representation of the crack-opening shape.

10.3 Past Validation of SQUIRT Models

The SQUIRT computer program was validated by comparing its predictions with published experimental data and with experimental data derived from the IPIRG Program. The SQUIRT thermal-hydraulic model predictions were compared with experimental data on two-phase flow through long tubes reported by Sozzi and Sutherland (Ref. 10.9), two-phase flow through slits reported by Collier et al. (Ref. 10.10), Amos and Shrock (Ref. 10.11), and Matsushima et al. (Ref. 10.12), and two-phase flow through actual cracked pipe reported by Collier et al. (Ref. 10.10). In general, the SQUIRT program tended to underpredict the experimental data obtained on artificial slits. This was attributed to possibly overestimating the nonequilibrium vapor generation rate for tight slits, although more work needs to be done to confirm this hypothesis. The SQUIRT program performed reasonably well in predicting the measured leak-rate data of Collier et al. (Ref. 10.10) in stress-corrosion cracks, but the scatter in the data was much greater than that observed with artificial slits. If the nonequilibrium vapor generation rate were changed to produce good agreement with the artificial slit data, then the SQUIRT program would predict leakage rates too high for the real crack data. However, a crack pathway loss coefficient for stress-corrosion cracks could be determined to provide a best fit to the data under these circumstances. More work is needed to resolve these ambiguities.

Additional data for experimental validation were developed by leak-rate tests performed using a circumferential fatigue crack in a carbon steel pipe with a girth weld (Ref. 10.1). To obtain reasonably good agreement between these experimental results and the SQUIRT predictions for leakage flow rates, a flow path loss coefficient of approximately 6 velocity heads per millimeter of crack flow path length had to be assumed. This implies that the tight fatigue crack in the girth weld causes the fluid to change direction many times while flowing through the crack.

The fracture-mechanics model for crack-opening-area analysis in SQUIRT was compared with experimental data as well as with the results of elastic-plastic finite element analyses from the Degraded Piping Program (Ref. 10.13). The test cases included circumferential cracks in both carbon steel and austenitic stainless steel pipes, as well as stainless steel submerged-arc welded pipes. The comparison of predicted and test results suggests that for circumferential cracks in unwelded pipes under bending, the GE/EPRI estimation method, combined with the assumption of an elliptical crack-opening profile provides adequately accurate estimates of crack-opening. For cracks in welds, the elliptical crack shape assumption appears to be reasonable; however, there is ambiguity in how one should model the presence of a weld using the GE/EPRI method.

10.4 Organization of the SQUIRT Code

The SQUIRT code comprises four different executable modules that were developed in response to various objectives of leak-rate calculations for LBB and pipe flaw evaluations. These are explained below.

The SQUIRT1 Module. The SQUIRT1 module solves for the center-crack-opening displacement and crack growth for a pipe as a function of applied load when the pipe geometry and initial crack sizes are given. It is essentially a stripped-down version of the NRCPIPE code (Ref. 10.3) developed previously for pure fracture-mechanics analyses.

The SQUIRT2 Module. The SQUIRT2 module solves for the leakage rate from a crack of specified dimensions when the fluid pressure, fluid temperature, and crack-morphology parameters are specified. Using this module, one can determine whether the predicted leak-rate from a cracked pipe will be detectable by the current leak-detection limits.

The SQUIRT3 Module. The SQUIRT3 module solves for the center-crack-opening displacement and pipe load when the leakage rate and initial crack length are specified. This module is useful for pipe flaw evaluations in which one can determine what load it will take for a leaking pipe to exceed current leak-rate detection limits.

The SQUIRT4 Module. The SQUIRT4 module solves for the crack length and center-crack-opening displacement when the pipe load and the leakage rate are specified. This usually involves numerical iteration between the thermal-hydraulic and fracture-mechanics parts of the code to solve for the unknown crack size. Obviously, an initial guess for crack length has to be specified. This module is very useful in determining the leakage size flaw for subsequent evaluations of its fracture stability in LBB applications.

10.5 Updates and Modifications in SQUIRT

During the Short Cracks in Piping and Piping Welds Program, the original SQUIRT code was updated by incorporating various refinements and modifications. During the course of this program, two new versions (Versions 2.2 and 2.3) were released with the changes described below.

10.5.1 Version 2.2 of the SQUIRT Code

Version 2.2 of the SQUIRT code was released on June 30, 1993. The following changes were incorporated in Version 2.2:

1. The fracture-mechanics modules of SQUIRT (SQUIRT1, NRC3M, and NRC4M) were modified to reflect recent changes in the NRCPIPE code and correct errors to make these modules completely compatible with the results from NRCPIPE.

2. A new module called SQUIRT4 was developed to calculate crack sizes for specified loadings and leakage rates.

3. The SQUIRT2 module was enhanced to allow for different crack lengths on the outside and inside of the pipe.

4. A minor error in the friction factor coefficient that affects the SQUIRT2 program was corrected. The SQUIRT3 and SQUIRT4 modules also reflect this correction.

5. Minor cosmetic improvements in the input-output options were also made.

10.5.2 Version 2.3 of the SQUIRT Code

Version 2.3 of the SQUIRT code was released on November 30, 1994. The following changes were incorporated in Version 2.3:

1. The fracture-mechanics modules of SQUIRT (SQUIRT1, NRCP3M, and NRC4M) were modified to reflect recent changes in the NRCPIPE code and correct errors to make these modules completely compatible with the results from NRCPIPE.

2. New GE/EPRI influence functions (e.g., h-, V-, and F-functions) which were previously developed at Battelle were incorporated as an option for elastic-plastic fracture-mechanics analysis. The original GE/EPRI functions developed functions were retained as an option.

3. A separate estimation scheme known as the LBB.ENG2 method, which is available in the NRCPIPE code, was incorporated as an option in all SQUIRT modules.

4. Minor cosmetic improvements in the input-output options were also made.

10.6 References

10.1 Paul, D., Ahmad, J., Scott, P., Flanigan, L., and Wilkowski, G., "Evaluation and Refinement of Leak-Rate Estimation Models," NUREG/CR-5128, Rev. 1, U.S. Nuclear Regulatory Commission, Washington, D.C., June 1994.

10.2 Schmidt, R. A., Wilkowski, G. M., and Mayfield, M. E., "The International Piping Integrity Research Group (IPIRG) Program: An Overview," *Transactions of the 11th International Conference on Structural Mechanics in Reactor Technology*, Vol. G2: Fracture Mechanics and Non-Destructive Evaluation - 2, Edited by H. Shibata, Tokyo, Japan, Paper No. G23/1, pp. 177-188, August 1991.

10.3 Wilkowski, G. M., and others, "Short Cracks in Piping and Piping Welds," Semiannual reports by Battelle, NUREG/CR-4599, Vols. 1 to 3, Nos. 1 and 2, U.S. Nuclear Regulatory Commission, Washington, D.C., May 1991 to March 1994.

10.4 Henry, R. E., and Fauske, H. K., "Two-Phase Critical Flow at Low Qualities, Part I: Experimental," *Nuclear Science and Engineering*, Vol. 41, pp. 79-91, 1970.

10.5 Henry, R. E., and Fauske, H. K., "Two-Phase Critical Flow at Low Qualities, Part II: Analysis," *Nuclear Science and Engineering*, Vol. 41, pp. 92-98, 1970.

10.6 Henry, R. E., "The Two-Phase Critical Discharge of Initially Saturated or Subcooled Liquid," *Nuclear Science and Engineering*, Vol. 41, pp. 336-342, 1970.

10.7 Kumar, V., German, M. D., and Shih, C. F., "An Engineering Approach to Elastic-Plastic Fracture Analysis," EPRI Report, NP-1931, Electric Power Research Institute, Palo Alto, CA, 1981.

10.8 Brust, F. W., "Approximate Methods for Fracture Analyses of Through-Wall Cracked Pipe," NUREG/CR-4853, U.S. Nuclear Regulatory Commission, Washington, D.C., February 1987.

10.9 Sozzi, G. L., and Sutherland, W. A., "Critical Flow of Saturated and Subcooled Water at High Pressure," NEDO-13418, 1975.

10.10 Collier, R. P., Stulen, F. B., Mayfield, M. E., Pape, D. B., and Scott, P. M., "Two-Phase Flow Through Intergranular Stress Corrosion Cracks and Resulting Acoustic Emission," EPRI Report No. NP-3540-LD, Electric Power Research Institute, Palo Alto, CA, 1984.

10.11 Amos, C., and Shrock, V., "Critical Discharge of Initially Subcooled Water Through Slits," NUREG/CR-3476, U.S. Nuclear Regulatory Commission, Washington, D.C., 1983.

10.12 Matsushima, E., Yano, T., and Okamoto, A., "Experimental Study of Leak Flow Rate Through Artificial Slits," SMiRT-9, Vol. G, pp. 287-292, 1987.

10.13 Wilkowski, G. M., Ahmad, J., Barnes, C. R., Brust, F., Ghadiali, N., Guerrieri, D., Jones, D., Kramer, G., Landow, M., Marschall, C. W., Olson, R., Papaspyropoulos, V., Pasupathi, V., Rosenfeld, M., Scott. P., and Vieth, P., "Degraded Piping Program - Phase II: Summary of Technical Results and Their Significance to Leak-Before-Break and In-Service Flaw Acceptance Criteria, March 1984 - January 1989," NUREG/CR-4082, Vol. 8, U.S. Nuclear Regulatory Commission, Washington, D.C., March 1989.

11.0 SUMMARY AND CONCLUSIONS

The objectives of this study were to review, evaluate, and refine current analytical models for conducting the crack-opening-area analysis of pipes with circumferential through-wall cracks. They were accomplished here in eight stages and are described below.

11.1 Review and Comparison of Predictive Models with Experimental Data

An in-depth review was conducted to evaluate the adequacy of current predictive models for performing crack-opening-area analyses of circumferentially cracked pipes. The results from twenty-five full-scale pipe fracture experiments, conducted in the Degraded Piping Program, the International Piping Integrity Research Group Program, and the Short Cracks in Piping and Piping Welds Program, were used to verify five different estimation methods as well as the finite element method. The key results and findings are summarized in the following:

From Finite Element Analyses

- The finite element predictions of the center-crack-opening displacement for Experiment 1.1.1.21 containing a short crack (θ/π = 6.25 percent) were in very good agreement with the experimental data from the pipe test. The corresponding load versus load-line displacement also compared well with the test data.

- The results from several finite element analyses showed that the crack-opening shape for a pipe would approximately follow an elliptical profile. Both large-diameter pipes with short cracks and small-diameter pipes with long cracks were analyzed under pure bending and combined bending and tension to reach this conclusion.

- The GE/EPRI influence functions were computed by finite-element analyses to determine the J-integral, crack-opening displacement, and other fracture parameters. The differences between the previously developed solutions (EPRI NP-3607) and the present results appear to be most important for small crack sizes (e.g., when θ/π = 1/16 and 1/8). The present solutions were developed using the three-dimensional solid elements (20-noded brick elements) and the deformation theory algorithm of ABAQUS. The solutions presented here are believed to be the more accurate of the two solutions because full three-dimensional elements were used instead of relying on shell elements. The influence functions in EPRI NP-3607 report appear to produce results that are too stiff, and, indeed, solutions for large n were not possible as convergence problems occurred. No convergence problems were experienced in the present work.

- For pipes under combined bending and pressure, the influence functions for a specific pipe (R_m/t = 10, θ/π = 1/16, and n = 5) were compared to determine the effects of hoop stress on a pipe. The comparisons of results suggest that the hoop stress due to pressure would increase h_1, and hence, the J-integral. The mid-thickness crack-opening displacement (h_2) was also increased slightly. This may be due to local crack bulging.

The load-point displacement (h_3) and the pipe rotation (h_4) were significantly affected due to stiffening of the pipe under additional hoop stresses.

From Estimation Analyses of Cracks in Base Metals

- For six pipe experiments with cracks in the base metal that involved either pure bending or tension loads, the LBB.ENG2 and GE/EPRI methods provided good predictions of crack-opening displacements when compared with the experimental data up to the load at crack initiation. The differences in the crack-opening solutions by the GE/EPRI method using the original and new influence functions were not significant. In general, the LBB.ENG2 method was more accurate than the GE/EPRI method in predicting crack-opening for large cracks, but the reverse was true when small cracks were considered. However, for the small cracks, the predictions of maximum load by the LBB.ENG2 method were closer to the experimental results when compared with those by the GE/EPRI method. The Paris/Tada and LBB.NRC methods generally underpredicted crack-opening for most of these experiments.

- For three pipe experiments containing base-metal cracks, but under combined bending and tension, there were mixed trends in the crack-opening predictions by the estimation methods. In all three experiments, the Paris/Tada and LBB.NRC methods underpredicted crack-opening with the former method underestimating the most. The LBB.ENG2 method underpredicted crack-opening displacement in two experiments (Experiment 4131-1 and 1-8), but overpredicted crack-opening displacement in one experiment (Experiment 4131-3). The predictive trends of the GE/EPRI method were similar to that of the LBB.ENG2 method for Experiments 4131-1 and 4131-3. However, for the Experiment 1-8, the predictions of crack-opening by the GE/EPRI method were excellent regardless of the choice in using the influence functions.

- The results for ten pipes with complex cracks[(a)] subjected to pure bending showed that in most cases, the exceptions being Experiments 4113-5, 4114-1, and 4114-2, the LBB.ENG2 estimation method overestimated crack-opening displacement at all load levels regardless of the J-R curves. This can be qualitatively explained by noting that for a complex-cracked pipe, an effective pipe thickness, $t^* = t - d$ was used in the estimation formulas for simple through-wall-cracked pipes. Consequently, the "equivalent" through-wall-cracked pipe assumed in an estimation model would have lower stiffness than the actual complex-cracked pipe and hence, the predicted crack-opening displacements were larger when compared with the experimental results. Obviously, when the surface crack becomes deeper (e.g., Experiments 4113-2, 4113-4, and 4113-6), the magnitudes of these overestimates of the crack-opening displacement would become larger and could be significantly different from the experimental results. Again, this general loss of accuracy can be attributed to the over-simplification in the

(a) A complex crack is defined as finite length circumferential through-wall crack with a surface crack in the remaining ligament of the circumferential plane. Sometimes referred to as a compound crack.

estimation formulas for through-wall-cracked pipes used for predicting crack-opening in complex-cracked pipes.

From Estimation Analyses of Cracks in Girth Welds

- There were mixed trends in the predictions of crack-opening for five welded pipe experiments that were subjected to pure bending. The Paris/Tada method significantly underpredicted crack-opening displacement in all five experiments. When the LBB.NRC method was used, the crack-opening displacements were underpredicted in three experiments, overpredicted in one experiment, and in good agreement in one experiment. The LBB.ENG2 and LBB.ENG3 methods underpredicted crack-opening in three experiments and overpredicted crack-opening in two experiments. The GE/EPRI method overestimated crack-opening displacements in all experiments except one in which case the calculated crack-opening displacements were slightly lower and in reasonably good agreement with the test data. For one of the experiments for which the GE/EPRI method overpredicted the crack-opening, the results also agreed well with the experimental measurements.

- The comparisons of the J-R curves obtained from compact tension specimens and η-factor analysis (pipe) in Experiments 4141-1 and 4141-5 revealed that differences in the weld thickness and procedure could provide widely different fracture toughness properties. Using the pipe J-R curves for these two experiments, the predicted crack-opening results by most estimation methods were in better agreement with the pipe fracture data. Among the five estimation methods, the LBB.ENG3 and LBB.NRC method provided the best results.

- The analysis of a bimetallic pipe experiment showed that reasonably good predictions of crack-opening could be obtained by using tensile properties of the A516 Grade 70 carbon steel pipe and J-R curve of A516 Grade 70/Inconel 182 weld fusion-line. In particular, the results from the GE/EPRI and LBB.ENG2 methods were in good agreement with the test data.

11.2 Statistical Evaluation of Current Predictive Models

Standard statistical analyses were performed to assess the accuracy of the predictive models in estimating the center-crack-opening displacement for pipes analyzed in this study. The statistics involved calculation of the mean and coefficient of variation (COV) of the predictive crack-opening ratio defined as the ratio between the experimental and predicted values of the center-crack-opening displacement when the applied load is 40 percent of the experimental maximum load. (Note, the fracture behavior at this load is essentially elastic.) The results showed the following:

From Analyses of Simple Through-Wall-Cracked Pipes

- When all TWC pipe experiments were considered, all of the predictive models underpredicted the mean value of the COD (i.e., mean ratio greater than 1). The

GE/EPRI methods (with the original and newly developed influence functions from this work) predicted experimental COD with very good accuracy in terms of the mean value of the crack-opening ratio, but their predicted COVs were much higher. The differences between the statistics for the GE/EPRI method based on the original influence functions and those from the present study were not significant. The LBB.ENG2 and LBB.ENG3 methods slightly underpredicted the mean experimental COD with much lower COVs. The LBB.NRC method underpredicted the COD more than the LBB.ENG2 or LBB.ENG3 methods with higher values of COV. Among all methods, the Paris/Tada method underpredicted COD by the largest margin in terms of both mean and COV of the predicted crack-opening ratio.

- For pipes under pure bending loads, the LBB.ENG2 (mean ratio = 1.07) and LBB.ENG3 (mean ratio = 1.10) methods slightly underpredicted the experimental COD when the mean values were compared. The LBB.NRC (mean ratio = 1.16) and Paris/Tada method (mean ratio = 1.60) also underpredicted the COD with the Paris/Tada method underpredicting the most. It is interesting to note that the GE/EPRI methods (mean ratio = 0.84 and 0.74 for original and newly developed influence functions, respectively) overpredicted the mean COD for this loading condition.

- For a pipe under pure tension from pressure loading, similar trends were exhibited by the GE/EPRI, LBB.ENG2, and LBB.ENG3 methods. The comparisons of the COD predictions by the LBB.ENG2 and LBB.ENG3 methods with the experimental data were excellent.

- For pipes under combined bending and tension, all methods considered in this study underpredicted the experimental COD. The qualitative behavior is similar to that exhibited for the results of all pipe experiments discussed earlier. On a quantitative scale, however, the magnitudes of underprediction were much higher regardless of the methods used. Once again, the Paris/Tada method significantly underpredicted the COD.

- The mean results for pipes with short cracks indicate that the crack-opening would be underpredicted by the Paris/Tada, LBB.NRC, LBB.ENG2, and LBB.ENG3 methods and overpredicted by the GE/EPRI method. A similar trend was found for pipes under pure bending. The results for pipes with cracks in girth welds also reveal a similar qualitative behavior. For the girth weld cracks, the LBB.ENG2 and LBB.ENG3 methods predicted crack-opening displacement with reasonable accuracy with mean ratios close to one.

From Analyses of Complex-Cracked Pipes

- Complex-cracked pipe experiments, i.e., a pipe with a 360-degree circumferential surface crack and a finite length through-wall crack, were also analyzed using only the LBB.ENG2 method. Regardless of whether a constraint factor was applied to the J-R curves, the LBB.ENG2 method overpredicted (in terms of the mean value) crack-opening displacement for pipes with complex cracks. This is clearly opposite to the

behavior exhibited by this method in analyzing simple through-wall-cracked pipes. Further breakdown of the statistics for shallow cracks ($d/t \leq 0.5$) and deep cracks ($d/t \geq 0.5$) reveals that this estimation method provides better predictions of the experimental COD if the depth of the 360-degree surface crack is smaller. For example, the mean values of the crack-opening ratios were 0.77 for shallow cracks and 0.33 for deep cracks. Nevertheless, the LBB.ENG2 predictions for complex-cracked pipes were much larger than the experimental COD values. This overprediction of the LBB.ENG2 method is due to the over-simplification in the estimation formulas for TWC pipes used for predicting the COD of complex-cracked pipes. Hence, further developments are necessary to improve crack-opening models for complex-cracked pipes.

- In analyzing pipes with a leaking crack that may potentially be a complex crack, it may not be always possible to estimate accurately the depth of the internal surface crack unless detailed nondestructive examination is performed. For such a crack, if the depth of the surface crack is overestimated, the current analysis methods would overpredict crack-opening. Hence, for a given leak rate, this will cause the crack length to be underestimated resulting overprediction of the pipe's maximum load-carrying capacity. On the other hand, if the depth of the surface crack is underestimated or ignored, the predictive methods would underestimate crack-opening, and hence, also underestimate the load-carrying capacity of the pipe.

11.3 Sensitivity Analysis

A sensitivity study was performed to evaluate the effects of crack-face pressure, Ramberg-Osgood fit parameters, and errors in elastic modulus on the crack-opening. The results showed that:

- In general, the crack-face pressure would increase the crack-opening displacement. The magnitude of this increase depends on the crack size, pressure on the crack face, and the applied remote moment. For a linear-elastic analysis, when the crack size is small ($\theta/\pi \leq 1/16$), the crack-face pressure can be neglected. For large crack sizes ($\theta/\pi \geq 1/4$), if the crack-face pressure is close to the pipe pressure and the applied remote moment is comparable to the equivalent moment due to the crack-face pressure, the effects of crack-face pressure can become important. However, since the ratio of the crack-face pressure to the pipe pressure increases with the crack-opening, the possibility of having large crack-face pressure and small applied moment is very unlikely. In that case, the effects of crack-face pressure for large cracks would also be negligible.

- The Ramberg-Osgood fit in various strain regions of actual tensile data showed distinct variations in the model parameters (α and n), particularly when the low-strain and high-strain regions were considered. The effects due to these variations on the crack-opening predictions were more significant for a stainless steel pipe than that for a carbon steel pipe. In particular, when α and n are based on low-strain fit, the predicted crack-opening displacements in the same stainless steel pipe were much lower than the experimental data.

- If the crack-opening analysis is linear-elastic, an accurate estimate of the elastic modulus can become important. In one particular experiment on a stainless steel pipe (Experiment 1.1.1.26), the elastic modulus was measured to be 157.5 GPa (22.84×10^6 psi). That is considerably lower than the handbook values. Typically, the elastic modulus for austenitic materials vary from 179.27 GPa (26×10^6 psi) to 182.7 GPa (26.5×10^6 psi). Hence, using these two handbook values for the elastic modulus instead of the measured one, the crack-opening displacement could be underpredicted by 13.8 percent and 16 percent, respectively.

11.4 Analysis of Off-Centered Cracks

An analytical effort was undertaken to investigate the crack-opening characteristics of a pipe with an off-centered crack. Methods were developed by both finite element and estimation analyses to predict the crack-opening area for an off-centered crack. The results showed that:

- When the cracks were off-centered, the crack-opening displacements in a pipe would be smaller than those for the centered cracks. Correspondingly, the crack-opening area would also be decreased for the off-centered cracks.

- The crack-opening area for a pipe with an off-centered crack can be determined by normal analysis procedures for a centered crack via resolution of applied moment and assuming an elliptical profile for the crack-opening shape. This was an important finding since for leak-rate calculations, accuracy in the prediction of crack-opening area is more significant than that of the entire crack-opening shape.

- From the numerical analyses, the effects of off-centered crack were determined considering only the crack-opening area for pipe fracture evaluations. Their effects on the load-carrying capacity and the fracture stability of a leaking crack had not been assessed. From qualitative viewpoint, one can, however, argue that when a crack is off-centered, the crack-driving force, be it stress-intensity factor in linear-elastic fracture or J-integral in elastic-plastic fracture, will be lower than that for a centered crack assuming that the bending plane is the same for normal moments and seismic moments. However, it is more likely that the bending planes will differ. Hence, an off-centered crack, which may increase the length of a leakage flaw due to reduced crack-opening, can have positive effects on the maximum load-carrying capacity of pipes. It would be interesting to see how they would be countered by the effects of crack-opening-area reduction.

11.5 Evaluation of Restraint of Pressure-Induced Bending

A numerical study was conducted to evaluate the effects of restraint of induced bending due to pressure on the crack-opening of a pipe with simple through-wall cracks. The results suggest that:

- The restraint of the induced bending due to an axial (pressure) tension increases the failure stresses, but can decrease the crack-opening at a given load. If the pipe system

restrains the bending (i.e., from cracks being close to a nozzle or restraint from the rest of the piping system) then the actual leak rate would be less than the leak-rate calculated by using analyses that assume that the pipe is free to rotate. This will cause the actual leakage crack size to be larger than calculated by the current analysis methods for the same leak rate.

- When the crack angle was small ($\theta/\pi \leq 1/8$), the restraint effects were also small and may be neglected. However, for larger crack angles ($\theta/\pi \geq 1/4$), the crack-opening displacement due to restraint of induced bending could be significantly smaller than the crack-opening displacement at unrestrained conditions. Hence, this effect should not be ignored in the crack-opening and leak-rate analyses. This was especially true for small-diameter pipes in which case the leaking crack size for leak-before-break (LBB) analysis could be large.

- From the numerical results presented in this report, the potential reduction of crack-opening area due to restraint of pressure-induced bending have been evaluated for some specific cases. On the other hand, it is also recognized that for a pipe which restrains bending from pressure loads, the load-carrying capacity of the pipe will also tend to increase. However, since the normal operating plus seismic loads have a higher percentage of bending than axial membrane loads, the beneficial effects on the fracture loads may not be as great on the relatively small leakage size flaws in LBB analyses. Nevertheless, the restraint of pressure-induced bending, which may increase the length of the leakage flaw, can have positive effects on the maximum load-carrying capacity of pipes. It would be useful to also quantify possible increase in the failure loads and then evaluate how it would counter the effects of crack-opening-area reduction.

  From one pipe system experiment in the International Piping Integrity Research Group Program (Phase 1), it was experimentally determined that a guillotine break did not occur until the growing through-wall crack was 95 percent around the pipe circumference. From pressure loads alone, it was expected that a break would occur once the crack reached 65 percent of the circumference. The 95-percent crack length corresponded to the pressure-induced failure if the induced bending was restrained. (This crack was located 3.4 pipe diameters from an elbow.) This is strong evidence of the effect of pressure-induced bending restraint on increasing load-carrying capacity in a pipe system when the crack becomes large, i.e., at least for analyses assessing fracture instability behavior.

11.6 Analysis of Girth Weld Nozzle Crack at a Thickness Transition

A pipe containing a crack in a girth weld at a nozzle with a thickness taper on both sides was analyzed to evaluate its crack-opening characteristics. Elastic-plastic finite element analyses were performed to assess the effects of a typical thickness transition and geometric constraint associated with heavy integrally reinforced nozzles on the crack-opening displacement of a carbon steel nozzle containing a circumferential through-wall crack. The results are summarized below.

- To simplify the finite element model, it was assumed that the nozzle could be modeled without the angular intersection into the cold-leg pipe. The length of the straight nozzle was varied to determine the effects of this length on the crack opening. From the results, the crack-opening displacements were not affected by the choice of the length of the nozzle. An analysis of an idealized nozzle geometry for modeling the combined nozzle and cold-leg pipe in a slanted configuration is a very useful simplification for crack-opening calculations.

- Due to thickness gradient on both sides of the crack, the component of crack-opening displacement in the thinner side was much larger than that in the thicker side, thereby breaking the symmetry of crack-opening shape with respect to the crack length. The differences in these components can be very significant when the applied moment is large enough to induce plasticity.

11.7 Evaluation of Weld Residual Stresses

A simplified analytical study was conducted to assess the magnitude of weld residual stresses in a pipe and their effects on the crack-opening-area analysis. Standard linear-elastic finite element analyses were performed to determine the effects of the residual stresses. The key results were:

- The prescribed residual stress field from ASME Section XI technical basis document IWB-3640 affected the crack-opening for the thicker-wall large-diameter pipe much less than that for the thinner-wall small-diameter pipe. For the large-diameter pipe at 1.08 times the ASME Service Level A stress limits with residual stresses, the center-crack-opening displacement:

  - increased by 4.4 percent at the inside surface,
  - decreased by 2.4 percent at the middle surface, and
  - increased by 3.3 percent at the outer surface of the pipe.

  For the small-diameter pipe when the residual stresses were included with stresses of 0.9 times the ASME Service Level A stress limit, the center-crack-opening displacement:

  - increased by 17.1 percent at the inside surface,
  - decreased by 11.7 percent at the mid-thickness, and
  - decreased by 31.7 percent at the outside surface.

- At more typical normal operating stresses, which can be much smaller than the applied stresses used in these analyses, the effects of residual stresses on crack-opening could be much higher. For example, when the applied stress is equal to 50-percent of ASME Service Level A stress, the center-crack-opening displacement for the thick-walled large diameter pipe would increase by 9.46 and 7.11 percent at the inside and outside surfaces, respectively, and decrease by 5.17 percent at the mid-thickness level. Correspondingly, the center-crack-opening displacement for the thin-walled small-diameter pipe would increase by 30.9 percent at the inner surface and decrease by 57.2

and 21.1 percent at the outer and middle surfaces of the pipe, respectively. Relative comparisons of the crack-opening results for these two pipes indicate that at any given applied load, the residual stress effects are more severe for the thin-walled small-diameter pipe than for the thick-walled large-diameter pipe.

- For both thicker-wall large-diameter pipe and thinner-wall small-diameter pipe, detailed plots of crack-opening displacement versus applied moment showed that at some value of this applied moment, the crack-opening could become zero when residual stresses were included. For the thinner-wall small-diameter pipe, the analysis predicted that due to the residual stress, the outer surface of the pipe would close (thus preventing any leakage) when the applied stress was equal to 28.6 percent of the ASME Service Level A stress limit. Similar calculations could also be made for the middle surface of both pipes, but the trends in the results suggest that for closure to occur, the applied stresses would have to be very small, i.e., 2.60 and 10.5 percent of the ASME Service Level A stress limits for the thicker-wall large-diameter and thinner-wall small-diameter pipes, respectively.

- The results of the crack-opening analysis presented in this study should be viewed as preliminary estimates for the residual stress effects. No efforts were undertaken to determine the accuracy of the approximate finite element analysis conducted in this study compared with more rigorous thermo-plastic finite element analysis, where the residual stress field can be numerically simulated. One major difference between these two approaches, is that modeling the residual stress field as a crack-face pressure, imposes a load-controlled stress field, whereas, the actual residual stresses are a local displacement-controlled stress field. The load-controlled crack-face-pressure modeling should produce a larger effect on the crack-opening, than the thermo-plastic modeling of the residual stresses (with unpinning of the nodes to determine the crack-opening displacement). Considering these aspects, the results from this analysis should overemphasize the predictions of the crack-opening displacement due to residual stresses. Nevertheless, the conclusion that the residual stress effects on the crack-opening for thinner-wall small-diameter pipe are more severe than the thicker-wall large-diameter pipe, is an important result.

11.8 Improved Model of Crack Morphology

An improved crack-morphology model was developed for performing leak-rate analyses. The model involved improved definitions of surface roughness, number of turns, and path deviation factors, which are key input parameters, as a function of center-crack-opening displacement for determining the leak rate in a cracked pipe. Simple linear models were developed based on local and global definitions of the crack-morphology variables that can be measured from the current service data. Standard statistical analyses of these data were conducted data to determine the probabilistic characteristics (e.g., mean and standard deviation) of the crack-morphology parameters for several types of cracking mechanisms and pipe materials. Using these statistics, one can evaluate the effects of crack-morphology variability on the leak rate or leakage size flaw for LBB or other applications.

11.9 Modifications of the SQUIRT Code

Two modified versions of the SQUIRT code, which was originally developed in the International Piping Integrity Research Group Program, were created to conduct improved leak-rate and crack-opening-area analyses. These modifications reflect recent changes in the fracture-mechanics modules including adding new GE/EPRI influence functions developed previously at Battelle. A separate estimation scheme, known as the LBB.ENG2 method, was also added to the already existing GE/EPRI method for elastic-plastic fracture-mechanics analyses. In addition, the modified versions of SQUIRT include corrections of minor bugs and errors that were identified during the course of the Short Cracks in Piping and Piping Welds Program. No work was done on the thermal-hydraulic analyses within the code.

NRC FORM 335 (2-89) NRCM 1102, 3201, 3202

U.S. NUCLEAR REGULATORY COMMISSION

BIBLIOGRAPHIC DATA SHEET

(See instructions on the reverse)

1. REPORT NUMBER (Assigned by NRC, Add Vol., Supp., Rev., and Addendum Numbers, if any.)

NUREG/CR-6300
BMI-2184

2. TITLE AND SUBTITLE

Refinement and Evaluation of Crack-Opening-Area Analyses for Circumferential Through-Wall Cracks in Pipes

3. DATE REPORT PUBLISHED

MONTH	YEAR
April	1995

4. FIN OR GRANT NUMBER

B5702

5. AUTHOR(S)

S. Rahman, F. Brust, N. Ghadiali, Y. H. Choi[1], P. Krishnaswamy, F. Moberg[2], B. Brickstad[2], G. Wilkowski

6. TYPE OF REPORT

Technical

7. PERIOD COVERED *(Inclusive Dates)*

3/90 - 1/95

8. PERFORMING ORGANIZATION – NAME AND ADDRESS *(If NRC, provide Division, Office or Region, U.S. Nuclear Regulatory Commission, and mailing address; if contractor, provide name and mailing address.)*

Battelle
505 King Avenue
Columbus, OH 43201-2693

[1]Korea Institute of Nuclear Safety
P.O. Box 16, Daeduk-danji, Taejeon Republic of Korea

[2]Swedish Plant Inspection Ltd. Alstromergatan 12
S-100 29 Stockholm, P.O. Box 49306 Sweden

9. SPONSORING ORGANIZATION – NAME AND ADDRESS *(If NRC, type "Same as above"; if contractor, provide NRC Division, Office or Region, U.S. Nuclear Regulatory Commission, and mailing address.)*

Division of Engineering Technology
Office of Nuclear Regulatory Research
U.S. Nuclear Regulatory Commission
Washington, D.C. 20555-0001

10. SUPPLEMENTARY NOTES

11. ABSTRACT *(200 words or less)*

Leak-before-break (LBB) analyses for circumferentially cracked pipes are currently being conducted in the nuclear industry to justify elimination of pipe whip restraints and jet impingement shields which are present because of the expected dynamic effects from pipe rupture. The application of the LBB methodology frequently requires calculation of leak rates. The leak rates depend on the crack- opening area of the through-wall crack in the pipe. In addition to LBB analyses which assume a hypothetical flaw size, there is also interest in the integrity of actual leaking cracks corresponding to current leakage detection requirements in NRC Regulatory Guide 1.45, or for assessing temporary repair of Class 2 and 3 pipes that have leaks as are being evaluated in ASME Section XI. This study was requested by the NRC to review, evaluate, and refine current analytical models for crack-opening-area analyses of pipes with circumferential through-wall cracks. Twenty-five pipe experiments were analyzed to determine the accuracy of the predictive models. Several practical aspects of crack-opening such as; crack-face pressure, off-center cracks, restraint of pressure-induced bending, cracks in thickness transition regions, weld residual stresses, crack-morphology models, and thermal-hydraulic analysis, were also investigated.

12. KEY WORDS/DESCRIPTORS *(List words or phrases that will assist researchers in locating the report.)*

Pipe, Fracture, Crack, Leak-before-break, J-integral, J-R curve, Leak rate, Residual stresses, crack-opening displacement, crack-opening area

13. AVAILABILITY STATEMENT

Unlimited

14. SECURITY CLASSIFICATION

(This Page) Unclassified

(This Report) Unclassified

15. NUMBER OF PAGES

16. PRICE